Inaugural dissertation

for

obtaining the doctoral degree

of the

Combined Faculty of Mathematics, Engineering and Natural Sciences

of the

Ruprecht - Karls - University

Heidelberg

Presented by

M.Sc. Simon Hänle-Kreidler

born in Ulm (Donau)

Oral examination: 21st February 2023

Characterization of novel substrates of SCF-FBXW7 in mitotic cell fate regulation

Referees: Prof. Dr. Ingrid Hoffmann
Prof. Dr. Frauke Melchior

Table of contents

Summary

Protein ubiquitylation is a post-translational modification, which can control various cellular processes. Ubiquitin is conjugated to a substrate by an enzymatic cascade comprising so-called ubiquitin writers: E1, E2 and E3 enzymes. More of the ubiquitin-code is continuously uncovered and functional relationships are established. The induction of proteasomal degradation is probably the most prominent function of protein ubiquitylation. The E3 ubiquitin ligases convey specificity by facilitating the substrate interaction. SKP1-CUL1-F-box protein complexes belong to the RING E3 ubiquitin ligases and are one of the largest groups of the over 600 human E3 ubiquitin ligases. Their substrate receptors, the F-box proteins, are interchangeable and they can therefore target a vast number of substrates. FBXW7 is one of the best characterized F-box proteins and acts as a tumor suppressor by targeting oncogenes like c-Myc, Cyclin E1 and NOTCH1 for degradation. Being the most frequently mutated F-box protein in human cancers, FBXW7 loss-of-function or deletion result in increased tumor proliferation and chemoresistance. FBXW7-deficiency promotes mitotic slippage in response to antimicrotubule drugs and the identification of FBXW7 substrates responsible for this phenotype remains a major task.

In the presented thesis, I aimed at identifying novel substrates of FBXW7 which are involved in mitotic slippage to better understand mitotic cell fate regulation. Using a proteomics approach, I identified the Histone 3 lysine 4 methyltransferase complex component WDR5 as FBXW7 candidate substrates and showed that FBXW7 regulates WDR5 protein levels by ubiquitylation. I verified that FBXW7 and WDR5 interact *in-vivo* and *in-vitro* and found that the overexpression of WDR5 and Cyclin E1 can promote mitotic slippage. Reciprocally, the depletion of WDR5 and Cyclin E1 reduced mitotic slippage induced by knockdown of FBXW7 and significantly reduced polyploidization after mitotic slippage. Although the methyltransferase enzymatic subunit KMT2D is a substrate of FBXW7 and cooperates with WDR5, knockdown of KMT2D did not affect mitotic cell fate.

Collectively, I identified WDR5 as a novel substrate of FBXW7 and showed that the FBXW7 substrates WDR5 and Cyclin E1 can promote mitotic slippage and are required for drug-induced polyploidy. My results help to better understand the mechanisms underlying chemotherapy resistance caused by treatment of cancers with antimicrotubule drugs.

Zusammenfassung

Die post-translationale Konjugation von Substraten mit dem Protein Ubiquitin, auch Ubiquitylierung genannt, ist eine Modifikation, die wichtige zelluläre Prozesse reguliert. Ubiquitin wird durch eine enzymatische Kaskade bestehend aus E1, E2 und E3 Enzymen an Substrate angeheftet, was je nach Art der Verlinkung der Ubiquitinketten verschiedene Funktionen ermöglicht. Die bekannteste Funktion der Ubiquitylierung ist wahrscheinlich die Erkennung und der Abbau der ubiquitylierten Substrate durch das Proteasom. Die E3 Ubiquitin-Ligasen interagieren mit dem Substrat und vermitteln daher die Spezifizität der Reaktion. Im menschlichen Genom wurden über 600 E3 Ubiquitin-Ligasen entdeckt, wobei die SKP1-CUL1-F-box Proteinkomplexe zu den größten und wichtigsten Gruppen zählt. F-box Proteine sind austauschbare Substratrezeptoren, wodurch diese Komplexe eine Vielzahl an Substraten ubiquitylieren kann. Der Tumorsuppressor FBXW7 ist eines der am besten untersuchten F-box Proteine und reguliert die Proteinmengen von bekannten Onkogenen wie c-Myc, Cyclin E1 und NOTCH1. Jedoch liegt FBXW7 bei Krebserkrankungen häufig mutiert vor und trägt dort zum Tumorwachstum und zur Chemoresistenz bei. Es wurde gezeigt, dass durch das Fehlen von funktionellem FBXW7 die Rate an mitotischen Zelltod während der Behandlung mit Mitosehemmstoffen sinkt. Daher ist die Identifizierung der für diesen Phänotypen verantwortlichen Substrate von großer Bedeutung.

Das Ziel meiner Doktorarbeit war es daher, neue Substrate von FBXW7 zu finden, die den mitotischen Zelltod beeinflussen. Durch Analyse des Interaktoms von FBXW7 konnte ich WDR5 als mögliches neues Substrat von FBXW7 ermitteln. Im Folgenden konnte ich zeigen, dass FBXW7 und WDR5 *in-vivo* und *in-vitro* interagieren und die Proteinmenge von WDR5 durch FBXW7 reguliert wird. Dazu ubiquityliert FBXW7 WDR5 und induziert dessen Abbau über das Proteasom. In Folge der Überexpression von WDR5 oder Cyclin E1 sinkt die Rate an mitotischen Zelltod von Krebszellen. Auf der anderen Seite kann der durch fehlendes FBXW7 verringerte mitotische Zelltod durch Herunterregulation von WDR5 und Cyclin E1 wieder verstärkt werden. Zudem werden WDR5 und Cyclin E1 für die Entstehung von polyploiden Zellen benötigt. Die Methyltransferase KMT2D, die ein bekanntes Substrat von FBXW7 ist und mit WDR5 interagiert, hat jedoch keinen Einfluss auf den mitotischen Zelltod.

Zusammengefasst konnte ich in dieser Arbeit WDR5 als neues Substrat von FBXW7 identifizieren und zeigen, dass WDR5 und Cyclin E1 sowohl den mitotischen Zelltod

beeinflussen, als auch für die Entstehung polyploider Zellen benötigt werden. Die erhobenen Daten tragen dazu bei, die Mechanismen der Chemotherapieresistenz gegenüber Spindelgiften besser zu verstehen.

1. Introduction

1.1 Protein degradation pathways

1.1.1 Protein ubiquitylation

The conjugation of proteins with ubiquitin is a multi-step process, which fulfills a vast variety of cellular functions. Initially, ubiquitylation was identified as an adenosine triphosphate (ATP)-dependent mechanism to target proteins for degradation via the 26S proteasome (Hershko et al. 1980; Ciechanover et al. 1980). An E1 ubiquitin activating enzyme catalyzes the activation of ubiquitin, a 76 amino-acid protein, by transferring it to a thiol site on itself (Ciechanover et al. 1981). Next, an E2 ubiquitin-carrier or -conjugating enzyme accepts the activated ubiquitin from the E1 via another thioester linkage and then localizes ubiquitin in close proximity to the substrate of the reaction. Finally, an E3 ubiquitin-ligase facilitates the interaction with the substrate, and thereby mediates substrate specificity (Hershko et al. 1983; Hershko 1996). Ubiquitin is linked to proteins by an isopeptide bond between its C-terminal glycine residue and the amino groups of lysine residues or the N-terminal residue of substrate proteins (Ciechanover and Ben-Saadon 2004). Strikingly, the ubiquitylation machinery was also found to catalyze the formation of polyubiquitin chains, in which the C-terminal glycine of ubiquitin is linked to lysine residues or the N-terminus of another ubiquitin molecule, which had been previously linked to a substrate (Chau et al. 1989; Hershko and Heller 1985; Hough et al. 1986).

While the human genome contains only two genes encoding for E1 enzymes, over 30 different E2 conjugating enzymes and over 600 E3 ubiquitin-ligases have been described. E3 ubiquitin-ligases can be categorized into different classes, depending on their conserved domains catalyzing the ubiquitylation reaction: Really interesting new gene (RING), homologous to the E6-associated protein (E6AP) carboxyl terminus (HECT) and RING-between-RING (RBR). RING E3 ligases bind the ubiquitin-loaded E2 conjugating enzymes to their zinc-finger or U-box domain and facilitate direct transfer of ubiquitin to the substrate. In contrast, HECT domain ligases contain an acceptor cysteine that accepts ubiquitin from the E2 by forming a thioester linkage with ubiquitin before transferring it to lysine residues on the substrate (Berndsen and Wolberger 2014; Metzger et al. 2012). The approximately 10 known RBR E3 ligases represent the smallest group of E3 ubiquitin-ligases. RBR ligases use a hybrid mechanism to ubiquitylate their substrates: While the RING1 domain recruits the loaded E2, RING2 contains a catalytic cysteine residue analogous to HECT ligases

and first binds ubiquitin covalently before transferring it to the substrate (Walden and Rittinger 2018). Although there are many monomeric E3 ligases, especially RING E3 ligases have been found to also exist in dimers or multisubunit complexes (Brzovic et al. 2001; Nalepa et al. 2006). The Cullin-RING ligases (CRL) superfamily and the anaphase-promoting complex/cyclosome (APC/C) are the most prominent examples (Hua and Vierstra 2011; Petroski and Deshaies 2005). This variety in E3 ligases allows the highly specific targeting of a wide range of substrates to regulate diverse biological processes (Nakayama and Nakayama 2006).

Up to date, the knowledge about the ubiquitin-proteasome system (UPS) has expanded tremendously and its proper function is required for fundamental cellular processes, such as cell cycle control, signaling, DNA repair and apoptosis (Vucic et al. 2011; Hershko and Ciechanover 1998; Metzger et al. 2012). Given this importance for cellular homeostasis, it is not surprising that dysfunction of the UPS is linked to many pathologies, genomic instability and tumorigenesis (Marshall and Vierstra 2019).

1.1.2 An overview on protein degradation

Proteins are the final products of transcription and translation processes in the cell. During translation, the ribosome connects amino acids via peptide bonds according to the messenger ribonucleic acid (mRNA) template to form polypeptides. Yet, the correct folding of polypeptides is required for their biological activity. Early work demonstrated that the information for protein folding is contained within its primary structure (Anfinsen 1973). Folding of many proteins was found to require molecular chaperones, which reduce misfolded species, prevent irreversible aggregation, and perform quality control (Kim et al. 2013). Folding already starts at the nascent polypeptide-chain upon exit from the ribosome and therefore happens co-translational (Nicola et al. 1999; Kaiser and Liu 2018). Correctly folded proteins are released when a stop codon is reached. However, different factors such as damaged or non-stop mRNAs can cause ribosome stalling and result in the formation of aberrant polypeptide products (Ito-Harashima et al. 2007; Wilson et al. 2007). These polypeptides can fold improperly and have severe effects on cellular fitness, causing various diseases, including neurodegeneration (Joazeiro 2017; Hartl 2017).

Not long ago, a conserved pathway was identified which represents the first line of defense against the accumulation of faulty translational products (Bengtson and Joazeiro 2010). Upon ribosome stalling, the ribosome-associated protein quality

control (RQC) pathway is initiated, and the newly formed polypeptides are targeted for proteasomal degradation. Key component is the RING E3 ubiquitin-ligase Listerin (LTN1), which ubiquitylates polypeptides localized in stalled 60S ribosomal subunits and promotes their degradation via the UPS (Bengtson and Joazeiro 2010; Brandman and Hegde 2016; Joazeiro 2019). The endoplasmatic reticulum-associated degradation (ERAD) system represents the second protein quality control system, which mainly performs quality control of secretory proteins (Vembar and Brodsky 2008).

During their life cycle, folded and functional proteins can be exposed to stresses, for example oxidative damage or heat, and thereby lose their folding. Central parts of the protein quality control system (PQC) are molecular chaperones, which recognize exposed hydrophobic surfaces of misfolded proteins, that are usually buried, and assist their refolding (Hartl et al. 2011; Kim et al. 2013). The majority of chaperones are the heat-shock proteins (HSPs), which are further divided into subgroups based on their molecular size. If the misfolding process fails, chaperones can promote the proteolytic degradation of terminally misfolded proteins (Ciechanover et al. 1995; Ellis and Minton 2006; Pauwels et al. 2007). While most misfolded proteins are directed to the UPS system by chaperones, the remaining fraction or aggregation-prone proteins are delivered to phagophores and are degraded by chaperone-mediated autophagy (Chiang et al. 1989; Cha-Molstad et al. 2015; Ciechanover and Kwon 2017).

Because the cellular pool of proteins is consistently refreshed by newly synthesized proteins, different mechanisms act in parallel to enable the regulation of protein abundance on a post-translational level.

The first protein degradation signals were described in 1986 by Alexander Varshavsky (Varshavsky 1991). He described that the N-terminal residue of a protein correlates to its *in-vivo* half-life. Members of the N-end rule pathway can recognize proteins by their N-degrons to induce their degradation by the 26S proteasome or via autophagy. To date, all 20 amino acids have been found to act as N-degrons in the correct sequence context and with specific post-translational modifications (PTMs). Regulated degradation by N-end rule pathway was shown to mediate a plethora of functions (Varshavsky 2017, 2019). One decade later, the first C-terminal degradation motif, a C-degron, was identified (Keiler et al. 1996). C-degrons are usually shielded after protein folding, however miss-localized proteins or proteolytic products more frequently present their C-terminus and are the main targets of this pathway. Analogical to N-

degrons, the surrounding sequence was found to dictate protein stability (Lin et al. 2018; Koren et al. 2018; Yeh et al. 2021; Varshavsky 2019).

Apart from the inherent degrons represented by the N-degrons, C-degrons, exposed hydrophobic patches and specific amino acid sequences within the primary structure, protein degradation can be induced by PTMs. These so-called acquired degrons can are marked by modifications, including phosphorylation or conjugation with the small ubiquitin-like modifier (SUMO) (Ravid and Hochstrasser 2008; Sriramachandran and Dohmen 2014). Adding another layer of regulation to protein degradation, these acquired degrons allow precise and rapid control of protein abundance in a timely and spatially controlled manner. For example, protein phosphorylation is the most common PTM for the recognition of substrates by CRLs (Willems et al. 2004).

Because the recognition of substrates by E3 ubiquitin-ligases is the most crucial and rate-limiting step in the ubiquitylation process, a variety of methods was developed to establish connections between E3 ubiquitin-ligases and their substrates (O'Connor and Huibregtse 2017). These connections can be utilized for the understanding of basic biological processes or pathologies, which are based on defects of the UPS.

Learnings from acquired degrons led to the development of the first proteolysis-targeting chimera (PROTAC) molecule by Sakamoto et al. 2001. PROTACs are small molecules, which allow the artificial targeting of a target protein by E3 ubiquitin-ligases (Sakamoto et al. 2001). The field has developed rapidly after the characterization of lenalidomide as a PROTAC utilizing the E3 ubiquitin-ligase cereblon (CRBN) (Lu et al. 2014; Fischer et al. 2014; Krönke et al. 2014). Novel PROTACs are developed continuously and might be used as drugs for certain pathologies in the future (Békés et al. 2022).

1.1.3 The 26S proteasome

The proteolytic heart of the UPS is the 26S proteasome, a huge protease-complex found in eukaryotic cells (Enenkel et al. 1998; Reits et al. 1997; Russell et al. 1999; Marshall and Vierstra 2019). It consists of two functionally distinct sub-complexes, the catalytic 20S core protease (CP) and two 19S regulatory particles (RP), which capture proteins designated for degradation (Groll et al. 1997; Finley 2009; Lander et al. 2012; Lasker et al. 2012). The CP contains catalytic sites for peptide bond cleavage and exhibits, amongst others, trypsin-like and caspase-like properties (Arendt and Hochstrasser 1997; Heinemeyer et al. 1997; Dick et al. 1998; Marshall and Vierstra

2019). The main regulator of the CP are the one or two RPs, which localize on the ends of the CP and facilitate the import of ubiquitylated substrates by opening of the α-ring pore and release of ubiquitin prior to substrate degradation (Bhattacharyya et al. 2014; Finley and Prado 2020). Substrate selection by the RP is performed in an ATP-dependent manner using a set of ubiquitin receptors (van Nocker et al. 1996; Verma et al. 2004). Lys48 poly-ubiquitylated proteins were earliest found to be degraded by the 26S proteasome (Hough et al. 1986). Intriguingly, ubiquitylation alone is not sufficient to drive the final degradation by the 26S proteasome, but also requires binding of an unstructured region in the substrate to the RP (Peth et al. 2010; Collins and Goldberg 2017).

In addition, the 26S proteasome is regulated on both transcriptional and post-translational level, which affects the abundance, assembly and activity of the subunits (Marshall and Vierstra 2019). Last, the absolute abundance of proteasomes is tightly controlled and their degradation by selective autophagy upon proteasomal dysfunction or nutrient starvation has been described (Cuervo et al. 1995; Gao et al. 2010; Marshall et al. 2015). Roughly half of all 20S CPs are free of RPs in cells and ubiquitin-independent degradation of loosely folded polypeptides may co-exist with the highly regulated 26S proteasome (Sahu and Glickman 2021).

Proteasome function is required for cellular fitness and proper protein homeostasis. Remarkably, the proteasome was identified as a valuable target in cancer therapy and different proteasome inhibitors have been approved for therapy, for example Bortezomib (Jang 2018).

1.1.4 Autophagy

The other major catabolic pathway involved in the regulation of protein abundance is autophagy (Galluzzi et al. 2017; Yu et al. 2018). Autophagy degrades cytoplasmic material by engulfment into membrane compartments and fusion with lysosomes, which contain an enzymatic set for the hydrolysis of a variety of cargo. In contrast to the 26S proteasome, which produces short peptides, lysosomal proteases fully catabolize proteins into single amino acids (Neefjes et al. 2011; Settembre et al. 2013). Similar to the UPS, autophagy is tightly regulated and large number of autophagy-related (ATG) proteins has been identified (Galluzzi et al. 2017). Strikingly, efficient autophagic processes have been associated with ubiquitin-like conjugation systems (Noda and Inagaki 2015; Antonioli et al. 2017).

For example, receptors for macroautophagy contain a conserved LC3-interacting region (LIR) or ubiquitin-binding domains (UBDs), by which they bring both ubiquitylated and non-modified targets into close proximity of forming autophagosomes (Birgisdottir et al. 2013; Khaminets et al. 2016). In addition, accumulations of ubiquitylated proteins tend to aggregate and are recognized by autophagy receptors (Lim and Yue 2015; Moscat et al. 2016).

The functional outcomes of autophagy processes can be diverse. One of the first described observations was cell death after accumulation of phagosomes and autolysosomes (Schweichel and Merker 1973). This form of regulated cell death is driven by dysfunctions or intervention of autophagic processes (Galluzzi et al. 2015). A graphical summary of the first chapters is shown in figure 1.

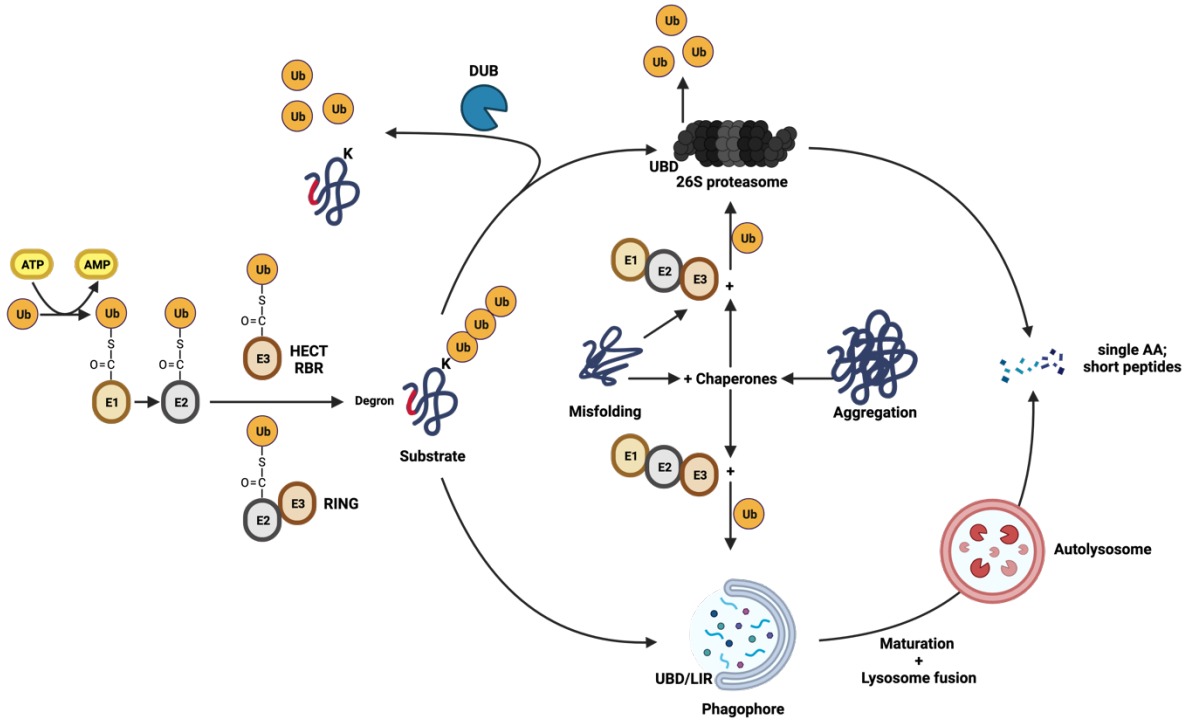

Figure 1: Overview on the two major protein degradation pathways.
Ubiquitin (Ub) is first transferred to the ubiquitin-activating enzyme E1 in an ATP-dependent manner. Ub is then transferred to the E2 conjugating enzyme and then covalently attached to lysine (K) residues on the substrate by E3 ubiquitin ligases. Really interesting new gene (RING) E3 ligases scaffold substrate and E2, while RING-between-RING (RBR) and homologous to the E6-associated protein carboxyl terminus (HECT) E3 ligases first bind ubiquitin and then transfer it onto the substrate. Substrates are recognized by specific degron sequences. Ubiquitylated substrates are targeted to the 26S proteasome and are recognized by ubiquitin binding domains (UBD), followed by ubiquitin release and substrate degradation. Deubiquitylating enzymes (DUB) can hydrolyze ubiquitin chains and stabilize their substrates. Ubiquitylated substrates can also be recognized by UBDs or LC3-interacting region (LIR) on forming phagophores and consequentially degraded by the autophagy pathway. Misfolded proteins and aggregates can be recognized by E3 ligases alone or with the help of molecular chaperones and be degraded by both the 26S proteasome and autophagy. Adapted from Marshall and Vierstra 2019 and Yu et al. 2018. Illustrations were created using the BioRender.com application

1.1.5 The ubiquitin code

As mentioned in the previous chapters, ubiquitylation is carried out by a complex cascade of enzymes, which can be summarized as ubiquitin writers. Ubiquitin readers comprise all proteins with ubiquitin-binding capacity and most of them contain conserved UBDs. In addition, E3 ubiquitin-ligases and deubiquitylating enzymes (DUB) are able to bind ubiquitin (Hu et al. 2002; Kamadurai et al. 2009). The latter form the class of ubiquitin erasers by catalyzing the hydrolysis of ubiquitin or polyubiquitin-chains (Clague et al. 2019).

Writers, readers and erasers together shape the proteome. In recent years, more of the functional relationships between ubiquitylation and its different functional outcomes have been uncovered, and by resembling a message-function relationship was therefore summarized as the ubiquitin code (Komander and Rape 2012; Oh et al. 2018).

Monoubiquitylation or polyubiquitin chains consisting of ubiquitin linked via the same Lys residue are classified as homotypic ubiquitylation and linkages using all seven Lys residues (Lys6, Lys11, Lys27, Lys29, Lys33, Lys48, Lys63) and the N-terminal amino group (M1) have been described (Peng et al. 2003; Xu et al. 2009). The canonical function of Lys48 linkages is to target proteins for proteasomal degradation, while Lys63 linkages have been found to play a role in cell signaling and DNA repair (Sobhian et al. 2007; Sims and Cohen 2009). The chain topology is recognized by ubiquitin readers with UBDs, which were found to exhibit high specificity for certain Lys-linkages (Dikic et al. 2009). For example, the proteasomal ubiquitin receptor S5a, which binds Lys11-, Lys48- and Lys63-linked, but not Lys6-linked polyubiquitin chains, with high affinity to target substrates for proteasomal degradation (Jin et al. 2008; Zhang et al. 2009).

Another level of complexity is added by heterotypic chains: mixtures of Lys-linkage types within one polyubiquitin-chain or the branching of chains at one ubiquitin moiety. In addition, conjugation of ubiquitin with ubiquitin-like modifiers (UBL) or PTMs can regulate the functional outcome (Ikeda and Dikic 2008; Dikic and Schulman 2022).

One of the most interesting PTMs of ubiquitin is the acetylation of its lysine residues. Acetylation has been found to interfere with or alter the formation of polyubiquitin chains and to reduce E3 ubiquitin-ligase autoubiquitylation, therefore significantly altering the ubiquitin code on a substrate (Ohtake et al. 2015; Kienle et al. 2022).

Further PTMs of ubiquitin and their functional outcomes were reviewed by Lei Song and Zhao-Qing Luo (Song and Luo 2019).
A myriad of functional outcomes can be achieved alone by the mechanisms described above. The final components regulating the ubiquitin code and therefore maintain the dynamic state of the cellular ubiquitome are the DUBs. They perform key roles in almost all cellular processes and, similar to ubiquitin readers, can possess specificity towards certain ubiquitin-chain topologies (Clague et al. 2019).
Imbalances caused by any component of this system can have detrimental effects on cellular fitness and the organism and be causative for severe pathologies like cancer. It will be interesting to see, whether the ubiquitin code can also be utilized for the specific alteration of cellular processes, for both research and medicine.

1.2 Cullin-RING E3 ubiquitin ligases (CRL)

The CRL system was first described at the end of the last millennium, where Cdc53, the yeast orthologue of Cullin 1 (CUL1), S-phase kinase-associated protein 1 (SKP1) with bound F-Box protein, and the E2 ubiquitin conjugating enzyme Cdc34 were shown to be required for the degradation of yeast cyclins (Schwob 1994; Bai et al. 1996; Willems et al. 1996). The field was first limited to research with a focus on yeast cell cycle regulation, however expanded rapidly after the identification of different F-box proteins, substrate receptors that bind SKP1 and their different functions (Li and Johnston 1997; Patton et al. 1998). These observations lead to the characterization of homologous systems also in higher eukaryotes, which now make up the CRL superfamily (Kipreos et al. 1996). An overview on the CRL family is shown in figure 2.

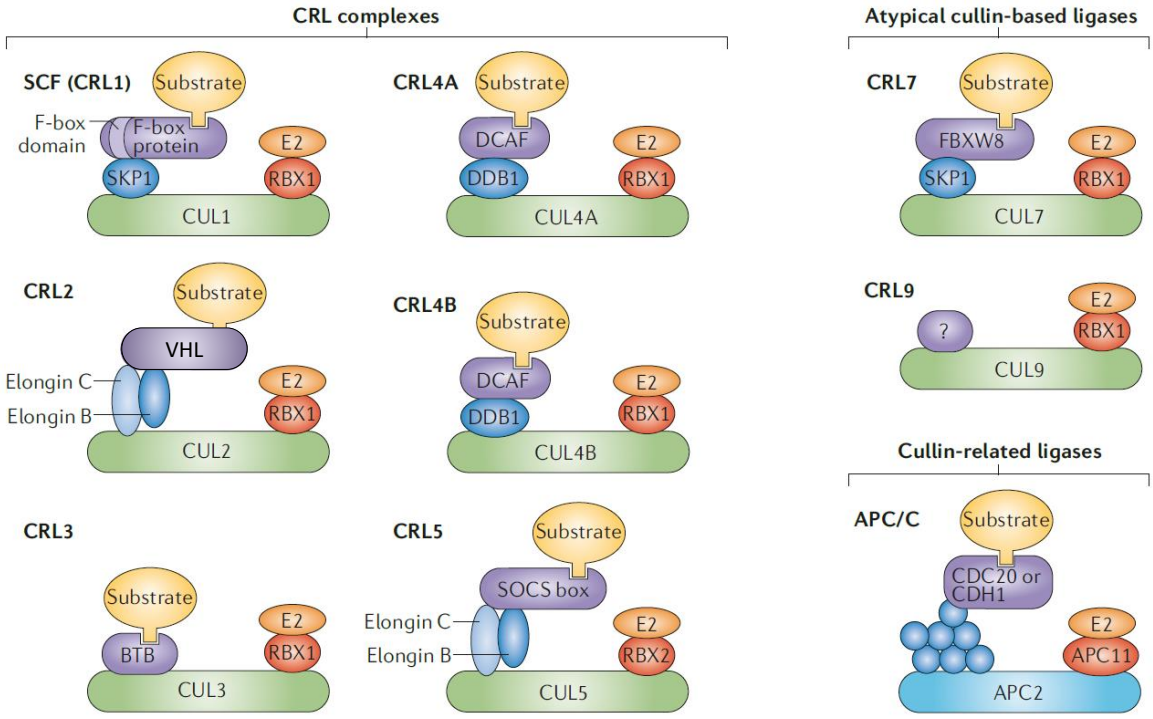

Figure 2: Cullin-RING ubiquitin ligase complexes (CRLs).
Cullin (CUL) proteins are the central scaffold of CRL complexes and bind to RING-box protein 1 (RBX1) or RBX2 with E3 ligase activity. CRL1, also known as S-phase kinase-associated protein 1 (SKP1)-CUL1-F-box protein (SCF) complex, binds SKP1 and F-box proteins as substrate adaptors and CRL2 and CRL5 bind elongins B and C to scaffold Von Hippel-Lindau (VHL) or suppressor of cytokine signaling (SOCS) box proteins, respectively. CUL3 uses Bric-a-brac/Tramtrack/Broad (BRB) substrate receptors. CRL4A and CRL4B bind DNA damage-binding protein 1 (DDB1) as adaptor for DDB1-CUL4-associated factor (DCAF) substrate receptors. CRL1-5 are considered canonical CRLs. CRL7 with SKP1 and F-box/WD40 repeat-containing protein 8 (FBXW8) as substrate receptor and the substrate receptor of CRL9 is not known. The anaphase-promoting complex/cyclosome (APC/C) E3 ligase complex is related to CRLs by its CUL-like APC2 subunit. Adapted from Skaar et al. 2013

Cullin proteins form the core scaffold of CRL complexes and interact directly with the catalytic subunit, the RING E3 ubiquitin ligases RING-box protein 1 (RBX1) or RBX2. CRLs are classified into six canonical CRLs with CUL1, CUL2, CUL3, CUL4A, CUL4B or CUL5 as backbone, while atypical CRLs contain CUL7 or CUL9. The multi-subunit E3 ubiquitin ligase APC/C is related the CRL family by the CUL-like APC2 subunit (Skaar et al. 2013). On the N-terminal region, CUL proteins bind to interchangeable substrate receptors (SR), either directly or indirectly through adaptor proteins. These SRs convey substrate specificity and are distinct for each CUL backbone: CUL1 interacts with SKP1 to recruit F-box protein SRs, CUL2 and CUL5 recruit Elongin B and C as adaptors to scaffold von Hippel-Lindau (VHL) proteins (to CUL2) or suppressor of cytokine signaling (SOCS)-box containing SRs (to CUL5), and CUL3 interacts with the Bric-a-brac/Tramtrack/Broad (BTB) SR. CUL4A and CUL4B bind to

the DNA damage-binding protein 1 (DDB1) adaptor to recruit DDB1-CUL4-associated factor (DCAF) SRs. (Skaar et al. 2013; Harper and Schulman 2021).

Both CRL activity and substrate specificity is tightly regulated by an intricate feedback-loop: Conjugation of the CUL winged-helix B (WHB) domain with the small UBL NEDD8 by an enzymatic cascade requiring E1, E2 and E3 enzymes, drives a conformational change which allows the recruitment of E2 ubiquitin conjugating enzymes and therefore activates the CRL (Lyapina et al. 2001; Cope et al. 2002; Duda et al. 2008; Scott et al. 2014; Bornstein et al. 2006; Baek et al. 2020).

During CRL activity, the COP9 signalosome deNEDDylase distinguishes between substrate-bound and substrate-free CRLs (Cavadini et al. 2016; Emberley et al. 2012; Enchev et al. 2012; Mosadeghi et al. 2016; Cope et al. 2002; Lyapina et al. 2001). CULs are only deNEDDylated when no substrate is bound to the SR, which increases in frequency as substrate levels decrease. In the next step, the Cullin-associated and neddylation-dissociated protein 1 (CAND1) binds unNEDDylated CRLs and catalyzes the exchange or removal of SRs, putting CRLs into standby-mode (Goldenberg et al. 2004; Pierce et al. 2013; Zheng et al. 2002a). CAND1 in turn is displaced from CRLs by NEDDylation (Liu et al. 2002). NEDDylation of CULs can be driven by binding of SRs loaded with substrates or by different signaling mechanisms (Chew and Hagen 2007; Fischer et al. 2011; Lydeard et al. 2013). As mentioned above, substrate recognition can be driven by intrinsic or acquired degrons. This principle also holds true for CLRs (Skaar et al. 2013). Given the plethora of substrates that are regulated by CRLs, dysregulation of their activity has been shown to cripple specific cellular functions and consequentially lead to the manifestation as diseases (Nguyen et al. 2017).

The modulation of CRL activity by small molecule drugs has therefore gained the interest of researchers and the pharmaceutical industry. The small molecule MLN4924 (pevonedistat) targets CRL activity by engaging with NAE1, the E1 for NEDDylation, which then catalyzes a stable NEDD8-MLN4924 adduct. This adduct blocks NAE1 activity and leads to global accumulation of CRL substrates (Soucy et al. 2009; Brownell et al. 2010; Petroski 2010). MLN4924 induced S-phase arrest and apoptosis of a human colon carcinoma cell line and is currently being evaluated in clinical trials (Soucy et al. 2009; Snow and Zeidner 2022).

Another group of small molecules which are of particular interest for CRLs are the molecular glues. Molecular glues contain multiple binding surfaces to artificially

facilitate protein-protein interactions and can therefore enable targeting of neo-substrates or re-establish dysfunctional SR-substrate binding, which can be for example caused by mutations of the substrates degron (Simonetta et al. 2019). In a third approach, small molecule inhibitors could be used to block the activity of CRLs with specific substrate receptors. Cell division control protein 4 (CDC4)-I2 is a specific allosteric inhibitor for the F-box protein CDC4 (Orlicky et al. 2010).

Most PROTACs utilize CRLs to target neo-substrates. The first developed PROTAC used the CRL1-F-box/WD repeat-containing protein 1A (FBXW1A/βTRCP) complex (Sakamoto et al. 2001). Later, also PROTACs utilizing CRL2-VHL and CRL4-CRBN have been characterized (Bondeson et al. 2015; Ito et al. 2010; Lu et al. 2014; Krönke et al. 2014; Matyskiela et al. 2016). It would be thrilling to see PROTACs being approved for future therapeutic use.

1.3 SKP1-CUL1-F-box protein (SCF) complexes

The best characterized subgroup of CRLs are the SKP1-CUL1-F-box protein (SCF) complexes (Feldman et al. 1997). Over 70 F-box proteins have been identified in humans, all of which have a conserved F-box domain that resembles a motif first found in Cyclin F (FBXO1) (Bai et al. 1996). In addition to their interaction with the adaptor protein SKP1, F-box proteins require a direct interaction with the CUL1 backbone (Zheng et al. 2002b).

F-box proteins are classified according to their substrate binding domain: FBXW with a WD40 domain, FBXL with a Leu-rich domain and FBXO with other domains (Jin et al. 2004). As mentioned in the previous chapter, SRs are interchangeable by CAND1-assisted release. Following the same principle, F-box proteins can be exchanged by CAND1 and therefore allow the targeting of a plethora of substrates (Skaar et al. 2013). In addition to the regulation of CRL activity by the NEDD8-COP9-CAND1 feedback relay, substrate recognition by the F-box proteins is the major rate-limiting step. A multitude of different modes of binding has been found for F-box proteins, including amongst others, the binding of unmodified degrons, phosphorylation-dependent degrons (phosphodegrons) and, vice-versa, inhibition of degron recognition by phosphorylation, or substrate binding which depends on compartmentation or subcellular localization (Abbas et al. 2013; D'Angiolella et al. 2010; D'Angiolella et al. 2012; Richter et al. 2020; Rossi et al. 2013; Welcker et al. 2003). In addition,

dimerization of F-box proteins was found to enhance the affinity for certain substrates (Hao et al. 2007; Welcker et al. 2013; Welcker et al. 2022).

F-box proteins are key regulators of the cell cycle, signaling and apoptosis and the perturbation of their function, for example by mutations of the F-box protein or the degron, amplification or deletion of the F-box protein or hijacking by microbial proteins, can be the basis for tumorigenesis and developmental diseases (Skaar et al. 2013).

There is an abundance of examples for F-box-mediated regulation of the cell cycle: FBXW5 targets epidermal growth factor receptor kinase substrate 8 (EPS8), spindle assembly abnormal protein 6 homolog (hSAS6) and mitotic centromere-associated kinesin (MCAK) to regulate mitotic progression, centriole duplication and ciliogenesis, respectively (Puklowski et al. 2011; Schweiggert et al. 2021; Werner et al. 2013). SCF-βTRCP targets the phosphatase CDC25A during S-phase in response to DNA damage and degrades the APC/C inhibitor early mitotic inhibitor 1 (EMI1) to allow progression beyond prometaphase (Busino et al. 2003; Margottin-Goguet et al. 2003). Further examples can be found in a recent review by Nana Zheng (Zheng et al. 2016).

Given their wide role in regulatory processes, it is not surprising that F-box proteins are also implicated in both, tumor suppression and oncogenic processes. FBXO1 targets centriolar coiled-coil protein of 110 kDa (CP110) for degradation to prevent centrosome amplification and degrades cell division cycle 6 (CDC6) to prevent DNA re-replication and therefore protects from genomic instability (D'Angiolella et al. 2010; Walter et al. 2016). Overexpression of SKP2 was found to promote the degradation of the cell cycle inhibitor p27 and to promote the development of T cell lymphoma when co-expressed with activated transforming protein N-Ras in mice (Latres et al. 2001). The tumor suppressor function of F-box/WD repeat-containing protein 7 (FBXW7) is well characterized and will be covered in section 1.4.3 (Yumimoto et al. 2020).

An example for viral hijacking is the herpesvirus-endoced protein vIRF-3, which binds to the F-box protein SKP2 to induce c-Myc expression and prevent its degradation (Baresova et al. 2012). Similarly, the adenovirus protein E1A specifically inhibits SCF-FBXW7 function by binding to CUL1 and RBX1 (Isobe et al. 2009).

1.4 F-box/WD repeat-containing protein 7 (FBXW7)

1.4.1 An introduction to FBXW7

The F-box protein cell division control protein 4 (CDC4) was first characterized in buddying yeast, where it mediates the degradation of the phosphorylated cyclin-

dependent kinase (CDK) inhibitor SIC1 and from there on emerged as an important cell cycle regulator (Feldman et al. 1997; Skowyra et al. 1997; Verma et al. 1997). The human orthologue FBXW7 is one of the most thoroughly characterized F-box proteins. The *FBXW7* gene produces three mRNAs coding for the three human FBXW7 isoforms (Spruck et al. 2002). Differing in their N-terminal exons that specify subcellular localization, all isoforms localize to specific compartments: FBXW7α localizes to the nucleus, FBXW7β to the cytoplasm and FBXW7γ is nucleolar. Overall, the FBXW7α isoform is more strongly expressed in many cell types (Spruck et al. 2002; Matsumoto et al. 2006). All isoforms share the WD40 domain, a β-sheet propeller that binds to phosphodegrons, the F-box domain for binding to SKP1 and a dimerization domain (D-domain) allowing FBXW7 dimerization, which promotes substrate degradation (Hao et al. 2007; Orlicky et al. 2003; Zhang and Koepp 2006; Welcker et al. 2013; Welcker et al. 2022).

Substrates of FBXW7 carry a conserved CDC4-phosphodegron motif, which allows for high affinity binding after phosphorylation by Ser or Thr protein kinases. These phosphorylations can be induced by different pathways to establish a tight regulation of FBXW7 activity. In most cases, glycogen synthase kinase 3 beta (GSK3β) phosphorylates Thr/Ser residues at position P0, which is followed by a Pro residue at P+1 and a negatively charged amino acid or another phosphorylated residue at P+4 (Nash et al. 2001; Hao et al. 2007; Welcker et al. 2013). Substrates of FBXW7 and their respective regulatory kinases were reviewed by Huiyin Lan (Lan and Sun 2021). FBXW7 binds to phosphorylated residues within degrons by an array of basic residues located within its WD40 domain (Orlicky et al. 2003; Hao et al. 2007). A recent publication by Neha Singh provided further insight into CDC4-phosphodegron sequence flexibility, showing that FBXW7 allows for some variety of residues within its target site (Singh et al. 2022).

An illustration of the SCF-FBXW7 complex and the FBXW7 domain architecture is shown in figure 3.

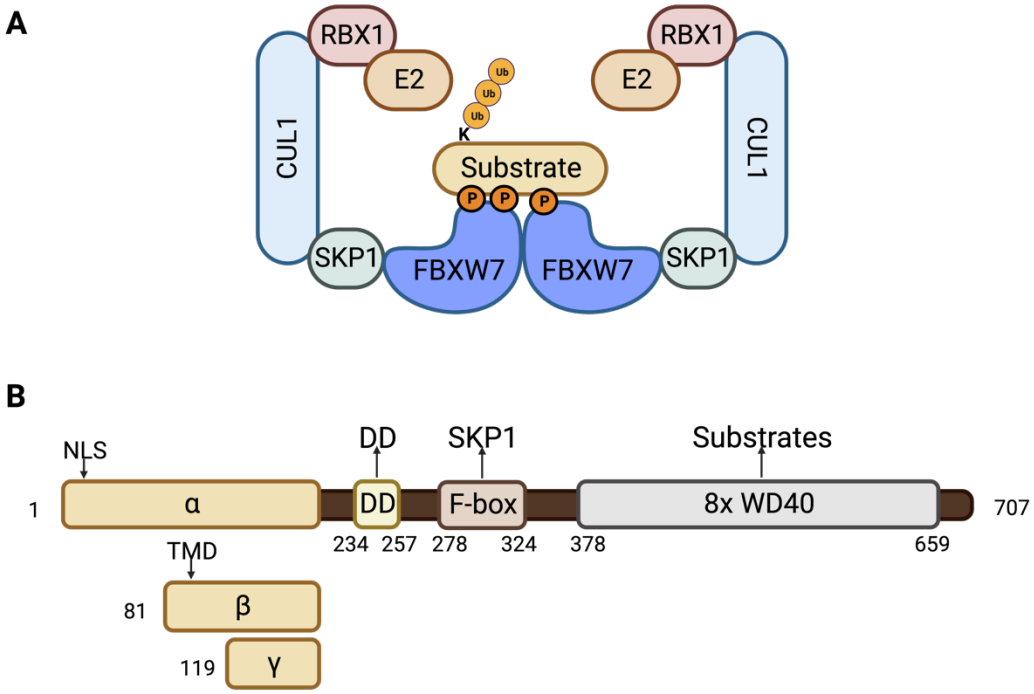

Figure 3: SCF-FBXW7 complex and FBXW7 domain architecture.
A CUL1 forms the central scaffold for binding the E3 ligase RING-box protein 1 (RBX1) and S-phase kinase-associated protein 1 (SKP1). F-box/WD40 repeat-containing protein 7 (FBXW7) is recruited to SKP1 via its F-box. FBXW7 dimerizes at the dimerization domain (DD) and binds phosphorylated (P) substrates to enable the transfer of ubiquitin (Ub) from the E2 conjugating enzyme. **B** FBXW7 is a 707 amino acid protein with three isoforms. The α-isoform contains a nuclear localization signal (NLS) and the β-isoform a transmembrane domain (TMD). Numbers denote the amino acids marking single domains. Adapted from Welcker and Clurman 2008 and Davis et al. 2014. Illustrations were created using the BioRender.com application

As mentioned in the previous chapter, F-box proteins fulfill important functions in the regulation of the cell cycle. Holding true also for FBXW7, one of the first identified substrates of SCF-FBXW7 was Cyclin E1 (Koepp et al. 2001; Moberg et al. 2001; Strohmaier et al. 2001). Cyclin E1 is an important cell cycle regulator and is required for the activity of CDK2 during S-phase (Sherr and Roberts 1999). Promoting autophosphorylation at Thr384 after GSK3β-mediated phosphorylation of Thr380, CDK2 activity creates a high-affinity CDC4-phosphodegron. Cyclin E1/CDK2 therefore regulates its own activity by recruiting FBXW7 (Won and Reed 1996; Welcker et al. 2003). An additional CDC4-phosphodegron is located at Thr62 (Welcker et al. 2003). More recently, the FBXW7 dimer was shown to engage with the Thr380 and Thr62 phosphodegrons simultaneously for increased avidity (Hao et al. 2007; Welcker et al. 2013). Therefore, FBXW7 regulates S-phase progression and prevents chromosomal instability (CIN) by ubiquitylating Cyclin E1 (Rajagopalan et al. 2004; Takada et al. 2017).

Similarly, FBXW7 controls the protein levels of the c-Myc proto-oncogene after Ras-dependent priming phosphorylation of Ser62 and GSK3β-mediated phosphorylation of Thr58 (Welcker et al. 2004; Yada et al. 2004). Recently, a second CDC4-phosphodegron was found at Thr244 and Thr248, which allows binding of an FBXW7-dimer and is required for efficient degradation of c-Myc (Welcker et al. 2022).

A big fraction of its targets are transcription factors and regulators of protein expression, for example neurogenic locus notch homolog protein 1 (NOTCH1) and the mediator of RNA polymerase II transcription subunits 13 (MED13) and MED13L (Hubbard et al. 1997; Davis et al. 2013). Recently, the SET-domain lysine methyltransferase 2D (KMT2D) was added to the collection. In particular, KMT2D degradation by FBXW7 alters histone methylation and therefore affects transcriptional signatures (Saffie et al. 2020). FBXW7 was also found to regulate the centriolar protein SAS6 and thereby controls centriole biogenesis (Badarudeen et al. 2020).

Being involved in apoptotic responses, Mcl-1 is one of the most interesting targets of FBXW7 but its exact role in FBXW7 regulation remains scarce (Kozopas et al. 1993; Inuzuka et al. 2011; Wertz et al. 2011). The relationship of Mcl-1 and FBXW7 will be further discussed in a later section.

Strikingly, the tumor suppressor p53 is Lys48 polyubiquitylated and degraded by FBXW7. GSK3β phosphorylates p53 Ser33 and DNA-dependent protein kinase (DNA-PK) or Ataxia telangiectasia mutated (ATM) kinase modify Ser37 in response to DNA damage by UV or radiation to suppress p53-dependent programs and to promote cell survival (Galindo-Moreno et al. 2019; Tripathi et al. 2019; Cui et al. 2020).

In addition to catalyzing Lys48 polyubiquitin chain formation, FBXW7 has been shown to perform Lys63 ubiquitylation of the non-homologous end joining (NHEJ) repair protein X-ray repair cross-complementing protein 4 (XRCC4) to facilitate DNA damage responses (Zhang et al. 2016a). This mechanism was later found to require the binding of FBXW7 to polyADP-ribose (PAR) via its WD40 domain, inducing its recruitment to DNA damage sites (Zhang et al. 2019). FBXW7-mediated Lys63 ubiquitylation of γ-catenin inhibits G2/M cell cycle transition to control cell proliferation (Li et al. 2018). These examples should serve to illustrate the importance of FBXW7-mediated ubiquitylation and an expanded list of substrates and their CDC4-phosphodegrons can be found in a recent review (Yumimoto and Nakayama 2020).

1.4.2 Regulation of FBXW7

It is not surprising that such an important player of key cellular functions is subject of tight regulation on multiple levels:

p53 has been shown to induce FBXW7 transcription in response to genotoxic stress, creating a feed-back loop. On the other hand, the transcription factor CCAAT-enhancer-binding protein δ (C/EBPδ) decreases FBXW7 expression (Kimura et al. 2003; Balamurugan et al. 2010).

A large number of microRNAs (miRNAs), for example miR-223, target the 3' untranslated region of the FBXW7 mRNA and thereby regulate mRNA stability and abundance (Yumimoto and Nakayama 2020).

As mentioned in the previous chapter, FBXW7 dimerization can enhance substrate degradation. Strikingly, dimerization deficient FBXW7 autoubiquitylates as a result of trans-ubiquitylation (Tang et al. 2007; Min et al. 2012; Welcker et al. 2013). The pseudo-substrate lysine-specific demethylase 1 (LSD1) prevents FBXW7 dimerization and leads to autoubiquitylation and degradation via the UPS and autophagy (Lan et al. 2019). Another regulator of FBXW7 complex assembly is the pseudophosphatase serine/threonine/tyrosine-interacting protein (STYX), which interacts with several F-box proteins, including FBXW7, and disables their recruitment into the SCF complex (Reiterer et al. 2017).

FBXW7 itself is subject to regulation by PTMs. Polo-like kinase 2 (PLK2) phosphorylates Ser176 on FBXW7, leading to its destabilization (Cizmecioglu et al. 2012). In contrast, phosphorylation of Ser227 by phosphoinositide 3-kinase (PI3K) inhibits autoubiquitylation and stabilizes FBXW7 levels (Mo et al. 2011; Schülein et al. 2011). Recently, it was shown by our group that the FBXO45-Myc-binding protein 2 (MYCBP2) complex ubiquitylates FBXW7 during mitosis to target it for proteasomal degradation (Richter et al. 2020). On the other hand, the DUB probable ubiquitin carboxyl-terminal hydrolase FAF-X (USP9X) antagonizes FBXW7 ubiquitylation, thereby increasing its protein stability (Khan et al. 2018).

By regulating FBXW7 abundance and function, the mentioned upstream regulations, amongst others, indirectly also affect FBXW7 substrate levels.

1.4.3 FBXW7 and cancer

FBXW7 was described as an important tumor suppressor, because it regulates many well-characterized oncogenes, including c-Myc, Cyclin E, Mcl-1 and NOTCH1 (Davis

et al. 2014). With over 3% mutation frequency, it is the most frequently mutated F-box protein found in human cancers (Yumimoto and Nakayama 2020). These mutations manifest as missense versions or cause a complete loss of FBXW7 expression. Strikingly, most mutations are found as heterozygous point mutations causing missense mutations of the three Arg residues, Arg465, Arg479, Arg505, which are required for the interaction with phosphodegrons of the substrate (Hao et al. 2007; Lan and Sun 2021). Cancers are hypothesized to select for this heterozygous FBXW7 ARG mutants, because FBXW7 ARG could have dominant negative effects by forming dimers with FBXW7 wild-type (WT) (Welcker and Clurman 2008; Davis et al. 2014).

FBXW7 mutations are found most frequently in T-cell acute lymphoblastic leukemia (T-ALL) and precursor T-cell lymphoblastic lymphoma (T-LBL) with 16.9% and 15.6%, respectively, adding up to over 30% for hematologic malignancies. In addition, over 20% of colorectal carcinomas carry FBXW7 mutations, making it one of the most frequently mutated genes in this cancer type (Yumimoto and Nakayama 2020).

Where FBXW7 is not mutated, alterations of its substrates are often observed, and mutations accumulate in the CDC4-phosphogedron. For example, 10% of NOTCH mutations in T-ALL affect PRO2514 in the phosphodegron (Bonn et al. 2013; Callens et al. 2012). In diffuse large B-cell lymphoma (DLBCL), c-Myc is frequently mutated and 43% of these mutations affect the phosphodegron (Yumimoto and Nakayama 2020).

FBXW7 is hypothesized to play a role in tumor initiation and clinical prognosis of many cancer types (Yeh et al. 2018). Cyclin E1 was identified as a driver of chromosomal instability almost 20 years ago and is thought to be a main mediator of tumorigenesis (Rajagopalan et al. 2004). Serving as a backup through mediating the G1 tetraploidy-checkpoint, p53-dependent cell cycle arrest was found to protect against Cyclin E1 deregulation and in line with this, mice co-depleted of FBXW7 and p53 developed highly invasive adenocarcinomas (Grim et al. 2012; Minella et al. 2002). Further examples of the clinical significance of FBXW7 substrates were recently reviewed by Jinyi Fan (Fan et al. 2022).

Furthermore, deregulation of FBXW7 does not only promote tumorigenesis but was also found to be involved in chemotherapy resistance against multiple approved cancer therapeutics, for example antimicrotubule drugs or tyrosine-kinase inhibitors (Yumimoto and Nakayama 2020; Fan et al. 2022).

Most frequently, upregulation of the antiapoptotic protein Mcl-1 by FBXW7 deficiency is correlated to therapy resistance. Generally, Mcl-1 is a widely accepted pro-survival protein of the B-cell lymphoma protein 2 (BCL-2) family and FBXW7 deficiency confers resistance towards Taxol and vincristine by upregulation of Mcl-1 protein levels (Inuzuka et al. 2011; Wertz et al. 2011; Gasca et al. 2016; Sloss et al. 2016; Wang et al. 2021b). The role of Mcl-1 in mitotic slippage will be further discussed in section 1.5.3. Strikingly, Mcl-1 inhibition was shown to restore the sensitivity of FBXW7-mutated cancers (Inuzuka et al. 2011; Tong et al. 2017; Song et al. 2020).
In addition, the FBXW7 substrates PLK1, Aurora kinase A and Cyclin E1 were also implied in FBXW7-dependent therapy resistance (Finkin et al. 2008; Gasca et al. 2016). SRY-box transcription factor 9 (SOX9) is degraded by FBXW7 in response to DNA damage and its overexpression mediates resistance against Cisplatin and UV-irradiation (Hong et al. 2016).
One possibility to restore the drug-sensitivity of cancers with FBXW7 deregulation is to promote FBXW7 expression or to prevent its degradation. For example, the drug decitabine inhibits hypermethylation of the FBXW7 promoter and consequentially increases FBXW7 protein abundance (Gu et al. 2008; Akhoondi et al. 2010; DiNardo et al. 2018). On the other hand, PLK1 inhibition stabilizes FBXW7 (Wang et al. 2021a). Since the E3 ligase complex FBXO45/MycBP2 specifically targets FBXW7 during mitosis, the combination of antimicrotubule drugs with intervention of FBXO45/MYCBP2 activity was proposed to promote mitotic cell death (Richter et al. 2020).
The intervention of FBXW7-mutated cancers can be facilitated by targeting its downstream effectors. Therefore, the identification of relevant substrates and pathways will support the development of targeted or combinational therapies (Fan et al. 2022).

1.5 Mitotic slippage

1.5.1 The mitotic cell cycle

The growth and division of cells follows a circular process, which can be divided into distinct phases. An overview of the cell cycle with particular focus on the steps involved in mitosis is shown in figure 4.

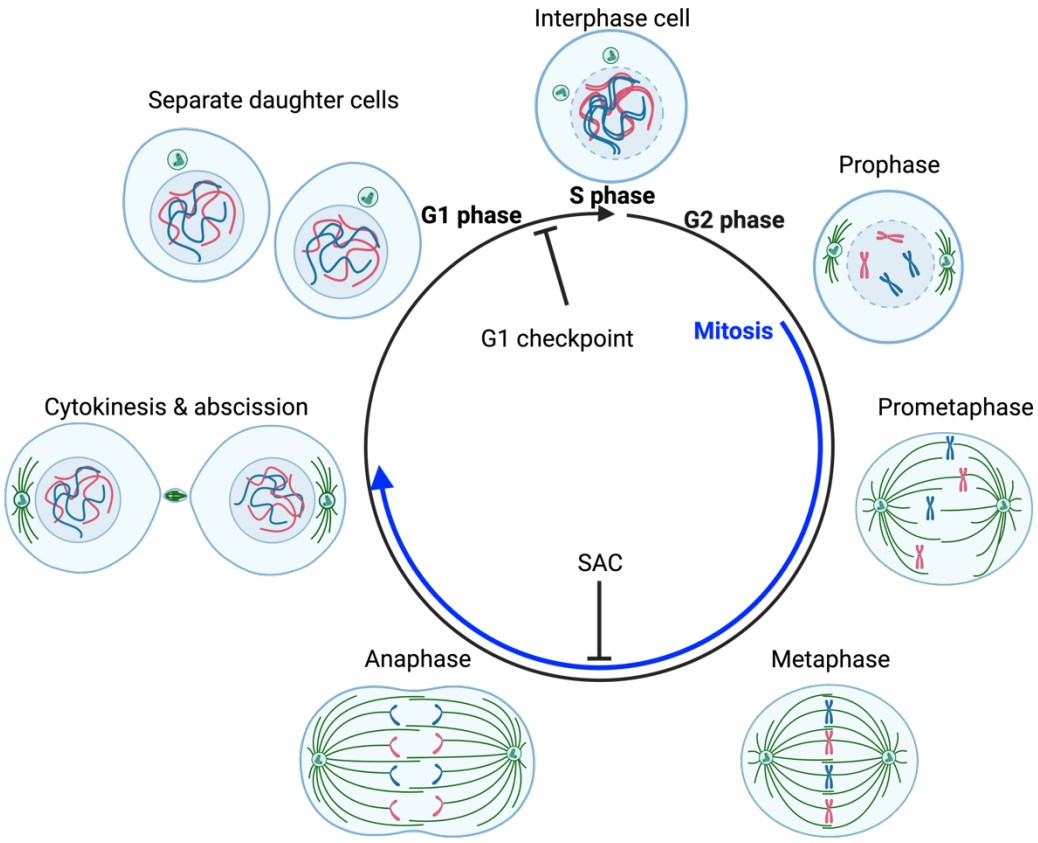

Figure 4: The mitotic cell division cycle.
Eukaryotic cells grow and replicate their genome during interphase and express proteins required for mitotic cell division in G2 phase. Mitotic entry starts with condensation of chromosomes and nuclear envelope breakdown in prophase, followed by the formation of the mitotic spindle apparatus and attachment of microtubules to kinetochores in prometaphase. Pulling forces align chromosomes in the metaphase plane before sister chromatids are pulled apart towards the cell poles in anaphase. During cytokinesis, two separate cells start to form around the separated genomic content, which separate their cell membranes in abscission. The G1 checkpoint serves as a surveillance point for DNA damage and mitotic defects and prevents progression through G1 phase. The spindle-assembly-checkpoint is activated upon defects in microtubule-kinetochore attachments in prometaphase or incomplete chromosome alignment and prevents progression to anaphase. Adapted from Matthews et al. 2022. Illustrations were created using the BioRender.com application

Generally, the cell division cycle consists of two major parts: The interphase with the duplication of cellular content and mitosis, the segregation of cellular content. Both phases are further divided into smaller steps, which are based on the distinct processes taking place. Especially Cyclin-CDK complexes and cell-cycle regulated transcription were shown to play a major part in coordinating these events and their activity is tightly controlled in an oscillatory fashion (Fisher 2012; Simmons Kovacs et al. 2008). As mentioned in previous chapters, also the UPS system plays a pivotal role (Teixeira and Reed 2013).

During the G1 phase of interphase, which takes place after cell division, cells grow and synthesize proteins required for S-phase. In S-phase, the genomic material is replicated and the microtubule-organizing center, the centrosome, is duplicated.

Interphase ends with the G2 phase, where more proteins are synthesized to prepare for cell division in mitosis. Mitosis was termed by Flemming in the 1880s and has since evolved to be one of the most complex cellular processes (Flemming 1882).

Mitosis begins with prophase, when DNA condenses to chromatin and individual chromosomes become visible. Cyclin B-CDK1 is a key regulatory kinase of mitotic commitment, and its activity is required throughout mitosis. CDK1 phosphorylates and activates CDC25, which in turn dephosphorylates and activates CDK1, serving as a self-amplifying molecular switch for mitotic entry by widespread phosphorylation of CDK1 substrates (Hoffmann et al. 1993; Dephoure et al. 2008; Blethrow et al. 2008). In addition, the mitotic kinases PLK1 and Aurora kinases A and B are activated to phosphorylate further mitotic substrates (Joukov and Nicolo 2018; Kettenbach et al. 2011).

These events lead to the condensation of chromosomes, nuclear envelope breakdown and activation of the APC/C E3 ligase complex (Fujimitsu et al. 2016; Zhang et al. 2016b). The two centrosomes then nucleate microtubules to form bilateral attachments with kinetochores located on each sister chromatid in prometaphase (Foley and Kapoor 2013; Hara and Fukagawa 2018). Chemo-mechanical processes result in the chromosomes to align in the division plane in metaphase and the degradation of Cyclin B1 by APC/C-CDC20 in parallel to dephosphorylation programs push cells towards mitotic exit. Sister chromatids are separated by pulling of the mitotic spindle towards the cell poles in anaphase. If microtubules fail to attach to the kinetochores or the chromosomes fail to align in the division plane, the spindle-assembly checkpoint (SAC) is activated, which inhibits Cyclin B1 degradation by blocking APC/C-CDC20 activity. Mitosis continues when the SAC is released after correcting all errors. After formation of the actomyosin contractile ring, the two daughter cells separate during abscission and enter the next interphase as separate entities (McIntosh 2016). In G1 phase, p53-dependent programs can arrest cell-cycle progression in response to DNA damage, mitotic errors or tetraploidy, and allow for DNA repair or the initiation of irreversible cell cycle exit and senescence (Andreassen et al. 2001; Huang and Zhou 2020; Janssen and Medema 2013; Margolis et al. 2003; Scully et al. 2019).

1.5.2 Mitotic slippage

As mentioned in the previous chapter, errors in kinetochore attachment or chromosome alignment lead to sustained activation of the SAC until defects are

resolved. Mechanistically, the kinase monopolar spindle 1 (MPS1) marks unattached kinetochores, which is promoted by Cyclin B1-CDK1 and Aurora kinase B. MPS1 phosphorylates kinetochore proteins to recruit budding uninhibited by benzimidazole 1 (BUB1)-BUB3 complexes followed by BUBR1-BUB3 heterodimers and mitotic arrest deficient 1 (MAD1)-MAD2 complex (Ji et al. 2015; Hiruma et al. 2015). The final mitotic checkpoint complex (MCC) consisting of MAD2, BUBR1 and BUB3 binds the APC/C substrate receptor CDC20 to inhibit APC/C-dependent degradation of Cyclin B1 and Securin, and therefore prevents progression towards anaphase (Fraschini et al. 2001; Hardwick et al. 2000; Sudakin et al. 2001). Once microtubule attachment and chromosome alignment are ensured, MCC assembly is stopped, and different pathways lead to the disassembly of the SAC and the release of CDC20 to activate the APC/C. The SAC antagonist p31-comet and the ATPase thyroid hormone receptor-interacting protein 13 (TRIP13) extract MAD2 from the MCC and, catalyzing a conformational change, inhibit it from entering new MCC complexes (Ma and Poon 2018). The SAC and its regulation by CDK1 were recently reviewed (Hayward et al. 2019).

Antimicrotubule drugs, such as taxanes or vinca-alkaloids, act directly on spindle microtubules and hinder their dynamics during mitosis, thereby inducing sustained activation of the SAC and prolonged mitotic arrest followed by apoptosis (Jordan and Wilson 2004). Cancer cells were found to escape this prolonged mitotic arrest and enter the next G1 phase without undergoing cytokinesis, a chemoresistance process termed mitotic slippage (Roberts et al. 1990; Rieder and Maiato 2004; Sudo et al. 2004). Mitotic arrest and mitotic cell fates are illustrated in figure 5.

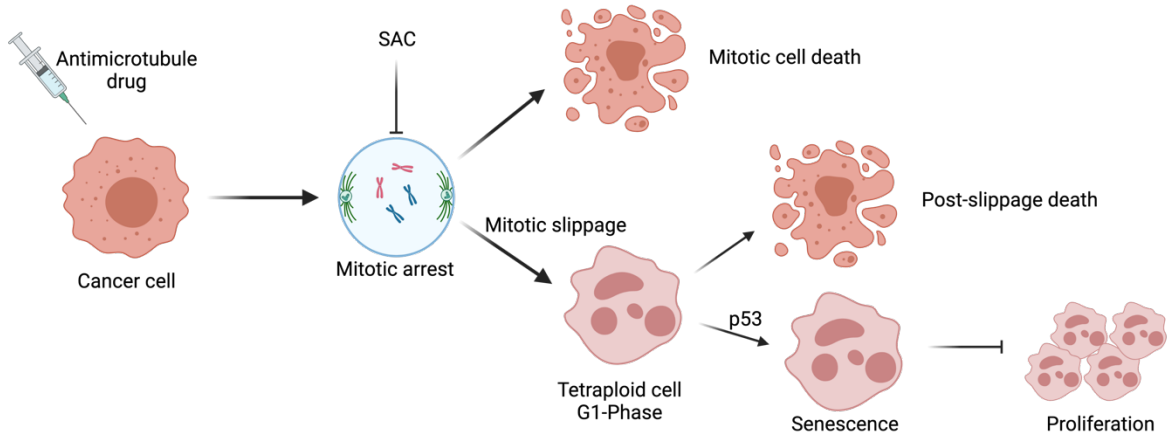

Figure 5: Cancer cells undergo mitotic slippage or death in mitosis in response to antimicrotubule drugs.
Treatment of cancers with antimicrotubule drugs leads to prolonged mitotic arrest by sustained activation of the spindle-assembly-checkpoint (SAC). Eventually, cancer cells either undergo mitotic cell death (apoptosis) or exit from mitosis without undergoing cytokinesis (mitotic slippage). The post-slippage resulting tetraploid cells enter the next cell cycle and undergo growth arrest or apoptosis through the p53-dependent G1 checkpoint. Depending, amongst others, on their p53 mutation status, cancer cells can escape from this growth arrest and continue to proliferate as genetically instable cells. Adapted from Cheng and Crasta 2017. Illustrations were created using the BioRender.com application.

The “competing networks-threshold” model describes a possible approach to explain a cells tendency to undergo mitotic slippage or mitotic cell death. Being required for the sustenance of the mitotic state, Cyclin B1 protein levels determine the commitment towards mitotic exit. Strikingly, Cyclin B1 levels were found to gradually decrease during prolonged mitotic arrest induced by antimicrotubule drugs (Balachandran et al. 2016; Brito and Rieder 2006). On the other hand, pro-apoptotic caspase activation induces apoptosis after passing a certain threshold (Díaz-Martínez et al. 2014; Gascoigne and Taylor 2008). Cells slipping from mitosis enter the next G1 phase with a tetraploid genomic content and often have accumulated DNA damage. As mentioned in the previous chapter, this activates a p53-dependent cell cycle arrest at the G1 checkpoint and further to senescence and cell death (Andreassen et al. 2001; Qian and Chen 2013; Vogel et al. 2004; Zhu et al. 2014). However, as p53 and related pathways are mutational hotspots in cancer, many cell types were found to escape from this arrest and to continue cycling into the next S-phase (Vogel et al. 2004; Welburn et al. 2010).

Cancer cells employ different mechanisms to escape from SAC induced arrest. For example, the SAC antagonists p31-comet and TRIP13 are upregulated in many cancers and their overexpression can overcome SAC-induced arrest in response to

antimicrotubule drugs (Habu and Matsumoto 2013; Lok et al. 2020; Ma et al. 2012; Ma and Poon 2016; Zeng et al. 2019). Although mutations of SAC components are rare in cancer, alteration of their gene expression is more common. Strikingly, cancer cells require a functional SAC, possibly to cope with chromosomal instability and to prevent mitotic catastrophe (Bailey et al. 2015b; Kwiatkowski et al. 2010; Matthews et al. 2022; Stolz et al. 2009). Further mechanisms are unraveled continuously, which will allow the development of targeted therapies for chemoresistant cancers.

For example, the induction of mitotic catastrophe by MPS1 or Aurora kinase B-inhibitors is a therapeutic mechanism currently under investigation in pre-clinical and clinical settings (Borah and Reddy 2021; Schulze et al. 2020). Small molecules and mitotic inhibitors for the treatment of antimicrotubule drug-resistant cancers were recently reviewed (Liu et al. 2019).

1.5.3 FBXW7 and mitotic slippage

FBXW7-deficiency promotes mitotic slippage and its overexpression increases the rate of mitotic cell death in response to treatment with antimicrotubule drugs (Finkin et al. 2008; Richter et al. 2020). Being upregulated by FBXW7 deficiency, Cyclin E1 and Aurora kinase A were the first substrates shown to be involved in the development of drug-induced polyploidy after treatment with the spindle poisons Taxol and vinblastine. FBXW7-deficient colorectal carcinoma cells lack induction of p27 at the G1 checkpoint and perform efficient endoreduplication, thereby promoting CIN and as a result high therapy resistance (Finkin et al. 2008; Lukow et al. 2021; Cheng and Crasta 2017). Different substrates of FBXW7 have since then been assessed for their role in mitotic slippage.

The targeting and degradation of Mcl-1 by FBXW7 was described as a novel pathway in the regulation of cellular apoptosis. Mcl-1 upregulation by FBXW7-deficiency promotes resistance towards different cancer therapeutics, including the BCL-2 inhibitor ABT-737 and antimicrotubule drugs (Inuzuka et al. 2011; Wertz et al. 2011; Sloss et al. 2016). Strikingly, the latter is mediated by an increased rate of mitotic slippage due to Mcl-1 deregulation (Wertz et al. 2011). Mcl-1 was therefore considered to sponge the apoptotic response induced by prolonged mitotic arrest and to serve as a timer in the “competing-networks threshold” model. However, more recent research questioned the FBXW7-dependent degradation of Mcl-1 during prolonged mitotic arrest by showing that Mcl-1 is rather degraded by the APC/C (Sloss et al. 2016; Allan

et al. 2018). Therefore, the role of Mcl-1 in mitotic slippage of FBXW7-deficient cancers is unclear.

Cyclin E1 was one of the first characterized substrates of FBXW7 and its oncogenic function was observed early on (Rajagopalan et al. 2004; Strohmaier et al. 2001). Causing chromosomal instability through deregulation of key mitotic players like the APC/C, centrosome-associated protein A (CENP-A) or CDC25, it is thought to be a key player in FBXW7-dependent tumorigenesis (Bagheri-Yarmand et al. 2010; Keck et al. 2007; Lau et al. 2013; Takada et al. 2017). Overexpression of Cyclin E1 alone is insufficient to promote drug-induced polyploidy but the deregulation of a low molecular weight isoform was suggested to promote mitotic slippage (Finkin et al. 2008; Bagheri-Yarmand et al. 2010). However, this was not experimentally proven.

c-Myc is a major determinant of mitotic cell fate: In contrast to Mcl-1, its overexpression results in increased sensitivity to antimitotic agents by upregulation of proapoptotic factors (Topham et al. 2015). The transcription factor forkhead box protein M1 (FOXM1) is a substrate of FBXW7 and FOXM1 upregulation represses BCL-2 modifying factor (BMF) expression and consequentially a reduction of cell death in mitosis (Vaz et al. 2021). However, this research only focused on FOXM1 alone and a connection to FBXW7-deficiency would be required.

Since FBXW7-deficiency deregulates a plethora of substrates and cellular mechanisms, the modulation of mitotic slippage is most likely the result of a multivalent process that integrates the effects of multiple substrates and a number of pathways. Therefore, the assessment of different FBXW7 substrates in mitotic slippage could help to combat this chemoresistance mechanism.

1.6 BIR repeat-containing ubiquitin-conjugating enzyme (BRUCE)

Inhibitors of apoptosis proteins (IAPs) are a family of proteins that are involved in the regulation of programmed cell death. IAPs can bind to caspases and other proapoptotic factors through Baculovirus IAP repeat domains (BIR) and thereby block their activity (Bartke et al. 2004; Goyal 2001; Verhagen et al. 2001). Many cancer types highly express different IAPs to prevent apoptosis, which promotes carcinogenesis and therapy resistance (Ghobrial et al. 2005). BIR repeat-containing ubiquitin-conjugating enzyme (BRUCE, BIRC6) is a giant 528 kDa and highly conserved IAP (Hauser et al. 1998).

It contains a single N-terminal BIR domain, which is responsible for caspase binding. BRUCE binds and inhibits several caspases and proapoptotic proteins, including caspases 3, 7 and 9, the serine protease high temperature requirement protein A2 (HtrA2) and DIABLO (Bartke et al. 2004; Hao et al. 2004). Interestingly, a ubiquitin-conjugating domain (UBC) that acts as E2/E3 chimera was found at the BRUCE C-terminus, enabling BRUCE to ubiquitylate its interaction partners, for example DIABLO and the IAP Survivin (Pohl 2008; Bartke et al. 2004). BRUCE interacts with and degrades p53 in hepatocellular carcinoma, thereby preventing apoptosis and promoting tumor growth (Tang et al. 2015). Reciprocally, BRUCE depletion leads to stabilization of p53 and subsequent growth arrest and activation of proapoptotic caspase pathways (Lopergolo et al. 2009). Multiple cancer cell lines express high levels of BRUCE and are resistant to apoptosis-inducing agents (Chen et al. 1999; Chu et al. 2008; Dong et al. 2013). To date, NRDP1 is the only known E3 ligase to mediate BRUCE degradation, thereby triggering apoptosis (Qiu et al. 2004).
BRUCE localizes to the midbody during cytokinesis as a central player in abscission and its depletion causes variable failures in cytokinesis. Intriguingly, ubiquitin is localized to the midbody during cytokinesis and BRUCE depletion perturbs these ubiquitin dynamics (Pohl and Jentsch 2008).

1.7 WD repeat-containing protein 5 (WDR5)

WD repeat-containing protein 5 (WDR5) is a highly conserved protein, which has been linked to a plethora of cellular processes. Its most thoroughly characterized function is as a core scaffolding component of histone H3 lysine 4 methyltransferase complexes (Miller et al. 2001). Therefore, WDR5 is required for the modification of histones and contributes to the regulation of gene expression (Wysocka et al. 2005).
Strikingly, WDR5 acts as a core scaffold in many protein complexes and facilitates interactions via conserved domains: WIN-binding motifs (WBM) on its partners interact with the WDR5 WIN-site, and, reciprocally, the WDR5 WBM site binds to other WIN-site containing proteins (Dias et al. 2014; Odho et al. 2010; Patel et al. 2008a). The WDR5 protein structure and the KMT2 methyltransferase complex are shown in figure 6.

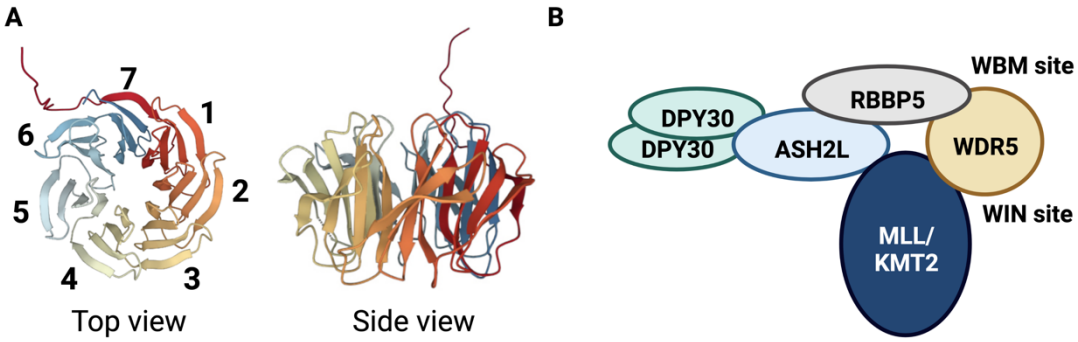

Figure 6: WDR5 structure and KMT2 methyltransferase complex.
A WDR5 consists of an unstructured N-terminal domain and seven WD40 repeats as indicated in the cartoon structure (Tian et al. 2020). **B** WDR5 acts as core scaffold of KMT2 methyltransferase complexes. WDR5 binds to mixed lineage leukemia (MLL)/KMT2 methyltransferases through its WIN site and to retinoblastoma-binding protein 5 (RBBP5) through its WIN-binding motif (WBM) site. Protein dpy-30 homolog (DPY30) and ASH2-like protein (ASH2L) are further subunits. Adapted from Guarnaccia, 2018.

WDR5 also exhibits non-canonical functions. For example it localized to the mitotic spindle and WIN-site mutation induces mitotic defects (Ali et al. 2014). One of its functions is to recruit protein complexes to microtubules which play key roles in mitotic integrity, for example KMT2A or KAT8 regulatory NSL complex subunit 1 (KANSL1) (Ali et al. 2014; Meunier et al. 2015; Orpinell et al. 2010). WDR5 localizes to the midbody to regulate abscission and its depletion increases the incidence of multinucleated cells (Bailey et al. 2015a). Another function of WDR5 is to regulate the localization of the kinesin-like protein KIF2A during mitosis to facilitate proper spindle assembly (Ali et al. 2017). In addition, it recruits the APC/C to histones during mitosis to modulate gene expression via histone ubiquitylation (Oh et al. 2020).

Being involved in a multitude of complexes, it is not surprising that WDR5 could be connected to tumorigenesis and its deregulation mediates pro-proliferative effects, chemoresistance and high levels of WDR5 expression correlate with poor patient survival (Chen et al. 2015; Dai et al. 2020; Gao et al. 2020; Neilsen et al. 2018). More functions of WDR5 were reviewed by Alissa duPuy Guarnaccia (Guarnaccia and Tansey 2018).

Small molecule inhibitors blocking WDR5's scaffolding function and PROTACS targeting WDR5 protein abundance are being developed as potential cancer therapeutics, showing promising preliminary results. It would be thrilling to see small molecules targeting WDR5 to be approved for treatment (Chacón Simon et al. 2020; Grebien et al. 2015; Tian et al. 2020; Yu et al. 2021).

1.8 Objectives

FBXW7 is a F-box protein and substrate receptor of the CRL1 E3 ubiquitin ligase complex (Feldman et al. 1997). It is considered a tumor suppressor, because it regulates the abundance of many oncogenes (Davis et al. 2014). FBXW7 is frequently mutated in cancer and FBXW7-deficiency has been linked to chemoresistance against multiple anticancer agents (Yumimoto and Nakayama 2020; Fan et al. 2022). Especially, FBXW7-deficiency promotes mitotic slippage in response to treatment with antimicrotubule drugs which ultimately leads to the emergence of drug-induced polyploidy (Finkin et al. 2008; Wertz et al. 2011; Richter et al. 2020). Different substrates of FBXW7 have been implicated as mediators of mitotic slippage, however the role of Mcl-1 in the induction of slippage of FBXW7-deficient cancers is a matter of debate (Sloss et al. 2016; Allan et al. 2018; Topham et al. 2015; Vaz et al. 2021).

Therefore, the identification and understanding of the players involved in this process and their respective downstream mechanisms will provide valuable insight in how to find vulnerabilities to combat FBXW7-mediated chemoresistance.

In the presented thesis, I utilized an immunoprecipitation-proteomics approach to specifically identify novel substrates of FBXW7, which are targeted during prolonged mitotic arrest induced by the microtubule destabilizing drug nocodazole. In order to validate hits from the screen, I performed immunoprecipitation experiments to confirm a specific interaction of putative substrates with the WD40 substrate binding domain of FBXW7.

In addition, I depleted candidate substrates from U2OS cells using RNA interference and assessed their influence on mitotic cell fate by live-cell imaging in the presence of nocodazole.

Overexpressing proteins in immortalized human cell lines and cancer cell lines, I aimed to assess their relationship with FBXW7 and FBXW7-mediated degradation via the ubiquitin-proteasome pathway. Finally, I depleted target proteins from FBXW7-deficient colorectal carcinoma cells to investigate their influence on the generation of drug-induced polyploidy and tried to identify the underlying mechanism.

2. Materials and Methods

2.1 Materials

2.1.1 Chemicals and reagents

Chemicals and reagents used in the presented thesis are summarized in table 1.

Table 1: List of chemicals and reagents

β-Mercaptoethanol	Sigma-Aldrich
0.05% Trypsin-EDTA	Thermo Fisher Scientific
1 kb DNA ladder	Thermo Fisher Scientific
100 bp DNA ladder	Thermo Fisher Scientific
Acetic acid	Sigma-Aldrich
Agarose	VWR
Ammonium peroxodisulfate (APS)	Carl Roth
Ampicillin	AppliChem
Apigenin	J&K Scientific
Aprotinin	Roche
Bicine	Carl-Roth
Bio-Rad Protein Assay	Bio-Rad
BIS-TRIS	Sigma-Aldrich
Bovine Serum Albumin (BSA)	Sigma-Aldrich
Bromophenol blue	Sigma-Aldrich
CHIR-99021	MedChemExpress
Coomassie Brilliant Blue G250	Carl Roth
Cycloheximide	Santa Cruz Biotechnology
Dimethylsulfoxide (DMSO)	Sigma-Aldrich
Dithiothreitol (DTT)	Carl Roth
DNA polymerase DeepVent	New England Biolabs
DNA polymerase GoTaq MasterMix	Promega
Doxycycline	Sigma-Aldrich
DPBS, no Calcium no Magnesium	Thermo Fisher Scientific
Dulbecco's Modified Eagle's Medium (DMEM)	Sigma-Aldrich
	Thermo Fisher Scientific
Ethanol	Sigma-Aldrich
Ethylenediaminetetraacetic acid (EDTA)	Carl Roth
Fetal bovine serum (FBS)	Thermo Fisher Scientific
Flag M2 affinity gel, 3xFlag peptide	Thermo Fisher Scientific
GFP-trap agarose	I. Hoffmann, DKFZ
Glutathione, reduced	Sigma-Aldrich
Glycerol	Thermo Fisher Scientific

Glycine	Carl Roth
Hydrochloric acid	VWR
Hygromycin B	Carl Roth
Immobilized reduced glutathione CL-4B Sepharose	Sigma-Aldrich
IPTG	Biomol
Isopropanol	VWR
Kanamycin	AppliChem
LB-Agar, LB-medium	Carl Roth
LDS Sample Buffer 4x	Thermo Fisher Scientific
Leupeptin	Roche
Lipofectamine 2000 and RNAiMax	Thermo Fisher Scientific
Lysozyme	Carl Roth
Magnesium chloride	Merck
Methanol	Sigma-Aldrich
MG132 (Z-Leu-Leu-Leu-al)	Sigma-Aldrich
Milk powder	Gerbu
MLN4924	Cell Signaling Technology
N-ethylmaleimide (NEM)	Sigma-Aldrich
N,N,N‘,N‘-Tetramethylethylenediamine (TEMED)	Carl Roth
Nocodazole	Merck
Nonidet NP40 (Igepal)	MP Biochemicals
Nuclease-free water	Dharmacon
OptiMEM	Thermo Fisher Scientific
Penicillin-Streptomycin	Sigma-Aldrich
Phenol/Chloroform/Isomylalcohol	Carl Roth
PIN	Roche
Polyethylenimine linear 25000 Da	Polysciences
Ponceau S solution	Serva
Primers	Sigma-Aldrich
Propidium iodide	Sigma-Aldrich
Protein A/G Sepharose	GE Healthcare
Protein ladder PageRuler prestained	Thermo Fisher Scientific
Restriction enzymes	New England Biolabs
RNAse	AppliChem
Rotiphorese Gel 30 acrylamide/bisacrylamide 37.5:1	Carl Roth
RPMI 1640	Sigma-Aldrich
Sodium azide	Merck
Sodium chloride	Sigma-Aldirch
Sodium dodecyl sulfate (SDS)	Carl Roth
Sodium fluoride	Merck

Sodium hydroxide	J.T. Baker
Sodium vanadate	Sigma-Aldrich
StainIN RED Nucleic Acid Stain	Highqu
T4 DNA ligase	Thermo Fisher Scientific
Taxol	Merck
Thymidine	Santa Cruz Biotechnology
TLCK (1-Chloro-3-tosylamido-7-amino-2-butanon)	Roche
TPCK (1-Chloro-3-tosylamido-7-amino-2-heptanon)	Roche
Tricine	Carl-Roth
TRIS base	Serva
	Sigma-Aldrich
Triton X-100	Sigma-Aldrich
TRIZOL	Thermo Fisher Scientific
Tween 20	Sigma-Aldrich
Western Chemiluminescence HRP-substrate	Merck

2.1.2 Laboratory equipment

Laboratory equipment used in the presented thesis is listed in table 2.

Table 2: Laboratory equipment

Cell counting chamber	Neubauer Improved	Brand
Cell culture incubator	C200	Labotect
Centrifuges	5415 R	Eppendorf
	5810 R	Eppendorf
	RC5C	Sorvall
Cull culture dishes	Cellstar	Greiner Bio-One
DNA gel electrophoresis	Wie Mini-Sub Cell	Bio-Rad
Electrotransfer unit	Mini Trans-Blot Cell	Bio-Rad
	Transblot Turbo	Bio-Rad
Filter paper		Whatman
Flow cytometer	FACSCalibur	BD
Fluorescence microscope	Cell Observer Z1	Zeiss
Freezer (-20°C)	Premium	Liebherr
Freezer (-80°C)	Ultralow	Sanyo
Fridge (4°C)	ProfiLine	Liebherr
Gel documentation	Gelstick	Intas
Glassware	Glass pipettes, measuring cylinders, flasks, bottles	Brand, Schott
Heat block	Thermomixer Compact	Eppendorf

Incubation shaker	Minitron	Infors HT
Light microscope	Eclipse TS100	Nikon
Live-cell imaging dish	x-well cell culture chamber	Sarstedt
Luminescent image analyzer	ImageQuant LAS 4000	GE Healthcare
Magnet stirrers	Ikamag RTC	IKA Labortechnik
Microplate absorbance reader	SPECTROstar Nano	BGM Labtech
Microwave		Sharp
Nitrocellulose membrane	Amersham Protran 0.45 µM	GE Healthcare
PAGE system	Mini Protean III	Bio-Rad
Parafilm	Parafilm M	New England Biolabs
PCR thermocycler	Mastercycler Nexus GX2	Eppendorf
pH-meter	Seven Easy	Mettler Toledo
Pipettes	Pipetman	Gilson
Pipettor	Pipetboy	Integra
Plasticware	Reaction tubes, falcon tubes, pipette tips, PCR tubes, petri dishes	Eppendorf, Nerbe, Falcon, Biozym, Greiner Bio-One, TPP
Power supply	PowerPac 200	Bio-Rad
Rocking platform shaker	Rocker 25	Labnet
Rotating wheel	Test tube rotator	Snijders
Shaking incubator	Minitron	Infors AG
Sonifier	Sonifier 250	Branson
Sterile Workbench	Safe2020	Thermo Fisher Scientific
Vortex shaker	VF2	IKA Labortechnik
Water bath	12B	Julabo EM
	WNB7	Memmert

2.1.3 Buffers and media

Buffers and media used in the presented thesis are listed in table 3.

Table 3: Buffers and media

4x Laemmli buffer	0.1M Tris-HCl pH 6.8
	4% SDS
	20% glycerol
	0.1 M DTT
	0.02% bromophenol blue
Bacteria lysis buffer	50 mM Tris-HCl pH 8.5 (WDR5) or pH 7.4 (Myc)
	300 mM NaCl

	0.1% NP40
	5% Glycerol
	5 mM EDTA
	1 mg/mL lysozyme
	Added before use:
	5 mM β-Mercaptoethanol
	10 µg/mL TPCK
	5 µg/mL TLCK
	0.1 mM Na_3VO_4
	1 µg/mL Aprotinin
	1 µg/mL Leupeptin
	10 µg/mL Trypsin inhibitor from soybean
Column washing buffer	Bacteria lysis buffer without lysozyme
Elution buffer	Bacteria lysis buffer without lysozyme
	10 mM reduced glutathione
In-vitro ubiquitylation assay buffer	50 mM Tris-HCl pH 7.5
	100 mM NaCl
	10 mM $MgCl_2$
	0.05% CHAPS
	Added before use:
	1 mM DTT
	0.1 mM Na_3VO_4
	1 µg/mL Aprotinin
	1 µg/mL Leupeptin
	10 µg/mL Trypsin inhibitor from soybean
NP40 lysis buffer	40 mM Tris-HCl pH 7.5
	150 mM NaCl
	5 mM EDTA
	10 mM β-glycerophosphate
	5 mM NaF
	0.5% NP40
	Added before use:
	1 mM DTT
	10 µg/mL TPCK
	5 µg/mL TLCK
	0.1 mM Na_3VO_4
	1 µg/mL Aprotinin
	1 µg/mL Leupeptin
	10 µg/mL Trypsin inhibitor from soybean
PBS	137 mM NaCl

	2.7 mM KCl
	1.8 mM KH_2PO_4
	10 mM Na_2HPO_4
	pH 7.4
PBST	0.1% Tween-20 in PBS
RIPA lysis buffer	50 mM Tris-HCl pH 7.4
	1% NP40
	0.5% Na-deoxycholate
	0.1% SDS
	150 mM NaCl
	2 mM EDTA
	50 mM NaF
	Added before use:
	1 mM DTT
	10 µg/mL TPCK
	5 µg/mL TLCK
	0.1 mM Na_3VO_4
	1 µg/mL Aprotinin
	1 µg/mL Leupeptin
	10 µg/mL Trypsin inhibitor from soybean
SDS running buffer	190 mM glycine
	25 mM Tris-HCl, pH 8.3
	0.1% SDS
TAE buffer	40 mM Tris-HCl pH 7.6
	20 mM acetic acid
	1 mM EDTA
TBS	50 mM Tris-HCl pH 7.4
	150 mM NaCl
Tris-Bicine gel transfer buffer	25 mM Bis-Tris pH 7.2
	25 mM bicine
	1 mM EDTA
	20% methanol
Tris-Tricine gel running buffer	50 mM Tris-HCl pH 8.2
	50 mM tricine
	0.1% SDS
Western blot blocking buffer	5% milk powder in PBST
Wet transfer buffer	25 mM Tris
	192 mM glycine
	20% methanol

2.1.4 Antibodies

2.1.4.1 Primary antibodies

Primary antibodies used in the presented thesis are summarized in table 4.

Table 4: Primary antibodies

Target protein	origin	Dilution WB	clone	source
α-Tubulin	mouse	1:5000	B-5-1-2	Sigma-Aldrich
Actin	mouse	1:5000	JLA21	Calbiochem
BIRC6/BRUCE	rabbit	1:10000	19609	Abcam
c-Myc	rabbit	1:1000	9402	Cell Signaling
Cyclin E1	mouse	1:1000	HE12	Santa Cruz
FBXW7α	rabbit	1:5000	A301-720A	Bethyl
Flag	mouse	1:5000	M2 (F3165)	Sigma-Aldrich
FYCO1	mouse	1:1000	A01	Abnova
GFP	rabbit	1:1000		I. Hoffmann, DKFZ
GSK3β	mouse	1:1000	E11	Santa Cruz
GST	rabbit	1:1000	Z-5	Santa Cruz
H3 pS10	rabbit	1:1000	06-570	Merck
HA-tag	mouse	1:1000	16B12	Babco
hSETD1A	rabbit	1:1000	A300-374A	Bethyl
KMT2D	rabbit	1:1000	A300-BL1185	Bethyl
Mcl-1	rabbit	1:1000	4572	Cell Signaling
MLL1	rabbit	1:1000	A300-289A	Bethyl
Myc (tag)	mouse	1:500	9E10	Santa Cruz
PLK1	mouse	1:1000	F-8	Santa Cruz
RBBP5	rabbit	1:1000	A300-109A	Bethyl
Ubiquitin	mouse	1:1000	P4D1	Santa Cruz
Vinculin	mouse	1:5000	hVIN-1	Sigma-Aldrich
WDR5	mouse	1:200 - 1:1000	G9	Santa Cruz

2.1.4.2 Secondary antibodies

Secondary antibodies used in the presented thesis are listed in table 5.

Table 5: Secondary antibodies

Target protein	origin	dilution	source
Mouse IgG	goat	1:5000	Novus
Rabbit IgG	donkey	1:5000	Jackson Laboratories

2.1.5 Small interfering RNAs (siRNAs)

Small interfering RNAs (siRNAs) used in the presented thesis are listed in table 6.

Table 6: Small interfering RNAs

siRNA name	Sequence sense (5'-3')	Published in
siGl2	CGUACGCGGAAUACUUCGAdTdT	
siFBXW7	ACAGGACAGUGUUUACAAAdTdT	(Busino et al. 2012)
siCyclin E1 #1	CCTCCAAAGTTGCACCAGTTTdTdT	(Takada et al. 2017)
siCyclin E1 #2	UGACUUACAUGAAGUGCUAdTdT	(Hänle-Kreidler et al. 2022)
siWDR5 #1	UUAGCAGUCACUCUUCCACUUdTdT	(Ali et al. 2014)
siWDR5 #2	GCUCAGAGGAUAACCUUGUdTdT	(Chen et al. 2015)
siBRUCE	GCAGUACAUGGUAUGAUUAdTdT	(Lopergolo et al. 2009)
siKMT2D	CCCACCUGAAUCAUCACCUdTdT	(Yang et al. 2020)
siGSK3β #1	GAAGUCAGCUAUACAGACAdTdT	(Hänle-Kreidler et al. 2022)
siGSK3β #2	GGUCACGUUUGGAAAGAAUdTdT	(Weikel et al. 2016)

2.1.6 Primers

Primers that were used in the presented thesis are listed in table 7.

Table 7: Primers

Primer name	Sequence (5'-3')	No.
FBXW7_A	GCATGAATTCGATGAATCAGGAACTGCTC	1
FBXW7_D	GCATAAGCTTTCACTTCATGTCCACATC	2
FBXW7_R465H_f	TACTTCCACTGTGCATTGTATGCATCTTCA	3
FBXW7_R465H_r	TGAAGATGCATACAATGCACAGTGGAAGTA	4
FBXW7_R479Q_f	AGCGGTTCTCAAGATGCCACT	5
FBXW7_R479Q_r	AACAACTCTTTTTTCATGAAGATGC	6
FBXW7_R505C_f	TGTTGCAGCAGTCTGCTGTGTTCAATATGA	7
FBXW7_R505C_r	TCATATTGAACACAGCAGACTGCTGCAACA	8
FBXW7_S462A/T463V/S465A_F	GTGGCCTGTATGCATCTTCATGAAAAAAG	9
FBXW7_S462A/T463V/S465A_R	AACGGCAGTATGCCCATATAAGGTG	10
WDR5_A	GTGAACCGTCAGATCCGCTAGCGATTAC	11
WDR5_D	GCTGATCAGCGAGCCGATCGAGTGA	12
WDR5_F133A_f	CACAGTAATTATGTCGCTTGCTGCAACTTCAAT	13
WDR5_F133A_r	ATTGAAGTTGCAGCAAGCGACATAATTACTGTG	14
WDR5_f_HindIII	AGCTAAGCTTATGGCGACGGAGGAGAAGAAG	15
WDR5_r_XhoI_resist O2	AGCTCTCGAGTCAACAATCGGATTTCCAAAGTTTAATTGTTTTGTCATTTTCTAGCGC	16
WDR5_T18A_f	AGCACAGCCAGCCCCTTCGTCA	17

WDR5_T18A_r	ATGACGAAGGGGCTGGCTGTGCT	18
WDR5_S54A_f	CTCCGTGAAATTCGCCCCGAATGGAGAGT	19
WDR5_S54A_r	ACTCTCCATTCGGGGCGAATTTCACGGAG	20
WDR5_qPCR_f	ATGCGACAGAGACCATCATAG	21
WDR5_qPCR_r	CGTGAGGATATGGGATGTGAA	22
GAPDH_qPCR_f	CAAGGCTGAGAACGGGAAG	23
GAPDH_qPCR_r	TGAAGACGCCAGTGGACTC	24
WDR5 delta 1-42_f	GAATTCGATATCAAGCTTGGCCACACCAAAGCAGTG	25
WDR5 delta 1-42_r	CACTGCTTTGGTGTGGCCAAGCTTGATATCGAATTC	26
WDR5 delta WD1_f	CTAAAGTTCACCCTTGCTATATCTGGTCACAAGCTG	27
WDR5 delta WD1_r	CAGCTTGTGACCAGATATAGCAAGGGTGAACTTTAG	28
WDR5 delta WD2_f	GGAAATTTGAGAAAACCATATCTGGACACAGTAATTATGTC	29
WDR5 delta WD2_r	GACATAATTACTGTGTCCAGATATGGTTTTCTCAAATTTCC	30
WDR5 delta WD3_f	CTGAAAACCCTGAAGGGAGCTCACTCGGATCCAGTC	31
WDR5 delta WD3_r	GACTGGATCCGAGTGAGCTCCCTTCAGGGTTTTCAG	32
WDR5 delta WD4_f	TGCCTCAAGACTTTGCCACTCATCGATGACGACAAC	33
WDR5 delta WD4_r	GTTGTCGTCATCGATGAGTGGCAAAGTCTTGAGGCA	34
WDR5 delta WD5_f	CTGAAGACGCTCATCGATGGCCACAAGAATGAGAAATAC	35
WDR5 delta WD5_r	GTATTTCTCATTCTTGTGGCCATCGATGAGCGTCTTCAG	36
WDR5 delta WD6_f	AAGACGTACACTGGCCACCTACAAGGCCACACAGATG	37
WDR5 delta WD6_r	CATCTGTGTGGCCTTGTAGGTGGCCAGTGTACGTCTT	38
WDR5 delta WD7_f	GAGATTGTACAGAAACTACAATAAGCGGCCGCTCGAGG	39
WDR5 delta WD7_r	CCTCGAGCGGCCGCTTATTGTAGTTTCTGTACAATCTC	40

2.1.7 Plasmids

Plasmids that were provided or generated in the presented thesis are listed in table 8.

Table 8: Plasmids

Plasmid name	Source	Primers	Enzymes
pcDNA3-Myc3-Cul1	Addgene #19896		
pCDNA3.1(+)-HA-CSNK2B	I. Hoffmann, DKFZ Heidelberg		
pcDNA5-2xFlag-2xHA-2xTEV-KMT2D	L. Busino, Philadelphia		
pcDNA5-2xFlag-2xHA-2xTEV-KMT2D_1-1323	L. Busino, Philadelphia		
pcDNA5-FRT-TO	Invitrogen		
pcDNA5-FRT-TO_WDR5	This work	13, 14	HindIII, XhoI
pcDNA5-FRT-TO_WDR5_F133A	This work	13-16	HindIII, XhoI

pCI-Flag-mBRUCE	Stefan Jentsch, Max-Planck-Institute for Biochemistry, Munich		
pCMV-3Tag1A-WDR5	I. Hoffmann, DKFZ		
pCMV-3Tag1C	Agilent Technologies		
pCMV-3Tag1C-FBXW7	I. Hoffmann, DKFZ, Heidelberg		
pCMV-3Tag1C-FBXW7_deltaFbox (284-321)	I. Hoffmann, DKFZ, Heidelberg		
pCMV-3Tag1C-FBXW7_R465H, R479Q, R505C	This work	1-8	EcoRI, HindIII
pCMV-3Tag1C-FBXW7_S462A, T463V, R465A	This work	9, 10	
pCMV-3Tag2A	Agilent Technologies		
pCMV-3Tag2A-CSNK2A1	I. Hoffmann, DKFZ Heidelberg		
pCMV-3Tag2A-CSNK2A2	I. Hoffmann, DKFZ Heidelberg		
pCMV-Tag5A-Myc-GSK3b	Addgene #16260		
pEGFP-C1	Clontech		
pEGFP-C1-FBXW7	I. Hoffmann, DKFZ		
pEGFP-C1-FBXW7_deltaFbox (284-321)	This work		EcoRI, ApaI
pEGFP-C1-FBXW7_R465H, R479Q, R505C	This work		EcoRI, ApaI
pEGFP-C2	Clontech		
pEGFP-C2-WDR5	This work		EcoRI, ApaI
pEGFP-C2-WDR5_F133A	This work	11-14	EcoRI, ApaI
pEGFP-C2-WDR5_S54A	This work	11, 12, 19, 20	EcoRI, ApaI
pEGFP-C2-WDR5_T18A	This work	11, 12, 17, 18	EcoRI, ApaI
pGEX-4T1	GE Healthcare		
pGEX-4T1-c-Myc	This work		BamHI, XhoI
pGEX-4T1-WDR5	This work		EcoRI, XhoI
pOG44	Invitrogen		
pPK-CMV-HA-UbiquitinC	F. Rösl, DKFZ Heidelberg		
pCMV-3Tag1A-WDR5 Δ1-42	This work	11, 12, 25, 26	HindIII, XhoI
pCMV-3Tag1A-WDR5 Δ43-82	This work	11, 12, 27, 28	HindIII, XhoI
pCMV-3Tag1A-WDR5 Δ83-126	This work	11, 12, 29, 30	HindIII, XhoI
pCMV-3Tag1A-WDR5 Δ128-168	This work	11, 12, 31, 32	HindIII, XhoI
pCMV-3Tag1A-WDR5 Δ169-208	This work	11, 12, 33, 34	HindIII, XhoI
pCMV-3Tag1A-WDR5 Δ212-253	This work	11, 12, 35, 36	HindIII, XhoI
pCMV-3Tag1A-WDR5 Δ256-296	This work	11, 12, 37, 38	HindIII, XhoI
pCMV-3Tag1A-WDR5 Δ299-333	This work	11, 12, 39, 40	HindIII, XhoI

2.1.8 Bacterial strains

Bacterial strains listed in table 9 were used for cloning and amplification of plasmid-DNA or for the production of recombinant proteins in the presented thesis.

Table 9: Bacterial strains

Strain	Genotype	Source
E. coli XL1-Blue	*recA1 endA1 gyrA96 thi-1 hsdR17 supE44 relA1 lac* [F' *proAB lacI*^{q}ZΔ*M15* Tn*10* (Tet^{r})]	Agilent Technologies
E. coli Top10 One Shot	F-*mcrA* Δ(*mrr-hsd*RMS-*mcr*BC) Φ80*Lac*ZΔM15 Δ *Lac*X74 *rec*A1 *ara*D139 Δ(*araleu*) 7697 *gal*U *gal*K *rps*L (StrR) *end*A1 *nup*G	ThermoFisher Scientific
E. coli DH5α MAX Efficiency	F^{-} Φ80*lac*ZΔM15 Δ(*lac*ZYA-*arg*F) U169 *rec*A1 *end*A1 *hsd*R17 (rk^{-}, mk^{+}) *pho*A *sup*E44 λ^{-} *thi*$^{-}$1 *gyr*A96 *rel*A1	ThermoFisher Scientific
E. coli Rosetta (DE3)	F^{-}*ompT hsDS*$_{B}$($r_B^{-}m_B^{-}$) *gal dcm* (DE3= pRARE2 (Cam^{R})	Merck

2.1.9 Cell lines

Cell lines listed in table 10 were used in the presented thesis.

Table 10: Cell lines

Name	Characteristics	Source
HCT116 FBXW7 $^{+/+}$	Human colorectal carcinoma cells	B. Vogelstein, Baltimore, USA
HCT116 FBXW7 $^{-/-}$		B. Vogelstein, Baltimore, USA
HeLa	Human epithelial cervix adenocarcinoma cells containing the HPV-18 sequence	ATCC
HEK293T	Human epithelial embryonic kidney cells expressing the SV-40 large T-antigen	DSMZ
U2OS	Human osteosarcoma cells	ATCC
DLD1 FBXW7 $^{+/+}$	Human colorectal adenocarcinoma cell line	B. Vogelstein, Baltimore, USA
DLD1 FBXW7 $^{-/-}$		B. Vogelstein, Baltimore, USA
U2OS T-Rex WDR5	Stable U2OS cell line expressing WDR5 homogenously after doxycycline addition	This work

U2OS T-Rex WDR5 F133A	Stable U2OS cell line expressing WDR5 F133A homogenously after doxycycline addition	This work
U2OS tet-Off Cyclin E1	Stable U2OS cell line expressing Cyclin E1 homogenously after doxycycline withdrawal	J. Bartek, Stockholm, Sweden

2.1.10 Kits

Commercially available kits listed in table 11 were used in the presented thesis.

Table 11: Kits

Kit name	Source
GenElute HP Plasmid Miniprep Kit	Sigma-Aldrich
GenElute HP Plasmid Midiprep Kit	Sigma-Aldrich
GenElute HP Plasmid Maxiprep Kit	Sigma-Aldrich
NucleoSpin Gel and PCR Clean-up Kit	Machery-Nagel
DNAse I Kit	Sigma-Aldrich
RevertAid First Strand cDNA Synthesis Kit	Thermo Fisher Scientific
*Power*SYBR Green PCR Master Mix	Thermo Fisher Scientific
Lamba Protein phosphatase	New England Biolabs

2.1.11 Antibiotics

Antibiotics listed in table 12 were used in the presented thesis.

Table 12: Antibiotics

Antibiotic	Stock concentration	Working concentration
Ampicillin	100 mg/mL	100 µg/mL
Kanamycin	50 mg/mL	50 µg/mL
Doxycycline	2 mg/mL	2 µg/mL
Hygromycin B	50 mg/mL	400 - 1000 µg/mL

2.2 Methods

2.2.1 Methods in molecular biology

2.2.1.1 Polymerase chain reaction (PCR) and site-directed mutagenesis

DNA sequences were amplified for cloning or site-directed mutagenesis using polymerase chain reaction (PCR). For subcloning, primers containing restriction sites were used upstream and downstream of the gene of interest to enable sticky-end ligations into the target backbone. For site-directed mutagenesis, homologous primers containing the desired mutation were designed additionally and the protocol from Heckman was followed (Heckman and Pease 2007). Briefly, two separate PCR reactions were performed with the forward and antisense mutagenesis and the reverse and sense mutagenesis primers. The products were used as templates for an overlapping PCR using only forward and reverse cloning primers.

PCR set-ups using two different systems are shown below:

10x ThermoPol Reaction buffer (NEB)	1x
Template DNA	50-200 ng
Forward primer	1.5 µM
Reverse primer	1.5 µM
dNTP mix	0.75 mM
DMSO	0.5%
DeepVent polymerase (NEB)	1 U
ddH_2O	ad 50 µL

GoTaq G2 Hotstart Green Master Mix (Promega)	1x
Template DNA	50-200 ng
Forward primer	1.5 µM
Reverse primer	1.5 µM
ddH_2O	ad 50 µL

Both polymerases

DeepVent polymerase was used as default tool, whereas GoTaq was used for high GC rich sequences and primers.

PCR reactions were performed in a thermocycler (Eppendorf) with following settings:

Initial denaturation	95°C, 5 min
Denaturation	95°C, 45 s
Annealing	44-72°C, 45 s
Elongation	72°C, 1 min/kb
Final elongation	72°C, 5 min
Cooling	4°C

The annealing temperature was predicted and set for each primer pair and the length of elongation was adjusted to the length of the amplicon. PCR products were analyzed by agarose gel electrophoresis and purified using NucleoSpin Gel and PCR Clean-up (Machery-Nagel).

2.2.1.2 Agarose gel electrophoresis

Nucleic acids were separated by agarose gel electrophoresis according to size. 0.7-2% agarose was boiled in 1x TAE buffer, supplemented with 0.05% StainIN RED Nucleic Acid Stain, and poured into a gel chamber. After polymerization, the gel was placed into an electrophoresis chamber (Bio-Rad) and covered with 1x TAE buffer. DNA samples were mixed with 6x DNA sample buffer and loaded to the wells of the gel. 1 kb or 100 bp DNA ladders were used as size references. Electrophoresis was carried out at 80-100V for 30-60 min. DNA was visualized under UV light at 366 nm wavelength.

2.2.1.3 Extraction of DNA fragments from agarose gels

Desired DNA fragments were cut from agarose gels under UV light at 366 nm wavelength and transferred to a reaction tube. DNA extraction was performed with the NucleoSpin Gel and PCR Clean-up Kit (Machery-Nagel) following the manufacturer's instructions. DNA was eluted with 20-30 µL ddH_2O and the DNA concentration determined according to section 2.2.1.8.

2.2.1.4 Restriction digest of DNA

Plasmid DNA and purified PCR products were digested with different pairs of restriction enzymes (NEB) for subcloning of inserts or mutant versions into target backbones via sticky ends. For fragments generated by PCR, the total product was digested. For

plasmids, 1-10 µg of DNA were used. All reactions were performed in a total volume of 20-30 µL with 1 µL of each restriction enzyme. Digests were incubated at 37°C for 2 h and inactivated at 65°C for 10 min. Digestion products were separated by agarose gel electrophoresis and the correct products extracted as described in 2.2.1.2 and 2.2.1.3.

2.2.1.5 Ligation of DNA fragments

Purified digestion products were combined by DNA ligation. 200 ng of linearized backbone were combined with a threefold molar amount of the insert or, in case of low yields, with the maximal available amount. Ligations were performed in 20 µL with 1x T4 DNA ligase buffer and 1 U of T4 DNA ligase (Thermo). Reactions were incubated at RT for 1-2 h and inactivated at 65°C for 10 min. Competent *E. coli* strains were transformed with half of the ligations as described in 2.2.1.6.

2.2.1.6 Transformation of chemically competent *E. coli*

For cloning and plasmid amplification, chemically competent *E. coli* XL1-Blue/Top10/DH5α were transformed with ligations or plasmid DNA. *E. coli* Rosetta (DE3) were transformed for the production of recombinant proteins. 200 ng of plasmid DNA or 10 µL of ligation reactions were mixed with 60-80 µL of competent bacteria and incubated on ice for 20 min, followed by heat-shock at 42°C for 45 sec. The bacteria were allowed to recover on ice for 2 min and then diluted with 800 µL pre-warmed LB medium and incubated at 37°C for 1 h with shaking at 600 rpm. For cloning, the bacteria were pelleted at 10000 g for 1 min and the pellet resuspended in 100 µL of the supernatant. The bacteria were spread on a LB agar plate containing the appropriate antibiotic. For plasmid amplification, 100 µL of the suspension were spread without prior pelleting. The LB agar plate was incubated at 37°C overnight and single colonies were used for downstream applications, such as plasmid DNA preparation or protein expression screening.

2.2.1.7 Isolation of plasmid DNA from *E. coli*

5 mL (Miniprep), 200 mL (Midiprep) or 400 mL (Maxiprep) cultures of *E. coli* XL1-Blue/Top10/DH5α containing plasmid DNA were prepared in LB medium with the appropriate antibiotic and incubated at 37°C overnight with constant shaking at 180 rpm. The bacteria were pelleted at 3200 g for 10 min and the plasmid DNA isolated

using GenElute HP Plasmid Mini/Midi/Maxiprep Kits (Sigma-Aldrich) according to the manufacturer's instructions. Final elutions were performed with ddH_2O and the DNA concentration determined as described in 2.2.1.8. Plasmid DNA from cloning was sequenced at LGC Genomics.

2.2.1.8 Determination of DNA and RNA concentration

DNA concentration and purity of plasmid DNA and DNA fragments, as well as the concentration of RNA extracts, were determined with a NanoDrop ND-1000 spectrophotometer (Thermo Fisher Scientific). ddH_2O was used as a blank and the optical density of the sample at 230, 260 and 280 nm wavelength determined. The specific extinction coefficient at 260 nm is 50 l/(mol*cm) for DNA and 40 for RNA. Ratios of OD_{260}/OD_{230} >1.8 and OD_{260}/OD_{280} >2.2 indicate that the DNA/RNA solution is of high purity.

2.2.1.9 Quantitative real-time PCR (qPCR)

Quantitative real-time PCR (qPCR) was performed to determine relative expression levels of genes between conditions.

2.2.1.9.1 mRNA extraction

Total RNA was extracted from cell pellets derived from sub-confluent cultures in 6 cm dishes. TRIzol reagent (Invitrogen) was used following the manufacturer's instructions. Total RNA pellets were dissolved in 30 µL RNAse-free H_2O by heating to 55°C for 10 min.

A total of 2.5-5 µg RNA were incubated with 1 U DNAse I (Sigma-Aldrich) in 10 µL 1x reaction buffer to digest potential DNA contaminants. The digest was performed at 37°C for 30 min and stopped by addition of 1 µL of 50 mM EDTA and incubation at 65°C for 10 min.

2.2.1.9.2 cDNA synthesis

First strand cDNA synthesis was performed using the RevertAid First Strand cDNA Synthesis Kit (Thermo Fisher Scientific) following the manufacturer's instructions. 2.5 µg of total RNA were used as template in 20 µL reaction volume. Reactions were incubated at 43°C for 1 h and inactivated at 70°C for 5 min.

2.2.1.9.3 Quantitative real-time PCR

Relative gene expression was determined by quantitative real-time PCR using *Power*SYBR Green PCR Master Mix (Thermo Fisher Scientific). The composition of qPCR reactions is shown below:

Template cDNA		1 µL
Forward primer 1.5 µM – 2.5 µM		4 µL
Reverse primer 1.5 µM – 2.5 µM		4 µL
2x MasterMix	10 µL	10 µL
ddH_2O		ad 20 µL

All reactions were prepared as triplicates. qPCR reactions were performed in a 96-well plate in a QuantStudio 5 cycler (Thermo Fisher Scientific).
Relative mRNA expression was calculated using the ΔΔCT method.

2.2.2 Methods in cell biology

2.2.2.1 Cell culture

Human cell lines were grown in a humidified atmosphere at 37°C and 5% CO_2. HEK293T, HeLa, U2OS and HCT116 cells were cultured in Dulbecco's Modified Eagle's Medium (DMEM) with 4.5 g/l glucose. DLD1 cells were grown in RPMI1640 with L-glutamine. Both media were supplemented with 10% fetal bovine serum (FBS) and 1% Penicillin-Streptomycin (100 U/mL penicillin, 0,1 mg/ml streptomycin). DMEM for U2OS tet-Off Cyclin E1 was supplemented with 2 µg/mL Doxycycline in the cell culture dish.
Cells were subcultured at 80-90% confluency. The medium was aspirated, cells washed once with sterile PBS and then detached by incubation with 0.05% Trypsin-EDTA solution at 37°C for 3-5 min. Detached cells were resuspended in fresh growth medium and diluted in a fresh cell culture dish to the desired ratio. All cell culture work was performed under sterile conditions and cell line identities were regularly confirmed by cell line authentication (Multiplexion, Heidelberg).

2.2.2.2 Harvesting and freezing of cells

For harvesting of cells, cultures were washed once with sterile PBS, detached with 0.05% Trypsin-EDTA at 37°C for 3-5 min and resuspended in growth medium.

HEK293T were harvested by washing cells of the dish with growth medium. Cell pellets were directly used for the preparation of lysates or stored at -80°C.
For the preparation of cryostocks, detached cells were collected in centrifuge tubes and pelleted at 330 g and 4°C for 3 min. Cell pellets were resuspended in growth medium supplemented with additional 10% FBS and 10% DMSO. Cell suspensions were frozen in 1.5 mL cryo vials using a freezing container (Nalgene, Thermo Fisher Scientific) at -80°C. For long-term storage, cryo vials were transferred to liquid nitrogen.

2.2.2.3 Transient transfection of mammalian cells

2.2.2.3.1 Transfection with plasmid DNA using polyethylenimine (PEI)

HEK293T were transiently transfected with plasmid DNA using polyethylenimine (PEI, Polysciences). Cells were seeded to the desired cell culture dishes and transfected after cultivation for at least 12 h. Transfection mixtures for 15 cm/10 cm dishes were prepared by diluting 10-20µg/7.5-15 µg of plasmid DNA with 4.6 mL/1.9 mL DMEM without FBS and 90 µL/34.2 µL PEI (1 mg/ml in ddH_2O, sterile filtered). Complex formation was induced by vortexing. After incubation for 10 min at RT, 13.9 mL/6.0 mL DMEM with 5% FBS were added to each transfection mix and vortexed briefly. The cell culture medium was aspirated from the target cultures and the transfection mix added. Cells were incubated for 24-48 h at 37°C, where the transfection mix was replaced with fresh growth medium after 24 h, if required.

2.2.2.3.2 Transfection with plasmid DNA and siRNA using Lipofectamine

U2OS and DLD1 cell lines were transfected with plasmid DNA using Lipofectamine 2000 (Thermo Fisher Scientific) following the manufacturer's instructions. Cells were seeded to 6-well plates or 10 cm dishes at least 12 h before transfection and were 60-80% confluent at the time of transfection. For the transfection of cells in 6-well plates/10 cm dishes, 2 µg/7.5 µg plasmid DNA were diluted in 250 µL/1 mL Opti-MEM (Thermo Fisher Scientific) and 4 µL/15 µL Lipofectamine 2000 in the same volumes in separate vials. Both dilutions were vortexed and incubated at RT for 4 min. DNA and lipid dilutions were combined, vortexed thoroughly and incubated at RT for 10 min. The cell culture medium was aspirated from target cultures and replaced with 1.5 mL/6 mL fresh complete medium (10% FBS, 1% P/S). The transfection mixes were added dropwise and cultures were incubated at least 6 h prior to medium exchange or passaging.

U2OS, HeLa and HCT116 were transfected with siRNA using Lipofectamine RNAiMax (Thermo Fisher Scientific) following the manufacturer's instructions. Cells were seeded at least 12 h before transfection and were 40-60% confluent at the first transfection. For the transfection of cells in 12-well/6-well plates, 1.2-1.5 µL/1.5-2.5 µL siRNA from 20 µM stocks were diluted in 150 µL Opti-MEM or DMEM without FBS. 3.75 µL/5 µL Lipofectamine RNAiMax were diluted in further 150 µL Opti-MEM or DMEM, all dilutions vortexed and incubated at RT for 4 min. siRNA and lipid dilutions were combined, vortexed thoroughly and incubated for 10 min at RT. The cell culture medium was aspirated from target cultures and replaced with 300 µL/700 µL growth medium with 5% FBS. Transfection mixes were added dropwise, resulting in 30-50 nM siRNA concentration, and cultures were incubated for 24 h before a second round of siRNA transfection was performed. 6 h after the second siRNA transfection, the cell culture medium was replaced, or cultures passaged. Cultures were harvested or used for experiments from 48 h after second siRNA transfection.

2.2.2.4 Generation of stable U2OS cell lines with inducible WDR5 expression

U2OS T-Rex inducible cell lines were generated following the manufacturer's instructions (Thermo Fisher Scientific). U2OS Flp-In-T-Rex (J.D. Pravin, Ohio State University) were seeded to 6-well dishes and incubated overnight. Cells were transfected with 1.8 µg pOG44 Flp-Recombinase and 0.2 µg pcDNA5/FRT/TO-WDR5 or WDR5 F133A using Lipofectamine 2000 as described in section 2.2.2.3.2. Plasmid DNA and Lipofectamine 2000 were diluted in 125 µL instead of 250 µL and 1.75 mL fresh growth medium added to the cells prior to addition of the transfection mixes. Cultures were incubated for 24 h and passaged to 10 cm dishes. After 48 h, 400 µg/mL Hygromycin B were added for three days followed by 1000 µg/mL for two days. Remaining cells were then cultured in fresh growth medium for seven days and single colonies picked by scraping with 20 µL pipette tips. Single colonies were transferred to 24-well plates and passaged to larger dishes before reaching confluency. The expression of WDR5 or WDR5 F133A was assessed by incubation with 2 µg/mL Doxycycline for 48-72 h.

2.2.2.5 Cell cycle synchronization

HEK293T and HCT116 were synchronized in G1/S phase using thymidine. Cells were treated with 2 mM thymidine for 22-24 h. For synchronization in prometaphase, cells

were released from thymidine-block by washing three times with PBS and incubation in fresh growth medium. 830 nM nocodazole (Merck), 500 nM Taxol (MP Biomedicals) or 100 nM vincristine were added to the growth medium directly or 4-5 h after release. Cultures were incubated for at least 15 h after release and harvested by trypsinization.

2.2.2.6 MG132, cycloheximide and small-molecule inhibitor treatment

Proteasomal protein degradation was inhibited in HEK293T using 10 µM MG132 (Sigma-Aldrich) for 5 h before harvesting. For cycloheximide chase assays, DLD1 cells were treated with 300 µg/mL cycloheximide (Santa Cruz Biotechnology) or HEK293T cells with 100 µg/mL cycloheximide in fresh growth medium. Cells were harvested by trypsinization at different time-points.

In order to inhibit enzymes with small molecules, 50 µM Apigenin (CK2), 5 µM CHIR-99021 (GSK3β) or 5 µM MLN4924 (NAE1) were added to the culture medium for 5 h prior to cell harvest.

2.2.2.7 Live-cell imaging

Mitotic cell fates of U2OS cells were analyzed by live-cell imaging. U2OS T-Rex WDR5, U2OS T-Rex WDR5 F133A and U2OS tet-Off Cyclin E1 were incubated in medium with and without 2 µg/mL doxycycline for 72 h before seeding to an 8-well µ-imaging dish (Sarstedt). U2OS and U2OS tet-Off Cyclin E1 were transfected with 30-40 nM siRNA as described in section 2.2.2.3.2. 24 h after the second siRNA transfection, cells were seeded to an 8-well imaging dish (Sarstedt). Cultures were incubated in imaging dishes for 24 h and reached density of 40-70%. Before live-cell imaging, 830 nM nocodazole and, where applicable, fresh 2 µg/ml doxycycline were added to the wells. Imaging dishes were placed into a humidified microscopy incubation chamber at 37°C and 5% CO_2 and positioned under a Zeiss Cell Observer Z1 inverted microscope with a 10x/0.3 EC PlnN Ph1 DICI objective. Cells arrested in mitosis were monitored by taking phase-contrast images of multiple positions every 10 min for up to 60 h using the Zeiss ZEN blue software. Mitotic cell fates were analyzed using ImageJ Fiji.

2.2.2.8 Flow cytometry analysis

For the analysis of cell ploidy after prolonged mitotic arrest, a propidium iodide (PI)-based DNA staining and flow cytometry assay was performed. HCT116 WT and KO

FBXW7 cell lines were seeded to 12-well dishes and transfected with siRNA was described under section 2.2.2.3.2. 6 h after the second siRNA transfection, cells were passaged to 6-well dishes and 2 mM thymidine were added. After synchronization in G1/S for 24 h, a thymidine-release was performed and fresh medium with 500 nM Taxol or 100 nM vincristine added. All cells, including cells floating in the culture medium, were collected after 20 h, washed once with PBS and fixed with ice-cold Ethanol.

For PI-staining, Ethanol was aspirated and cell pellets were rehydrated in PBS at RT for 15 min. PBS was then aspirated and cells stained with 30 µg/mL PI and 10 µg/mL RNAse at RT for 15 min in the dark. DNA content was determined on a FACSCalibur (BD) and raw data analyzed using FlowJo v10 (BD).

2.2.3 Methods in protein biochemistry

2.2.3.1 Preparation of protein extracts from mammalian cells

Cell extracts from all cell lines were prepared using NP40 or RIPA buffer. After cells were harvested as described in 2.2.2.2, cell pellets were resuspended in a 3-5-fold volume of NP40 buffer for immunoprecipitations or RIPA buffer for all other applications. Cell lysates were incubated on ice for 30 min with vigorous vortexing every 10 min. Lysates were then clarified from insoluble components by centrifugation at 16100 g and 4°C for 20 min in an Eppendorf 5415 R centrifuge. After transferring supernatants to fresh tubes, protein concentration was determined as described under 2.2.3.2. For analysis by SDS-PAGE, samples of cell lysates were mixed with equal volumes of 2x Laemmli buffer or 2x LDS buffer (Thermo Fisher Scientific) and denatured at 95°C for 5 min or 72°C for 10 min, respectively.

2.2.3.2 Determination of protein concentration by Bradford assay

Protein concentrations were determined by Bradford assay with Bio-Rad Protein assay. 1 µL of protein extract or different amounts of a BSA standard were diluted in 800 µL ddH_2O and mixed with 200 µL of assay dye. After incubation at RT for 5 min, 200 µL of each sample were transferred to a clear-bottom 96-well plate and the $OD_{595\ nm}$ was determined with a SPECTROstar Nano (BMG Labtech). Protein concentrations were calculated based on the BSA standard curve.

2.2.3.3 SDS polyacrylamide gel electrophoresis (SDS-PAGE)

SDS polyacrylamide gel electrophoresis (SDS-PAGE) was performed to separate protein extracts or other protein samples according to their molecular weight. Polyacrylamide gels were prepared with the Mini-Protean vertical electrophoresis system (Bio-Rad). Separating gels were prepared depending on the size of the target proteins and contained 6-15% acrylamide/bisacrylamide, 375 mM Tris-HCl pH 8.8, 0.1% SDS, 0.1% APS and 0.1% TEMED. Stacking gels contained 125 mM Tris-HCl pH 6.8, 0.1% SDS, 0.1% APS and 0.1% TEMED. For the analysis of large proteins above 300 kDa mass, Tris-Acetate gels were prepared (Cubillos-Rojas et al. 2019). Tris-Acetate gels contained 5% acrylamide/bisacrylamide, 200 mM Tris-acetate pH 7.0, 0.1% APS and 0.1% TEMED. After polymerization, gels were transferred to SDS-PAGE chambers, chambers filled with SDS-running buffer (Tris-HCl gels) or Tris-Tricine (Tris-Acetate gels) buffer and protein samples in Laemmli or LDS buffer loaded. Protein molecular weight markers were used as size reference. SDS-PAGEs were run at constant voltage of 80-105 V for 2 h.

2.2.3.4 Western blotting

After separation of proteins by SDS-PAGE, they were transferred to nitrocellulose membranes by Western blotting. Transfers from Tris-HCl gels were performed using a wet blotting chamber (Mini Trans-Blot Cell, Bio-Rad) and wet blot buffer or the Trans-Blot Turbo semi-dry system (Bio-Rad). Wet blots were run at 100 V for 60 min and semi-dry blots at 2.5 A for 15 min. Proteins from Tris-Acetate gels were transferred by wet blotting in Tris-Bicine buffer at 200 mA and 4°C for 2 h.

Transferred proteins were stained with Ponceau S solution to assess transfer quality. Membranes were then blocked with 5% milk powder in PBST at RT for at least 20 min with gentle shaking. Target proteins were detected by incubation with primary antibodies at RT for 2 h or 4°C overnight, followed by three washing cycles with PBST at RT for 10 min. Fresh blocking buffer with the species-specific HRP-conjugated secondary antibody was added and membranes incubated at RT for further 1-2 h. Excess secondary antibodies were washed off three times with PBST for 10 min and signals were detected using Immobilon Western Chemiluminescence HRP-substrate (Merck) according to the manufacturer's instructions. Signals were detected in an ImageQuant LAS 4000 (GE) and quantifications were performed using ImageJ Fiji.

2.2.3.5 Immunoprecipitation assays

2.2.3.5.1 Immunoprecipitation of Flag-tagged proteins using Flag M2 affinity beads

Flag-tagged proteins were immunoprecipitated using α-Flag M2 beads (Sigma-Aldrich). Cell extracts were prepared as described under section 2.2.3.1. 10-20 µL bed volume of affinity beads were used for each sample. All centrifugation steps were performed at 6000 g and 4°C for 2 min in an Eppendorf 5414 R centrifuge. Beads were prepared by washing twice with TBS, once with 0.1 M glycine-HCl pH 3.5 and three times with TBS. Prepared beads were added to 4-15 mg of each extract, volumes were normalized to the highest volume with NP40 buffer and immunoprecipitations were incubated at 4°C overnight on a rotating wheel. Unbound proteins were washed off 3-5 times with NP40 lysis buffer. To dephosphorylate proteins bound to beads, beads were washed three times in NP40 special (0.1 mM EDTA, without Na_3VO_4) and resuspended in 40 µL NP40 special. 5 µL 10x NEB PMP buffer, 5 µL 10 mM $MnCl_2$ and 1 µL of Lambda Protein Phosphatase (New England Biolabs) were added and the reaction incubated at 30°C for 3 h with shaking. Unbound proteins were washed off three times with NP40 lysis buffer. For all Flag-immunoprecipitations, bound proteins were eluted by incubation with 50 µL NP40 buffer containing 200 ng/µL 3x Flag peptide (Thermo Fisher Scientific) on ice for 30 min. Beads were pelleted by centrifugation and the supernatant transferred to a fresh tube. Samples were denatured by addition of 4x Laemmli buffer or 4x LDS buffer and incubation at 95°C for 5 min or 72°C for 10 min, respectively. Immunoprecipitations were analyzed by SDS-PAGE and Western blotting.

2.2.3.5.2 Immunoprecipitation of GFP-tagged proteins using GFP-trap affinity beads

GFP-tagged proteins were immunoprecipitated using GFP-trap affinity beads. Cell extracts were prepared as described under section 2.2.3.1. 10 µL bed volume of affinity beads were used for each sample. All centrifugation steps were performed at 5000 g and 4°C for 2 min. GFP-trap beads were prepared by washing once with ddH_2O and twice with NP40 lysis buffer. Prepared beads were added to 2-10 mg of each extract and volumes were normalized with NP40 lysis buffer. Immunoprecipitations were performed on a rotating wheel at 4°C overnight. Unbound proteins were washed off three times with NP40 buffer and bound proteins were eluted by incubation in 50 µL of

2x Laemmli or 2x LDS buffer at 95°C for 5 min or 72°C for 10 min, respectively. After centrifugation, supernatants were analyzed by SDS-PAGE and Western blotting.

2.2.3.5.3 Immunoprecipitation of endogenous proteins using protein A or protein G Sepharose

Endogenous WDR5 or FBXW7 were immunoprecipitated using specific antibodies and protein A or protein G Sepharose beads (GE). Four times 12 mg extracts from HEK293T cells were prepared as described under section 2.2.3.1. 4 µg of mouse anti-WDR5 (G9, Santa Cruz Biotechnology) or 4 µg rabbit anti-FBXW7 (A301-720, Bethyl) were added to one extract, each. 4 µg of non-specific mouse-IgG or rabbit-IgG were used as controls. Extracts were incubated with antibodies on a rotating wheel at 4°C overnight. All centrifugation steps were performed at 4000 g and 4°C for 2 min. 15 µL bed volume protein A or protein G beads were prepared for each immunoprecipitation by washing once in ddH_2O and twice with NP40 buffer. Beads were added to extract-antibody mixes and incubated on a rotating wheel at 4°C for 2 h. Unbound proteins were washed off three times with NP40 buffer adjusted to 600 mM NaCl and bound proteins eluted by incubation in 50 µL 2x Laemmli buffer at 95°C for 5 min. Supernatants were analyzed by SDS-PAGE and Western blotting.

2.2.3.6 Mass spectrometry analysis

Flag-immunoprecipitation followed by mass spectrometry (MS) was performed to identify novel FBXW7 substrates. pCMV-3Tag1C-FBXW7 S462A, T463V, R465A, a mutant which is unable to bind substrates, was used as negative control. HEK293T were transfected with pCMV-3Tag1C-FBXW7, FBXW7 mutant or EV as described under 2.2.2.3.1 and cultures were either grown without synchronization or synchronized in prometaphase as described in section 2.2.2.5. Flag-immunoprecipitations were performed with 20-30 mg extract and 50 µL bed volume following the protocol described in 2.2.3.5.1. Bound proteins were eluted with 50 µL NP40 buffer with 500 ng/mL 3x Flag-peptide and denatured by incubation with 4x Laemmli buffer at 95°C for 5 min. 35 µL of each sample, and in total four replicates of each condition, were submitted to the MS-based Protein Analysis Unit of the DKFZ, Heidelberg. Following steps were performed by the core facility: Protein samples were loaded to a 1D-SDS-PAGE and gel pieces cut out, cysteines reduced by adding DTT and carbamidomethylated using iodoacetamide followed by overnight digestion with

Trypsin. Peptides were loaded on a cartridge trap column, packed with Acclaim PepMap300 C18, 5 µm, 300 Å wide pores (Thermo Fisher Scientific) and separated in a 120 min gradient from 3% to 40% acetonitrile on a nanoEase MZ Peptide analytical column, 300Å, 1.7 µm, 75 µm x 200 mm (Waters GmbH). Eluted peptides were analyzed by an online coupled Q-Exactive-HF-X mass spectrometer.
Data analysis was carried out by MaxQuant (V. 1.6.3.3). Proteins and peptides were identified with an FDR cutoff of 0.01. Quantification was done using a label free quantification approach based on the MaxLFQ algorithm (Cox et al. 2014). Label-free quantification (LFQ) results were first compared between Flag-FBXW7 WT IPs and Flag-EV for both, non-synchronized and prometaphase populations using unpaired, two-tailed Student's t-test. In the next step, the significantly enriched proteins were compared between Flag-FBXW7 WT and Flag-FBXW7 mutant by another unpaired, two-tailed Student's t-test. $p < 0.05$ was considered significant, n=4.

2.2.3.7 *In-vivo* ubiquitylation assays

In-vivo ubiquitylation of Flag-WDR5 was assessed by co-expression of pCMV-3Tag1A-WDR5 with pPK-CMV-HA-UbiquitinC and pEGFP-C1-FBXW7 or mutant constructs in HEK293T cells. 10 µM MG132 (Sigma-Aldrich) were added for 4-5 h before harvesting. Cell extracts were prepared as described under 2.2.3.1 with NP40 lysis buffer containing 20 mM NEM. Flag-tagged WDR5 was immunoprecipitated following the steps described under 2.2.3.5.1 and NP40 lysis buffer with 20 mM NEM was used for washing. Eluted proteins were denatured with 2x LDS buffer at 72°C for 10 min and analyzed by SDS-PAGE and Western blotting.

2.2.3.8 Expression and purification of recombinant GST-WDR5 and GST-c-Myc

E. coli Rosetta (DE3) transformed with pGEX-4T1-WDR5 or pGEX-4T1-c-Myc (described under 2.2.1.6) were used to express recombinant proteins. 5 mL LB medium with ampicillin were inoculated with a single colony and grown at 37°C and 180 rpm overnight. Overnight cultures were used to inoculate 400 mL LB with ampicillin by 1:100 dilution and were cultivated at 37°C and 180 rpm until they reached an $OD_{600} = 0.5$. Cultures were then cooled down on ice, 400 µM IPTG added and cultivated at 18°C and 180 rpm overnight.
Bacteria were harvested using a F10-6x500Y rotor (Piramoon Technology) in a Sorvall RC5C centrifuge at 5000 rpm and 4°C for 30 min. Pellets were resuspended in 20 mL

lysis buffer and lysed by sonication using a Branson Sonifier 250 at 30% output and 50% cycle duty for ten rounds of 20 s. Lysates were clarified by centrifugation in a Sorvall F-28/50 rotor at 20200 g and 4°C for 30 min and supernatants moved to fresh reaction tubes. 600 µL bed volume of immobilized glutathione CL-4B beads (Sigma-Aldrich) were equilibrated with lysis buffer and added to the supernatants. Protein binding was performed at 4°C on a rotating wheel for 2 h. Beads were collected in a Poly-Prep chromatography column (Bio-Rad) and washed three times with 10 mL washing buffer. Three elutions with each 600 µL elution buffer were performed and all fractions pooled.

Eluates were dialyzed against washing buffer with 1 mM DTT instead of 5 mM β-Mercaptoethanol using a 500 Da MW cut-off dialysis membrane at 4°C with gentle stirring overnight. Dialyzed products were cleared from aggregates by centrifugation at 16100 g and 4°C for 20 min. Final products were analyzed by SDS-PAGE and Coomassie-staining and aliquots were frozen in liquid nitrogen and stored at -80°C.

2.2.3.9 GST pull-down assays

The direct interaction of GST-WDR5 and His-FBXW7/SKP1 was assessed by a GST pull-down assay. 10 µg of purified GST-WDR5 or an equimolar amount of GST and 10 µg of His-FBXW7/SKP1 were combined in 200 µL NL40 buffer and incubated on a rotating wheel at 4°C for 1 h. 10 µL immobilized glutathione CL-4B beads were equilibrated with NP40 buffer for each pulldown and added in 200 µL NP40 to the protein mix. Proteins were bound by incubation on a rotating wheel at 4°C for 2 h and unbound proteins were washed off four times with NP40 buffer. Bound proteins were eluted by incubation with 25 µL 2x Laemmli buffer at 95°C for 5 min. Protein interactions were analyzed by SDS-PAGE and Western blotting.

2.2.3.10 *In-vitro* ubiquitylation assays

Ubiquitylation of GST-WDR5 and GST-c-Myc was assessed by an *in-vitro* ubiquitylation assay with recombinant proteins and Flag-FBXW7 complexes precipitated from HEK293T cells. Flag-FBXW7 or Flag-FBXW7 R465H R479Q R505C was co-expressed in HEK293T with Myc-Cullin1 as described under 2.2.2.3.1. Flag-immunoprecipitations were performed following the steps outlined under 2.2.3.5.1 but no elution step was performed.

Beads were washed once in ubiquitin assay buffer (50 mM Tris-HCl pH 7.50, 100 mM NaCl, 10 mM $MgCl_2$, 0.05% CHAPS, 0.1 mM NA_3VO_4, 1 µg/ml Aprotinin, 1 µg/ml Leupeptin, 10 µg/ml Trypsin inhibitor from soybean). For ubiquitylation reactions, 200 nM GST-WDR5 or GST-c-Myc were combined with 170 nM UBA1, 250 nM UBCH5b and 250 nM CDC34, 200 nM His-GSK3β, 30 µM Ubiquitin and α-Flag M2 beads with immobilized Flag-FBXW7/Cullin1 in 20 µL total volume assay buffer and incubated at 37°C and 500 rpm for 90 min. Reactions were terminated by addition of 2x LDS buffer and incubation at 72°C for 10 min. Samples were analyzed by SDS-PAGE and Western blotting.

2.2.4 Statistical analysis

Statistical analysis was performed with GraphPad Prism v9. Quantitative data was collected from at least three independent experiments and are represented as mean ± SD for each experiment. Statistical significance was determined using unpaired, two-tailed, Student's t test, with Welch's correction where applicable, or one-way ANOVA with Tukey post-hoc test, as indicated in each figure legend. p values of less than 0.05 were considered statistically significant (ns $p > 0.05$, * $p < 0.05$, ** $p < 0.01$, *** $p < 0.001$, **** $p < 0.0001$).

3. Results

3.1 Identification of FBXW7 candidate substrates by co-immunoprecipitation and mass spectrometry analysis

I used a Flag-immunoprecipitation (IP)/mass spectrometry (MS)-based approach to identify novel substrates of FBXW7. In addition, I designed the approach in a way to be able to distinguish proteins, which are specifically bound during prolonged mitotic arrest induced by antimicrotubule drugs. An illustration of the approach can be found in Figure 6 A, left part. HEK293T were transfected with Flag-empty vector (EV), Flag-FBXW7 wild-type (WT) or a Flag-FBXW7 WD40 domain S462A, T463V, R465A mutant, which is unable to interact with substrates (Hao et al. 2007). While as a control HEK293T cells were left untreated after transfection of Flag-FBXW7 or Flag-FBXW7 WD40 mutant expressing HEK293T, a second set of cells expressing either Flag-FBXW7 or FLAG-FBXW7 WD40 was first synchronized with thymidine and then released into medium containing nocodazole to induce prolonged mitotic arrest. After nocodazole treatment, most HEK293T cells showed the rounded-up mitotic morphology. I performed Flag-IPs from the cell lysates and submitted the elution fractions to the DKFZ MS-based protein analysis unit for MS-analysis (Fig. 7 A, right part).

Western blot experiments confirmed equal expression of the constructs (Fig. 7 B). Upregulation of PLK1 and the absence of Cyclin E1 showed that most cells were synchronized in prometaphase. As a positive control, I could show that the FBXW7 substrate c-Myc co-precipitated with Flag-FBXW7 WT but not with the WD40 domain mutant.

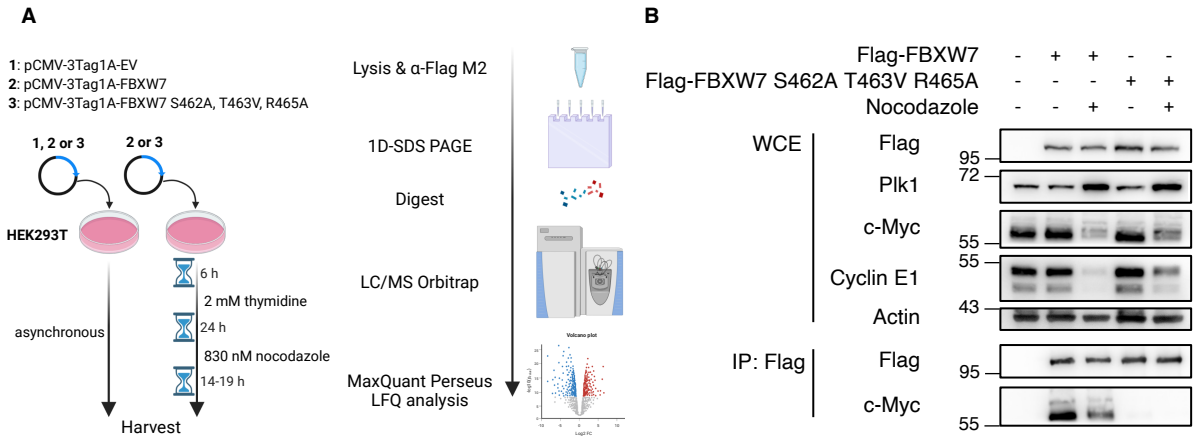

Figure 7: Mass spectrometry screen to identify novel substrates of FBXW7.
A Schematic representation showing the method of FBXW7 substrate identification. HEK293T were transfected with Flag-FBXW7, FBXW7 WD40 domain mutant (S462A, T463V, R465A) or EV as a control. For each condition, half of the cultures were left untreated for 48 h, while the other half was first pre-synchronized in G1/S with 2 mM thymidine and then blocked in prometaphase with 830 nM nocodazole after thymidine-release. Cell pellets were lysed after harvest and Flag-IPs were performed. Eluates were analyzed by the DKFZ MS-based Protein Analysis Unit using SDS-PAGE, tryptic digest and LC/MS using a label-free approach. Results received from the core facility were analyzed following a protocol for label-free quantification. **B** Inputs and eluted proteins from IPs following the protocol from **A** were analyzed by Western blotting. LC – liquid chromatography, MS – mass spectrometry, LFQ – label-free quantification, WCE – whole cell extract, IP – immunoprecipitation. Illustrations were created using the BioRender.com application.

I used the Perseus software platform to compare the label-free quantification (LFQ) results between each condition (Tyanova et al. 2016). LFQ values represent a normalized score for each protein, which compares the peptide intensity to the theoretically possible number of peptides (Cox et al. 2014).

I first compared the abundance of peptides between the Flag-FBXW7 WT IPs in asynchronously growing or mitotic cells to the EV control to subtract non-specific proteins. Non-specific proteins could be for example proteins interacting with the α-Flag M2 beads. The remaining pool of proteins should therefore only interact with Flag-FBXW7 or backbone proteins of the SCF complex. In the next step, LFQ values of these proteins were compared between Flag-FBXW7 WT and the WD40 domain mutant. Proteins, which were enriched in the IP of the WT construct compared to the substrate binding deficient mutant, could therefore be considered candidate substrates. This comparison was performed once for either non-synchronized or mitotic conditions (Fig. 8 A & B). In both conditions, known FBXW7 substrates could be identified. For example, members of the Mediator complex, c-Myc, p53, NFKB2 and NOTCH1 were found, validating the approach for the identification of FBXW7 substrates (Yumimoto and Nakayama 2020). In addition, the SCF components SKP1, RBX1, CUL1 and NEDD8 and the recently published regulators of FBXW7, MYCBP2

and FBXO45 could be identified in both FBXW7 WT and mutant IPs to similar extent (Richter et al. 2020). Moreover, using in the same approach, I identified several novel candidate substrates (see list Appendix 6.1). Of particular interest were the putative FBXW7 substrates BIRC6/BRUCE and FYCO1, because they were significantly enriched in the samples of Flag-FBXW7 IPs from mitotic HEK293T compared to the non-synchronized sample (Fig. 8 C). These results show that novel putative substrates of SCF-FBXW7 were identified by Flag-IP/MS, which can be the basis for further characterization by interaction studies and functional assays to assess their role in mitotic slippage.

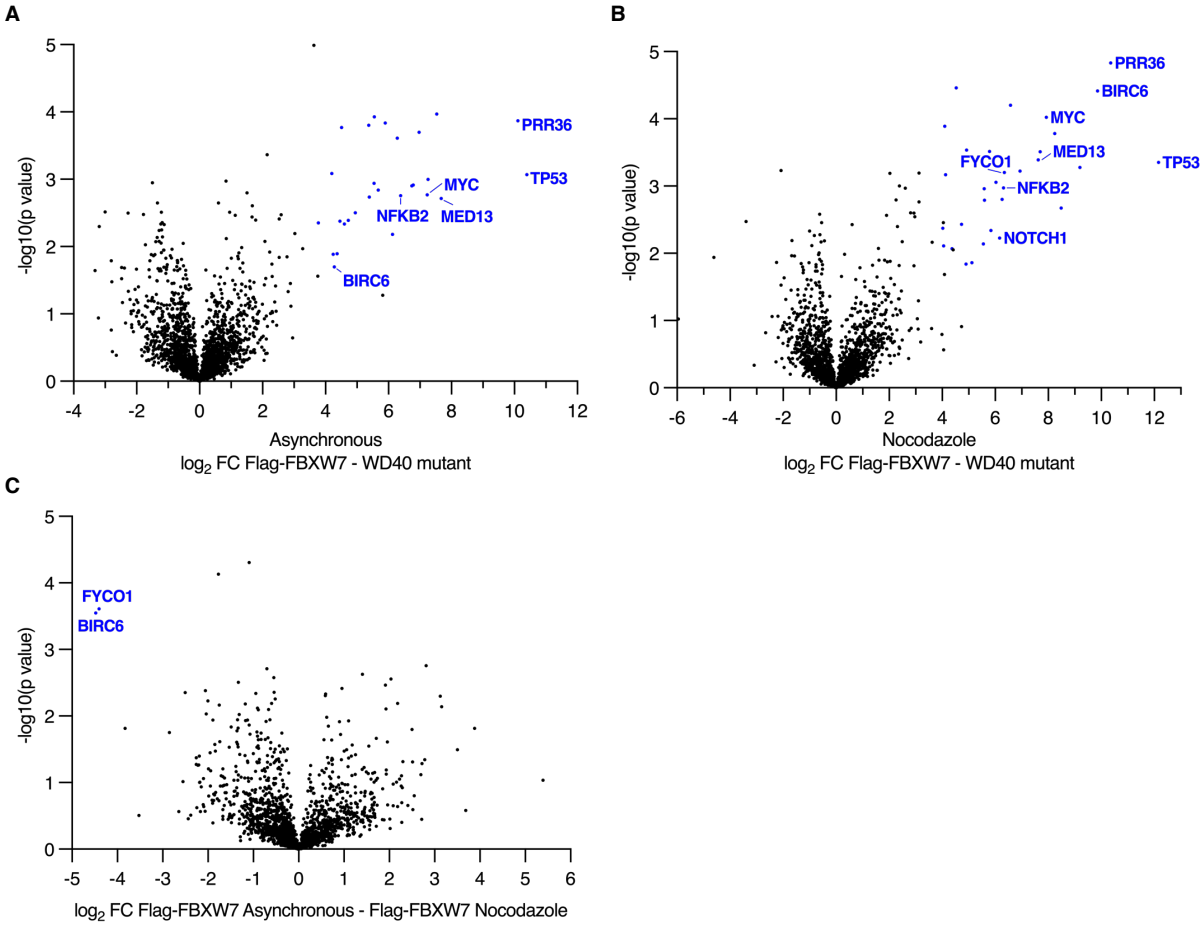

Figure 8: New putative substrates of FBXW7 were identified by IP-MS.
Results from the IP-based MS-screen (Fig. 6) were analyzed using MaxQuant Perseus. LFQ values were compared between each condition by student's t-test. Volcano plots were created with S_0 = 0 and FDR=0.05, n=4. Blue dots represent significantly enriched proteins between the samples depicted below the x-axis. **A** Abundance of co-precipitated proteins was compared between Flag-FBXW7 WT and Flag-FBXW7 WD40 mutant S462A, T463V, R465A derived from non-synchronized cultures and **B** from cultures synchronized in prometaphase. **C** Mitotic interactors were identified by comparing abundances of proteins co-precipitated with Flag-FBXW7 WT from non-synchronized and prometaphase arrested HEK293T cells. FC - fold change

3.2 Characterization of BRUCE as a novel interaction partner of FBXW7

I identified novel interactors and putative candidate substrates of SCF-FBXW7 (Fig. 8). For example, BIRC6/BRUCE was enriched in IPs from both non-synchronized and prometaphase HEK293T lysates. BRUCE is a member of the inhibitor of apoptosis proteins (IAPs) and can counteract proapoptotic signaling (Bartke et al. 2004; Hao et al. 2004). Many cancer cell types highly express different IAPs to prevent apoptosis, which promotes carcinogenesis and therapy resistance (Ghobrial et al. 2005). In addition, BRUCE plays important roles in mitosis (Pohl and Jentsch 2008). Therefore, I decided to investigate whether BRUCE is a novel substrate of FBXW7.

3.2.1 FBXW7 binds BRUCE in mitotic cells through its WD40 domain

According to the results from IP/MS (Fig. 8), BRUCE specifically interacted with Flag-FBXW7 WT but not with the WD40 mutant and co-precipitated significantly more from lysates of mitotic HEK293T than from asynchronous cells.

In order to verify these results, I transfected HEK293T with Flag-FBXW7 WT or the cancer-relevant WD40 mutant R479Q, which is unable to interact with substrates (Hao et al. 2007). The interaction of Flag-FBXW7 with endogenous BRUCE was compared between non-synchronized HEK293T cells and those blocked in prometaphase with nocodazole using Flag-IP followed by Western blotting (Fig. 8 A). Small amounts of BRUCE co-eluted with Flag-FBXW7 from non-synchronized lysates, whereas a significant higher amount was bound to Flag-FBXW7 from prometaphase lysates. FBXW7 R479Q mutation abolished BRUCE binding in both cases. I transfected HEK293T with Flag-tagged murine BRUCE, to assess whether BRUCE could also co-immunoprecipitate endogenous FBXW7 to find out whether there was a difference between non-synchronized and nocodazole-treated cells. I used murine BRUCE, because the construct could be supplied rapidly from within Germany and BRUCE is highly conserved between mice and humans. Western blot analysis revealed that small amounts of FBXW7 co-eluted with Flag-mBRUCE from non-synchronized lysates, while a significantly higher amount was bound to Flag-mBRUCE in mitotic cells (Fig. 9). These results indicate that FBXW7 and BRUCE interact specifically during mitosis and that the interaction is mediated by the WD40 domain of FBXW7.

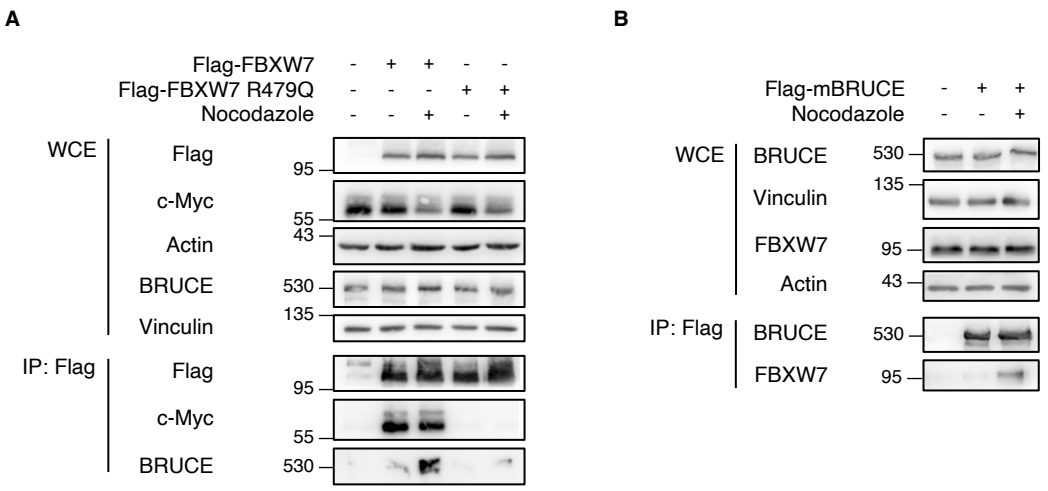

Figure 9: BRUCE interacts with FBXW7 in mitosis and the interaction is mediated by the WD40 domain of FBXW7.
A HEK293T cells were transfected with Flag-FBXW7, Flag-FBXW7 R479Q or Flag-EV as control and proteins were overexpressed for 48 h. 6 hours after transfection, indicated cultures were pre-synchronized with 2 mM thymidine for 24 h and released into 830 nM nocodazole for 19 h. Flag-IPs were performed and inputs and eluates analyzed by Western blotting. **B** HEK293T cells were transfected with Flag-mBRUCE or Flag-EV as control and the proteins were overexpressed for 48 h. Where indicated, cultures were pre-synchronized with 2 mM thymidine for 24 h and released into 830 nM nocodazole for 19 h. Flag-IPs were performed and inputs and eluates analyzed by Western blotting. WCE – whole cell extract, IP: immunoprecipitation.

3.2.2 GSK3β activity is required for the interaction between BRUCE and FBXW7

Ubiquitylation of substrates of SCF-FBXW7 requires the interaction of FBXW7 with phosphodegrons on its targets (Nash et al. 2001; Hao et al. 2007). FBXW7 phosphodegrons are conserved sequence motifs with some flexibility in their sequence but they always require phosphorylation of a serine or threonine residue for high affinity binding to the WD40 domain of FBXW7 (Singh et al. 2022).

In order to elucidate whether the interaction between FBXW7 and BRUCE requires a specific kinase, I used small molecule inhibitors against different important cell-cycle regulatory kinases. I expressed Flag-FBXW7 in HEK293T and synchronized the cultures first with thymidine, followed by a release into medium containing nocodazole. The small molecule inhibitors were added after the cells reached the prometaphase block. The interaction of Flag-FBXW7 and BRUCE was assessed by Flag-IP and Western blotting. The amount of co-precipitated BRUCE was reduced by inhibition of CDK1, CDK2, GSK3β and Aurora kinase B, while the interaction was stabilized by inhibition of PLK1 or Cullin-RING ligase activity (Fig. 10 A). This experiment was performed in collaboration with Bosco Sungho-Han, University of Heidelberg. Because CDK1 and Aurora B inhibition leads to mitotic exit, I compared the mitotic index of each

treatment by detecting Histone H3 S10 phosphorylation (Fig. 10 B) (Carpinelli and Moll 2008; Girdler et al. 2006; Kaestner et al. 2009; Murray et al. 1989; Murray 2004). While treatment with RO-3306 and Hesperadin strongly and Roscovitine slightly reduced the mitotic population, CHIR99021 showed no effect. PLK1 inhibition led to an even stronger H3 S10 phosphorylation. Because the co-precipitation of FBXW7 and BRCUCE is strongest in mitotic cells, the effects of CDK1, CDK2 and Aurora B were considered possible artifacts and the kinases excluded. Only GSK3β inhibition reduced the interaction of Flag-FBXW7 and BRUCE and did not affect the mitotic arrest. I used the Eukaryotic Linear Motif resource (ELM) to screen the BRUCE primary structure for FBXW7 degron sequences and GSK3β consensus sites (Fig. 10 C) (Kumar et al. 2022). In total, seven FBXW7 degron motifs were identified, of which six matched the GSK3β consensus sequence. Taken together, GSK3β is required for the interaction between BRUCE and FBXW7 during mitosis and there are multiple possible binding sites within the BRUCE amino acid sequence.

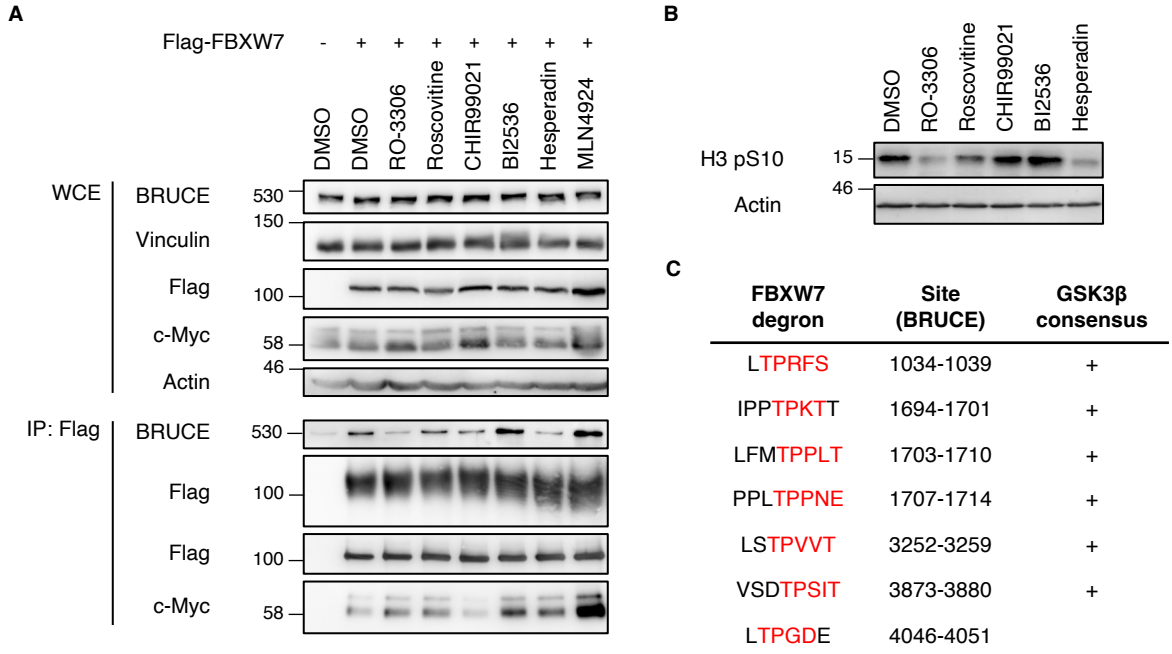

Figure 10: The interaction between FBXW7 and BRUCE is regulated by GSK3β.
A HEK293T were transfected with Flag-FBXW7 or Flag-EV as control. All cultures were pre-synchronized by addition of 2 mM thymidine 6 hours after transfection and released into 830 nM nocodazole after 24 h. 12 h after thymidine-release, cells were treated with either 10 µM RO-3306 (CDK1), 10 µM Roscovitine (CDK2), 5 µM CHIR99021 (GSK3β), 100 nM BI2536 (PLK1), 500 nM Hesperadin (Aurora kinase B), 1 µM MLN4924 (NAE1) or DMSO for 3 h. Lysates were subjected to Flag-IP and inputs and eluates analyzed by Western blotting. This experiment was performed in collaboration with Bosco Sungho-Han, University of Heidelberg. **B** Inputs with Flag-FBXW7 overexpression from **A** were analyzed for histone H3 S10 phosphorylation by Western blotting. **C** FBXW7 degron sequences [TS],P,X,X,[TSED] and GSK3β consensus sites were predicted on the BRUCE amino acid sequence using the Eukaryotic Linear Motif resource ELM. Highlighted amino acids indicate putative degron sequences. WCE – whole cell extract, IP – immunoprecipitation.

3.2.3 BRUCE depletion affects mitotic slippage

FBXW7 has been linked to chemoresistance and its depletion promotes mitotic slippage, while its upregulation favors mitotic cell death in response to treatment with antimicrotubule drugs (Wertz et al. 2011; Richter et al. 2020). As FBXW7 functions as a tumor suppressor, its depletion might result in the upregulation of target proteins that are able to promote cell survival or enforce an escape from prometaphase arrest.

In order to assess whether BRUCE affects mitotic cell fate, I depleted BRUCE in U2OS cells using siRNA (Fig. 11 A) and performed live-cell imaging in the presence of nocodazole (Fig. 11 B). Cells entering mitotic arrest were followed and their mitotic cell fate was determined. BRUCE depletion significantly decreased mitotic slippage of U2OS cells from 76.0±2.8% in the control to 43.0±15.6%. Although the absence of BRUCE might result in a lower apoptotic threshold, neither the duration from mitotic entry to slippage, nor to cell death was affected. These results suggest that BRUCE is required for mitotic slippage in response to nocodazole.

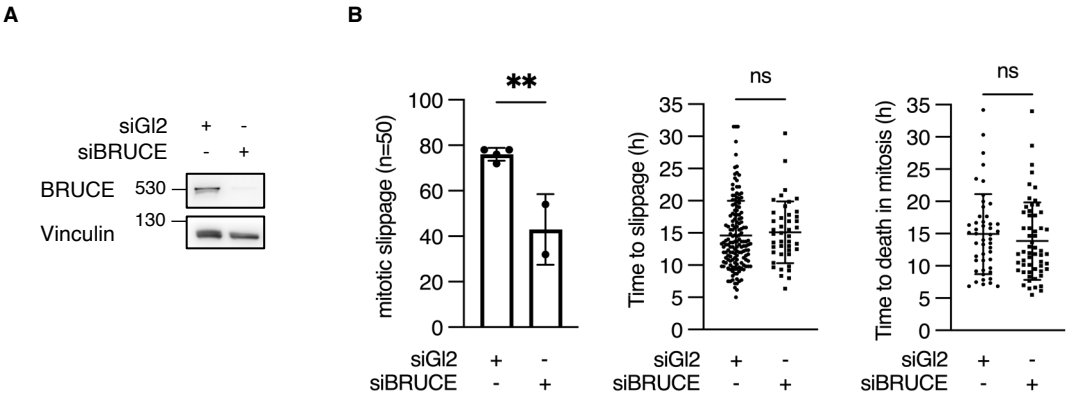

Figure 11: BRUCE depletion decreases mitotic slippage.
A U2OS cells were transfected with siRNA targeting BRUCE or Gl2 for 72 h. Cell lysates were analyzed by Western blotting. **B** 830 nM nocodazole were added to U2OS from **A** and mitotic cell fates were assessed by live-cell imaging. The time from mitotic entry to slippage or cell death was quantified for each analyzed cell. For each condition, n=50 cells were analyzed. ** $p < 0.01$, ns $p > 0.05$, unpaired, two-tailed student's t-test, n=2-4.

3.2.4 BRUCE protein levels are not regulated by FBXW7

To date, only the E3 ligase NRDP1 has been shown to regulated BRUCE protein levels via the ubiquitin-proteasome system (Qiu et al. 2004). I have shown that BRUCE fulfills typical criteria of a FBXW7 substrate. Therefore, I assessed whether BRUCE protein levels were regulated by FBXW7. I depleted FBXW7 in U2OS and analyzed BRUCE protein levels by Western blotting (Fig. 12 A). Intriguingly, BRUCE protein levels were not increased in absence of FBXW7 (Fig. 12 B). These results suggest that BRUCE

specifically interacts with the WD40 domain of FBXW7 but that this interaction could have other functions than targeting BRUCE for proteasomal degradation.

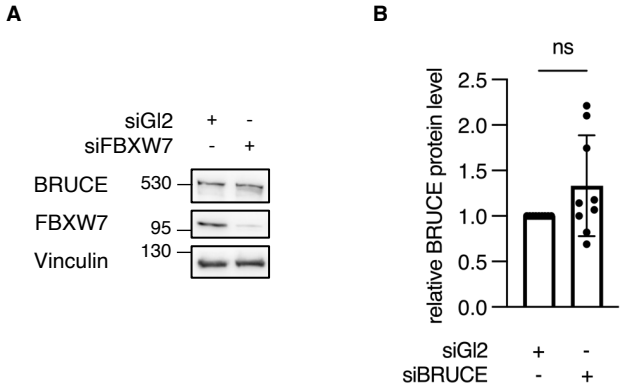

Figure 12: BRUCE protein levels are not regulated by FBXW7.
A U2OS cells were transfected with siRNA targeting FBXW7 or Gl2 for 72 h. Cell lysates were analyzed by Western blotting. **B** BRUCE protein levels were normalized using Vinculin and compared between conditions shown in **A**. ns $p > 0.05$, unpaired, two-tailed student's t-test with Welch's correction, n=9.

3.3 Characterization of WDR5 as a novel substrate of FBXW7

3.3.1 Identification of KMT2D and WDR5 as FBXW7 candidate substrates by Flag-immunoprecipitation and mass spectrometry

In addition to BRUCE, I assessed the influence of FBXW7 depletion on the protein levels of the other hit from the screen, FYVE and coiled-coil domain autophagy adaptor 1 (FYCO1) (Fig. 8 C, Appendix 6.2). However, FYCO1 was not stabilized after knockdown of FBXW7 in U2OS or HeLa cells.

Therefore, I analyzed screens that were aimed at FBXW7 substrate identification from literature and the Hoffmann lab for additional candidates (Saffie et al. 2020; Hänle-Kreidler et al. 2022). A reoccurring hit was the methyltransferase KMT2D, together with its complex members WDR5 and ASH2L, which are shown in my analysis of the FBXW7 substrate screen performed by Kai Richter (Fig. 13 A). Here, peptides of the published FBXW7 substrates c-Myc and p53 were significantly enriched in the Flag-FBXW7 WT IP compared to the WD40 domain mutant, thereby validating the approach. KMT2D is one of six SET-domain KMT2 methyltransferases, but of these the only published interactor of FBXW7 (Saffie et al. 2020).

I assessed whether other methyltransferases of this class, KMT2A and SETD1A, could interact with FBXW7. Western blot analysis of Flag-FBXW7 immunoprecipitations revealed that the FBXW7 substrates KMT2D and c-Myc, as well the methyltransferase complex member WDR5, only co-precipitated with WT FBXW7 and that their abundance was increased by the Cullin-RING ligase inhibitor MLN4924 (Fig. 13 B). In

contrast, neither KMT2A nor SETD1A co-precipitated with FBXW7. This suggests, that KMT2D is specifically targeted and regulated by FBXW7, but not other proteins of the same family (Hänle-Kreidler et al. 2022).

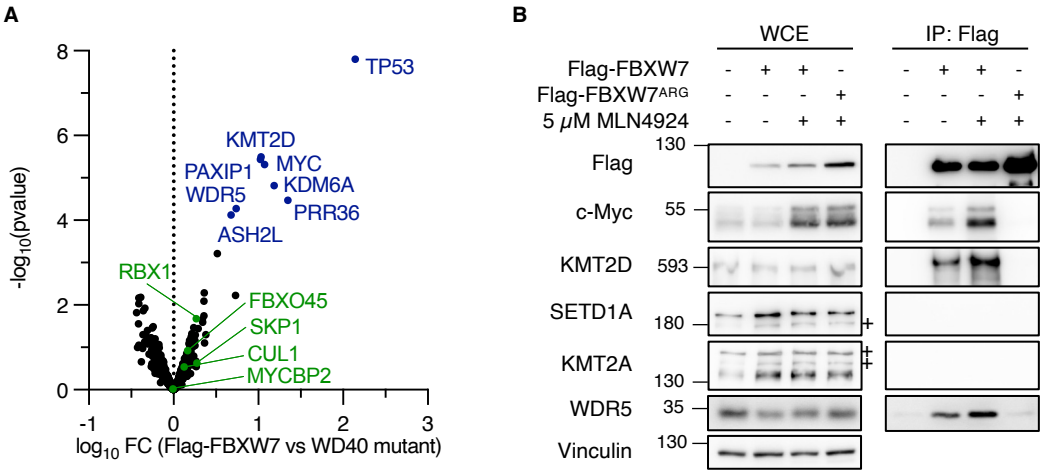

Figure 13: KMT2D and WDR5 were identified as FBXW7 candidate substrates.
I assessed an FBXW7 substrate screen performed by Kai Richter for FBXW7 candidate substrates. The screen was performed by Flag-IP/MS from HEK293T cells expressing Flag-FBXW7 or Flag-FBXW7 T439I, S462A, T463A, R465A. Eluates were analyzed by the EMBL Proteomics Core Facility using TMT10-plex labeling and mass spectrometry. Significance was determined via t-statistics using LIMMA R-package. Enrichments were considered significant when peptide quantity changed at least 50% and the adjusted p-value after Benjamini and Hochberg was below 5%, n=2. **A** Volcano plot showing proteins identified in the Flag-IP/MS approach. Proteins labeled in green are known FBXW7 complex members and regulators and proteins in blue are significantly enriched interactors. **B** HEK293T were transfected with Flag-FBXW7, Flag-FBXW7^{ARG} (R465H, R479Q, R505C) mutant or Flag-EV and proteins were expressed for 48 h. Where indicated, 5 µM MLN4924 (NAE1 inhibitor) were added for 5 h prior to harvest. Lysates were subjected to Flag-IP and inputs and eluates analyzed by Western blotting. FC – fold change, WCE – whole cell extract, IP – immunoprecipitation. + denotes non-specific bands. (Hänle-Kreidler et al. 2022)

3.3.2 Casein kinase 2 (CK2) regulates the binding of KMT2D to FBXW7

Saffie et al. recently established that KMT2D is a novel substrate of FBXW7 and that, like other FBXW7 substrates, it needs to be phosphorylated to establish an interaction with FBXW7. The interaction site was narrowed down to a N-terminal site between AA 535-727, but the kinase(s) regulating the interaction was/were not identified (Saffie et al. 2020). In order to investigate the phospho-regulation of KMT2D, I co-expressed an N-terminal fragment of KMT2D (1-1323) with GFP-FBXW7 in HEK293T cells and inhibited the activity of important cell-cycle regulating kinases by using small molecule inhibitors. Western blot analysis of the GFP-IPs showed that the interaction of the N-terminal fragment of KMT2D and GFP-FBXW7 was not affected by any of the kinase inhibitors but stabilized by the Cullin-RING ligase inhibitor MLN4924 (Fig. 14 A). As positive control, the interaction of FBXW7 and c-Myc was reduced by inhibition of GSK3β and stabilized by blockage of the mitotic kinases CDK1 and Aurora (Welcker

et al. 2022; Welcker et al. 2004; Yada et al. 2004). To narrow down kinases which could potentially phosphorylate KMT2D within the interaction interphase (535-727), I used the prediction tool NetPhos 3.1 (Blom et al. 1999). There are several potential FBXW7 degrons within this site and GSK3β was the most frequent hit for Serine and Threonine residues within this fragment. In addition, p38 MAPK and casein kinase 2 (CK2) appeared as hits in the prediction. I repeated the GFP-FBXW7 immunoprecipitations from Fig. 8 A but now used Losmapimod to block p38 MAPK (Fig. 14 B) or Apigenin to inhibit CK2 (Fig. 14 C). While p38 MAPK did not affect the interaction of KMT2D and FBXW7, Apigenin strongly reduced but not completely abolished their co-precipitation (Fig. 14 D).

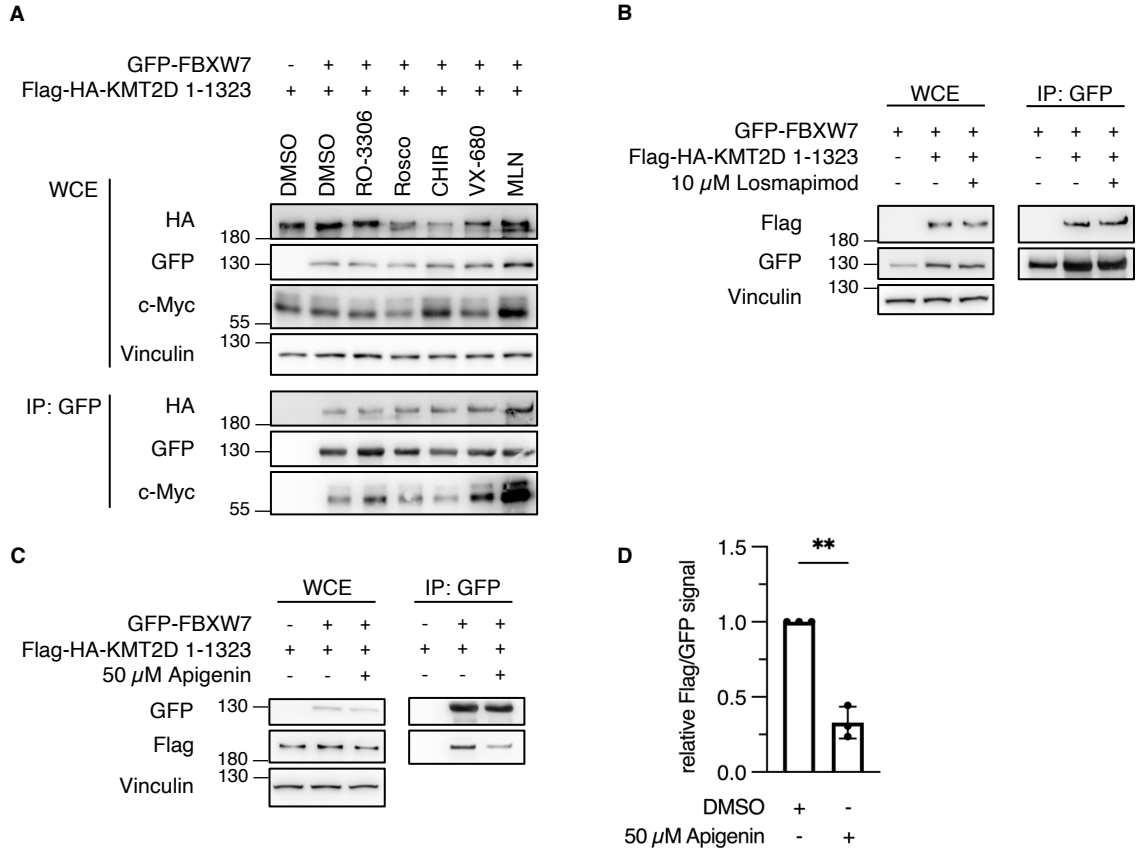

Figure 14: The interaction between FBXW7 and KMT2D is regulated by CK2.
A HEK293T cells were co-transfected with GFP or GFP-FBXW7 and Flag-HA-KMT2D AA 1-1323 fragment, containing the FBXW7 binding site, and proteins were overexpressed for 48 h. During the last 5 h, 10 µM RO-3306 (CDK1), 10 µM Roscovitine (CDK2), 5 µM CHIR99021, 500 nM VX-680 (Pan-Aurora), 1 µM MLN4924 (NAE1) or DMSO were added to the cultures. GFP-IPs were performed from lysates and inputs and eluates were analyzed by Western blotting. **B** HEK293T cells were co-transfected with GFP or GFP-FBXW7 and Flag-HA-KMT2D 1-1323 and proteins were overexpressed for 48 h. During the last 5 h, 10 µM Losmapimod (p38 MAPK) or DMSO were added to the cultures. GFP-IPs were performed from lysates and inputs and eluates were analyzed by Western blotting. **C** HEK293T cells were co-transfected with GFP or GFP-FBXW7 and Flag-HA-KMT2D 1-1323 and proteins were overexpressed for 48 h. During the last 5 h, 50 µM Apigenin (CK2) or DMSO were added to the cultures. GFP-IPs were performed from lysates and inputs and eluates were analyzed by Western blotting. **D** relative interaction was determined by normalizing Flag signal intensity to GFP signal intensity. ** $p > 0.01$, unpaired, two-tailed student's t-test with Welch's correction, n=3. WCE – whole cell extract, IP – immunoprecipitation.

To further validate this finding, I co-expressed the single subunits of CK2 with FBXW7 and KMT2D 1-1323 to assess their influence on the interaction of KMT2D and FBXW7. CK2 is a tetramer of two β regulatory and two α and/or α' catalytic subunits (Litchfield 2003). GFP-FBXW7 immunoprecipitations and Western blotting revealed that the interaction with the N-terminal fragment of KMT2D was stabilized by single co-expression of each CK2 subunit (Fig. 15 A). In addition, I transfected HEK293T cells with only Flag-HA-KMT2D 1-1323 and the single CK2 subunits and performed Flag-IPs and Western blotting to analyze the interaction of the KMT2D fragment with endogenous FBXW7 (Fig. 15 B). Overexpression of the CK2 subunits increased the interaction between KMT2D 1-1323 and endogenous FBXW7 to a similar extent compared to the GFP-FBXW7 IP. These results indicate that the multi-subunit kinase CK2 is required for the binding of KMT2D to FBXW7

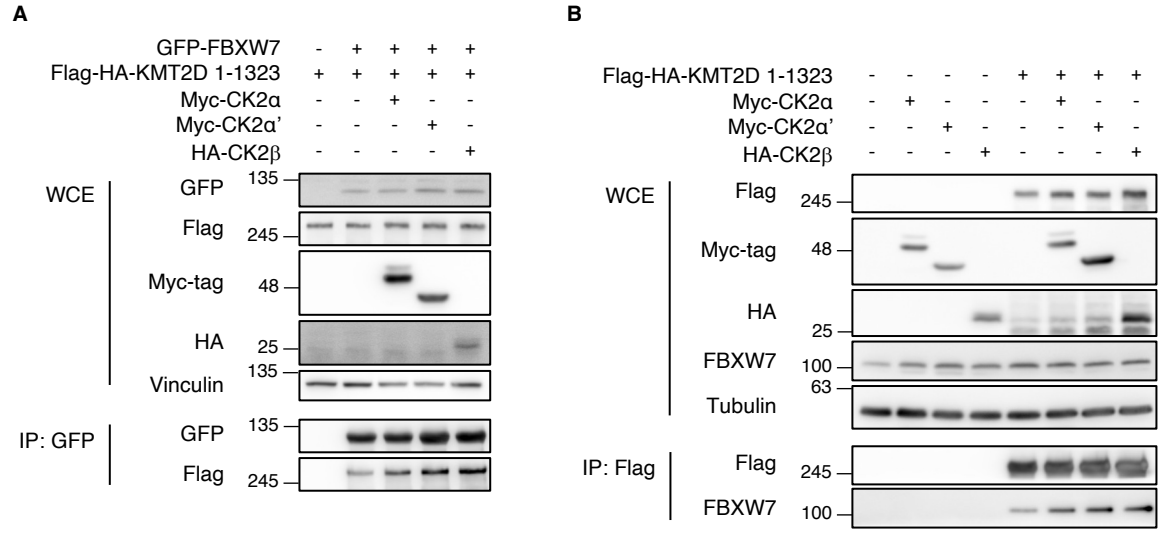

Figure 15: Overexpression of Casein kinase 2 subunits promotes FBXW7/KMT2D interaction.
A HEK293T cells were co-transfected with GFP or GFP-FBXW7, Flag-HA-KMT2D 1-1323 and tagged CK2 subunits. Proteins were overexpressed for 48 h and GFP-IPs performed from the lysates. Inputs and eluates were analyzed by Western blotting. **B** HEK293T were co-transfected with Flag-EV or Flag-HA-KMT2D 1-1323 and tagged CK2 subunits. Proteins were overexpressed for 48 h and Flag-IPs performed from the lysates. Inputs and eluates were analyzed by Western blotting. WCE – whole cell extract, IP – immunoprecipitation.

3.3.3 KMT2D does not affect mitotic slippage

KMT2D has recently been published as novel substrate of FBXW7 and its levels were shown to be inversely correlated to chemoresistance in different cancer types (Saffie et al. 2020; Dawkins et al. 2016; Li et al. 2019; Lv et al. 2019).

To investigate if KMT2D depletion could also promote mitotic cell death in response to antimicrotubule drugs, I depleted KMT2D alone and in combination with FBXW7 from U2OS cells using siRNAs and determined their mitotic cell fates in the presence of nocodazole (Fig. 16 A). Intriguingly, KMT2D protein levels were not upregulated by FBXW7 depletion in U2OS cells, despite that Saffie et al. 2020 characterized KMT2D as a substrate of FBXW7. Knockdown of FBXW7 significantly increased slippage from 68.0±7.1 % to 82.7±3.1%, while KMT2D depletion alone or in combination with FBXW7 depletion did not affect mitotic cell cate. These results show that KMT2D does not regulate chemoresistance by mitotic slippage (Hänle-Kreidler et al. 2022).

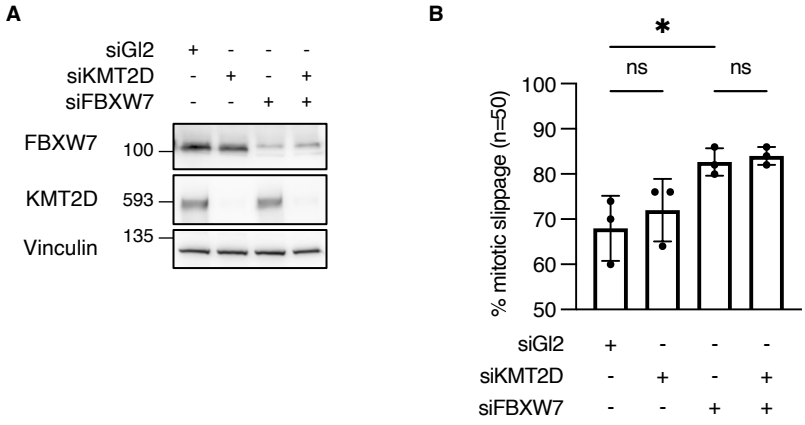

Figure 16: The FBXW7 substrate KMT2D does not affect mitotic slippage.
A U2OS cells were transfected with siRNA targeting Gl2, KMT2D or FBXW7, either alone or in combination, for 72 h. Cell lysates were analyzed by Western blotting. **B** 830 nM nocodazole were added to U2OS from **A** and mitotic cell fates were assessed by live-cell imaging. For each condition, n=50 cells were analyzed. * $p < 0.05$, ns $p > 0.05$, one-way ANOVA with Tukey post-hoc test, n=3. (Hänle-Kreidler et al. 2022).

3.3.4 WDR5 protein levels are regulated by FBXW7

Another interesting protein, which specifically co-precipitated with FBXW7 WT but not with the WD40 mutant, was the WD repeat-containing protein 5 (WDR5). WDR5 is a cellular multitasker and plays an important role in multiple protein complexes, including the KMT2D methyltransferase complex and several cellular pathways (Guarnaccia and Tansey 2018). Intriguingly, WDR5 was reported to regulate the expression of several oncogenes and has been implicated in both, cell cycle regulation and chemoresistance (Chen et al. 2015; Dai et al. 2020; Neilsen et al. 2018). Since FBXW7 targets a number

of oncogenes and cell cycle regulators for degradation, I decided to characterize WDR5 as a putative substrate of FBXW7. In contrast to KMT2D, for which I could not observe upregulation by Western blotting, it was shown that WDR5 protein levels were upregulated in HCT116 FBXW7 knockout (KO) cell lines as well as in HeLa cells after depletion of FBXW7 with siRNA (Richter 2017).

I reproduced these findings by Richter 2017 using the two colorectal carcinoma cell lines HCT116 and DLD1 and compared WDR5 protein levels between the WT cell line and FBXW7 knockouts by Western blotting (Fig. 17 A-D). WDR5 was clearly stabilized in response to FBXW7 KO in both cell lines. An upregulation of protein levels can be caused by deregulation at multiple steps. For example, increased transcription or altered post-translational modifications can equally affect the abundance of a target protein. As SCF-FBXW7 is an E3 ligase, it regulates its substrates by post-translational modification. In order to exclude any changes in protein expression, I performed quantitative real-time PCR (qPCR) and compared relative WDR5 expression between HCT116 WT and FBXW7 KO, as well as between HeLa with or without FBXW7 knockdown by siRNA (Fig. 17 E & F). WDR5 expression was not affected by FBXW7-deficieny. These results support the hypothesis that FBXW7 regulates WDR5 protein levels via ubiquitylation (Hänle-Kreidler et al. 2022).

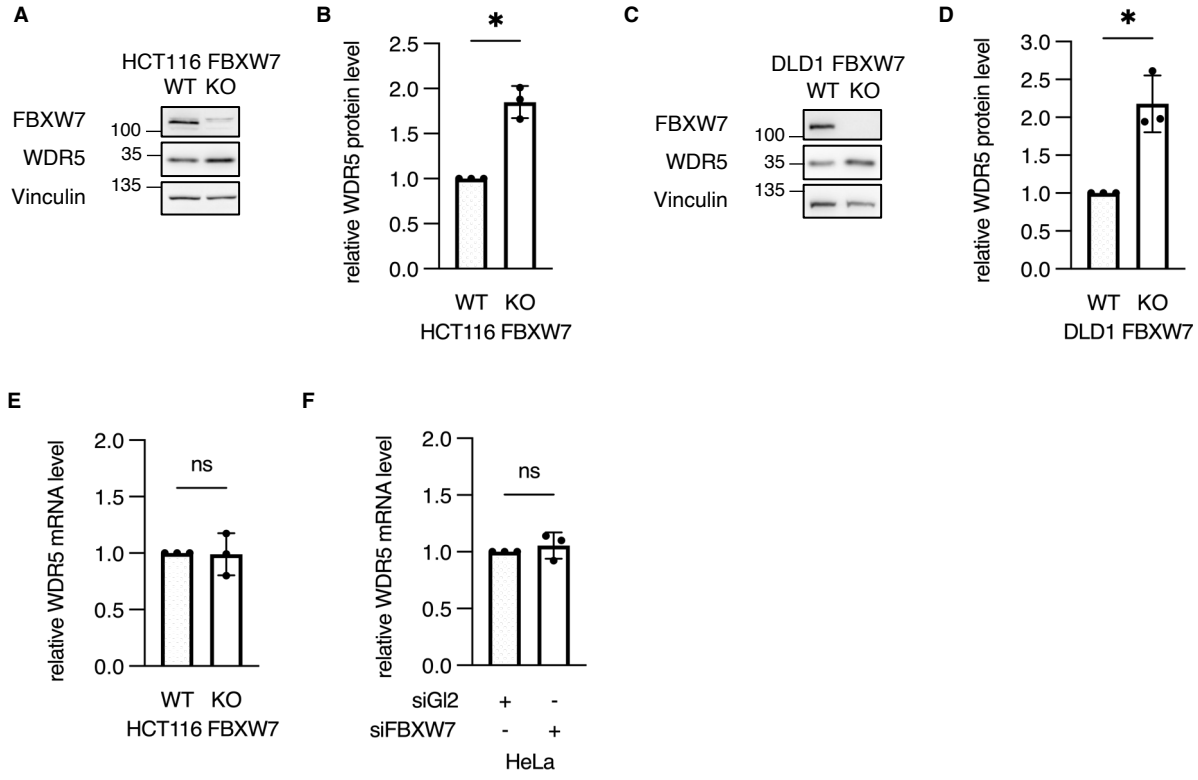

Figure 17: WDR5 protein levels are upregulated when FBXW7 is depleted from cells.
A Lysates from HCT116 WT or FBXW7 KO were analyzed by Western blotting. **B** WDR5 signal intensity from **A** was normalized to Vinculin signal intensity. * $p < 0.05$, unpaired, two-way student's t-test with Welch's correction, n=3. **C** Lysates from DLD1 WT or FBXW7 KO were analyzed by Western blotting. **D** WDR5 signal intensity from **C** was normalized to Vinculin signal intensity. * $p < 0.05$, unpaired, two-way student's t-test with Welch's correction, n=3. **E** total RNA was extracted from HCT116 WT and FBXW7 KO cell pellets and relative WDR5 mRNA levels were determined by qPCR using the ΔΔCT method with GAPDH for normalization. ns $p > 0.05$, unpaired, two-way student's t-test with Welch's correction, n=3. **F** HeLa cells were transfected with siRNA targeting FBXW7 or Gl2 for 72 h. total RNA was extracted from cell pellets and relative WDR5 mRNA levels were determined by qPCR using the ΔΔCT method with GAPDH for normalization. ns $p > 0.05$, unpaired, two-way student's t-test with Welch's correction, n=3. WT – wild type, KO – knockout. (Hänle-Kreidler et al. 2022).

3.3.5 WDR5 protein levels and binding to FBXW7 are regulated independent of the WDR5 WIN site and c-Myc

KMT2D has recently been described as a novel substrate of SCF-FBXW7 (Saffie et al. 2020). Therefore, the co-precipitation of WDR5 with FBXW7 and upregulation by FBXW7 depletion could be due to its interaction with KMT2D. Following the same rationale, the known FBXW7 substrate c-Myc interacts specifically with the WBM site of WDR5 and might therefore play a role in the regulation of WDR5 (Thomas et al. 2015).

To test if FBXW7 binding to WDR5 occurs independently of KMT2D, I depleted KMT2D from HCT116 WT and FBXW7 KO cell lines and analyzed WDR5 protein levels by Western blotting (Fig. 18 A & B). Although KMT2D was almost completely depleted from both cell lines, WDR5 protein levels were not altered compared to the respective siGl2-transfected controls. Since WDR5 directly interacts with KMT2D in methyltransferase complexes, I performed GFP-immunoprecipitations of WT and the WIN site mutant WDR5 F133A to assess a possible indirect relationship between FBXW7 and WDR5 (Piunti and Shilatifard 2016). F133 is required for the interaction of WDR5 with KMT2 methyltransferases (Guarnaccia et al. 2021; Patel et al. 2008b). Western blotting revealed that co-precipitation of KMT2D was almost completely abolished, while the amount of FBXW7 did not change (Fig. 18 C & D). In addition, I transfected HEK293T with Flag-FBXW7 alone or in combination with Myc tagged c-Myc to investigate whether c-Myc could facilitate the co-precipitation of WDR5 with FBXW7. Overexpression of c-Myc decreased the amount of WDR5 in the Flag-FBXW7 IP compared to the EV control (Fig. 18 E). Together, these results suggest that WDR5 can interact with FBXW7 independently of either KMT2D and c-Myc and that KMT2D abundance does not influence WDR5 protein levels (Hänle-Kreidler et al. 2022).

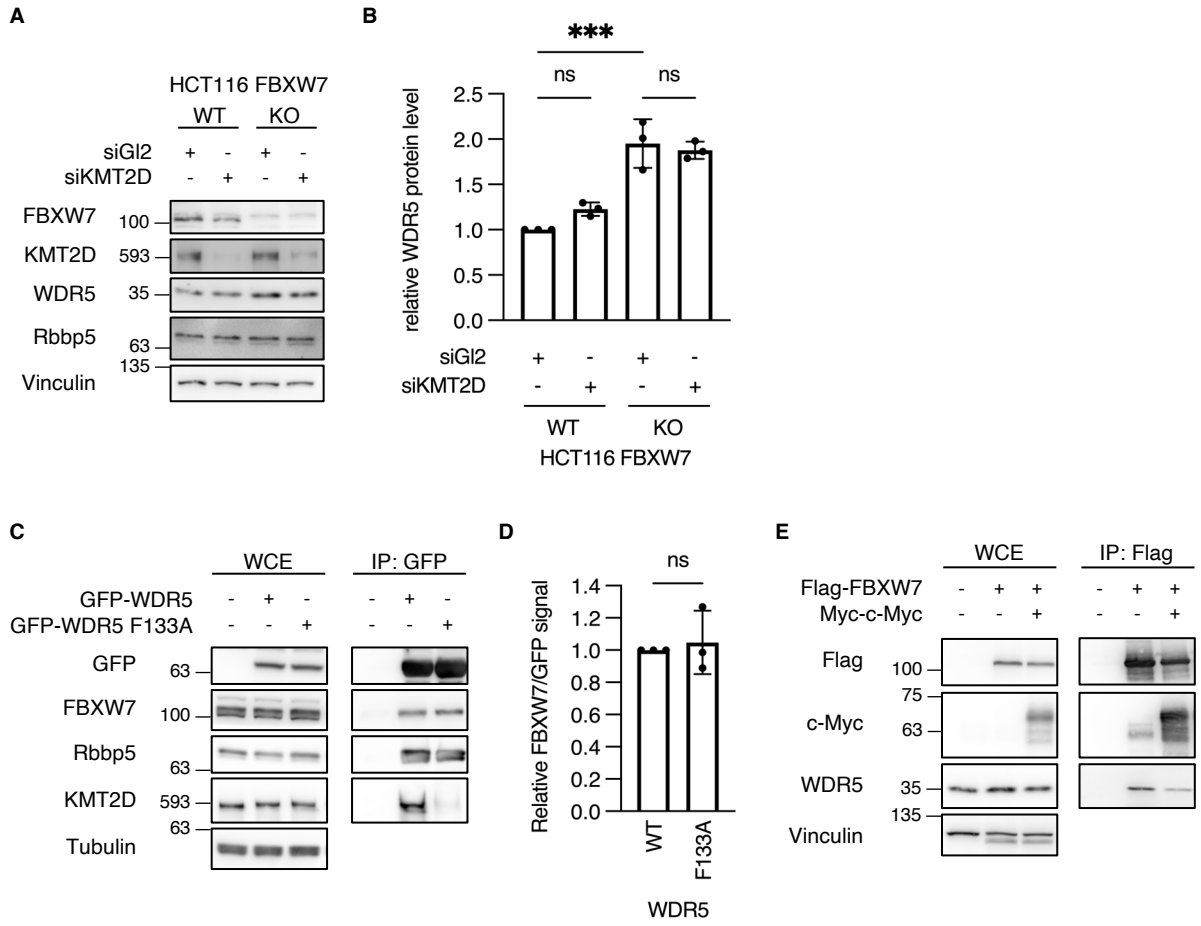

Figure 18: WDR5 protein levels are regulated by FBXW7 independently of KMT2D and c-Myc.
A HCT116 WT and FBXW7 KO were transfected with siRNA targeting KMT2D or Gl2 for 72 h. Cell lysates were analyzed by Western blotting. **B** WDR5 signal intensities from **A** were normalized to Vinculin signal intensities. *** $p < 0.001$, ns $p > 0.05$, one-way ANOVA with Tukey post-hoc test, n=3. **C** HEK293T cells were transfected with GFP, GFP-WDR5 or GFP-WDR5 F133A mutant and proteins were overexpressed for 24 h. GFP-IPs were performed from cell lysates and inputs and eluates analyzed by Western blotting. **D** FBXW7 signal intensities from **C** were normalized to GFP signal intensities. ns $p > 0.05$, unpaired, two-tailed student's t-test with Welch's correction, n=3. **E** HEK293T were transfected with Flag-FBXW7 and Myc-c-Myc, either alone or in combination. Flag-EV and Myc-EV were used as controls and proteins were overexpressed for 48 h. Flag-IPs were performed from cell lysates and inputs and eluates analyzed by Western blotting. WCE – whole cell extract, IP – immunoprecipitation. (Hänle-Kreidler et al. 2022).

3.3.6 WDR5 and FBXW7 interact *in-vivo* and *in-vitro*

Interactions between FBXW7 and substrates are facilitated by direct binding of the WD40 domain of FBXW7 to conserved phosphodegrons located on substrates (Hao et al. 2007; Welcker et al. 2013). Since the co-precipitation of FBXW7 and WDR5 did not require a functional WIN site or c-Myc (Fig. 18), I assessed the direct interaction of FBXW7 and WDR5 both *in-vivo* and *in-vitro*.

I precipitated endogenous WDR5 or FBXW7 from lysates of HEK293T cells using specific antibodies and used normal mouse or rabbit IgG as controls. Western blotting of the eluates revealed that FBXW7 specifically co-precipitated with endogenous

WDR5 and vice-versa, while the control antibodies bound little or none of the proteins (Fig. 19 A). In order to assess whether both proteins can directly interact, I expressed recombinant GST-WDR5 in *E. coli* Rosetta and affinity purified the protein from the lysate. I received recombinant His-FBXW7/Skp1 complex purified from Sf21 from Frauke Melchior (ZMBH, Heidelberg). GST or GST-WDR5 were incubated with His-FBXW7/SKP1 and GST pulldowns were performed. His-FBXW7 was pulled down with GST-WDR5 but not with GST alone (Fig. 19 B), indicating a direct interaction between both proteins *in-vitro* and *in-vivo* (Hänle-Kreidler et al. 2022).

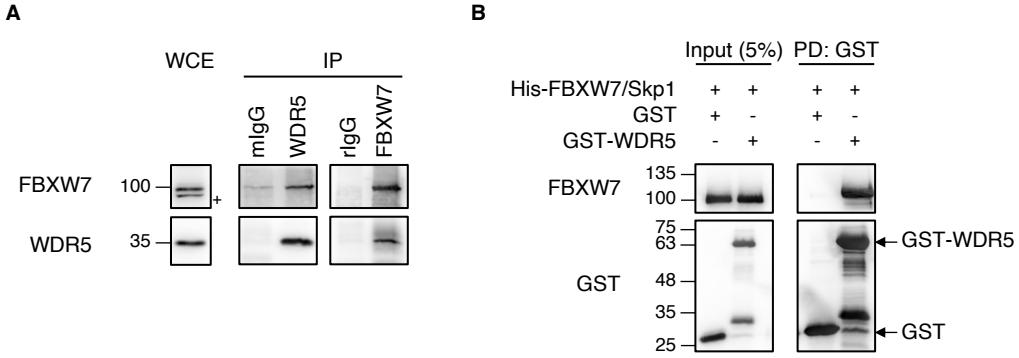

Figure 19: WDR5 and FBXW7 interact with each other *in-vivo* and *in-vitro*.
A Endogenous WDR5 or FBXW7 were precipitated from HEK293T lysates using mouse anti-WDR5 and rabbit anti-FBXW7 antibodies overnight. Antibodies were captured using protein G (mouse) or protein A (rabbit) Sepharose for 2 h. Inputs and eluates were analyzed by Western blotting. **B** GST or GST-WDR5 were expressed in *E. coli* Rosetta (DE3) and purified with immobilized glutathione CL-4B Sepharose. 10 µg of GST-WDR5 or equimolar amounts of GST were incubated with 10 µg of His-FBXW7/Skp1 for 2 h, followed by GST-pulldown with immobilized glutathione CL-4B Sepharose. Inputs and eluates were analyzed by Western blotting. WCE – whole cell extract, IP – immunoprecipitation, PD – pulldown, + denotes a non-specific band. (Hänle-Kreidler et al. 2022).

3.3.7 WDR5 protein stability is regulated by FBXW7

SCF-FBXW7 activity negatively affects the protein stability of the majority of its substrates by Lys48 ubiquitylation. Polyubiquitylation of substrates on Lys48 leads to their recognition by the 26S proteasome, followed by their degradation (Hough et al. 1986). Because I observed upregulated WDR5 protein levels in the absence of FBXW7, I investigated whether FBXW7 negatively affects WDR5 protein stability.

I transfected DLD1 WT and FBXW7 KO cell lines with Flag-WDR5 and blocked their protein translation with the ribosomal inhibitor cycloheximide. Analysis of protein levels by Western blotting revealed that Flag-WDR5 protein levels decreased in both cell lines over time, however more rapidly in FBXW7 proficient DLD1 WT cells with a half-life of 8.8 h compared 20.7 h in the FBXW7 KO cell line (Fig. 20 A & B). Next, I inhibited

protein degradation by the 26S proteasome with MG132 to assess whether Flag-WDR5 degradation is mediated by the UPS. Flag-WDR5 was stabilized in DLD1 cells treated with MG132 compared to the DMSO control (Fig. 20 C & D). To assess if the stability of endogenous WDR5 is similarly affected by the FBXW7 status, I performed cycloheximide chase experiments with DLD1 WT and FBXW7 KO cell lines and analyzed WDR5 protein levels by Western blotting (Fig. 20 E). FBXW7 deletion also stabilized endogenous WDR5 compared to the WT cell line. In addition, the time-course data showed that endogenous WDR5, with a half-life of 25.4 h, was more stable compared to Flag-WDR5, which showed a half-life of 8.8 h (Fig. 20 B & F). Because FBXW7 requires the activity of the SCF backbone to regulate the stability of its substrates, I investigated whether a FBXW7 F-box deletion mutant, which cannot bind to SKP1, would show a dominant-negative effect. HEK293T cells were transfected with Flag-FBXW7 ΔF-box, Flag-FBXW7 WT or Flag-EV and WDR5 protein stability was again assessed by a cycloheximide chase and Western blotting (Fig. 20 G). The half-life of WDR5 reduced by half from 29.5 h to 16.0 h in HEK293T cells with Flag-FBXW7 WT overexpression (Fig. 20 H). In contrast, the half-life of endogenous WDR5 was doubled by Flag-FBXW7 ΔF-box compared to the Flag-EV control. These results showed that WDR5 is a stable protein and that SCF-FBXW7 regulates WDR5 protein stability via the ubiquitin-proteasome system (Hänle-Kreidler et al. 2022).

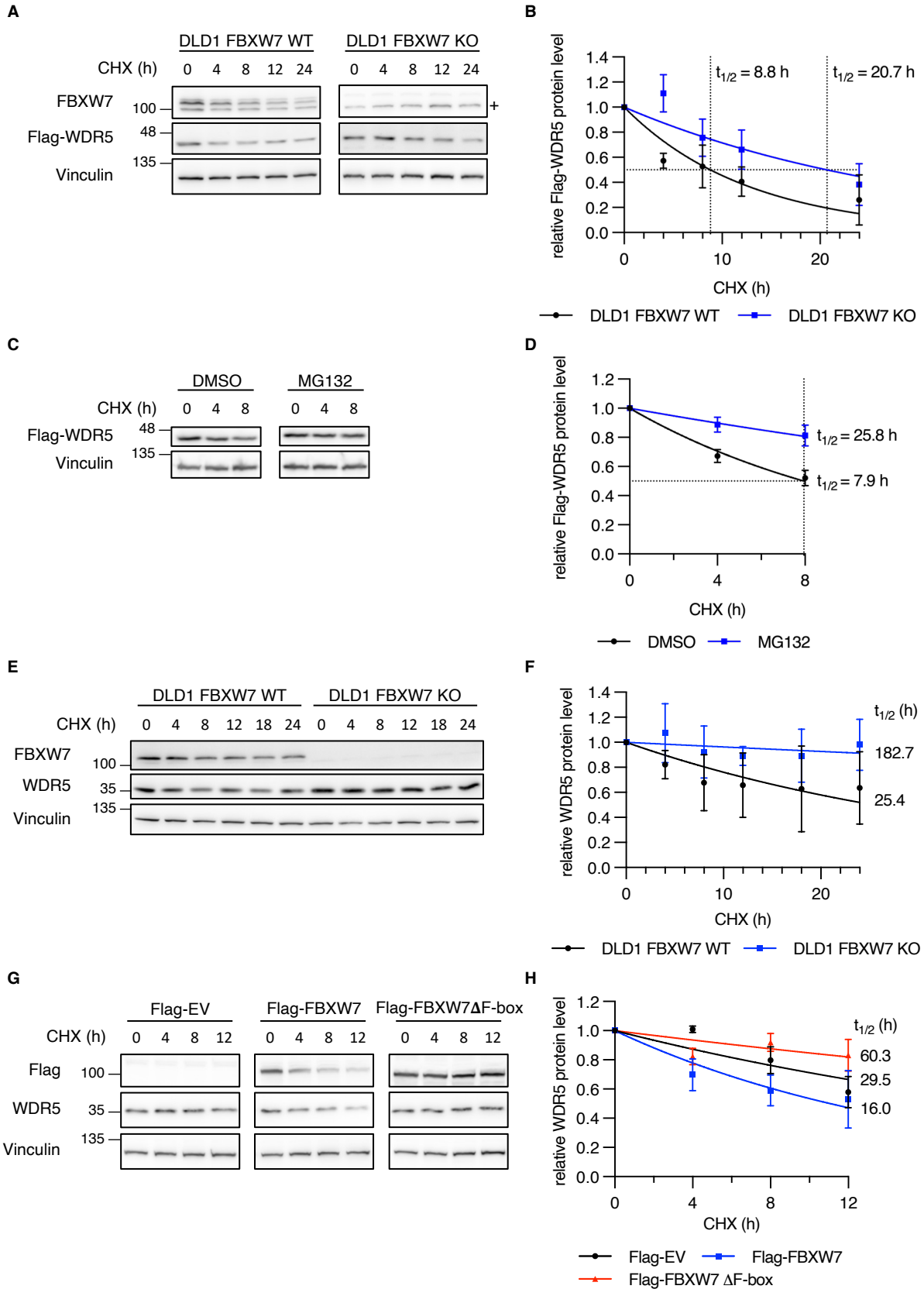
A
DLD1 FBXW7 WT
DLD1 FBXW7 KO
CHX (h)
0 4 8 12 24
0 4 8 12 24
FBXW7
Flag-WDR5
Vinculin
100
48
135
+
B
relative Flag-WDR5 protein level
t1/2 = 8.8 h
t1/2 = 20.7 h
CHX (h)
DLD1 FBXW7 WT
DLD1 FBXW7 KO
C
DMSO
MG132
CHX (h)
0 4 8
0 4 8
Flag-WDR5
Vinculin
48
135
D
relative Flag-WDR5 protein level
t1/2 = 25.8 h
t1/2 = 7.9 h
CHX (h)
DMSO
MG132
E
DLD1 FBXW7 WT
DLD1 FBXW7 KO
CHX (h)
0 4 8 12 18 24 0 4 8 12 18 24
FBXW7
WDR5
Vinculin
100
35
135
F
relative WDR5 protein level
t1/2 (h)
182.7
25.4
CHX (h)
DLD1 FBXW7 WT
DLD1 FBXW7 KO
G
Flag-EV
Flag-FBXW7
Flag-FBXW7ΔF-box
CHX (h)
0 4 8 12
0 4 8 12
0 4 8 12
Flag
WDR5
Vinculin
100
35
135
H
relative WDR5 protein level
t1/2 (h)
60.3
29.5
16.0
CHX (h)
Flag-EV
Flag-FBXW7
Flag-FBXW7 ΔF-box

Figure 20: WDR5 protein stability is regulated by FBXW7.
A DLD1 WT and FBXW7 KO cell lines were transfected with Flag-WDR5 and the protein was overexpressed for 24 h. 300 µg/mL cycloheximide were added and cells were harvested at the indicated time-points. Lysates were analyzed by Western blotting. **B** Flag signal intensities form **A** were normalized to Vinculin signal intensities. Time-course data was fitted to a one-phase decay model to determined protein half-lives, n=3. **C** DLD1 WT were transfected with Flag-WDR5 and the protein was overexpressed for 24 h. 10 µM MG132 or DMSO were added for 3 h before cultures were treated with 300 µg/mL cycloheximide. Cells were harvested at the indicated time-points and lysates were analyzed by Western blotting. **D** Flag signal intensities form **C** were normalized to Vinculin signal intensities. Time-course data was fitted to a one-phase decay model to determined protein half-lives, n=3. **E** DLD1 WT and FBXW7 KO cells were treated with 300 µg/mL cycloheximide and cells were harvested at the indicated time-points. Lysates were analyzed by Western blotting. **F** WDR5 signal intensities from **E** were normalized to Vinculin signal intensities. Time-course data was fitted to a one-phase decay model to determined protein half-lives, n=3. **G** HEK293T cells were transfected with Flag-FBXW7, Flag-FBXW7 ΔF-box (284-321 deletion) mutant or Flag-EV and proteins were overexpressed for 48. 100 µg/mL cycloheximide were added and were cells harvested at the indicated time-points. Lysates were analyzed by Western blotting. **H** WDR5 signal intensities from **G** were normalized to Vinculin signal intensities. Time-course data was fitted to a one-phase decay model to determined protein half-lives, n=3. (Hänle-Kreidler et al. 2022).

3.3.8 SCF-FBXW7 promotes WDR5 ubiquitylation

SCF-FBXW7 facilitates polyubiquitylation of its substrates with Lys48 or Lys63 ubiquitin chains, which promotes proteasomal degradation or translocation of the conjugated protein (Yumimoto and Nakayama 2020). While FBXW7 facilitates substrate interaction, the RING E3 ligase RBX1 transfers ubiquitin from the E2 ubiquitin-conjugating enzyme to lysine residues on the bound substrate.

Because I observed WDR5 destabilization by FBXW7 (Fig. 17 & Fig. 20), I assessed whether FBXW7 could also promote polyubiquitylation of WDR5. I performed an *in-vivo* ubiquitylation assay by transfecting HEK293T cells with Flag-WDR5, HA-Ubiquitin and GFP-FBXW7 WT or mutant versions as control. The cells were treated with MG132 to inhibit the 26S proteasome and consequentially accumulate ubiquitylated proteins. Flag-WDR5 immunoprecipitates were analyzed by Western blotting. Flag-WDR5 was readily ubiquitylated without FBXW7 overexpression, however FBXW7 WT overexpression slightly increased WDR5 ubiquitylation while the ΔF-box and the WD40 domain mutant did not (Fig. 21 A). In addition, I expressed Flag-FBXW7 or Flag-FBXW7^{ARG} mutant and Myc-CUL1 in HEK293T cells and immobilized the SCF-complexes on α-Flag M2 beads. Using these complexes, I performed *in-vitro* ubiquitylation assays of recombinant GST-WDR5 or GST-c-Myc purified from *E. coli*. Purified E1, E2 and ubiquitin were kind gifts from Frauke Melchior (ZMBH, Heidelberg). Western blotting revealed that GST-WDR5 and GST-c-Myc were stronger ubiquitylated by SCF-FBXW7 but not by SCF-FBXW7^{ARG}. In addition, this difference was also visible for GST-WDR5 without the addition of GSK3β. These results suggest

that FBXW7 promotes the proteasomal degradation of WDR5 by polyubiquitylation (Hänle-Kreidler et al. 2022).

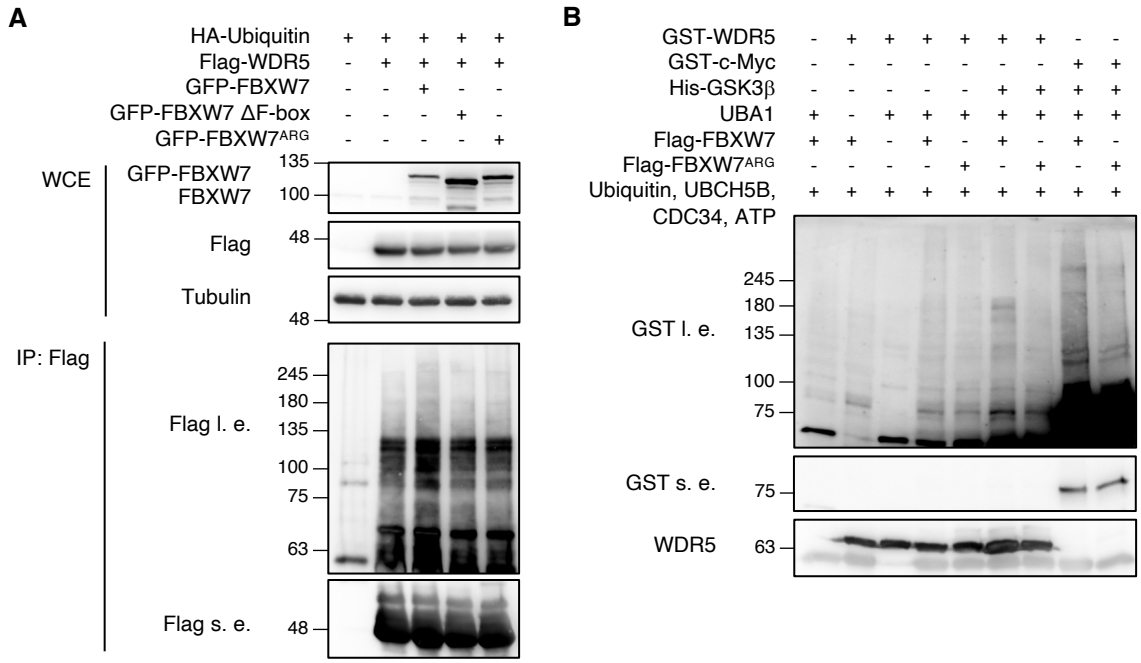

Figure 21: FBXW7 promotes WDR5 ubiquitylation.
A HEK293T cells were co-transfected with HA-Ubiquitin, Flag-EV or Flag-WDR5 and GFP or GFP-FBXW7 WT and mutant versions (ΔF-Box: 284-321 deletion, ARG: R465H, R479Q, R505C). Proteins were overexpressed for 24 h and the 26S proteasome was inhibited with 10 µM MG132 for 5 h. Flag-IPs were performed from lysates and inputs and eluates were analyzed by Western blotting. **B** HEK293T cells were co-transfected with Flag-FBXW7 or Flag-FBXW7^{ARG} and Myc-Cullin1 and proteins were overexpressed for 48 h. Flag-IPs were performed from lysates to immobilize the complexes on α-Flag M2 beads. *In-vitro* ubiquitylation assays of 200 nM GST-WDR5 or GST-c-Myc contained 170 nM UBA1, 250 nM UBCH5B and CDC34, 30 µM Ubiquitin, 200 nM His-GSK3β, 5 mM ATP and immobilized FBXW7 constructs as indicated. Reactions were incubated at 37°C for 90 min and analyzed by Western blotting. WCE – whole cell extract, IP – immunoprecipitation, l. e. – long exposure, s. e. – short exposure. (Hänle-Kreidler et al. 2022).

3.3.9 GSK3β and FBXW7 cooperate to regulate WDR5 protein levels

Target engagement of FBXW7 requires the phosphorylation of conserved phospho-degrons on its substrates. This interaction then enables ubiquitylation by the E3 ligase activity of the SCF complex and proteasomal degradation (Won and Reed 1996; Welcker et al. 2003). A set of different kinases has been shown to facilitate phosphorylation of degrons but GSK3β plays a critical role in targeting many cancer-relevant substrates (Lan and Sun 2021).

I transfected HEK293T cells with Flag-FBXW7 and performed Flag-immunoprecipitations but treated the α-Flag-M2 beads with λ-phosphatase to dephosphorylate the bound protein fraction. Western blot analysis showed that WDR5 co-precipitation with Flag-FBXW7 was strongly reduced by phosphatase-treatment

(Fig. 22 A). In addition, the reduction in the amounts of co-precipitated KMT2D and c-Myc, two FBXW7 substrates which have been reported to require phosphorylation for their interaction with FBXW7, showed that the λ-phosphatase was active (Welcker et al. 2004; Yada et al. 2004; Saffie et al. 2020). In order to assess whether GSK3β activity is required for the interaction between FBXW7 and WDR5, I transfected HEK293T cells with GFP-WDR5 and blocked GSK3β activity with the small molecule inhibitor CHIR99021. The amount of co-precipitated FBXW7 was markedly reduced by GSK3β inhibition compared to the control (Fig. 17 B & C). These results indicate that WDR5 is a substrate of GSK3β and that phosphorylation is required for the interaction with FBXW7 *in-vivo* (Hänle-Kreidler et al. 2022).

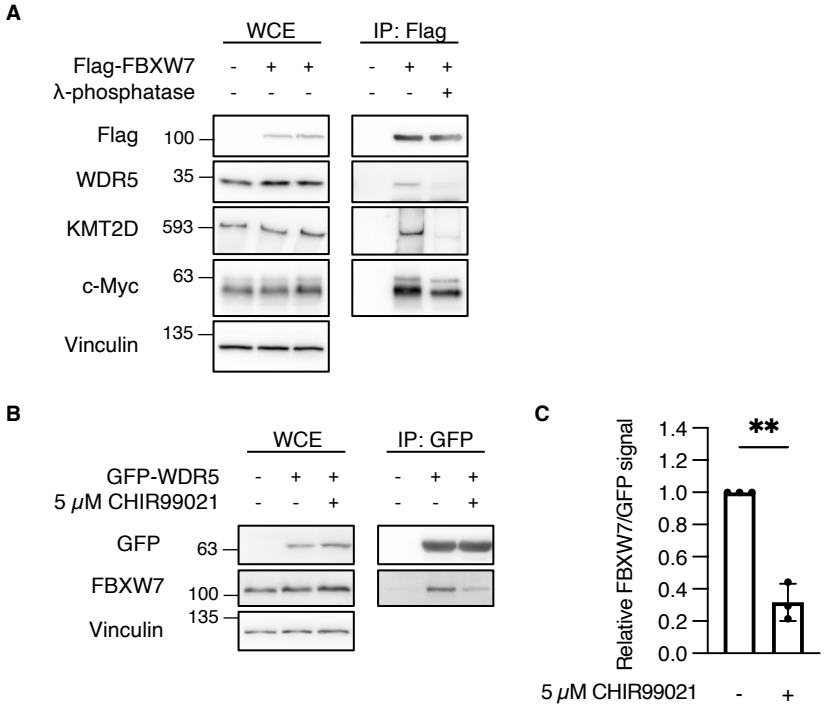

Figure 22: The interaction between FBXW7 and WDR5 is regulated by phosphorylation.
A HEK293T were transfected with Flag-FBXW7 or Flag-EV and proteins were overexpressed for 48 h. Flag-IPs were performed from lysates. The indicated IP was dephosphorylated with λ-phosphatase for 3 h. Inputs and eluates were analyzed by Western blotting. **B** HEK293T cells were transfected with GFP or GFP-WDR5 and proteins were overexpressed for 24 h. 5 µM CHIR99021 or DMSO were added for 5 h before harvest. GFP-IPs were performed from cell lysates and inputs and eluates were analyzed by Western blotting. **C** FBXW7 signal intensities from **B** were normalized to GFP signal intensities. ** $p < 0.01$, unpaired, two-tailed student's t-test with Welch's correction, n=3. WCE – whole cell extract, IP – immunoprecipitation. (Hänle-Kreidler et al. 2022).

In the next step, I investigated if GSK3β could also influence WDR5 protein levels. Depletion of GSK3β in U2OS cells and Western blot analysis of the cell lysates showed that WDR5 was stabilized in the absence of GSK3β (Fig. 23 A & B). As GSK3β needs to directly interact with its substrates to facilitate phosphorylation, I performed GFP-

immunoprecipitations of GFP-WDR5 to assess the interaction with endogenous or co-expressed GSK3β (Dajani et al. 2003). Western blot analysis revealed that both, endogenous and overexpressed GSK3β, co-precipitated more with GFP-WDR5 in comparison to the GFP control (Fig. 23 C). Since GSK3β activity was required for the interaction of WDR5 with FBXW7 *in-vivo* (Fig. 22 B), I performed *in-vivo* ubiquitylation assays to assess if GSK3β inhibition could reduce WDR5 ubiquitylation by FBXW7. Flag-WDR5 was stronger ubiquitylated by FBXW7 overexpression compared to the control and this increased ubiquitylation was strongly reduced by the small molecule inhibitor CHIR99021 (Fig. 23 D). As a control, the CRL inhibitor MLN4924 completely abolished WDR5 ubiquitylation by FBXW7. Taken together, these results suggest that GSK3β cooperates with FBXW7 to regulate WDR5 protein levels via the ubiquitin-proteasome system (Hänle-Kreidler et al. 2022).

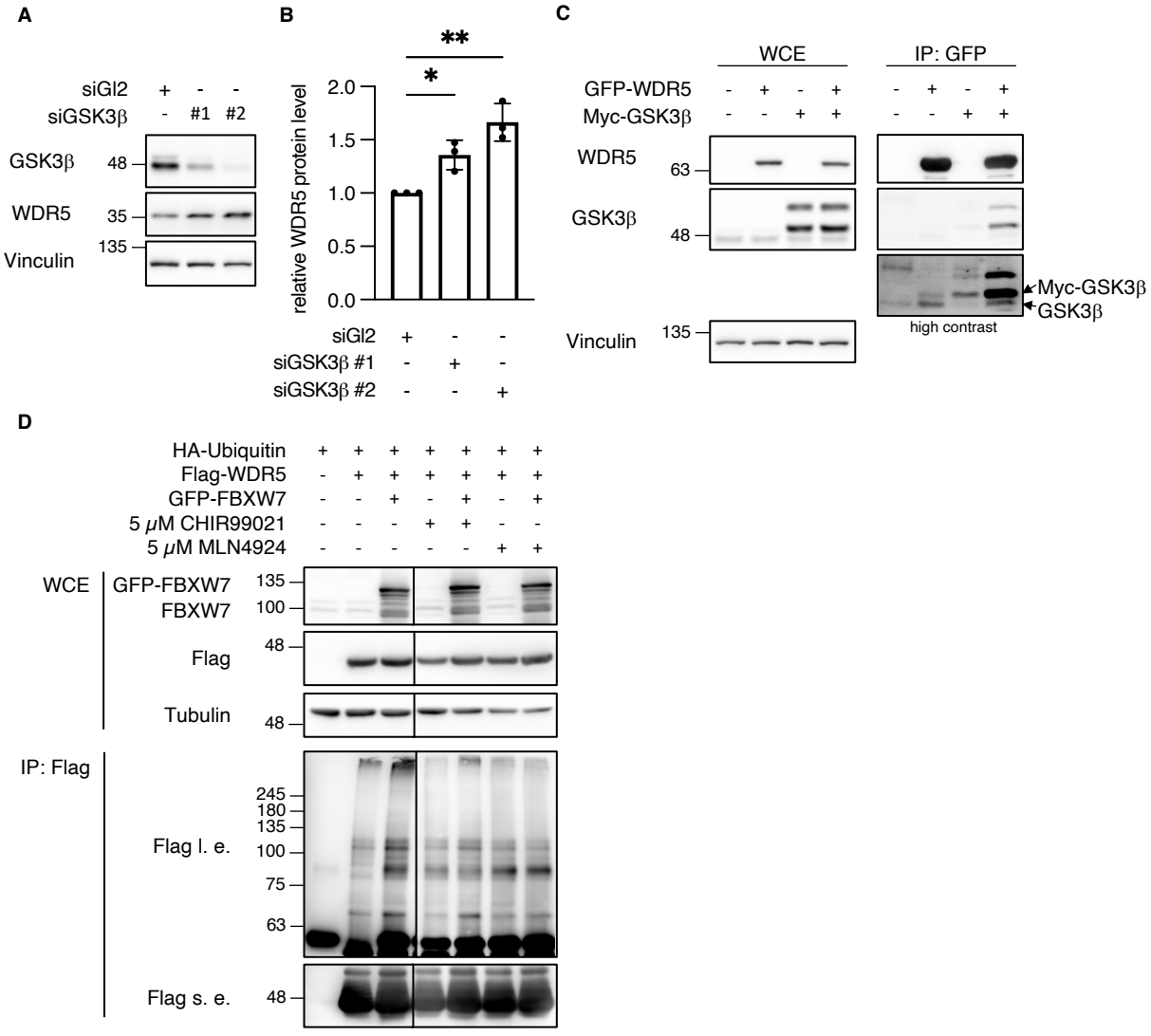

Figure 23: Regulation of WDR5 protein levels by FBXW7 is dependent on GSK3β.
A U2OS cells were transfected with siRNA targeting GSK3β or Gl2 for 72 h. Lysates were analyzed by Western blotting. **B** WDR5 signal intensities from **A** were normalized to Vinculin signal intensities. ** $p < 0.01$, * $p < 0.05$, one-way ANOVA with Tukey post-hoc test, n=3. **C** HEK293T cells were transfected with GFP-WDR5 and Myc-GSK3β either alone or in combination. GFP and Myc-EV were used as controls. Proteins were overexpressed for 24 h and GFP-IPs were performed from lysates. Inputs and eluates were analyzed by Western blotting. **D** HEK293T cells were co-transfected with HA-Ubiquitin, Flag-EV or Flag-WDR5 and GFP or GFP-FBXW7 WT and mutant versions (ΔF-Box: 284-321 deletion, ARG: R465H, R479Q, R505C). Proteins were overexpressed for 24 h, followed by addition of 5 µM CHIR99021 (GSK3β), 5 µM MLN4924 (NAE1) or DMSO for 4 h. 10 µM MG132 were then added to all dishes for 5 h. Flag-IPs were performed from lysates and inputs and eluates were analyzed by Western blotting. The image was cropped at the line to remove additional experimental settings. WCE – whole cell extract, IP – immunoprecipitation, l. e. – long exposure, s. e. – short exposure. (Hänle-Kreidler et al. 2022).

3.3.10 Two putative phosphodegrons within WDR5 are not responsible for FBXW7 binding

SCF-FBXW7 interacts with its substrates via conserved phoshodegron motifs on the substrates (Davis et al. 2014). I used ELM to predict possible FBXW7 degrons and GSK3β consensus sites on the WDR5 primary structure (Kumar et al. 2022). Only two sites matched the FBXW7 binding motif, of which one was also a predicted GSK3β site (Fig. 24 A). I applied site-directed mutagenesis to mutate the first serine or threonine amino acid residues of the motifs and performed GFP-WDR5 IPs to assess their interaction with endogenous FBXW7. Western blotting revealed that both mutants co-precipitated similar amounts of FBXW7 compared to the GFP-WDR5 WT control. Therefore, I conclude that none of the predicted FBXW7 motifs are required for the interaction.

To narrow down the binding site on WDR5, I generated eight deletion mutants with deletions of either a WD40 repeat or the N-terminal disordered domain (Fig. 24 C). Co-expression of these deletion mutants with Myc-FBXW7 followed Flag-immunoprecipitation showed that more FBXW7 protein co-eluted when either the disordered domain of WDR5 or the WD40 repeats 1 or 2 were deleted (Fig. 24 D). Flag-WDR5 ΔWD40 6 (AA 256-296 deletion) co-precipitated the least amount of FBXW7 but did not completely abolish the interaction. However, there is no putative FBXW7 degron motif located within this site. These results suggest that the WD40 repeat 6 of WDR5 binds to FBXW7 independent of a FBXW7 degron motif.

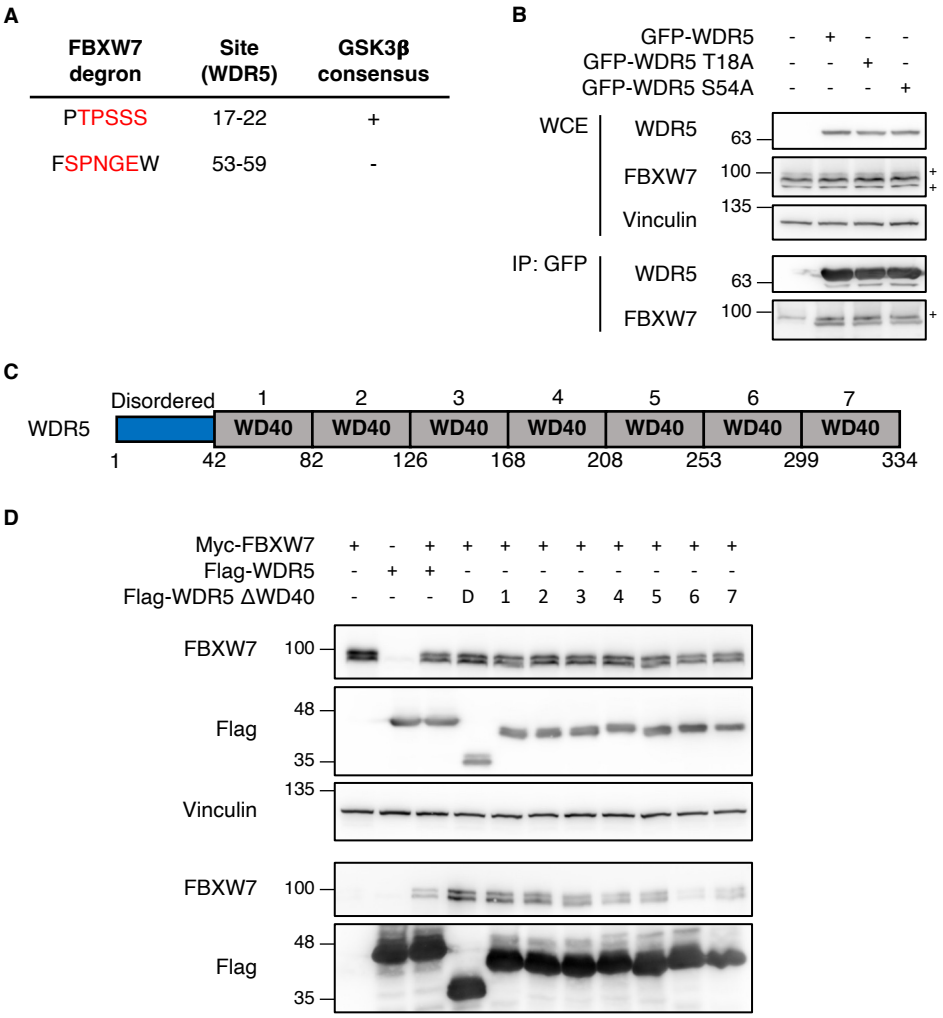

Figure 24: The interaction between FBXW7 and WDR5 is not mediated by two predicted FBXW7 degron sequences.
A FBXW7 degron sequences [TS],P,X,X,[TSED] and GSK3β consensus sites were predicted on the WDR5 amino acid sequence using the Eukaryotic Linear Motif resource ELM. Highlighted amino acids indicate putative degron sequences. **B** HEK293T cells were transfected with GFP or GFP-WDR5 and mutant versions and proteins were overexpressed for 24 h. GFP-IPs were performed from cell lysates and inputs and eluates analyzed by Western blotting. **C** Schematic illustration of WDR5 domain architecture. **D** HEK293T were transfected with Myc-FBXW7 and Flag-WDR5 or Flag-WDR5 deletion mutants, either alone or in combination, and proteins were overexpressed for 24 h. Flag-EV and Myc-EV were used as controls. Flag-IPs were performed from cell lysates and inputs and eluates were analyzed by Western blotting. WCE – whole cell extract, IP – immunoprecipitation, + denotes non-specific bands, D – disordered

3.4 The FBXW7 substrates WDR5 and Cyclin E1 are involved in chemotherapy resistance

3.4.1 WDR5 overexpression promotes mitotic slippage

WDR5 had previously been linked to chemoresistance (Chen et al. 2015; Neilsen et al. 2018). In addition, it is involved in mitotic progression and the transcriptional regulation of key mitotic proteins like Cyclin B1 and CDC20 (Chen et al. 2015; Zhou et

al. 2021). These findings suggest that WDR5 might be an interesting candidate to assess its influence on chemoresistance via mitotic slippage.

Therefore, I generated stable U2OS T-Rex cell lines with inducible expression of WT WDR5 or the WIN site mutant WDR5 F133A to assess whether WDR5 overexpression alone could also influence mitotic slippage (Fig. 25 B & D). I performed live-cell imaging with both cell lines in the presence of nocodazole to induce prolonged mitotic arrest and quantified the fraction of cells undergoing mitotic slippage. Examples of mitotic slippage and apoptosis are shown in figure 25 A. While overexpression of WT WDR5 significantly increased mitotic slippage from 62.7±4.2% to 72.0±2.0% (Fig. 25 C), the WIN site mutant did not: 86.0±0.0% to 84.0±5.3% (Fig. 25 D). Despite that WDR5 had been shown to regulate the expression of important mitotic proteins and regulators of apoptosis, the overexpression of the WDR5 constructs did not alter the duration from mitotic entry to slippage or cell death (Fig. 25, C & D). These data show that upregulation of WDR5 can also facilitate chemoresistance in form of mitotic slippage and that the WDR5 WIN site might play an important role (Hänle-Kreidler et al. 2022).

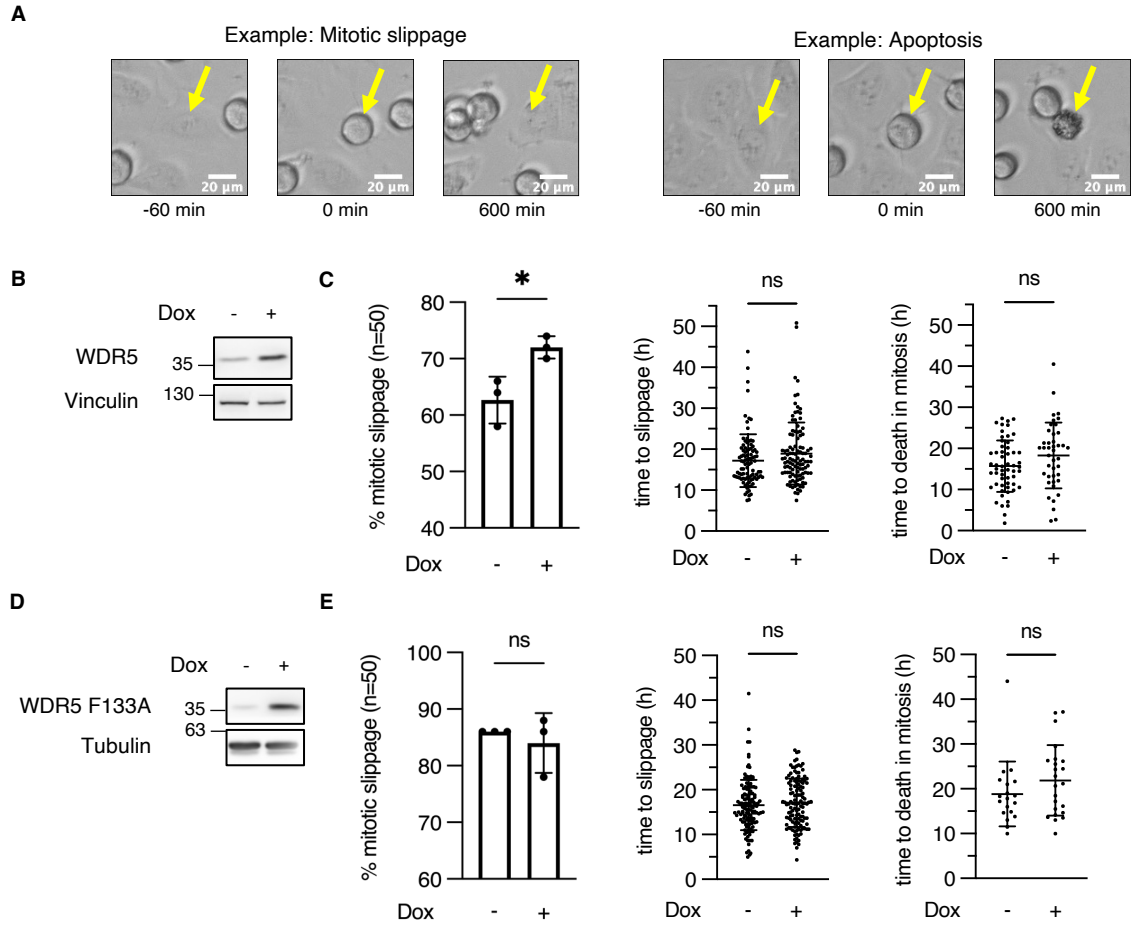

Figure 25: WDR5 overexpression increases mitotic slippage and requires functional WIN site. **A** Representative still-images from live-cell imaging of U2OS T-Rex WDR5 showing different mitotic cell fates in presence of 830 nM nocodazole. Cells undergoing mitotic arrest followed by slippage or mitotic cell death are indicated. **B** U2OS T-Rex WDR5 were incubated with or without 2 µg/mL doxycycline for 96 h to induce WDR5 expression. Cell lysates were analyzed by Western blotting. **C** 830 nM nocodazole were added to U2OS T-Rex WDR5 from **B** and mitotic cell fates were assessed by live-cell imaging. The time from mitotic entry to slippage or cell death was quantified for each analyzed cell. For each condition, n=50 cells were analyzed. * $p < 0.05$, ns $p > 0.05$, unpaired, two-tailed students t-test, n=3. **D** U2OS T-Rex WDR5 F133A were incubated with or without 2 µg/mL doxycycline for 96 h to induce WDR5 F133A expression. Cell lysates were analyzed by Western blotting. **E** 830 nM nocodazole were added to U2OS T-Rex WDR5 F133A from **D** and mitotic cell fates were assessed by live-cell imaging. The time from mitotic entry to slippage or cell death was quantified for each analyzed cell. For each condition, n=50 cells were analyzed. ns $p > 0.05$, unpaired, two-tailed students t-test, left chart with Welch's correction, n=3. Dox – doxycycline. (Hänle-Kreidler et al. 2022).

3.4.2 Cyclin E1 overexpression promotes mitotic slippage

To date, a vast number of substrates of FBXW7 have been described in the literature and many of these proteins function in cell cycle regulation and control (Yumimoto and Nakayama 2020). Of these substrates, only Mcl-1 and FOXM1 were previously shown to promote mitotic slippage (Wertz et al. 2011; Vaz et al. 2021). In addition, depletion of Cyclin E1 or Aurora kinase A reduced drug-induced polyploidy of FBXW7 knockout HCT116 but overexpression of Cyclin E1 alone was insufficient to phenocopy FBXW7 knockout (Finkin et al. 2008). Cyclin E1 has been suggested to promote mitotic slippage but this hypothesis was not confirmed by live-cell imaging (Bagheri-Yarmand et al. 2010).

In order to test this hypothesis, I used U2OS tet-Off Cyclin E1 cells provided by Jiri Bartek (Karolinska Institute, Stockholm, Sweden) to compare Cyclin E1 overexpression and FBXW7 knockdown with control treatments (Bartkova et al. 2005). Cyclin E1 was upregulated by FBXW7 depletion and doxycycline withdrawal to similar extend and was even further upregulated by the combination of both treatments (Fig. 26 A). In the presence of nocodazole, mitotic slippage was significantly increased from 45.3±2.3% to 60.7±5.0% by knockdown of FBXW7. Overexpression of Cyclin E1 also increased mitotic slippage significantly to 56.7±3.1%, while the combination of siFBXW7 and Cyclin E1 overexpression did not have any further effect (Fig. 26 B). None of the experimental conditions affected the duration from mitotic entry to slippage. Only the additional depletion of FBXW7 in Cyclin E1 overexpressing cells delayed mitotic cell death significantly compared to Cyclin E1 overexpression alone (Fig. 26 B). These results show that also Cyclin E1 overexpression alone can increase mitotic slippage to a similar degree as shown for FBXW7 depletion (Hänle-Kreidler et al. 2022).

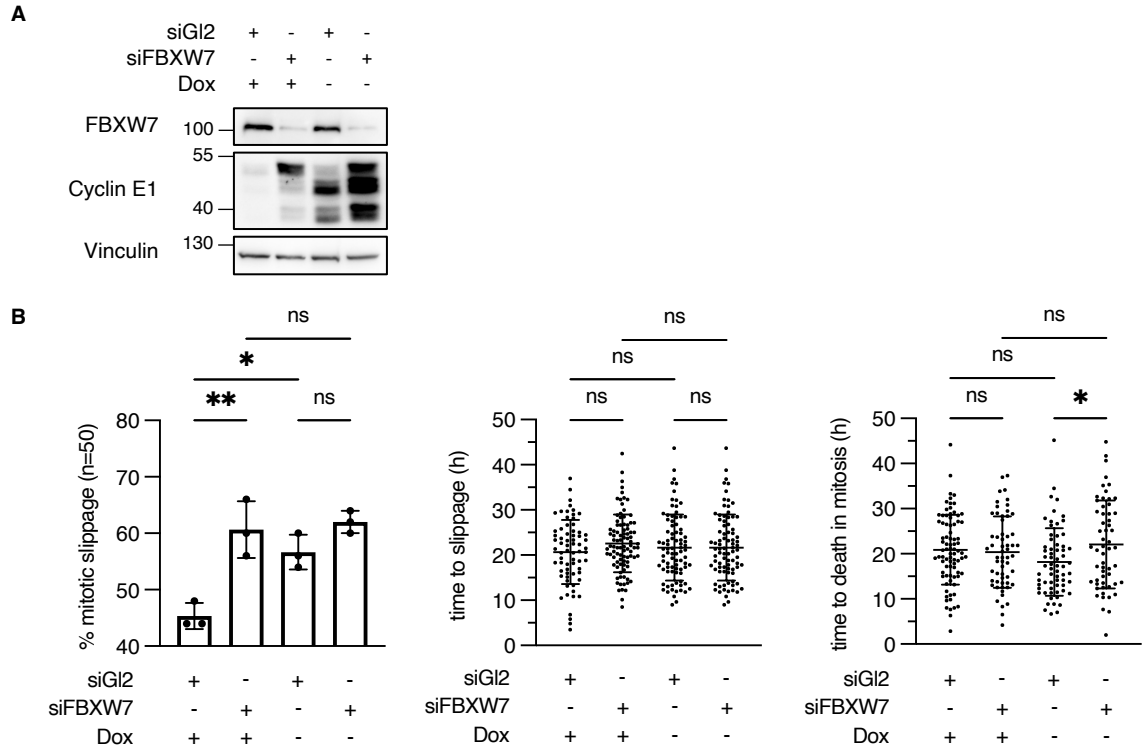

Figure 26: Cyclin E1 overexpression promotes mitotic slippage.
A U2OS tet-Off Cyclin E1 were incubated with or without 2 µg/mL doxycycline for 96 h. In parallel, cells were transfected with siRNA targeting Gl2 or FBXW7 for 72 h. Cell lysates were analyzed by Western blotting. **B** 830 nM nocodazole were added to U2OS tet-Off Cyclin E1 from **A** and mitotic cell fates were assessed by live-cell imaging. The time from mitotic entry to slippage or cell death was quantified for each analyzed cell. For each condition, n=50 cells were analyzed. ** $p < 0.01$, * $p < 0.05$, ns $p > 0.05$, one-way ANOVA with Tukey post-hoc test, n=3. Dox – doxycycline. (Hänle-Kreidler et al. 2022).

3.4.3 WDR5 is required for increased chemoresistance after loss of FBXW7

My results show that both WDR5 and Cyclin E1 were able to promote mitotic slippage when overexpressed in U2OS cells (Fig. 25 & 26). FBXW7 depletion most likely increases mitotic slippage by effects and functions of its deregulated substrates. Therefore, I assessed whether co-depletion of WDR5 or Cyclin E1 could rescue the effect of FBXW7. I performed live-cell imaging experiments of U2OS cells transfected with different combinations of siRNAs and quantified the mitotic cell fates. Western blot analysis revealed that the siRNA transfections strongly reduced the protein levels of their targets (Fig. 27 A). FBXW7 depletion increased mitotic slippage from 70.0±2.0% to 82.0±2.0% but knockdown of Cyclin E1, WDR5 or the combination of both did not affect mitotic slippage compared to the siGl2-transfected control (Fig. 27 B). The knockdown of Cyclin E1 alone was insufficient to rescue the increased slippage by siFBXW7. In contrast, WDR5 depletion significantly reduced mitotic slippage to

68.7±4.6% and the combination of WDR5 and Cyclin E1 depletion decreased the rate even further to 64.0±2.0%. Again, I quantified the durations from mitotic entry to mitotic slippage or cell death to investigate changes in prolonged mitotic arrest. Strikingly, none of the conditions affected the durations of the prolonged mitotic arrest (Fig. 27, C & D). These results show that WDR5 depletion rescues the increase in mitotic slippage caused by loss of FBXW7 and that the combination of WDR5 and Cyclin E1 depletion has an even more pronounced effect (Hänle-Kreidler et al. 2022).

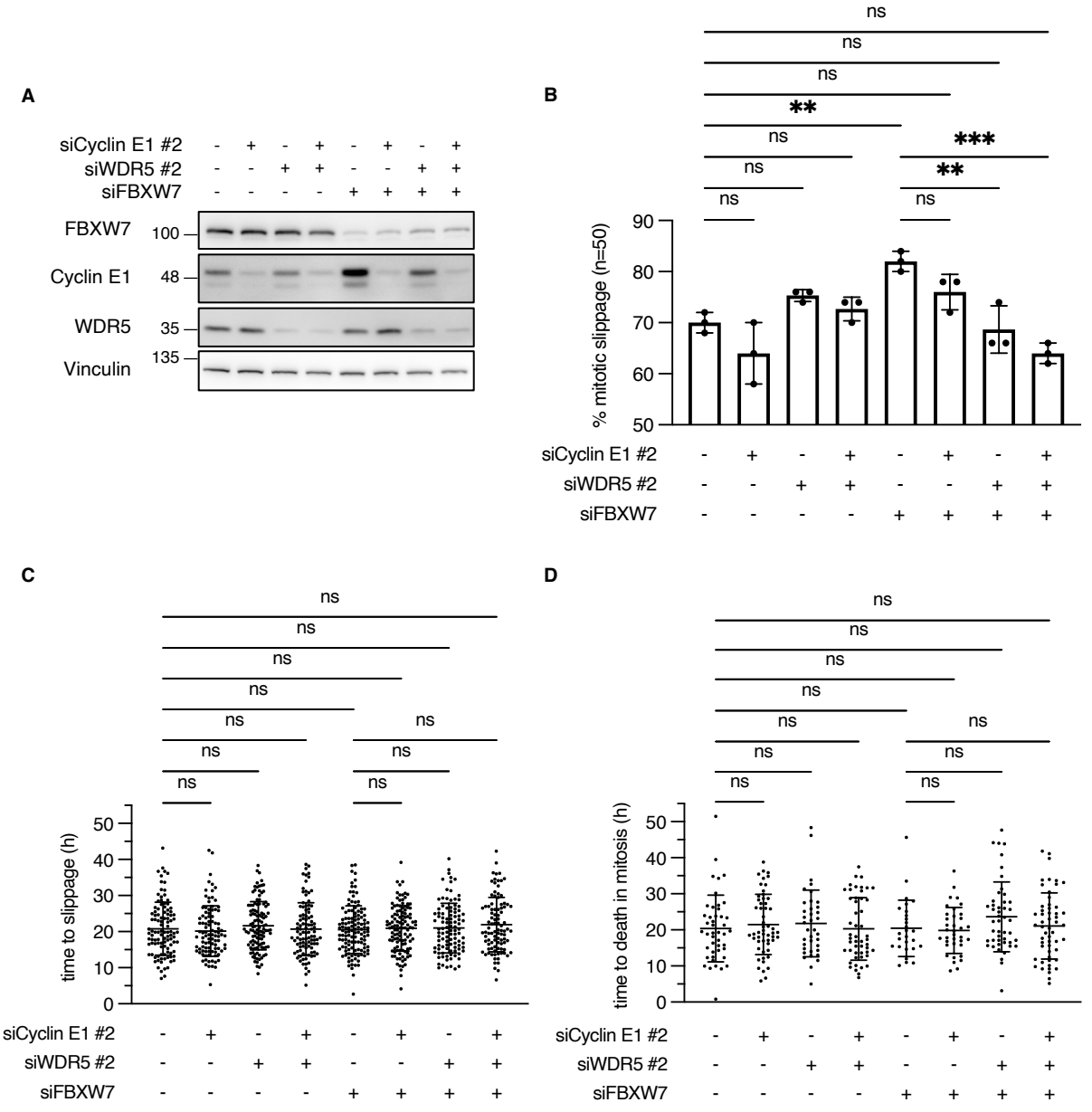

Figure 27: WDR5 depletion rescues the increase in chemoresistance after FBXW7 knockdown. **A** U2OS cells were transfected with siRNA targeting Cyclin E1, WDR5, FBXW7 or Gl2, either alone or in combination, for 72 h. Cell lysates were analyzed by Western blotting. **B** 830 nM nocodazole were added to U2OS from **A** and mitotic cell fates were assessed by live-cell imaging. The time from mitotic entry to slippage **C** or cell death **D** was quantified for each analyzed cell. For each condition, n=50 cells were analyzed. *** $p < 0.001$, ** $p < 0.01$, * $p < 0.05$, ns $p > 0.05$, one-way ANOVA with Tukey post-hoc test, n=3. (Hänle-Kreidler et al. 2022).

3.4.4 WDR5 and Cyclin E1 are required for polyploidization of FBXW7-depleted cancer cells in response to treatment with antimicrotubule drugs

FBXW7 ablation has early been connected to chromosomal instability and the formation of polyploid cells caused by deregulation of its substrates (Rajagopalan et al. 2004; Finkin et al. 2008; Takada et al. 2017). In addition, Finkin et al. showed that FBXW7 inactivation leads to significantly more mitotic slippage and an increased formation of polyploid cells after treatment with antimicrotubule drugs, such as Taxol or vinblastine, and that Cyclin E1 and Aurora kinase A are required for this effect (Finkin et al. 2008).

To assess whether WDR5 depletion could affect drug-induced polyploidy of FBXW7 inactivated cancer cells, I used an adapted protocol from Wertz et al. 2011 to quantify the ploidy of HCT116 cells by PI-staining and flow cytometry (Fig. 28 A) (Wertz et al. 2011). I depleted Cyclin E1, WDR5 or KMT2D from HCT116 FBXW7 KO cells to compare their DNA content with HCT116 WT and HCT116 FBXW7 KO which were transfected with siGl2 as control. The knockdown-efficiency was controlled for each set-up by Western blotting (Fig. 28 C). All siRNA transfections led to a strong reduction in the protein levels of their respective targets. The cells were synchronized in G1/S phase with thymidine to reduce differences in cell cycle progression and then released into Taxol or vincristine containing medium. The first cells entered mitosis usually 10 h after release from the block. The cell ploidy histograms of Taxol-treated HCT116 reveal that the main population of HCT116 WT cells was arrested with a 4N DNA content equal to cells in G2/M-phase (Fig. 28 B). In comparison, HCT116 FBXW7 KO cells also contained a major population with 4N DNA content but the formation of polyploid cells was visible as a right-sided shoulder in the histogram. Cyclin E1 was knocked down as a control, as it had already been shown to influence drug-induced polyploidy (Finkin et al. 2008).

I observed that WDR5 depletion in the HCT116 FBXW7 KO cell line significantly reduced the fraction of polyploid cells (>4N) after treatment with Taxol or vincristine compared to the siGl2 control (Fig. 28 B, D & E). The effect size of WDR5 depletion was similar to that of siCyclin E1. Interestingly, the combined knockdown of WDR5 and Cyclin E1 did not further reduce polyploidization in the presence of Taxol or vincristine. Depletion of the methyltransferase KMT2D did not affect ploidy, showing that the observed effects are specific for WDR5. These results suggest that WDR5 is a novel player in drug-induced polyploidization of FBXW7-deficient cancer cells and that

WDR5 and Cyclin E1 might act via similar mechanisms, as their combined depletion did not have synergistic effects (Hänle-Kreidler et al. 2022).

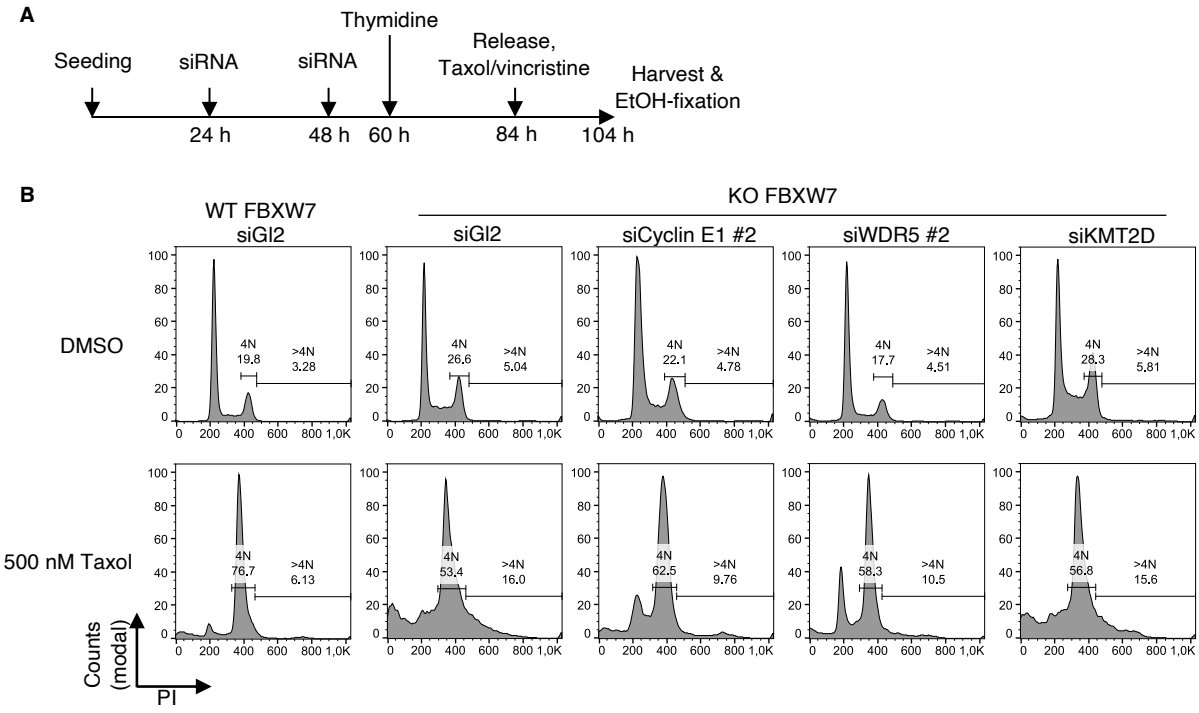
A
Seeding
siRNA
siRNA
Thymidine
Release,
Taxol/vincristine
Harvest &
EtOH-fixation
24 h
48 h
60 h
84 h
104 h
B
WT FBXW7
siGl2
KO FBXW7
siGl2
siCyclin E1 #2
siWDR5 #2
siKMT2D
DMSO
500 nM Taxol
4N 19.8
>4N 3.28
4N 26.6
>4N 5.04
4N 22.1
>4N 4.78
4N 17.7
>4N 4.51
4N 28.3
>4N 5.81
4N 76.7
>4N 6.13
4N 53.4
>4N 16.0
4N 62.5
>4N 9.76
4N 58.3
>4N 10.5
4N 56.8
>4N 15.6
Counts (modal)
PI
C
HCT116 FBXW7 WT KO
siCyclin E1 #1
siCyclin E1 #2
siWDR5 #1
siWDR5 #2
siKMT2D
FBXW7
Cyclin E1
WDR5
KMT2D
Vinculin
100
48
35
35
593
135
D
500 nM Taxol
ns
****
***
**
****
****
**
% > 4N cells
HCT116 FBXW7 WT KO
siCyclin E1 #1
siCyclin E1 #2
siWDR5 #1
siWDR5 #2
siKMT2D
E
100 nM vincristine
ns
***
**
*
****
****
***
% > 4N cells
HCT116 FBXW7 WT KO
siCyclin E1 #1
siCyclin E1 #2
siWDR5 #1
siWDR5 #2
siKMT2D

Figure 28: WDR5 and Cyclin E1 are equally required for drug-induced polyploidy in response to anti-microtubule drugs.
A Schematic depicting the experimental design of transfection and synchronization protocol to determine drug-induced polyploidy of HCT116 WT and FBXW7 KO cell lines. Cells were transfected with siRNA at the indicated time-points, synchronized with 2 mM thymidine for 24 h and released into medium containing 500 nM Taxol or 100 nM vincristine. 20 h after release, cells were harvested and fixed with Ethanol. **B** HCT116 WT and FBXW7 KO cell lines were transfected with siRNA targeting Gl2, Cyclin E1, WDR5 or KMT2D, either alone or in combination, and were synchronized following the protocol from **A**. Ploidy was determined using PI-staining and flow-cytometry. Non-synchronized cells were used as reference. Cells with 4N genomic content (G2/M-phase) and cells with more than 4N were quantified. **C** Lysates of non-synchronized HCT116 WT and KO FBXW7 from **B** were analyzed by Western blotting. **D** The fraction of >4N HCT116 WT and KO FBXW7 cells from **B** was quantified after mitotic arrest with 500 nM Taxol or **E** 100 nM vincristine. **** $p < 0.0001$, *** $p < 0.001$, ** $p < 0.01$, * $p < 0.05$, ns $p > 0.05$, one-way ANOVA with Tukey post-hoc test, n=3-4. WT – wild type, KO – knockout, PI – propidium iodide. (Hänle-Kreidler et al. 2022).

3.4.5 WDR5 depletion overrides Mcl-1 upregulation caused by loss of FBXW7

I have shown that WDR5 overexpression can promote mitotic slippage and that WDR5 is a novel player in drug-induced polyploidization. How WDR5 mechanistically influences these cellular responses to antimicrotubule drugs remains unclear. As WDR5 plays an important role during mitosis, both as scaffolding protein and as transcriptional regulator, a number of possible mechanisms could be postulated (Ali et al. 2014; Ali et al. 2017; Thomas et al. 2015; Zhou et al. 2021). The antiapoptotic protein Mcl-1 influences mitotic slippage but is also regulated by FBXW7 and WDR5 (Wertz et al. 2011; Chen et al. 2015). I therefore assessed whether WDR5 depletion could rescue the effect of FBXW7 on WDR5 protein levels.

I depleted WDR5 and/or FBXW7 in HeLa cells and quantified Mcl-1 protein levels after Western blotting (Fig. 29 A). In accordance with the literature, knockdown of FBXW7 significantly increased Mcl-1 levels and WDR5 depletion led to a strong downregulation (Fig. 29 B). Strikingly, Mcl-1 protein levels did not differ between co-depletion of FBXW7 and WDR5 and WDR5 depletion alone. These results suggest that WDR5 has a greater influence on Mcl-1 protein abundance compared to FBXW7 and that the effects of WDR5 could be due to its regulation of Mcl-1.

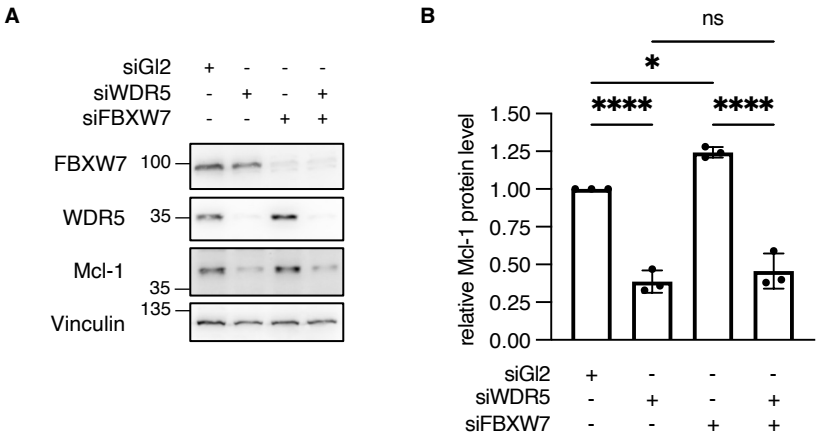

Figure 29: WDR5 knockdown reduces Mcl-1 protein levels indifferent of FBXW7 status.
A HeLa cells were transfected with siRNA targeting Gl2, WDR5 or FBXW7, either alone or in combination, for 72 h. Cell lysates were analyzed by Western blotting. **B** Mcl-1 signal intensities from **A** were normalized to Vinculin signal intensities. **** $p < 0.0001$, * $p < 0.05$, ns $p > 0.05$, one-way ANOVA with Tukey post-hoc test, n=3.

4. Discussion

SCF-FBXW7 is an important tumor suppressor because it regulates the abundance of many oncogenes (Davis et al. 2014). Unfortunately, it is the most frequently mutated F-box protein in human cancers and FBXW7-deficiency has been linked to tumor progression and chemoresistance (Yumimoto and Nakayama 2020; Fan et al. 2022). Its depletion causes mitotic slippage in response to antimicrotubule agents, followed by polyploidization and genomic instability (Finkin et al. 2008). Different mediators of FBXW7-dependent mitotic slippage have been proposed, yet the identification of the substrates involved in mitotic slippage remains a major task (Wertz et al. 2011; Allan et al. 2018; Topham et al. 2015). In the presented thesis, I aimed at identifying and characterizing novel substrates of FBXW7, uncovering their regulation by FBXW7, and assessing their function in mitotic slippage.

4.1 Identification of novel FBXW7 substrates

I decided to perform a FBXW7-substrate screen in cooperation with the DKFZ core facility to potentially identify candidate substrates of FBXW7. The core facility offered a label-free quantification (LFQ) approach, thereby differing from the previously performed TMT10plex-based approach (Hänle-Kreidler et al. 2022).

I mutated Flag-tagged FBXW7 in order to generate the previously published FBXW7 S462A, T463V, R465A WD40 domain mutant version, which is unable to interact with phosphodegrons (Hao et al. 2007). This mutant was employed as a negative control to specifically identify WD40 domain binders, hence candidate substrates. In addition, HEK293T cells expressing FBXW7 constructs were left untreated or were synchronized in prometaphase using nocodazole. This comparison would allow me to identify mitotic substrates of FBXW7, which could be degraded during prolonged mitotic arrest, like Cyclin B1 gradually decreases despite an active SAC (Brito and Rieder 2006).

I validated the screen by Western blotting (Fig. 7 B) and during the LFQ analysis (Fig. 8) using known FBXW7 interactors and substrates. PLK1 levels are upregulated during mitosis and Cyclin E1 is degraded during S-phase (Ekholm and Reed 2000; Petronczki et al. 2008). Both markers verified a good synchrony of the populations treated with nocodazole. The previously published FBXW7 substrates c-Myc, NFKB2, MED13, p53 and NOTCH1 were significantly enriched in Flag-FBXW7 WT IPs compared to the WD40 mutant version, which validated the approach. I also found that

the SCF components CUL1, SKP1, RBX1 and NEDD8, and the previously published regulators of FBXW7, FBXO45 and MYCBP2, did not differ between the samples (Appendix table 1 and table 2) (Richter et al. 2020). Therefore, similar levels of the FBXW7 constructs were present in the co-precipitation experiments.
Using this approach, BRUCE and FYCO1 were identified as mitotic candidate substrates of FBXW7. In addition, a few other potential substrates were identified, which co-precipitated with FBXW7 also during interphase (Appendix 6.1).

4.2 BRUCE is a putative substrate of FBXW7

BRUCE is a member of the IAP protein family and a regulator of apoptosis. It can bind to caspases and other proapoptotic factors and thereby block their activity (Bartke et al. 2004; Hao et al. 2004). Furthermore, BRUCE carries a ubiquitin-conjugating domain and targets caspases, DIABLO and p53 for degradation through its E2/E3 chimera activity (Tang et al. 2015). As IAPs are frequently deregulated in cancer, also BRUCE was shown to be upregulated in cancer cells and thereby convey poor prognosis and chemoresistance (Garrison et al. 2015; Hu et al. 2015).
To validate the findings from the FBXW7 substrate screen (Fig. 8), I performed reciprocal half-endogenous immunoprecipitations of FBXW7 and BRUCE (Fig. 9). Confirming the MS results, BRUCE specifically co-precipitated with Flag-FBXW7 WT from nocodazole-treated cells and endogenous FBXW7 was enriched in the Flag-mBRUCE IP from mitotic cells. This mitosis-restricted interaction could be the basis of an interesting mechanism between BRUCE and FBXW7, to specifically regulate mitotic functions of BRUCE. Similarly, a mitosis-restricted regulation of FBXW7 by the E3 ligase complex FBXO45/MYCBP2 was recently identified (Richter et al. 2020).
FBXW7 binds its substrates by interacting with conserved CDC4-phosphodegrons (Davis et al. 2014). The inhibition of different important kinases with small molecules revealed that only GSK3β inhibition reduced the interaction of FBXW7 and BRUCE without affecting the nocodazole-induced mitotic arrest. CDK2 activity is mainly required during S-Phase and G2 but also mitotic functions of CDK2 have been reported, which could explain the decrease in H3 S10 phosphorylation by the CDK2 inhibitor Roscovitine (Fig. 10 B) (Clemm von Hohenberg et al. 2022; Rosenblatt et al. 1992; Guadagno and Newport 1996). In addition, Roscovitine targets CDK7, another regulator of Cyclin B1/CDK1 activity (Larochelle et al. 2007).

The activity of CDK1 and Aurora kinase B are required to maintain the mitotic status, therefore RO-3306 and Hesperadin greatly decreased H3 S10 phosphorylation (Carpinelli and Moll 2008; Girdler et al. 2006; Kaestner et al. 2009; Murray et al. 1989; Murray 2004) . As the cells used in these IPs were presumably pushed out of mitosis, the mitosis-restricted interaction between FBXW7 and BRUCE was terminated. However, an influence of CDK1 or Aurora kinase B on their interaction cannot be excluded. Inhibition of PLK1 stabilized the interaction comparably to CRL inhibition with MLN4924, therefore PLK1 activity could have a negative impact on BRUCEs ability to bind to FBXW7. The interaction of PLK1 and CDK1 with BRUCE has been previously shown, supporting the possibility that PLK1, CDK1 and GSK3β could all be involved in the regulation of BRUCE (Pohl and Jentsch 2008).

BRUCE phosphorylation on Thr1035 and Thr1710 had been reported in phospho-proteomics studies, but to investigate the absolute requirement of BRUCE phosphorylation for the interaction, a dephosphorylation step would have to be added to a Flag-FBXW7 IP (Hornbeck et al. 2015). Furthermore, interaction mapping using truncated versions of BRUCE could be used to identify the interaction site.

Being in line with the role of BRUCE as an inhibitor of apoptosis, knockdown of BRUCE significantly increased death in mitosis and hence sensitized U2OS cells to nocodazole (Fig. 11) (Verhagen et al. 2001). Interestingly, the time spent in mitotic arrest was not altered. According to the “competing-networks threshold” model, a decrease in apoptotic threshold should decrease the time to death in mitosis. For example, the overexpression of Mcl-1 in DLD1 cells delayed death in mitosis but not the time to slippage (Sloss et al. 2016). In contrast, knockdown of c-Myc greatly delayed death in mitosis but not mitotic slippage (Topham et al. 2015). Depletion of BRUCE causes cytokinesis-associated apoptosis, suggesting an influence of BRUCE on the apoptotic commitment rather at the end of mitotic arrest, which could be the reason that no delay of apoptosis was observed (Pohl and Jentsch 2008).

In order to be involved in FBXW7-mediated mitotic slippage, BRUCE needs to be regulated by FBXW7 in a way that promotes mitotic slippage in the absence of FBXW7. Strikingly, BRUCE protein levels were not stabilized after depletion of FBXW7 (Fig. 12), indicating that BRUCE is not targeted towards the proteasome by FBXW7. I experienced the quantification of BRUCE protein abundance by Western blotting as challenging, because of the protein size of over 500 kDa. Therefore, a regulation of BRUCE by FBXW7 cannot be excluded and it would be interesting to see whether

BRUCE is Lys48 or Lys63 ubiquitylated by FBXW7 during mitotic arrest. Given the size of BRUCE, *in-vivo* ubiquitylation assays could be difficult. To date, NRDP1 remains the only E3 ubiquitin ligase targeting BRUCE and its possible regulation by FBXW7 remains subject of further investigation (Qiu et al. 2004). For example, FBXW7 could interact with and ubiquitylate BRUCE to alter its localization or activity.

Besides BRUCE, I also assessed a possible regulation of FYCO1 protein levels by FBXW7 but did not observe stabilization FYCO1 (Appendix 6.2). BRUCE and FYCO1 are both regulators of autophagy and it would be interesting to see whether FBXW7 regulates BRUCE and/or FYCO1 to alter autophagy-related processes, for example by Lys63 ubiquitylation (Ebner et al. 2018; Jia and Bonifacino 2019; Pankiv et al. 2010; Xiao et al. 2021). Nevertheless, my work and previous studies show that BRUCE is an interesting target in cancer therapy and further work is required to utilize this knowledge to benefit patients (Lamers et al. 2012; Luk et al. 2017).

4.3 KMT2D is phosphorylated by Casein kinase 2 to interact with FBXW7 but does not influence mitotic slippage

I screened the literature for unrelated FBXW7 substrate screens and compared them with FBXW7 screens performed in our group to find further candidate substrates of FBXW7 (Saffie et al. 2020; Richter et al. 2020; Hänle-Kreidler et al. 2022). A reoccurring hit was the SET-domain methyltransferase KMT2D together with its interactors WDR5, RB-binding protein 5 (RBBP5) and ASH2-like protein (ASH2L).

Chromatin-modifying enzymes are frequently deregulated in cancer and correlate with tumor progression and drug resistance (Toh et al. 2017; Zhao et al. 2021). The role of KMT2D seems to be context specific, because both oncogenic and tumor suppressor functions have been reported (Dauch et al. 2022; Kim et al. 2014; Lv et al. 2018; Ma et al. 2022; Wang et al. 2022; Xiong et al. 2018; Saffie et al. 2020)

Saffie et al. recently identified KMT2D as a novel substrate of FBXW7 but did not completely uncover the underlying regulation. As I showed that KMT2D seems to be the only KMT2-methyltransferase being targeted by FBXW7, knowing their exact relationship might therefore be as useful tool for further research (Fig. 13).

Using small molecule inhibitors and overexpression of CK2 subunits, I showed that CK2 activity regulates the interaction between KMT2D and FBXW7 (Fig. 14 and 15). However, to provide evidence that this regulation also influences the degradation of

KMT2D by FBXW7, further experiments like cycloheximide chases or ubiquitylation assays would need to be performed.

CK2 is a constitutively active kinase and therefore a lateral signal transducer (Borgo et al. 2021). This means that KMT2D could be continuously phosphorylated by CK2 without upstream cues and that the CDC4-phosphodegron be recognized by FBXW7. This could be a general mechanism of FBXW7 to continuously regulate the abundance of KTM2D. However, further investigation is required to assess under which conditions KMT2D is phosphorylated by CK2 and which functions this regulation serves. The identification of the exact phosphorylation and interaction site could help to answer these questions.

Despite its tumorigenic and tumor suppressive functions, knockdown of KMT2D did not affect the mitotic cell fate of U2OS cells in response to nocodazole. However, it cannot be excluded that this observation could be cell line- and drug-specific.

4.4 WDR5 is a novel substrate of SCF-FBXW7

I analyzed data from pre-existing experiments in the Hoffmann lab, where it was shown that the KMT2D methyltransferase complex component WDR5 is upregulated by FBXW7-deficiency or depletion (Richter 2017). Previous studies showed that WDR5 is frequently deregulated in cancer and that it is an important regulator of mitosis and proliferation but also a promoter of tumorigenesis and chemoresistance (Ali et al. 2014; Ali et al. 2017; Chen et al. 2015; Bailey et al. 2015a). Given the tumor suppressor function of FBXW7, I therefore investigated whether FBXW7 regulates WDR5 protein levels.

Along with this data, my experiments show that WDR5 protein levels are increased when FBXW7 is depleted in different cell lines (Fig. 17) (Richter 2017). WDR5 expression was previously shown to be upregulated by N-Myc in neuroblastoma and an indirect effect due to deregulation of WDR5 expression could not be excluded (Sun et al. 2015). By performing qPCR, I showed that WDR5 mRNA levels were not affected by FBXW7 status (Fig. 17), suggesting that WDR5 is indeed deregulated on the protein level.

Because WDR5 is a scaffolding component in many protein complexes, two key questions needed to be addressed: First, whether the interaction between WDR5 and FBXW7 is direct and, second, if the upregulation of WDR5 protein levels are indirectly caused by deregulation of its interactors (Guarnaccia and Tansey 2018).

An indirect regulation of members of protein complexes has been shown in the literature. For example, non-proportional protein synthesis can lead to an excess of one or more subunits that fail to assemble to functional complexes, so-called “orphaned subunits”. These proteins can be less stable if not incorporated into complexes and are degraded to correct subunit stoichiometry (Goldberg and Dice 1974; Mueller et al. 2015; Taggart et al. 2020). An interesting mechanism herein is the shielding of degrons by protein-protein interactions within complexes (Guharoy et al. 2022). For example, a degron within Cyclin B1 is shielded through its interaction with CDK1 (Levasseur et al. 2019). On the other hand, protein complexes have been shown to be degraded en bloc when ubiquitylation sites and the unstructured recognition site are localized on different complex subunits (Prakash et al. 2009).

Therefore, WDR5 protein levels could be stabilized through an increased abundance of complex members, for example the FBXW7 substrates KMT2D or c-Myc (Saffie et al. 2020; Thomas et al. 2015).

Depletion of KMT2D did not decrease WDR5 protein levels in HCT116 FBXW7 KO, indicating that WDR5 is not regulated through such a mechanism (Fig. 18). In line with this, my results also showed that KMT2D and c-Myc do not dictate the co-precipitation of WDR5 and FBXW7. c-Myc overexpression even decreased the co-elution of WDR5 with Flag-FBXW7, indicating a competition for FBXW7 binding.

Nevertheless, the interaction of FBXW7 and WDR5 could be facilitated indirectly via uncharacterized proteins. Therefore, I performed reciprocal immunoprecipitation of endogenous WDR5 and FBXW7 and showed that both proteins interact without overexpression. Using recombinant proteins, I verified that the both proteins can indeed interact *in-vitro*. It would be interesting to determine the dissociation constant for their interaction. My experiments therefore pointed towards a direct regulation of WDR5 by FBXW7.

The only previously published E3 ligase regulating WDR5 is CUL4-DDB1, but different functional outcomes have been reported: While first results showed that WDR5 was not degraded by CUL4-DDB1 and that the depletion of CUL4 rather increased histone methylation, more recent research suggested that WDR5 is indeed ubiquitylated by nuclear CUL4B-DDB1 and degraded to regulate neuronal gene expression (Higa et al. 2006; Nakagawa and Xiong 2011a, 2011b). In addition, it was shown that WD40-repeat containing proteins could act as substrate receptor through their interaction with

DDB1 and WDR5 could therefore function in a similar manner (Jin et al. 2006; Angers et al. 2006).

I therefore analyzed whether the protein stability and ubiquitylation of WDR5 is affected by FBXW7. Using the ribosomal inhibitor cycloheximide that blocks protein synthesis, I showed that overexpressed and endogenous WDR5 are destabilized by FBXW7 and that WDR5 is degraded via the 26S proteasome (Fig. 20). I determined a half-live of 25-30 h for endogenous WDR5 in DLD1 and HEK293T cells, which is more stable compared to the study of Tadashi Nakagawa (Nakagawa and Xiong 2011b). In fact, WDR5 appeared to be a rather stable protein in my experiments which suggests that its regulation by FBXW7 does not have a cell-cycle related function. Proteins involved in cell-cycle regulation need to be degraded rapidly to enable a tight regulation within distinct phases. For example, the FBXW7 substrate c-Myc has a half-life of about 30 min (Gregory and Hann 2000). On the other hand, WDR5 is required to maintain cell viability and rapid depletion of WDR5 could lead to uncontrolled cell death (Neilsen et al. 2018). In addition, its presence in complexes could possibly protect it from rapid degradation. Protein stability assessment with a WDR5 WIN-site and WBM-site mutant could be used to answer this question.

FBXW7 promotes Lys48- or Lys63-linked polyubiquitylation of its substrates, hence I investigated whether WDR5 is also ubiquitylated by FBXW7. Using *in-vivo* and *in-vitro* ubiquitylation assays, I showed that WDR5 ubiquitylation is increased by FBXW7 WT but not the mutant controls (Fig. 21). I usually did not observe a strong difference in WDR5 ubiquitylation between GFP-EV or GFP-FBXW7 WT overexpression, which fits to my finding that WDR5 is a stable protein and therefore not efficiently marked for degradation. An additional experiment would be required to assess whether the observed polyubiquitylation is indeed Lys48-linked or if there are other topologies involved. These results indicate that WDR5 is polyubiquitylated and degraded by FBXW7. WDR5 itself has been recognized as oncogene and a regulation of WDR5 protein levels by FBXW7 could therefore be a novel tumor suppressive function of FBXW7 (Lu et al. 2018).

FBXW7 recognizes its substrates via conserved CDC4-phosphodegrons and in most cases GSK3β catalyzes the phosphorylation required for binding (Lan and Sun 2021). My results showed that phosphorylation is required for the interaction of FBXW7 and WDR5, similarly to the previous published substrates KMT2D and c-Myc (Fig. 22) (Saffie et al. 2020; Welcker et al. 2004; Yada et al. 2004). Strikingly, the interaction

with c-Myc was not completely abolished by the treatment with λ-phosphatase. This could be due to c-Myc carrying multiple CDC4-phosphodegrons and an uncomplete dephosphorylation, potentially through high affinity binding on FBXW7 (Welcker et al. 2022). Furthermore, inhibition of GSK3β with the small molecule CHIR99021 strongly reduced the interaction of FBXW7 and WDR5 (Fig. 22). I performed the reciprocal immunoprecipitation experiment and observed less reduction of WDR5 co-elution with Flag-FBXW7 by CHIR99021, suggesting that there could be some interaction of WDR5 and FBXW7 without phosphorylation or that other kinases might be involved (Hänle-Kreidler and Hoffmann, unpublished results). Indeed, WDR5 and FBXW7 interacted *in-vitro* without prior phosphorylation (Fig. 19). Another possibility is that GSKβ-mediated phosphorylation frees WDR5 from protein complexes and enables the interaction with FBXW7. This hypothesis could be tested by identifying the phosphorylation site and experiments with non-phosphorylatable WDR5 mutant.

I further showed that GSK3β is required for the regulation of WDR5 protein levels by polyubiquitylation and that GSK3β co-precipitates with WDR5 (Fig. 23). Interestingly, inhibition of GSK3β in the *in-vivo* ubiquitylation assay did not completely abolish WDR5 ubiquitylation as seen with the NEDDylation inhibitor MLN4924, suggesting that either GSK3β was not completely inhibited or that the remaining interaction seen in figure 21 is sufficient to enable some ubiquitylation of WDR5. GSK3β can therefore mark WDR5 for recognition by FBXW7 and then further for proteasomal degradation. It would be interesting to assess which functions this regulation fulfills in untransformed cells and if it requires certain circumstances, such as specific cell cycle phases or upstream signals.

The CDC4-phosphodegron is a conserved [TS], P, X, X, [TSED] motif, although recent data showed that FBXW7 allows for more flexibility in the degron structure (Singh et al. 2022). Using the Eukaryotic Linear Motif tool, I predicted two different degrons within the WDR5 amino acid sequence. However, substitution of either residue to alanine did not affect the interaction with FBXW7 (Fig. 24). WDR5 has been shown to be phosphorylated at different sites *in-vivo*, including Thr18, Thr29, Ser49 and Ser54, and all sites could be checked to identify the phosphodegron motif (Hornbeck et al. 2015). Another approach could be interaction mapping, as shown in figure 24 C and D. Here, the interaction of FBXW7 and WDR5 was reduced most markedly by deletion of WDR5 WD40 repeat 6 but none of the constructs completely lost the interaction. As the WD40 repeats of WDR5 organize in an intricate WD40 propeller structure, deletion of WD40

repeats could completely alter the tertiary structure and such mutants have therefore to be used with care and appropriate controls (Schuetz et al. 2006). In my experiments, WDR5 and FBXW7 could often be detected in the control IP, indicating that further optimization of the experimental conditions could help achieving a clear result. In addition, *in-vitro* interaction studies using purified truncated WDR5 constructs could help to identify the interaction site.

Taken together, I showed that WDR5 protein levels are upregulated in FBXW7-deficient cells, because SCF-FBXW7 regulates WDR5 protein stability by polyubiquitylation. In addition, GSK3β is required for efficient regulation of WDR5 by FBXW7 but the identification of the interaction site and CDC4-phosphodegron requires further studies.

4.5 WDR5 and Cyclin E1 promote mitotic slippage and are required for drug-induced polyploidy

The treatment of cancers with antimicrotubule drugs leads to prolonged mitotic arrest, followed by mitotic cell death or mitotic exit without cytokinesis (Roberts et al. 1990; Rieder and Maiato 2004; Sudo et al. 2004). FBXW7 was shown to regulate mitotic cell fate and FBXW7-deficiency promotes chemoresistance towards antimicrotubule drugs by promoting mitotic slippage (Wertz et al. 2011; Richter et al. 2020). Hence, the aim of this thesis to better understand the mechanisms underlying chemoresistance by identifying down-stream targets of FBXW7 substrates involved in mitotic slippage.

I showed that the overexpression of WDR5 WT but not WDR5 F133A, a WIN-site mutant, in U2OS cells promotes mitotic slippage in the presence of nocodazole and therefore identified WDR5 as a novel player in mitotic slippage (Fig. 25). Given the role of the WIN site in mediating protein-protein interactions, it is not surprising that WDR5-mediated mitotic slippage is disrupted by WIN site mutation. Interestingly, no effects on prolonged mitotic arrest were observed. Different mechanisms could be imagined how the overexpression of WDR5 promotes mitotic slippage: WDR5 promotes the expression of Mcl-1 and could therefore increase the antiapoptotic capacities (Chen et al. 2015). Histone H3 lysine 4 (H3K4) methylation reduces MAD2 available for SAC formation, because active MAD2 binds H3K4me3 signatures, increased histone methylation by overexpression of WDR5 could weaken the SAC (Schibler et al. 2016). In addition, these cells showed an increased resistance to microtubule depolymerization. Recently, WDR5 has been characterized as a novel substrate

adaptor of the APC/C E3 ubiquitin ligase and it is possible, that it could redirect mitotic substrate specificity in a way that promotes chemoresistance (Oh et al. 2020). More work is required to characterize the mechanism involved in WDR5-mediated chemoresistance.

It is possible that the observed increase of mitotic slippage caused by FBXW7-deficiency is the cumulative effect of multiple deregulated substrates and pathways.

Cyclin E1 overexpression deregulates the APC/C, CENP-A and mitotic fidelity and has been proposed as a mediator of mitotic slippage (Keck et al. 2007; Bagheri-Yarmand et al. 2010; Lau et al. 2013; Takada et al. 2017). I showed that the overexpression of Cyclin E1 is sufficient to induce mitotic slippage to a similar extent as FBXW7 depletion (Fig. 25). Similar to WDR5, different possible mechanisms of action can be derived for how Cyclin E1 mediates mitotic slippage. Interestingly, WDR5 has also been shown to regulate Cyclin E1 protein expression, indicating that both pathways could overlap (Chen et al. 2015). However, my finding, that the co-depletion of Cyclin E1 and WDR5 rescued mitotic slippage of U2OS after knockdown of FBXW7 more strongly, suggests that both proteins also act through unique mechanisms and therefore have an additive effect on mitotic cell fate (Fig. 27). Strikingly, almost all mitotic slippage experiments showed no alteration of prolonged mitotic arrest, pointing out that SAC activity or Cyclin B1 kinetics were unaffected.

Mitotic slippage is the first crucial step in the emergence of chromosomal instability after treatment with antimicrotubule drugs (Sinha et al. 2019). FBXW7-deficiency greatly increases drug-induced polyploidy and the depletion of its substrates Cyclin E1 and Aurora kinase A was shown to partially rescue this phenotype (Finkin et al. 2008). In addition, knockdown of Mcl-1 also reduces drug-induced polyploidy (Wertz et al. 2011).

I therefore assessed whether WDR5 could also influence polyploidization in response to antimicrotubule drugs. I chose to deplete WDR5 from HCT116 FXBW7 KO, because previous evidence suggested that the overexpression of single substrates might not suffice to drive polyploidization (Finkin et al. 2008).

Treatment with Taxol efficiently arrested HCT116 WT in mitosis, indicated by a uniform G2/M population (Fig. 28). HCT116 FBXW7 KO slipped from mitosis and began the next endoreplication leading to polyploidization, as visible by the forming right-sided shoulder in the histogram. I depleted Cyclin E1 as a control and achieved a similar reduction in drug-induced polyploidy compared to the literature precedence (Finkin et

al. 2008). Depletion of WDR5 had a similar or slightly less strong effect, but still significantly reduced polyploidization of HCT116 FBXW7 KO cells. Strikingly, the co-depletion of Cyclin E1 and WDR5 did not have an additive effect as compared to their effect on mitotic slippage. This could indicate that both proteins might act through the same pathways in the efficient replication of DNA HCT116 FBXW7 KO cells after slippage. Indeed, both proteins are involved in DNA replication: Cyclin E1 was early shown to promote S-phase and later that it supports DNA replication by loading minichromosome maintenance protein complex (MCM) into prereplication DNA to promote S-phase entry (Strausfeld et al. 1996; Geng et al. 2007). Intriguingly, downregulation of WDR5 also reduces recruitment of MCM proteins onto replication origins and suppresses DNA replication (Lu et al. 2016). In addition, inhibition of WDR5 downregulates genes involved in DNA replication as well as important cell-cycle regulators (Aho et al. 2019). However, further research is required to elucidate the mechanisms of Cyclin E1 and WDR5-dependent drug-induced polyploidization in FBXW7-deficient cancer cells.

Based on previous studies showing that WDR5 regulates Mcl-1 protein expression, and that Mcl-1 is an important protein involved in chemoresistance and drug-induced polyploidy, I assessed whether depletion of WDR5 could reduce Mcl-1 protein levels after knockdown of FBXW7 (Fig. 29) (Inuzuka et al. 2011; Wertz et al. 2011; Chen et al. 2015). As shown in the literature, knockdown of FBXW7 stabilized Mcl-1 while knockdown of WDR5 drastically decreased Mcl-1 protein levels. Strikingly, the siRNA-mediated knockdown of WDR5 and FBXW7 together resulted in the same Mcl-1 protein abundance as after WDR5 knockdown alone. This indicates that WDR5 plays a major role in the regulation of Mcl-1 protein abundance and that one mechanism of how WDR5 promotes chemoresistance could be through increasing Mcl-1 protein abundance.

Collectively, the literature and my data support that WDR5 is a driver of chemoresistance. However, it cannot be excluded that multiple pathways mediate the effects of WDR5 overexpression. Similarly, FBXW7-deficiency most likely leads to mitotic slippage and drug-induced polyploidy through the deregulation of multiple substrates that culminate in one phenotype. Therefore, it will be interesting to see whether the inhibition of WDR5 in combination with targeting of other FBXW7 substrates could generate additive effects in the fight against chemoresistance.

4.6 Working model

FBXW7 is an important tumor suppressor protein and is frequently mutated in cancers (Davis et al. 2014). FBXW7-deficiency exhibits different outcomes in cancers, one of them is an increased chemoresistance against antimicrotubule drugs through mitotic slippage (Wertz et al. 2011; Richter et al. 2020).

In the presented thesis, I screened for novel and mitotic substrates of SCF-FBXW7 and identified the IAP BRUCE and WDR5 as novel candidate substrates. I showed that BRUCE influences mitotic slippage but its regulation by FBXW7 remains unclear.

I characterized WDR5 as a novel substrate of FBXW7 and showed that FBXW7 regulates the protein abundance of WDR5 in cooperation with GSK3β. Furthermore, the overexpression of the FBXW7 substrates WDR5 and Cyclin E1 promotes mitotic slippage, and their depletion reduces mitotic slippage and drug-induced polyploidization of FBXW7-deficient cancer cells (Hänle-Kreidler et al. 2022). WDR5 might promote slippage through the regulation of Mcl-1 but also other mechanisms are possible. The working model is summarized in figure 30.

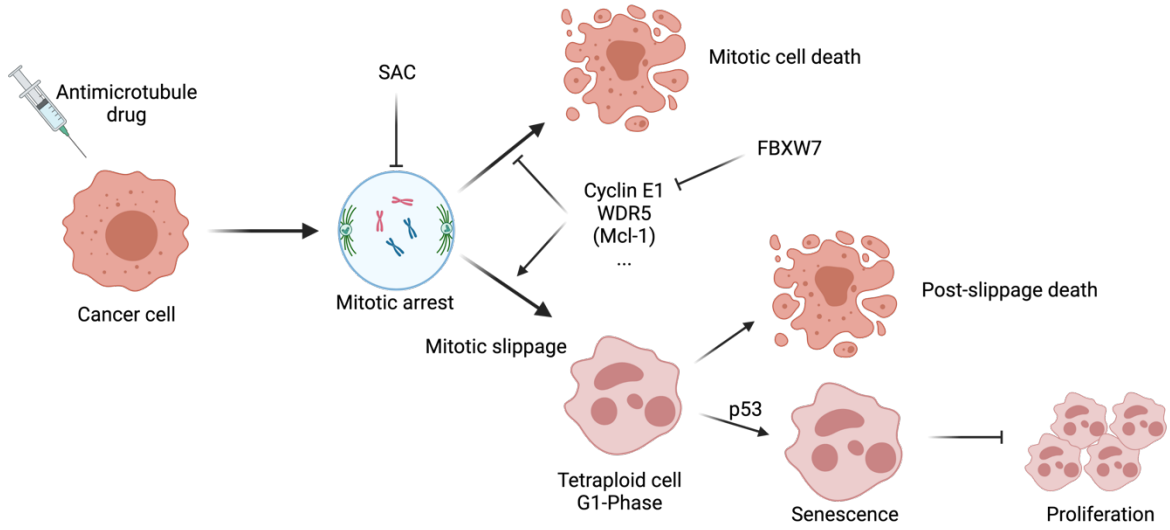

Figure 30: FBXW7 targets Cyclin E1 and WDR5 to prevent mitotic slippage and polyploidy in response to antimicrotubule drugs.
Treatment of cancers with antimicrotubule drugs leads to prolonged mitotic arrest by sustained activation of the spindle-assembly-checkpoint (SAC). Eventually, cancer cells either undergo mitotic cell death (apoptosis) or exit from mitosis without undergoing cytokinesis (mitotic slippage). These tetraploid cells enter the next cell cycle and undergo growth arrest or apoptosis through the p53-dependend G1 checkpoint. Depending, amongst others, on their p53 mutation status, cancer cells can escape from this growth arrest and continue to proliferate as genetically instable cells. WDR5 and Cyclin E1 are substrates of FBXW7, and FBXW7-deficiency promotes mitotic slippage by upregulation of their protein levels. Adapted from Cheng and Crasta, 2017. Illustrations were created using the BioRender.com application.

4.7 Future perspectives

I would like to summarize the remaining open questions from this thesis in this section. As mentioned above, chemoresistance through FBXW7-deficiency is most likely the cumulative outcome of multiple deregulated substrates and their downstream effects. Further screening could therefore help to identify other known or novel FBXW7 substrates involved in mitotic slippage.

The screening rationale used in this project could be optimized for the testing of multiple candidates in parallel. By combining the results of different FBXW7 substrate screens performed with different methods, possible matrix effects could be avoided to deliver the best available pool of candidates (O'Connor and Huibregtse 2017). Novel substrate candidates could be screened for targeting by FBXW7 using an *in-vitro* ubiquitylation assay on protein microarrays (Schweiggert et al. 2021). One possible problem could be the requirement of phosphorylation of the CDC4-phosphodegron in this reaction. Another screening modality could be the *in-vivo* fluorescent tagging of candidates to determine if FBXW7 status affects their turnover (Khmelinskii et al. 2012). The assessment of mitotic slippage by live-cell imaging remains the main bottleneck and an alternative assay or surrogate readout could help to increase throughput. Using substrate screening and a reliable functional assay, multiple FBXW7 candidate substrates could be assessed in parallel.

Keeping in mind that FBXW7 was also shown to promote Lys63 polyubiquitylation, it would be interesting to assess whether these substrates are also involved in mitotic slippage (Zhang et al. 2016a). Here, FBXW7-deficiency would rather disrupt signaling pathways or protein complexes.

I showed that BRUCE is a novel candidate substrate of FBXW7, but I did not observe a regulation of BRUCE protein levels by FBXW7. Whether FBXW7 promotes Lys63 ubiquitylation of BRUCE to regulate its functions, for example by affecting its mitotic localization or activity, is a possibility that could be tested in future experiment.

WDR5 is a novel substrate of FBXW7 and promotes mitotic slippage in FBXW7-deficient cells (Hänle-Kreidler et al. 2022). It would be interesting to see whether FBXW7 is involved in the regulation of canonical functions of WDR5, for example histone methylation. In this study, I did not identify the CDC4-phosphodegron on WDR5. Further binding studies are therefore required to find the interaction surface and GSK3β phosphorylation site, for example by interaction mapping or phosphor-

proteomics. Mutation of the interaction site could help to uncover more of the functional relationship between FBXW7 and WDR5.

Furthermore, it would be helpful to investigate whether WDR5 exerts its role in mitotic slippage through its canonical methyltransferase complex function or as a part of other protein complexes. To investigate the functions of WDR5 in mitotic slippage, it would be possible to assess the interactome of WDR5 during prolonged mitotic arrest and to compare the WDR5-dependent transcriptome between non-synchronized and nocodazole-treated cells. In doing so, potential pathways or mechanisms of how WDR5 promotes chemoresistance could potentially be identified.

In addition to this work, previous studies have suggested targeting of WDR5 as an investigational therapy for cancer. In fact, the inhibition of WDR5 scaffolding functions with small molecules or its degradation by specific PROTACs showed promising results (Grebien et al. 2015; Yu et al. 2021; Li et al. 2022). Further live-cell imaging experiments could include the use of these compounds to assess their effects on mitotic cell fate. Because I have shown that WDR5 promotes mitotic slippage, I would expect WDR5 inhibitors to promote mitotic cell death (Hänle-Kreidler et al. 2022).

Furthermore, FBXW7-deficiency promotes chemoresistance against multiple cancer therapeutics (Fan et al. 2022). It would be interesting to assess the effect of WDR5 knockdown or inhibition on the resistance against these therapeutics. The frequency of WDR5 mutations in cancer is low, which suggests that WDR5 is also essential for cellular processes in cancer (Neilsen et al. 2018). Therefore, WDR5 represents an ideal target for the development of further inhibitors.

5. References

Abbas, Tarek; Mueller, Adam C.; Shibata, Etsuko; Keaton, Mignon; Rossi, Mario; Dutta, Anindya (2013): CRL1-FBXO11 promotes Cdt2 ubiquitylation and degradation and regulates Pr-Set7/Set8-mediated cellular migration. In *Molecular cell* 49 (6), pp. 1147–1158. DOI: 10.1016/j.molcel.2013.02.003.

Aho, Erin R.; Wang, Jing; Gogliotti, Rocco D.; Howard, Gregory C.; Phan, Jason; Acharya, Pankaj et al. (2019): Displacement of WDR5 from Chromatin by a WIN Site Inhibitor with Picomolar Affinity. In *Cell reports* 26 (11), 2916-2928.e13. DOI: 10.1016/j.celrep.2019.02.047.

Akhoondi, Shahab; Lindström, Linda; Widschwendter, Martin; Corcoran, Martin; Bergh, Jonas; Spruck, Charles et al. (2010): Inactivation of FBXW7/hCDC4-β expression by promoter hypermethylation is associated with favorable prognosis in primary breast cancer. In *Breast cancer research : BCR* 12 (6), R105. DOI: 10.1186/bcr2788.

Ali, Aamir; Veeranki, Sailaja Naga; Chinchole, Akash; Tyagi, Shweta (2017): MLL/WDR5 Complex Regulates Kif2A Localization to Ensure Chromosome Congression and Proper Spindle Assembly during Mitosis. In *Developmental cell* 41 (6), 605-622.e7. DOI: 10.1016/j.devcel.2017.05.023.

Ali, Aamir; Veeranki, Sailaja Naga; Tyagi, Shweta (2014): A SET-domain-independent role of WRAD complex in cell-cycle regulatory function of mixed lineage leukemia. In *Nucleic acids research* 42 (12), pp. 7611–7624. DOI: 10.1093/nar/gku458.

Allan, Lindsey A.; Skowyra, Agnieszka; Rogers, Katie I.; Zeller, Désirée; Clarke, Paul R. (2018): Atypical APC/C-dependent degradation of Mcl-1 provides an apoptotic timer during mitotic arrest. In *The EMBO journal* 37 (17). DOI: 10.15252/embj.201796831.

Andreassen, P. R.; Lohez, O. D.; Lacroix, F. B.; Margolis, R. L. (2001): Tetraploid state induces p53-dependent arrest of nontransformed mammalian cells in G1. In *Molecular biology of the cell* 12 (5), pp. 1315–1328. DOI: 10.1091/mbc.12.5.1315.

Anfinsen, C. B. (1973): Principles that govern the folding of protein chains. In *Science (New York, N.Y.)* 181 (4096), pp. 223–230. DOI: 10.1126/science.181.4096.223.

Angers, Stephane; Li, Ti; Yi, Xianhua; MacCoss, Michael J.; Moon, Randall T.; Zheng, Ning (2006): Molecular architecture and assembly of the DDB1-CUL4A ubiquitin ligase machinery. In *Nature* 443 (7111), pp. 590–593. DOI: 10.1038/nature05175.

Antonioli, Manuela; Di Rienzo, Martina; Piacentini, Mauro; Fimia, Gian Maria (2017): Emerging Mechanisms in Initiating and Terminating Autophagy. In *Trends in biochemical sciences* 42 (1), pp. 28–41. DOI: 10.1016/j.tibs.2016.09.008.

Arendt, C. S.; Hochstrasser, M. (1997): Identification of the yeast 20S proteasome catalytic centers and subunit interactions required for active-site formation. In *Proceedings of the National Academy of Sciences of the United States of America* 94 (14), pp. 7156–7161. DOI: 10.1073/pnas.94.14.7156.

Badarudeen, Binshad; Gupta, Ria; Nair, Sreeja V.; Chandrasekharan, Aneesh; Manna, Tapas K. (2020): The ubiquitin ligase FBXW7 targets the centriolar assembly protein HsSAS-6 for degradation and thereby regulates centriole duplication. In *The Journal of biological chemistry* 295 (14), pp. 4428–4437. DOI: 10.1074/jbc.AC119.012178.

Baek, Kheewoong; Krist, David T.; Prabu, J. Rajan; Hill, Spencer; Klügel, Maren; Neumaier, Lisa-Marie et al. (2020): NEDD8 nucleates a multivalent cullin-RING-UBE2D ubiquitin ligation assembly. In *Nature* 578 (7795), pp. 461–466. DOI: 10.1038/s41586-020-2000-y.

Bagheri-Yarmand, Rozita; Nanos-Webb, Angela; Biernacka, Anna; Bui, Tuyen; Keyomarsi, Khandan (2010): Cyclin E deregulation impairs mitotic progression through premature activation of Cdc25C. In *Cancer research* 70 (12), pp. 5085–5095. DOI: 10.1158/0008-5472.CAN-09-4095.

Bai, Chang; Sen, Partha; Hofmann, Kay; Ma, Lei; Goebl, Mark; Harper, J.Wade; Elledge, Stephen J. (1996): SKP1 Connects Cell Cycle Regulators to the Ubiquitin Proteolysis Machinery through a Novel Motif, the F-Box. In *Cell* 86 (2), pp. 263–274. DOI: 10.1016/s0092-8674(00)80098-7.

Bailey, Jeffrey K.; Fields, Alexander T.; Cheng, Kaijian; Lee, Albert; Wagenaar, Eric; Lagrois, Remy et al. (2015a): WD repeat-containing protein 5 (WDR5) localizes to the midbody and regulates abscission. In *The Journal of biological chemistry* 290 (14), pp. 8987–9001. DOI: 10.1074/jbc.M114.623611.

Bailey, Melanie L.; Singh, Tejomayee; Mero, Patricia; Moffat, Jason; Hieter, Philip (2015b): Dependence of Human Colorectal Cells Lacking the FBW7 Tumor Suppressor on the Spindle Assembly Checkpoint. In *Genetics* 201 (3), pp. 885–895. DOI: 10.1534/genetics.115.180653.

Balachandran, Riju S.; Heighington, Cassandra S.; Starostina, Natalia G.; Anderson, James W.; Owen, David L.; Vasudevan, Srividya; Kipreos, Edward T. (2016): The ubiquitin ligase CRL2ZYG11 targets cyclin B1 for degradation in a conserved pathway that facilitates mitotic slippage. In *The Journal of cell biology* 215 (2), pp. 151–166. DOI: 10.1083/jcb.201601083.

Balamurugan, Kuppusamy; Wang, Ju-Ming; Tsai, Hsin-Hwa; Sharan, Shikha; Anver, Miriam; Leighty, Robert; Sterneck, Esta (2010): The tumour suppressor C/EBPδ inhibits FBXW7 expression and promotes mammary tumour metastasis. In *The EMBO journal* 29 (24), pp. 4106–4117. DOI: 10.1038/emboj.2010.280.

Baresova, Petra; Pitha, Paula M.; Lubyova, Barbora (2012): Kaposi sarcoma-associated herpesvirus vIRF-3 protein binds to F-box of Skp2 protein and acts as a regulator of c-Myc protein function and stability. In *The Journal of biological chemistry* 287 (20), pp. 16199–16208. DOI: 10.1074/jbc.M111.335216.

Bartke, Till; Pohl, Christian; Pyrowolakis, George; Jentsch, Stefan (2004): Dual role of BRUCE as an antiapoptotic IAP and a chimeric E2/E3 ubiquitin ligase. In *Molecular cell* 14 (6), pp. 801–811. DOI: 10.1016/j.molcel.2004.05.018.

Bartkova, Jirina; Horejsí, Zuzana; Koed, Karen; Krämer, Alwin; Tort, Frederic; Zieger, Karsten et al. (2005): DNA damage response as a candidate anti-cancer barrier in early human tumorigenesis. In *Nature* 434 (7035), pp. 864–870. DOI: 10.1038/nature03482.

Békés, Miklós; Langley, David R.; Crews, Craig M. (2022): PROTAC targeted protein degraders: the past is prologue. In *Nature reviews. Drug discovery* 21 (3), pp. 181–200. DOI: 10.1038/s41573-021-00371-6.

Bengtson, Mario H.; Joazeiro, Claudio A. P. (2010): Role of a ribosome-associated E3 ubiquitin ligase in protein quality control. In *Nature* 467 (7314), pp. 470–473. DOI: 10.1038/nature09371.

Berndsen, Christopher E.; Wolberger, Cynthia (2014): New insights into ubiquitin E3 ligase mechanism. In *Nature structural & molecular biology* 21 (4), pp. 301–307. DOI: 10.1038/nsmb.2780.

Bhattacharyya, Sucharita; Yu, Houqing; Mim, Carsten; Matouschek, Andreas (2014): Regulated protein turnover: snapshots of the proteasome in action. In *Nature reviews. Molecular cell biology* 15 (2), pp. 122–133. DOI: 10.1038/nrm3741.

Birgisdottir, Åsa Birna; Lamark, Trond; Johansen, Terje (2013): The LIR motif - crucial for selective autophagy. In *Journal of cell science* 126 (Pt 15), pp. 3237–3247. DOI: 10.1242/jcs.126128.

Blethrow, Justin D.; Glavy, Joseph S.; Morgan, David O.; Shokat, Kevan M. (2008): Covalent capture of kinase-specific phosphopeptides reveals Cdk1-cyclin B substrates. In *Proceedings of the National Academy of Sciences of the United States of America* 105 (5), pp. 1442–1447. DOI: 10.1073/pnas.0708966105.

Blom, N.; Gammeltoft, S.; Brunak, S. (1999): Sequence and structure-based prediction of eukaryotic protein phosphorylation sites. In *Journal of molecular biology* 294 (5), pp. 1351–1362. DOI: 10.1006/jmbi.1999.3310.

Bondeson, Daniel P.; Mares, Alina; Smith, Ian E. D.; Ko, Eunhwa; Campos, Sebastien; Miah, Afjal H. et al. (2015): Catalytic in vivo protein knockdown by small-molecule PROTACs. In *Nature chemical biology* 11 (8), pp. 611–617. DOI: 10.1038/nchembio.1858.

Bonn, Bettina R.; Rohde, Marius; Zimmermann, Martin; Krieger, David; Oschlies, Ilske; Niggli, Felix et al. (2013): Incidence and prognostic relevance of genetic variations in T-cell lymphoblastic lymphoma in childhood and adolescence. In *Blood* 121 (16), pp. 3153–3160. DOI: 10.1182/blood-2012-12-474148.

Borah, Naheed Arfin; Reddy, Mamatha M. (2021): Aurora Kinase B Inhibition: A Potential Therapeutic Strategy for Cancer. In *Molecules (Basel, Switzerland)* 26 (7). DOI: 10.3390/molecules26071981.

Borgo, Christian; D'Amore, Claudio; Sarno, Stefania; Salvi, Mauro; Ruzzene, Maria (2021): Protein kinase CK2: a potential therapeutic target for diverse human diseases. In *Sig Transduct Target Ther* 6 (1), p. 183. DOI: 10.1038/s41392-021-00567-7.

Bornstein, Gil; Ganoth, Dvora; Hershko, Avram (2006): Regulation of neddylation and deneddylation of cullin1 in SCFSkp2 ubiquitin ligase by F-box protein and substrate. In *Proceedings of the National Academy of Sciences of the United States of America* 103 (31), pp. 11515–11520. DOI: 10.1073/pnas.0603921103.

Brandman, Onn; Hegde, Ramanujan S. (2016): Ribosome-associated protein quality control. In *Nature structural & molecular biology* 23 (1), pp. 7–15. DOI: 10.1038/nsmb.3147.

Brito, Daniela A.; Rieder, Conly L. (2006): Mitotic checkpoint slippage in humans occurs via cyclin B destruction in the presence of an active checkpoint. In *Current Biology* 16 (12), pp. 1194–1200. DOI: 10.1016/j.cub.2006.04.043.

Brownell, James E.; Sintchak, Michael D.; Gavin, James M.; Liao, Hua; Bruzzese, Frank J.; Bump, Nancy J. et al. (2010): Substrate-assisted inhibition of ubiquitin-like protein-activating enzymes: the NEDD8 E1 inhibitor MLN4924 forms a NEDD8-AMP mimetic in situ. In *Molecular cell* 37 (1), pp. 102–111. DOI: 10.1016/j.molcel.2009.12.024.

Brzovic, P. S.; Rajagopal, P.; Hoyt, D. W.; King, M. C.; Klevit, R. E. (2001): Structure of a BRCA1-BARD1 heterodimeric RING-RING complex. In *Nature structural biology* 8 (10), pp. 833–837. DOI: 10.1038/nsb1001-833.

Busino, Luca; Donzelli, Maddalena; Chiesa, Massimo; Guardavaccaro, Daniele; Ganoth, Dvora; Dorrello, N. Valerio et al. (2003): Degradation of Cdc25A by beta-TrCP during S phase and in response to DNA damage. In *Nature* 426 (6962), pp. 87–91. DOI: 10.1038/nature02082.

Busino, Luca; Millman, Scott E.; Scotto, Luigi; Kyratsous, Christos A.; Basrur, Venkatesha; O'Connor, Owen et al. (2012): Fbxw7α- and GSK3-mediated degradation of p100 is a pro-survival mechanism in multiple myeloma. In *Nature cell biology* 14 (4), pp. 375–385. DOI: 10.1038/ncb2463.

Callens, Celine; Baleydier, Frederic; Lengline, Etienne; Ben Abdelali, Raouf; Petit, Arnaud; Villarese, Patrick et al. (2012): Clinical impact of NOTCH1 and/or FBXW7 mutations, FLASH deletion, and TCR status in pediatric T-cell lymphoblastic lymphoma. In *Journal of clinical oncology : official journal of the American Society of Clinical Oncology* 30 (16), pp. 1966–1973. DOI: 10.1200/JCO.2011.39.7661.

Carpinelli, Patrizia; Moll, Jürgen (2008): Aurora kinase inhibitors: identification and preclinical validation of their biomarkers. In *Expert opinion on therapeutic targets* 12 (1), pp. 69–80. DOI: 10.1517/14728222.12.1.69.

Cavadini, Simone; Fischer, Eric S.; Bunker, Richard D.; Potenza, Alessandro; Lingaraju, Gondichatnahalli M.; Goldie, Kenneth N. et al. (2016): Cullin-RING ubiquitin E3 ligase regulation by the COP9 signalosome. In *Nature* 531 (7596), pp. 598–603. DOI: 10.1038/nature17416.

Chacón Simon, Selena; Wang, Feng; Thomas, Lance R.; Phan, Jason; Zhao, Bin; Olejniczak, Edward T. et al. (2020): Discovery of WD Repeat-Containing Protein 5 (WDR5)-MYC Inhibitors Using Fragment-Based Methods and Structure-Based Design. In *Journal of medicinal chemistry* 63 (8), pp. 4315–4333. DOI: 10.1021/acs.jmedchem.0c00224.

Cha-Molstad, Hyunjoo; Sung, Ki Sa; Hwang, Joonsung; Kim, Kyoung A.; Yu, Ji Eun; Yoo, Young Dong et al. (2015): Amino-terminal arginylation targets endoplasmic reticulum chaperone BiP for autophagy through p62 binding. In *Nature cell biology* 17 (7), pp. 917–929. DOI: 10.1038/ncb3177.

Chau, V.; Tobias, J. W.; Bachmair, A.; Marriott, D.; Ecker, D. J.; Gonda, D. K.; Varshavsky, A. (1989): A multiubiquitin chain is confined to specific lysine in a targeted short-lived protein. In *Science (New York, N.Y.)* 243 (4898), pp. 1576–1583. DOI: 10.1126/science.2538923.

Chen, Xu; Xie, Weibin; Gu, Peng; Cai, Qingqing; Wang, Bo; Xie, Yun et al. (2015): Upregulated WDR5 promotes proliferation, self-renewal and chemoresistance in bladder cancer via mediating H3K4 trimethylation. In *Scientific reports* 5, p. 8293. DOI: 10.1038/srep08293.

Chen, Z.; Naito, M.; Hori, S.; Mashima, T.; Yamori, T.; Tsuruo, T. (1999): A human IAP-family gene, apollon, expressed in human brain cancer cells. In *Biochemical and Biophysical Research Communications* 264 (3), pp. 847–854. DOI: 10.1006/bbrc.1999.1585.

Cheng, Bing; Crasta, Karen (2017): Consequences of mitotic slippage for antimicrotubule drug therapy. In *Endocrine-related cancer* 24 (9), T97-T106. DOI: 10.1530/ERC-17-0147.

Chew, Eng-Hui; Hagen, Thilo (2007): Substrate-mediated regulation of cullin neddylation. In *The Journal of biological chemistry* 282 (23), pp. 17032–17040. DOI: 10.1074/jbc.M701153200.

Chiang, H. L.; Terlecky, S. R.; Plant, C. P.; Dice, J. F. (1989): A role for a 70-kilodalton heat shock protein in lysosomal degradation of intracellular proteins. In *Science (New York, N.Y.)* 246 (4928), pp. 382–385. DOI: 10.1126/science.2799391.

Chu, L.; Gu, J.; Sun, L.; Qian, Q.; Qian, C.; Liu, X. (2008): Oncolytic adenovirus-mediated shRNA against Apollon inhibits tumor cell growth and enhances antitumor effect of 5-fluorouracil. In *Gene therapy* 15 (7), pp. 484–494. DOI: 10.1038/gt.2008.6.

Ciechanover, A.; Heller, H.; Elias, S.; Haas, A. L.; Hershko, A. (1980): ATP-dependent conjugation of reticulocyte proteins with the polypeptide required for protein degradation. In *Proceedings of the National Academy of Sciences of the United States of America* 77 (3), pp. 1365–1368. DOI: 10.1073/pnas.77.3.1365.

Ciechanover, A.; Heller, H.; Katz-Etzion, R.; Hershko, A. (1981): Activation of the heat-stable polypeptide of the ATP-dependent proteolytic system. In *Proceedings of the National Academy of Sciences of the United States of America* 78 (2), pp. 761–765. DOI: 10.1073/pnas.78.2.761.

Ciechanover, A.; Laszlo, A.; Bercovich, B.; Stancovski, I.; Alkalay, I.; Ben-Neriah, Y.; Orian, A. (1995): The ubiquitin-mediated proteolytic system: involvement of molecular chaperones, degradation of oncoproteins, and activation of transcriptional regulators. In *Cold Spring Harbor symposia on quantitative biology* 60, pp. 491–501. DOI: 10.1101/sqb.1995.060.01.053.

Ciechanover, Aaron; Ben-Saadon, Ronen (2004): N-terminal ubiquitination: more protein substrates join in. In *Trends in cell biology* 14 (3), pp. 103–106. DOI: 10.1016/j.tcb.2004.01.004.

Ciechanover, Aaron; Kwon, Yong Tae (2017): Protein Quality Control by Molecular Chaperones in Neurodegeneration. In *Frontiers in neuroscience* 11, p. 185. DOI: 10.3389/fnins.2017.00185.

Cizmecioglu, Onur; Krause, Annekatrin; Bahtz, Ramona; Ehret, Lena; Malek, Nisar; Hoffmann, Ingrid (2012): Plk2 regulates centriole duplication through phosphorylation-mediated degradation of Fbxw7 (human Cdc4). In *Journal of cell science* 125 (Pt 4), pp. 981–992. DOI: 10.1242/jcs.095075.

Clague, Michael J.; Urbé, Sylvie; Komander, David (2019): Breaking the chains: deubiquitylating enzyme specificity begets function. In *Nature reviews. Molecular cell biology* 20 (6), pp. 338–352. DOI: 10.1038/s41580-019-0099-1.

Clemm von Hohenberg, Katharina; Müller, Sandra; Schleich, Sibylle; Meister, Matthias; Bohlen, Jonathan; Hofmann, Thomas G.; Teleman, Aurelio A. (2022): Cyclin B/CDK1 and Cyclin A/CDK2 phosphorylate DENR to promote mitotic protein translation and faithful cell division. In *Nature communications* 13 (1), p. 668. DOI: 10.1038/s41467-022-28265-0.

Collins, Galen Andrew; Goldberg, Alfred L. (2017): The Logic of the 26S Proteasome. In *Cell* 169 (5), pp. 792–806. DOI: 10.1016/j.cell.2017.04.023.

Cope, Gregory A.; Suh, Greg S. B.; Aravind, L.; Schwarz, Sylvia E.; Zipursky, S. Lawrence; Koonin, Eugene V.; Deshaies, Raymond J. (2002): Role of predicted metalloprotease motif of Jab1/Csn5 in cleavage of Nedd8 from Cul1. In *Science (New York, N.Y.)* 298 (5593), pp. 608–611. DOI: 10.1126/science.1075901.

Cox, Jürgen; Hein, Marco Y.; Luber, Christian A.; Paron, Igor; Nagaraj, Nagarjuna; Mann, Matthias (2014): Accurate proteome-wide label-free quantification by delayed normalization and maximal peptide ratio extraction, termed MaxLFQ. In *Molecular & cellular proteomics : MCP* 13 (9), pp. 2513–2526. DOI: 10.1074/mcp.M113.031591.

Cubillos-Rojas, Monica; Amair-Pinedo, Fabiola; Tato, Irantzu; Bartrons, Ramon; Ventura, Francesc; Rosa, Jose Luis (2019): Tris-Acetate Polyacrylamide Gradient Gels for the Simultaneous Electrophoretic Analysis of Proteins of Very High and Low Molecular Mass. In *Methods in molecular biology (Clifton, N.J.)* 1855, pp. 269–277. DOI: 10.1007/978-1-4939-8793-1_22.

Cuervo, A. M.; Palmer, A.; Rivett, A. J.; Knecht, E. (1995): Degradation of proteasomes by lysosomes in rat liver. In *European journal of biochemistry* 227 (3), pp. 792–800. DOI: 10.1111/j.1432-1033.1995.tb20203.x.

Cui, Danrui; Xiong, Xiufang; Shu, Jianfeng; Dai, Xiaoqing; Sun, Yi; Zhao, Yongchao (2020): FBXW7 Confers Radiation Survival by Targeting p53 for Degradation. In *Cell reports* 30 (2), 497-509.e4. DOI: 10.1016/j.celrep.2019.12.032.

Dai, Bin; Xiao, Zhiyong; Zhu, Guangtong; Mao, Beibei; Huang, Hui; Guan, Feng et al. (2020): WD Repeat Domain 5 Promotes Invasion, Metastasis and Tumor Growth in Glioma Through Up-Regulated

Zinc Finger E-Box Binding Homeobox 1 Expression. In *Cancer management and research* 12, pp. 3223–3235. DOI: 10.2147/CMAR.S237582.

Dajani, Rana; Fraser, Elizabeth; Roe, S. Mark; Yeo, Maggie; Good, Valerie M.; Thompson, Vivienne et al. (2003): Structural basis for recruitment of glycogen synthase kinase 3beta to the axin-APC scaffold complex. In *The EMBO journal* 22 (3), pp. 494–501. DOI: 10.1093/emboj/cdg068.

D'Angiolella, Vincenzo; Donato, Valerio; Forrester, Frances M.; Jeong, Yeon-Tae; Pellacani, Claudia; Kudo, Yasusei et al. (2012): Cyclin F-mediated degradation of ribonucleotide reductase M2 controls genome integrity and DNA repair. In *Cell* 149 (5), pp. 1023–1034. DOI: 10.1016/j.cell.2012.03.043.

D'Angiolella, Vincenzo; Donato, Valerio; Vijayakumar, Sangeetha; Saraf, Anita; Florens, Laurence; Washburn, Michael P. et al. (2010): SCF(Cyclin F) controls centrosome homeostasis and mitotic fidelity through CP110 degradation. In *Nature* 466 (7302), pp. 138–142. DOI: 10.1038/nature09140.

Dauch, Cara; Shim, Sharon; Cole, Matthew Wyatt; Pollock, Nijole C.; Beer, Abigail J.; Ramroop, Johnny et al. (2022): KMT2D loss drives aggressive tumor phenotypes in cutaneous squamous cell carcinoma. In *American Journal of Cancer Research* 12 (3), pp. 1309–1322.

Davis, Michael A.; Larimore, Elizabeth A.; Fissel, Brian M.; Swanger, Jherek; Taatjes, Dylan J.; Clurman, Bruce E. (2013): The SCF-Fbw7 ubiquitin ligase degrades MED13 and MED13L and regulates CDK8 module association with Mediator. In *Genes & development* 27 (2), pp. 151–156. DOI: 10.1101/gad.207720.112.

Davis, Ryan J.; Welcker, Markus; Clurman, Bruce E. (2014): Tumor suppression by the Fbw7 ubiquitin ligase: mechanisms and opportunities. In *Cancer cell* 26 (4), pp. 455–464. DOI: 10.1016/j.ccell.2014.09.013.

Dawkins, Joshua B. N.; Wang, Jun; Maniati, Eleni; Heward, James A.; Koniali, Lola; Kocher, Hemant M. et al. (2016): Reduced Expression of Histone Methyltransferases KMT2C and KMT2D Correlates with Improved Outcome in Pancreatic Ductal Adenocarcinoma. In *Cancer research* 76 (16), pp. 4861–4871. DOI: 10.1158/0008-5472.CAN-16-0481.

Dephoure, Noah; Zhou, Chunshui; Villén, Judit; Beausoleil, Sean A.; Bakalarski, Corey E.; Elledge, Stephen J.; Gygi, Steven P. (2008): A quantitative atlas of mitotic phosphorylation. In *Proceedings of the National Academy of Sciences of the United States of America* 105 (31), pp. 10762–10767. DOI: 10.1073/pnas.0805139105.

Dias, Jorge; van Nguyen, Nhuong; Georgiev, Plamen; Gaub, Aline; Brettschneider, Janine; Cusack, Stephen et al. (2014): Structural analysis of the KANSL1/WDR5/KANSL2 complex reveals that WDR5 is required for efficient assembly and chromatin targeting of the NSL complex. In *Genes & development* 28 (9), pp. 929–942. DOI: 10.1101/gad.240200.114.

Díaz-Martínez, Laura A.; Karamysheva, Zemfira N.; Warrington, Ross; Li, Bing; Wei, Shuguang; Xie, Xian-Jin et al. (2014): Genome-wide siRNA screen reveals coupling between mitotic apoptosis and adaptation. In *The EMBO journal* 33 (17), pp. 1960–1976. DOI: 10.15252/embj.201487826.

Dick, T. P.; Nussbaum, A. K.; Deeg, M.; Heinemeyer, W.; Groll, M.; Schirle, M. et al. (1998): Contribution of proteasomal beta-subunits to the cleavage of peptide substrates analyzed with yeast mutants. In *The Journal of biological chemistry* 273 (40), pp. 25637–25646. DOI: 10.1074/jbc.273.40.25637.

Dikic, Ivan; Schulman, Brenda A. (2022): An expanded lexicon for the ubiquitin code. In *Nature reviews. Molecular cell biology*. DOI: 10.1038/s41580-022-00543-1.

Dikic, Ivan; Wakatsuki, Soichi; Walters, Kylie J. (2009): Ubiquitin-binding domains - from structures to functions. In *Nature reviews. Molecular cell biology* 10 (10), pp. 659–671. DOI: 10.1038/nrm2767.

DiNardo, Courtney D.; Pratz, Keith W.; Letai, Anthony; Jonas, Brian A.; Wei, Andrew H.; Thirman, Michael et al. (2018): Safety and preliminary efficacy of venetoclax with decitabine or azacitidine in elderly patients with previously untreated acute myeloid leukaemia: a non-randomised, open-label, phase 1b study. In *The Lancet Oncology* 19 (2), pp. 216–228. DOI: 10.1016/S1470-2045(18)30010-X.

Dong, Xin; Lin, Dong; Low, Chris; Vucic, Emily A.; English, John C.; Yee, John et al. (2013): Elevated expression of BIRC6 protein in non-small-cell lung cancers is associated with cancer recurrence and chemoresistance. In *Journal of thoracic oncology : official publication of the International Association for the Study of Lung Cancer* 8 (2), pp. 161–170. DOI: 10.1097/JTO.0b013e31827d5237.

Duda, David M.; Borg, Laura A.; Scott, Daniel C.; Hunt, Harold W.; Hammel, Michal; Schulman, Brenda A. (2008): Structural insights into NEDD8 activation of cullin-RING ligases: conformational control of conjugation. In *Cell* 134 (6), pp. 995–1006. DOI: 10.1016/j.cell.2008.07.022.

Ebner, Petra; Poetsch, Isabella; Deszcz, Luiza; Hoffmann, Thomas; Zuber, Johannes; Ikeda, Fumiyo (2018): The IAP family member BRUCE regulates autophagosome-lysosome fusion. In *Nature communications* 9 (1), p. 599. DOI: 10.1038/s41467-018-02823-x.

Ekholm, Susanna V.; Reed, Steven I. (2000): Regulation of G1 cyclin-dependent kinases in the mammalian cell cycle. In *Current opinion in cell biology* 12 (6), pp. 676–684. DOI: 10.1016/s0955-0674(00)00151-4.

Ellis, R. John; Minton, Allen P. (2006): Protein aggregation in crowded environments. In *Biological chemistry* 387 (5), pp. 485–497. DOI: 10.1515/BC.2006.064.

Emberley, Ethan D.; Mosadeghi, Ruzbeh; Deshaies, Raymond J. (2012): Deconjugation of Nedd8 from Cul1 is directly regulated by Skp1-F-box and substrate, and the COP9 signalosome inhibits deneddylated SCF by a noncatalytic mechanism. In *The Journal of biological chemistry* 287 (35), pp. 29679–29689. DOI: 10.1074/jbc.M112.352484.

Enchev, Radoslav I.; Scott, Daniel C.; Da Fonseca, Paula C. A.; Schreiber, Anne; Monda, Julie K.; Schulman, Brenda A. et al. (2012): Structural basis for a reciprocal regulation between SCF and CSN. In *Cell reports* 2 (3), pp. 616–627. DOI: 10.1016/j.celrep.2012.08.019.

Enenkel, C.; Lehmann, A.; Kloetzel, P. M. (1998): Subcellular distribution of proteasomes implicates a major location of protein degradation in the nuclear envelope-ER network in yeast. In *The EMBO journal* 17 (21), pp. 6144–6154. DOI: 10.1093/emboj/17.21.6144.

Fan, Jingyi; Bellon, Marcia; Ju, Mingyi; Zhao, Lin; Wei, Minjie; Fu, Liwu; Nicot, Christophe (2022): Clinical significance of FBXW7 loss of function in human cancers. In *Molecular cancer* 21 (1), p. 87. DOI: 10.1186/s12943-022-01548-2.

Feldman, R.M.Renny; Correll, Craig C.; Kaplan, Kenneth B.; Deshaies, Raymond J. (1997): A Complex of Cdc4p, Skp1p, and Cdc53p/Cullin Catalyzes Ubiquitination of the Phosphorylated CDK Inhibitor Sic1p. In *Cell* 91 (2), pp. 221–230. DOI: 10.1016/s0092-8674(00)80404-3.

Finkin, S.; Aylon, Y.; Anzi, S.; Oren, M.; Shaulian, E. (2008): Fbw7 regulates the activity of endoreduplication mediators and the p53 pathway to prevent drug-induced polyploidy. In *Oncogene* 27 (32), pp. 4411–4421. DOI: 10.1038/onc.2008.77.

Finley, Daniel (2009): Recognition and processing of ubiquitin-protein conjugates by the proteasome. In *Annual review of biochemistry* 78, pp. 477–513. DOI: 10.1146/annurev.biochem.78.081507.101607.

Finley, Daniel; Prado, Miguel A. (2020): The Proteasome and Its Network: Engineering for Adaptability. In *Cold Spring Harbor perspectives in biology* 12 (1). DOI: 10.1101/cshperspect.a033985.

Fischer, Eric S.; Böhm, Kerstin; Lydeard, John R.; Yang, Haidi; Stadler, Michael B.; Cavadini, Simone et al. (2014): Structure of the DDB1-CRBN E3 ubiquitin ligase in complex with thalidomide. In *Nature* 512 (7512), pp. 49–53. DOI: 10.1038/nature13527.

Fischer, Eric S.; Scrima, Andrea; Böhm, Kerstin; Matsumoto, Syota; Lingaraju, Gondichatnahalli M.; Faty, Mahamadou et al. (2011): The molecular basis of CRL4DDB2/CSA ubiquitin ligase architecture, targeting, and activation. In *Cell* 147 (5), pp. 1024–1039. DOI: 10.1016/j.cell.2011.10.035.

Fisher, Robert P. (2012): The CDK Network: Linking Cycles of Cell Division and Gene Expression. In *Genes & cancer* 3 (11-12), pp. 731–738. DOI: 10.1177/1947601912473308.

Flemming (1882): Zellsubstanz, Kern und Zelltheilung: F.C.W. Vogel.

Foley, Emily A.; Kapoor, Tarun M. (2013): Microtubule attachment and spindle assembly checkpoint signalling at the kinetochore. In *Nature reviews. Molecular cell biology* 14 (1), pp. 25–37. DOI: 10.1038/nrm3494.

Fraschini, R.; Beretta, A.; Sironi, L.; Musacchio, A.; Lucchini, G.; Piatti, S. (2001): Bub3 interaction with Mad2, Mad3 and Cdc20 is mediated by WD40 repeats and does not require intact kinetochores. In *The EMBO journal* 20 (23), pp. 6648–6659. DOI: 10.1093/emboj/20.23.6648.

Fujimitsu, Kazuyuki; Grimaldi, Margaret; Yamano, Hiroyuki (2016): Cyclin-dependent kinase 1-dependent activation of APC/C ubiquitin ligase. In *Science (New York, N.Y.)* 352 (6289), pp. 1121–1124. DOI: 10.1126/science.aad3925.

Galindo-Moreno, María; Giráldez, Servando; Limón-Mortés, M. Cristina; Belmonte-Fernández, Alejandro; Reed, Steven I.; Sáez, Carmen et al. (2019): SCF(FBXW7)-mediated degradation of p53 promotes cell recovery after UV-induced DNA damage. In *FASEB journal : official publication of the Federation of American Societies for Experimental Biology* 33 (10), pp. 11420–11430. DOI: 10.1096/fj.201900885R.

Galluzzi, L.; Bravo-San Pedro, J. M.; Vitale, I.; Aaronson, S. A.; Abrams, J. M.; Adam, D. et al. (2015): Essential versus accessory aspects of cell death: recommendations of the NCCD 2015. In *Cell death and differentiation* 22 (1), pp. 58–73. DOI: 10.1038/cdd.2014.137.

Galluzzi, Lorenzo; Baehrecke, Eric H.; Ballabio, Andrea; Boya, Patricia; Bravo-San Pedro, José Manuel; Cecconi, Francesco et al. (2017): Molecular definitions of autophagy and related processes. In *The EMBO journal* 36 (13), pp. 1811–1836. DOI: 10.15252/embj.201796697.

Gao, Weiwu; Jia, Zhengcai; Tian, Yi; Yang, Penghui; Sun, Hui; Wang, Chenhui et al. (2020): HBx Protein Contributes to Liver Carcinogenesis by H3K4me3 Modification Through Stabilizing WD Repeat Domain 5 Protein. In *Hepatology (Baltimore, Md.)* 71 (5), pp. 1678–1695. DOI: 10.1002/hep.30947.

Gao, Wentao; Kang, Jeong Han; Liao, Yong; Ding, Wen-Xing; Gambotto, Andrea A.; Watkins, Simon C. et al. (2010): Biochemical isolation and characterization of the tubulovesicular LC3-positive autophagosomal compartment. In *The Journal of biological chemistry* 285 (2), pp. 1371–1383. DOI: 10.1074/jbc.M109.054197.

Garrison, Jason B.; Ge, Chunmin; Che, Lixiao; Pullum, Derek A.; Peng, Guang; Khan, Sohaib et al. (2015): Knockdown of the Inhibitor of Apoptosis BRUCE Sensitizes Resistant Breast Cancer Cells to Chemotherapeutic Agents. In *Journal of cancer science & therapy* 7 (4), pp. 121–126. DOI: 10.4172/1948-5956.1000335.

Gasca, Jessica; Flores, Maria Luz; Giráldez, Servando; Ruiz-Borrego, Manuel; Tortolero, María; Romero, Francisco et al. (2016): Loss of FBXW7 and accumulation of MCL1 and PLK1 promote paclitaxel resistance in breast cancer. In *Oncotarget* 7 (33), pp. 52751–52765. DOI: 10.18632/oncotarget.10481.

Gascoigne, Karen E.; Taylor, Stephen S. (2008): Cancer cells display profound intra- and interline variation following prolonged exposure to antimitotic drugs. In *Cancer cell* 14 (2), pp. 111–122. DOI: 10.1016/j.ccr.2008.07.002.

Geng, Yan; Lee, Young-Mi; Welcker, Markus; Swanger, Jherek; Zagozdzon, Agnieszka; Winer, Joel D. et al. (2007): Kinase-independent function of cyclin E. In *Molecular cell* 25 (1), pp. 127–139. DOI: 10.1016/j.molcel.2006.11.029.

Ghobrial, Irene M.; Witzig, Thomas E.; Adjei, Alex A. (2005): Targeting apoptosis pathways in cancer therapy. In *CA: a cancer journal for clinicians* 55 (3), pp. 178–194. DOI: 10.3322/canjclin.55.3.178.

Girdler, Fiona; Gascoigne, Karen E.; Eyers, Patrick A.; Hartmuth, Sonya; Crafter, Claire; Foote, Kevin M. et al. (2006): Validating Aurora B as an anti-cancer drug target. In *Journal of cell science* 119 (Pt 17), pp. 3664–3675. DOI: 10.1242/jcs.03145.

Goldberg, A. L.; Dice, J. F. (1974): Intracellular protein degradation in mammalian and bacterial cells. In *Annual review of biochemistry* 43 (0), pp. 835–869. DOI: 10.1146/annurev.bi.43.070174.004155.

Goldenberg, Seth J.; Cascio, Thomas C.; Shumway, Stuart D.; Garbutt, Kenneth C.; Liu, Jidong; Xiong, Yue; Zheng, Ning (2004): Structure of the Cand1-Cul1-Roc1 complex reveals regulatory mechanisms for the assembly of the multisubunit cullin-dependent ubiquitin ligases. In *Cell* 119 (4), pp. 517–528. DOI: 10.1016/j.cell.2004.10.019.

Goyal, Lakshmi (2001): Cell Death Inhibition. In *Cell* 104 (6), pp. 805–808. DOI: 10.1016/s0092-8674(01)00276-8.

Grebien, Florian; Vedadi, Masoud; Getlik, Matthäus; Giambruno, Roberto; Grover, Amit; Avellino, Roberto et al. (2015): Pharmacological targeting of the Wdr5-MLL interaction in C/EBPα N-terminal leukemia. In *Nature chemical biology* 11 (8), pp. 571–578. DOI: 10.1038/nchembio.1859.

Gregory, M. A.; Hann, S. R. (2000): c-Myc proteolysis by the ubiquitin-proteasome pathway: stabilization of c-Myc in Burkitt's lymphoma cells. In *Molecular and cellular biology* 20 (7), pp. 2423–2435. DOI: 10.1128/mcb.20.7.2423-2435.2000.

Grim, Jonathan E.; Knoblaugh, Sue E.; Guthrie, Katherine A.; Hagar, Amanda; Swanger, Jherek; Hespelt, Jessica et al. (2012): Fbw7 and p53 cooperatively suppress advanced and chromosomally

unstable intestinal cancer. In *Molecular and cellular biology* 32 (11), pp. 2160–2167. DOI: 10.1128/mcb.00305-12.

Groll, M.; Ditzel, L.; Löwe, J.; Stock, D.; Bochtler, M.; Bartunik, H. D.; Huber, R. (1997): Structure of 20S proteasome from yeast at 2.4 A resolution. In *Nature* 386 (6624), pp. 463–471. DOI: 10.1038/386463a0.

Gu, Zhaodi; Mitsui, Hidetoshi; Inomata, Kenichi; Honda, Masako; Endo, Chiaki; Sakurada, Akira et al. (2008): The methylation status of FBXW7 beta-form correlates with histological subtype in human thymoma. In *Biochemical and Biophysical Research Communications* 377 (2), pp. 685–688. DOI: 10.1016/j.bbrc.2008.10.047.

Guadagno, Thomas M.; Newport, John W. (1996): Cdk2 Kinase Is Required for Entry into Mitosis as a Positive Regulator of Cdc2–Cyclin B Kinase Activity. In *Cell* 84 (1), pp. 73–82. DOI: 10.1016/s0092-8674(00)80994-0.

Guarnaccia, Alissa D.; Rose, Kristie L.; Wang, Jing; Zhao, Bin; Popay, Tessa M.; Wang, Christina E. et al. (2021): Impact of WIN site inhibitor on the WDR5 interactome. In *Cell reports* 34 (3), p. 108636. DOI: 10.1016/j.celrep.2020.108636.

Guarnaccia, Alissa duPuy; Tansey, William Patrick (2018): Moonlighting with WDR5: A Cellular Multitasker. In *Journal of clinical medicine* 7 (2). DOI: 10.3390/jcm7020021.

Guharoy, Mainak; Lazar, Tamas; Macossay-Castillo, Mauricio; Tompa, Peter (2022): Degron masking outlines degronons, co-degrading functional modules in the proteome. In *Communications biology* 5 (1), p. 445. DOI: 10.1038/s42003-022-03391-z.

Habu, Toshiyuki; Matsumoto, Tomohiro (2013): p31(comet) inactivates the chemically induced Mad2-dependent spindle assembly checkpoint and leads to resistance to anti-mitotic drugs. In *SpringerPlus* 2, p. 562. DOI: 10.1186/2193-1801-2-562.

Hänle-Kreidler, Simon; Richter, Kai T.; Hoffmann, Ingrid (2022): The SCF-FBXW7 E3 ubiquitin ligase triggers degradation of Histone 3 Lysine 4 methyltransferase complex component WDR5 to prevent mitotic slippage. In *The Journal of biological chemistry*, p. 102703. DOI: 10.1016/j.jbc.2022.102703.

Hao, Bing; Oehlmann, Stephanie; Sowa, Mathew E.; Harper, J. Wade; Pavletich, Nikola P. (2007): Structure of a Fbw7-Skp1-cyclin E complex: multisite-phosphorylated substrate recognition by SCF ubiquitin ligases. In *Molecular cell* 26 (1), pp. 131–143. DOI: 10.1016/j.molcel.2007.02.022.

Hao, Yanyan; Sekine, Keiko; Kawabata, Atsushi; Nakamura, Hitoshi; Ishioka, Toshiyasu; Ohata, Hirokazu et al. (2004): Apollon ubiquitinates SMAC and caspase-9, and has an essential cytoprotection function. In *Nature cell biology* 6 (9), pp. 849–860. DOI: 10.1038/ncb1159.

Hara, Masatoshi; Fukagawa, Tatsuo (2018): Kinetochore assembly and disassembly during mitotic entry and exit. In *Current opinion in cell biology* 52, pp. 73–81. DOI: 10.1016/j.ceb.2018.02.005.

Hardwick, K. G.; Johnston, R. C.; Smith, D. L.; Murray, A. W. (2000): MAD3 encodes a novel component of the spindle checkpoint which interacts with Bub3p, Cdc20p, and Mad2p. In *The Journal of cell biology* 148 (5), pp. 871–882. DOI: 10.1083/jcb.148.5.871.

Harper, J. Wade; Schulman, Brenda A. (2021): Cullin-RING Ubiquitin Ligase Regulatory Circuits: A Quarter Century Beyond the F-Box Hypothesis. In *Annual review of biochemistry* 90, pp. 403–429. DOI: 10.1146/annurev-biochem-090120-013613.

Hartl, F. Ulrich (2017): Protein Misfolding Diseases. In *Annual review of biochemistry* 86, pp. 21–26. DOI: 10.1146/annurev-biochem-061516-044518.

Hartl, F. Ulrich; Bracher, Andreas; Hayer-Hartl, Manajit (2011): Molecular chaperones in protein folding and proteostasis. In *Nature* 475 (7356), pp. 324–332. DOI: 10.1038/nature10317.

Hauser, H. P.; Bardroff, M.; Pyrowolakis, G.; Jentsch, S. (1998): A giant ubiquitin-conjugating enzyme related to IAP apoptosis inhibitors. In *The Journal of cell biology* 141 (6), pp. 1415–1422. DOI: 10.1083/jcb.141.6.1415.

Hayward, Daniel; Alfonso-Pérez, Tatiana; Gruneberg, Ulrike (2019): Orchestration of the spindle assembly checkpoint by CDK1-cyclin B1. In *FEBS letters* 593 (20), pp. 2889–2907. DOI: 10.1002/1873-3468.13591.

Heckman, Karin L.; Pease, Larry R. (2007): Gene splicing and mutagenesis by PCR-driven overlap extension. In *Nature protocols* 2 (4), pp. 924–932. DOI: 10.1038/nprot.2007.132.

Heinemeyer, W.; Fischer, M.; Krimmer, T.; Stachon, U.; Wolf, D. H. (1997): The active sites of the eukaryotic 20 S proteasome and their involvement in subunit precursor processing. In *The Journal of biological chemistry* 272 (40), pp. 25200–25209. DOI: 10.1074/jbc.272.40.25200.

Hershko, A.; Ciechanover, A. (1998): The ubiquitin system. In *Annual review of biochemistry* 67, pp. 425–479. DOI: 10.1146/annurev.biochem.67.1.425.

Hershko, A.; Ciechanover, A.; Heller, H.; Haas, A. L.; Rose, I. A. (1980): Proposed role of ATP in protein breakdown: conjugation of protein with multiple chains of the polypeptide of ATP-dependent proteolysis. In *Proceedings of the National Academy of Sciences of the United States of America* 77 (4), pp. 1783–1786. DOI: 10.1073/pnas.77.4.1783.

Hershko, A.; Heller, H.; Elias, S.; Ciechanover, A. (1983): Components of ubiquitin-protein ligase system. Resolution, affinity purification, and role in protein breakdown. In *The Journal of biological chemistry* 258 (13), pp. 8206–8214.

Hershko, Avram (1996): Lessons from the discovery ofthe ubiquitin system. In *Trends in biochemical sciences* 21 (11), pp. 445–449. DOI: 10.1016/s0968-0004(96)10054-2.

Hershko, Avram; Heller, Hannah (1985): Occurrence of a polyubiquitin structure in ubiquitin-protein conjugates. In *Biochemical and Biophysical Research Communications* 128 (3), pp. 1079–1086. DOI: 10.1016/0006-291X(85)91050-2.

Higa, Leigh Ann; Wu, Min; Ye, Tao; Kobayashi, Ryuji; Sun, Hong; Zhang, Hui (2006): CUL4-DDB1 ubiquitin ligase interacts with multiple WD40-repeat proteins and regulates histone methylation. In *Nature cell biology* 8 (11), pp. 1277–1283. DOI: 10.1038/ncb1490.

Hiruma, Yoshitaka; Sacristan, Carlos; Pachis, Spyridon T.; Adamopoulos, Athanassios; Kuijt, Timo; Ubbink, Marcellus et al. (2015): CELL DIVISION CYCLE. Competition between MPS1 and microtubules at kinetochores regulates spindle checkpoint signaling. In *Science (New York, N.Y.)* 348 (6240), pp. 1264–1267. DOI: 10.1126/science.aaa4055.

Hoffmann, I.; Clarke, P. R.; Marcote, M. J.; Karsenti, E.; Draetta, G. (1993): Phosphorylation and activation of human cdc25-C by cdc2--cyclin B and its involvement in the self-amplification of MPF at mitosis. In *The EMBO journal* 12 (1), pp. 53–63. DOI: 10.1002/j.1460-2075.1993.tb05631.x.

Hong, Xuehui; Liu, Wenyu; Song, Ruipeng; Shah, Jamie J.; Feng, Xing; Tsang, Chi Kwan et al. (2016): SOX9 is targeted for proteasomal degradation by the E3 ligase FBW7 in response to DNA damage. In *Nucleic acids research* 44 (18), pp. 8855–8869. DOI: 10.1093/nar/gkw748.

Hornbeck, Peter V.; Zhang, Bin; Murray, Beth; Kornhauser, Jon M.; Latham, Vaughan; Skrzypek, Elzbieta (2015): PhosphoSitePlus, 2014: mutations, PTMs and recalibrations. In *Nucleic acids research* 43 (Database issue), D512-20. DOI: 10.1093/nar/gku1267.

Hough, R.; Pratt, G.; Rechsteiner, M. (1986): Ubiquitin-lysozyme conjugates. Identification and characterization of an ATP-dependent protease from rabbit reticulocyte lysates. In *The Journal of biological chemistry* 261 (5), pp. 2400–2408.

Hu, Min; Li, Pingwei; Li, Muyang; Li, Wenyu; Yao, Tingting; Wu, Jia-Wei et al. (2002): Crystal Structure of a UBP-Family Deubiquitinating Enzyme in Isolation and in Complex with Ubiquitin Aldehyde. In *Cell* 111 (7), pp. 1041–1054. DOI: 10.1016/s0092-8674(02)01199-6.

Hu, Tingting; Weng, Shuqiang; Tang, Wenqing; Xue, Ruyi; Chen, She; Cai, Guoxiang et al. (2015): Overexpression of BIRC6 Is a Predictor of Prognosis for Colorectal Cancer. In *PloS one* 10 (5), e0125281. DOI: 10.1371/journal.pone.0125281.

Hua, Zhihua; Vierstra, Richard D. (2011): The cullin-RING ubiquitin-protein ligases. In *Annual review of plant biology* 62, pp. 299–334. DOI: 10.1146/annurev-arplant-042809-112256.

Huang, Rui-Xue; Zhou, Ping-Kun (2020): DNA damage response signaling pathways and targets for radiotherapy sensitization in cancer. In *Signal transduction and targeted therapy* 5 (1), p. 60. DOI: 10.1038/s41392-020-0150-x.

Hubbard, E. J.; Wu, G.; Kitajewski, J.; Greenwald, I. (1997): sel-10, a negative regulator of lin-12 activity in Caenorhabditis elegans, encodes a member of the CDC4 family of proteins. In *Genes & development* 11 (23), pp. 3182–3193. DOI: 10.1101/gad.11.23.3182.

Ikeda, Fumiyo; Dikic, Ivan (2008): Atypical ubiquitin chains: new molecular signals. 'Protein Modifications: Beyond the Usual Suspects' review series. In *EMBO reports* 9 (6), pp. 536–542. DOI: 10.1038/embor.2008.93.

Inuzuka, Hiroyuki; Shaik, Shavali; Onoyama, Ichiro; Gao, Daming; Tseng, Alan; Maser, Richard S. et al. (2011): SCF(FBW7) regulates cellular apoptosis by targeting MCL1 for ubiquitylation and destruction. In *Nature* 471 (7336), pp. 104–109. DOI: 10.1038/nature09732.

Isobe, Tomoyasu; Hattori, Takayuki; Kitagawa, Kyoko; Uchida, Chiharu; Kotake, Yojiro; Kosugi, Isao et al. (2009): Adenovirus E1A inhibits SCF(Fbw7) ubiquitin ligase. In *The Journal of biological chemistry* 284 (41), pp. 27766–27779. DOI: 10.1074/jbc.M109.006809.

Ito, Takumi; Ando, Hideki; Suzuki, Takayuki; Ogura, Toshihiko; Hotta, Kentaro; Imamura, Yoshimasa et al. (2010): Identification of a primary target of thalidomide teratogenicity. In *Science (New York, N.Y.)* 327 (5971), pp. 1345–1350. DOI: 10.1126/science.1177319.

Ito-Harashima, Sayoko; Kuroha, Kazushige; Tatematsu, Tsuyako; Inada, Toshifumi (2007): Translation of the poly(A) tail plays crucial roles in nonstop mRNA surveillance via translation repression and protein destabilization by proteasome in yeast. In *Genes & development* 21 (5), pp. 519–524. DOI: 10.1101/gad.1490207.

Jang, Ho Hee (2018): Regulation of Protein Degradation by Proteasomes in Cancer. In *Journal of cancer prevention* 23 (4), pp. 153–161. DOI: 10.15430/JCP.2018.23.4.153.

Janssen, A.; Medema, R. H. (2013): Genetic instability: tipping the balance. In *Oncogene* 32 (38), pp. 4459–4470. DOI: 10.1038/onc.2012.576.

Ji, Zhejian; Gao, Haishan; Yu, Hongtao (2015): CELL DIVISION CYCLE. Kinetochore attachment sensed by competitive Mps1 and microtubule binding to Ndc80C. In *Science (New York, N.Y.)* 348 (6240), pp. 1260–1264. DOI: 10.1126/science.aaa4029.

Jia, Rui; Bonifacino, Juan S. (2019): Negative regulation of autophagy by UBA6-BIRC6-mediated ubiquitination of LC3. In *eLife* 8. DOI: 10.7554/eLife.50034.

Jin, Jianping; Arias, Emily E.; Chen, Jing; Harper, J. Wade; Walter, Johannes C. (2006): A family of diverse Cul4-Ddb1-interacting proteins includes Cdt2, which is required for S phase destruction of the replication factor Cdt1. In *Molecular cell* 23 (5), pp. 709–721. DOI: 10.1016/j.molcel.2006.08.010.

Jin, Jianping; Cardozo, Timothy; Lovering, Ruth C.; Elledge, Stephen J.; Pagano, Michele; Harper, J. Wade (2004): Systematic analysis and nomenclature of mammalian F-box proteins. In *Genes & development* 18 (21), pp. 2573–2580. DOI: 10.1101/gad.1255304.

Jin, Lingyan; Williamson, Adam; Banerjee, Sudeep; Philipp, Isabelle; Rape, Michael (2008): Mechanism of ubiquitin-chain formation by the human anaphase-promoting complex. In *Cell* 133 (4), pp. 653–665. DOI: 10.1016/j.cell.2008.04.012.

Joazeiro, Claudio A. P. (2017): Ribosomal Stalling During Translation: Providing Substrates for Ribosome-Associated Protein Quality Control. In *Annual review of cell and developmental biology* 33, pp. 343–368. DOI: 10.1146/annurev-cellbio-111315-125249.

Joazeiro, Claudio A. P. (2019): Mechanisms and functions of ribosome-associated protein quality control. In *Nature reviews. Molecular cell biology* 20 (6), pp. 368–383. DOI: 10.1038/s41580-019-0118-2.

Jordan, Mary Ann; Wilson, Leslie (2004): Microtubules as a target for anticancer drugs. In *Nature reviews. Cancer* 4 (4), pp. 253–265. DOI: 10.1038/nrc1317.

Joukov, Vladimir; Nicolo, Arcangela de (2018): Aurora-PLK1 cascades as key signaling modules in the regulation of mitosis. In *Science signaling* 11 (543). DOI: 10.1126/scisignal.aar4195.

Kaestner, Phillip; Stolz, Ailine; Bastians, Holger (2009): Determinants for the efficiency of anticancer drugs targeting either Aurora-A or Aurora-B kinases in human colon carcinoma cells. In *Molecular cancer therapeutics* 8 (7), pp. 2046–2056. DOI: 10.1158/1535-7163.MCT-09-0323.

Kaiser, Christian M.; Liu, Kaixian (2018): Folding up and Moving on-Nascent Protein Folding on the Ribosome. In *Journal of molecular biology* 430 (22), pp. 4580–4591. DOI: 10.1016/j.jmb.2018.06.050.

Kamadurai, Hari B.; Souphron, Judith; Scott, Daniel C.; Duda, David M.; Miller, Darcie J.; Stringer, Daniel et al. (2009): Insights into ubiquitin transfer cascades from a structure of a UbcH5B approximately

ubiquitin-HECT(NEDD4L) complex. In *Molecular cell* 36 (6), pp. 1095–1102. DOI: 10.1016/j.molcel.2009.11.010.

Keck, Jamie M.; Summers, Matthew K.; Tedesco, Donato; Ekholm-Reed, Susanna; Chuang, Li-Chiou; Jackson, Peter K.; Reed, Steven I. (2007): Cyclin E overexpression impairs progression through mitosis by inhibiting APC(Cdh1). In *The Journal of cell biology* 178 (3), pp. 371–385. DOI: 10.1083/jcb.200703202.

Keiler, K. C.; Waller, P. R.; Sauer, R. T. (1996): Role of a peptide tagging system in degradation of proteins synthesized from damaged messenger RNA. In *Science (New York, N.Y.)* 271 (5251), pp. 990–993. DOI: 10.1126/science.271.5251.990.

Kettenbach, Arminja N.; Schweppe, Devin K.; Faherty, Brendan K.; Pechenick, Dov; Pletnev, Alexandre A.; Gerber, Scott A. (2011): Quantitative phosphoproteomics identifies substrates and functional modules of Aurora and Polo-like kinase activities in mitotic cells. In *Science signaling* 4 (179), rs5. DOI: 10.1126/scisignal.2001497.

Khaminets, Aliaksandr; Behl, Christian; Dikic, Ivan (2016): Ubiquitin-Dependent And Independent Signals In Selective Autophagy. In *Trends in cell biology* 26 (1), pp. 6–16. DOI: 10.1016/j.tcb.2015.08.010.

Khan, Omar M.; Carvalho, Joana; Spencer-Dene, Bradley; Mitter, Richard; Frith, David; Snijders, Ambrosius P. et al. (2018): The deubiquitinase USP9X regulates FBW7 stability and suppresses colorectal cancer. In *The Journal of clinical investigation* 128 (4), pp. 1326–1337. DOI: 10.1172/JCI97325.

Khmelinskii, Anton; Keller, Philipp J.; Bartosik, Anna; Meurer, Matthias; Barry, Joseph D.; Mardin, Balca R. et al. (2012): Tandem fluorescent protein timers for in vivo analysis of protein dynamics. In *Nature biotechnology* 30 (7), pp. 708–714. DOI: 10.1038/nbt.2281.

Kienle, Simon Maria; Schneider, Tobias; Stuber, Katrin; Globisch, Christoph; Jansen, Jasmin; Stengel, Florian et al. (2022): Electrostatic and steric effects underlie acetylation-induced changes in ubiquitin structure and function. In *Nature communications* 13 (1), p. 5435. DOI: 10.1038/s41467-022-33087-1.

Kim, Jae-Hwan; Sharma, Amrish; Dhar, Shilpa S.; Lee, Sung-Hun; Gu, Bingnan; Chan, Chia-Hsin et al. (2014): UTX and MLL4 coordinately regulate transcriptional programs for cell proliferation and invasiveness in breast cancer cells. In *Cancer research* 74 (6), pp. 1705–1717. DOI: 10.1158/0008-5472.CAN-13-1896.

Kim, Yujin E.; Hipp, Mark S.; Bracher, Andreas; Hayer-Hartl, Manajit; Hartl, F. Ulrich (2013): Molecular chaperone functions in protein folding and proteostasis. In *Annual review of biochemistry* 82, pp. 323–355. DOI: 10.1146/annurev-biochem-060208-092442.

Kimura, Takashi; Gotoh, Mitsukazu; Nakamura, Yusuke; Arakawa, Hirofumi (2003): hCDC4b, a regulator of cyclin E, as a direct transcriptional target of p53. In *Cancer science* 94 (5), pp. 431–436. DOI: 10.1111/j.1349-7006.2003.tb01460.x.

Kipreos, Edward T.; Lander, Lois E.; Wing, John P.; He, Wei Wu; Hedgecock, Edward M. (1996): cul-1 Is Required for Cell Cycle Exit in C. elegans and Identifies a Novel Gene Family. In *Cell* 85 (6), pp. 829–839. DOI: 10.1016/s0092-8674(00)81267-2.

Koepp, D. M.; Schaefer, L. K.; Ye, X.; Keyomarsi, K.; Chu, C.; Harper, J. W.; Elledge, S. J. (2001): Phosphorylation-dependent ubiquitination of cyclin E by the SCFFbw7 ubiquitin ligase. In *Science (New York, N.Y.)* 294 (5540), pp. 173–177. DOI: 10.1126/science.1065203.

Komander, David; Rape, Michael (2012): The ubiquitin code. In *Annual review of biochemistry* 81, pp. 203–229. DOI: 10.1146/annurev-biochem-060310-170328.

Koren, Itay; Timms, Richard T.; Kula, Tomasz; Xu, Qikai; Li, Mamie Z.; Elledge, Stephen J. (2018): The Eukaryotic Proteome Is Shaped by E3 Ubiquitin Ligases Targeting C-Terminal Degrons. In *Cell* 173 (7), 1622-1635.e14. DOI: 10.1016/j.cell.2018.04.028.

Kozopas, K. M.; Yang, T.; Buchan, H. L.; Zhou, P.; Craig, R. W. (1993): MCL1, a gene expressed in programmed myeloid cell differentiation, has sequence similarity to BCL2. In *Proceedings of the National Academy of Sciences of the United States of America* 90 (8), pp. 3516–3520. DOI: 10.1073/pnas.90.8.3516.

Krönke, Jan; Udeshi, Namrata D.; Narla, Anupama; Grauman, Peter; Hurst, Slater N.; McConkey, Marie et al. (2014): Lenalidomide causes selective degradation of IKZF1 and IKZF3 in multiple myeloma cells. In *Science (New York, N.Y.)* 343 (6168), pp. 301–305. DOI: 10.1126/science.1244851.

Kumar, Manjeet; Michael, Sushama; Alvarado-Valverde, Jesús; Mészáros, Bálint; Sámano-Sánchez, Hugo; Zeke, András et al. (2022): The Eukaryotic Linear Motif resource: 2022 release. In *Nucleic acids research* 50 (D1), D497-D508. DOI: 10.1093/nar/gkab975.

Kwiatkowski, Nicholas; Jelluma, Nannette; Filippakopoulos, Panagis; Soundararajan, Meera; Manak, Michael S.; Kwon, Mijung et al. (2010): Small-molecule kinase inhibitors provide insight into Mps1 cell cycle function. In *Nature chemical biology* 6 (5), pp. 359–368. DOI: 10.1038/nchembio.345.

Lamers, Fieke; Schild, Linda; Koster, Jan; Speleman, Frank; Øra, Ingrid; Westerhout, Ellen M. et al. (2012): Identification of BIRC6 as a novel intervention target for neuroblastoma therapy. In *BMC cancer* 12, p. 285. DOI: 10.1186/1471-2407-12-285.

Lan, Huiyin; Sun, Yi (2021): Tumor Suppressor FBXW7 and Its Regulation of DNA Damage Response and Repair. In *Frontiers in cell and developmental biology* 9, p. 751574. DOI: 10.3389/fcell.2021.751574.

Lan, Huiyin; Tan, Mingjia; Zhang, Qiang; Yang, Fei; Wang, Siyuan; Li, Hua et al. (2019): LSD1 destabilizes FBXW7 and abrogates FBXW7 functions independent of its demethylase activity. In *Proceedings of the National Academy of Sciences of the United States of America* 116 (25), pp. 12311–12320. DOI: 10.1073/pnas.1902012116).

Lander, Gabriel C.; Estrin, Eric; Matyskiela, Mary E.; Bashore, Charlene; Nogales, Eva; Martin, Andreas (2012): Complete subunit architecture of the proteasome regulatory particle. In *Nature* 482 (7384), pp. 186–191. DOI: 10.1038/nature10774.

Larochelle, Stéphane; Merrick, Karl A.; Terret, Marie-Emilie; Wohlbold, Lara; Barboza, Nora M.; Zhang, Chao et al. (2007): Requirements for Cdk7 in the assembly of Cdk1/cyclin B and activation of Cdk2 revealed by chemical genetics in human cells. In *Molecular cell* 25 (6), pp. 839–850. DOI: 10.1016/j.molcel.2007.02.003.

Lasker, Keren; Förster, Friedrich; Bohn, Stefan; Walzthoeni, Thomas; Villa, Elizabeth; Unverdorben, Pia et al. (2012): Molecular architecture of the 26S proteasome holocomplex determined by an integrative approach. In *Proceedings of the National Academy of Sciences of the United States of America* 109 (5), pp. 1380–1387. DOI: 10.1073/pnas.1120559109.

Latres, E.; Chiarle, R.; Schulman, B. A.; Pavletich, N. P.; Pellicer, A.; Inghirami, G.; Pagano, M. (2001): Role of the F-box protein Skp2 in lymphomagenesis. In *Proceedings of the National Academy of Sciences of the United States of America* 98 (5), pp. 2515–2520. DOI: 10.1073/pnas.041475098.

Lau, Alan W.; Inuzuka, Hiroyuki; Fukushima, Hidefumi; Wan, Lixin; Liu, Pengda; Gao, Daming et al. (2013): Regulation of APC(Cdh1) E3 ligase activity by the Fbw7/cyclin E signaling axis contributes to the tumor suppressor function of Fbw7. In *Cell research* 23 (7), pp. 947–961. DOI: 10.1038/cr.2013.67.

Levasseur, Mark D.; Thomas, Christopher; Davies, Owen R.; Higgins, Jonathan M. G.; Madgwick, Suzanne (2019): Aneuploidy in Oocytes Is Prevented by Sustained CDK1 Activity through Degron Masking in Cyclin B1. In *Developmental cell* 48 (5), 672-684.e5. DOI: 10.1016/j.devcel.2019.01.008.

Li, Dongxu; Yu, Xufen; Kottur, Jithesh; Gong, Weida; Zhang, Zhao; Storey, Aaron J. et al. (2022): Discovery of a dual WDR5 and Ikaros PROTAC degrader as an anti-cancer therapeutic. In *Oncogene* 41 (24), pp. 3328–3340. DOI: 10.1038/s41388-022-02340-8.

Li, F. N.; Johnston, M. (1997): Grr1 of Saccharomyces cerevisiae is connected to the ubiquitin proteolysis machinery through Skp1: coupling glucose sensing to gene expression and the cell cycle. In *The EMBO journal* 16 (18), pp. 5629–5638. DOI: 10.1093/emboj/16.18.5629.

Li, Si-Si; Jiang, Wei-Liang; Xiao, Wen-Qin; Li, Kai; Zhang, Ye-Fei; Guo, Xing-Ya et al. (2019): KMT2D deficiency enhances the anti-cancer activity of L48H37 in pancreatic ductal adenocarcinoma. In *World journal of gastrointestinal oncology* 11 (8), pp. 599–621. DOI: 10.4251/wjgo.v11.i8.599.

Li, Yu; Hu, Kaishun; Xiao, Xing; Wu, Wenjing; Yan, Haiyan; Chen, Hengxing et al. (2018): FBW7 suppresses cell proliferation and G2/M cell cycle transition via promoting γ-catenin K63-linked ubiquitylation. In *Biochemical and Biophysical Research Communications* 497 (2), pp. 473–479. DOI: 10.1016/j.bbrc.2018.01.192.

Lim, Junghyun; Yue, Zhenyu (2015): Neuronal aggregates: formation, clearance, and spreading. In *Developmental cell* 32 (4), pp. 491–501. DOI: 10.1016/j.devcel.2015.02.002.

Lin, Hsiu-Chuan; Yeh, Chi-Wei; Chen, Yen-Fu; Lee, Ting-Ting; Hsieh, Pei-Yun; Rusnac, Domnita V. et al. (2018): C-Terminal End-Directed Protein Elimination by CRL2 Ubiquitin Ligases. In *Molecular cell* 70 (4), 602-613.e3. DOI: 10.1016/j.molcel.2018.04.006.

Litchfield, David W. (2003): Protein kinase CK2: structure, regulation and role in cellular decisions of life and death. In *The Biochemical journal* 369 (Pt 1), pp. 1–15. DOI: 10.1042/BJ20021469.

Liu, Jidong; Furukawa, Manabu; Matsumoto, Tomohiro; Xiong, Yue (2002): NEDD8 Modification of CUL1 Dissociates p120CAND1, an Inhibitor of CUL1-SKP1 Binding and SCF Ligases. In *Molecular cell* 10 (6), pp. 1511–1518. DOI: 10.1016/s1097-2765(02)00783-9.

Liu, Xinran; Chen, Yuchen; Li, Yangkai; Petersen, Robert B.; Huang, Kun (2019): Targeting mitosis exit: A brake for cancer cell proliferation. In *Biochimica et biophysica acta. Reviews on cancer* 1871 (1), pp. 179–191. DOI: 10.1016/j.bbcan.2018.12.007.

Lok, Tsun Ming; Wang, Yang; Xu, Wendy Kaichun; Xie, Siwei; Ma, Hoi Tang; Poon, Randy Y. C. (2020): Mitotic slippage is determined by p31comet and the weakening of the spindle-assembly checkpoint. In *Oncogene* 39 (13), pp. 2819–2834. DOI: 10.1038/s41388-020-1187-6.

Lopergolo, A.; Pennati, M.; Gandellini, P.; Orlotti, N. I.; Poma, P.; Daidone, M. G. et al. (2009): Apollon gene silencing induces apoptosis in breast cancer cells through p53 stabilisation and caspase-3 activation. In *British journal of cancer* 100 (5), pp. 739–746. DOI: 10.1038/sj.bjc.6604927.

Lu, Fei; Wu, Xiaojun; Yin, Feng; Chia-Fang Lee, Christina; Yu, Min; Mihaylov, Ivailo S. et al. (2016): Regulation of DNA replication and chromosomal polyploidy by the MLL-WDR5-RBBP5 methyltransferases. In *Biology open* 5 (10), pp. 1449–1460. DOI: 10.1242/bio.019729.

Lu, Gang; Middleton, Richard E.; Sun, Huahang; Naniong, MarkVic; Ott, Christopher J.; Mitsiades, Constantine S. et al. (2014): The myeloma drug lenalidomide promotes the cereblon-dependent destruction of Ikaros proteins. In *Science (New York, N.Y.)* 343 (6168), pp. 305–309. DOI: 10.1126/science.1244917.

Lu, Kebin; Tao, He; Si, Xiaomin; Chen, Qingjuan (2018): The Histone H3 Lysine 4 Presenter WDR5 as an Oncogenic Protein and Novel Epigenetic Target in Cancer. In *Frontiers in oncology* 8, p. 502. DOI: 10.3389/fonc.2018.00502.

Luk, Iris Sze Ue; Shrestha, Raunak; Xue, Hui; Wang, Yuwei; Zhang, Fang; Lin, Dong et al. (2017): BIRC6 Targeting as Potential Therapy for Advanced, Enzalutamide-Resistant Prostate Cancer. In *Clinical cancer research : an official journal of the American Association for Cancer Research* 23 (6), pp. 1542–1551. DOI: 10.1158/1078-0432.CCR-16-0718.

Lukow, Devon A.; Sausville, Erin L.; Suri, Pavit; Chunduri, Narendra Kumar; Wieland, Angela; Leu, Justin et al. (2021): Chromosomal instability accelerates the evolution of resistance to anti-cancer therapies. In *Developmental cell* 56 (17), 2427-2439.e4. DOI: 10.1016/j.devcel.2021.07.009.

Lv, Shidong; Ji, Liyan; Chen, Bin; Liu, Shuqiang; Lei, Chengyong; Liu, Xi et al. (2018): Histone methyltransferase KMT2D sustains prostate carcinogenesis and metastasis via epigenetically activating LIFR and KLF4. In *Oncogene* 37 (10), pp. 1354–1368. DOI: 10.1038/s41388-017-0026-x.

Lv, Shidong; Wen, Haoran; Shan, Xiongwei; Li, Jianhua; Wu, Yaobin; Yu, Xinpei et al. (2019): Loss of KMT2D induces prostate cancer ROS-mediated DNA damage by suppressing the enhancer activity and DNA binding of antioxidant transcription factor FOXO3. In *Epigenetics* 14 (12), pp. 1194–1208. DOI: 10.1080/15592294.2019.1634985.

Lyapina, S.; Cope, G.; Shevchenko, A.; Serino, G.; Tsuge, T.; Zhou, C. et al. (2001): Promotion of NEDD-CUL1 conjugate cleavage by COP9 signalosome. In *Science (New York, N.Y.)* 292 (5520), pp. 1382–1385. DOI: 10.1126/science.1059780.

Lydeard, John R.; Schulman, Brenda A.; Harper, J. Wade (2013): Building and remodelling Cullin-RING E3 ubiquitin ligases. In *EMBO reports* 14 (12), pp. 1050–1061. DOI: 10.1038/embor.2013.173.

Ma, Emily; Zlobin, Andrei; Wyatt, Debra; Ng, Jeffrey; Dingwall, Andrew; Osipo, Clodia (2022): Abstract P3-05-03: KMT2D as a novel therapeutic target for HER2+ breast cancers. In *Cancer research* 82 (4_Supplement), P3-05-03-P3-05-03. DOI: 10.1158/1538-7445.SABCS21-P3-05-03.

Ma, Hoi Tang; Chan, Yan Yan; Chen, Xiao; On, Kin Fan; Poon, Randy Y. C. (2012): Depletion of p31comet protein promotes sensitivity to antimitotic drugs. In *The Journal of biological chemistry* 287 (25), pp. 21561–21569. DOI: 10.1074/jbc.M112.364356.

Ma, Hoi Tang; Poon, Randy Y. C. (2018): TRIP13 Functions in the Establishment of the Spindle Assembly Checkpoint by Replenishing O-MAD2. In *Cell reports* 22 (6), pp. 1439–1450. DOI: 10.1016/j.celrep.2018.01.027.

Ma, Hoi Tang; Poon, Randy Yat Choi (2016): TRIP13 Regulates Both the Activation and Inactivation of the Spindle-Assembly Checkpoint. In *Cell reports* 14 (5), pp. 1086–1099. DOI: 10.1016/j.celrep.2016.01.001.

Margolis, Robert L.; Lohez, Olivier D.; Andreassen, Paul R. (2003): G1 tetraploidy checkpoint and the suppression of tumorigenesis. In *Journal of cellular biochemistry* 88 (4), pp. 673–683. DOI: 10.1002/jcb.10411.

Margottin-Goguet, Florence; Hsu, Jerry Y.; Loktev, Alexander; Hsieh, Harn-Mei; Reimann, Julie D.R; Jackson, Peter K. (2003): Prophase Destruction of Emi1 by the SCFβTrCP/Slimb Ubiquitin Ligase Activates the Anaphase Promoting Complex to Allow Progression beyond Prometaphase. In *Developmental cell* 4 (6), pp. 813–826. DOI: 10.1016/s1534-5807(03)00153-9.

Marshall, Richard S.; Li, Faqiang; Gemperline, David C.; Book, Adam J.; Vierstra, Richard D. (2015): Autophagic Degradation of the 26S Proteasome Is Mediated by the Dual ATG8/Ubiquitin Receptor RPN10 in Arabidopsis. In *Molecular cell* 58 (6), pp. 1053–1066. DOI: 10.1016/j.molcel.2015.04.023.

Marshall, Richard S.; Vierstra, Richard D. (2019): Dynamic Regulation of the 26S Proteasome: From Synthesis to Degradation. In *Frontiers in Molecular Biosciences* 6, p. 40. DOI: 10.3389/fmolb.2019.00040.

Matsumoto, Akinobu; Onoyama, Ichiro; Nakayama, Keiichi I. (2006): Expression of mouse Fbxw7 isoforms is regulated in a cell cycle- or p53-dependent manner. In *Biochemical and Biophysical Research Communications* 350 (1), pp. 114–119. DOI: 10.1016/j.bbrc.2006.09.003.

Matthews, Helen K.; Bertoli, Cosetta; Bruin, Robertus A. M. de (2022): Cell cycle control in cancer. In *Nature reviews. Molecular cell biology* 23 (1), pp. 74–88. DOI: 10.1038/s41580-021-00404-3.

Matyskiela, Mary E.; Lu, Gang; Ito, Takumi; Pagarigan, Barbra; Lu, Chin-Chun; Miller, Karen et al. (2016): A novel cereblon modulator recruits GSPT1 to the CRL4(CRBN) ubiquitin ligase. In *Nature* 535 (7611), pp. 252–257. DOI: 10.1038/nature18611.

McIntosh, J. Richard (2016): Mitosis. In *Cold Spring Harbor perspectives in biology* 8 (9). DOI: 10.1101/cshperspect.a023218.

Metzger, Meredith B.; Hristova, Ventzislava A.; Weissman, Allan M. (2012): HECT and RING finger families of E3 ubiquitin ligases at a glance. In *Journal of cell science* 125 (Pt 3), pp. 531–537. DOI: 10.1242/jcs.091777.

Meunier, Sylvain; Shvedunova, Maria; van Nguyen, Nhuong; Avila, Leonor; Vernos, Isabelle; Akhtar, Asifa (2015): An epigenetic regulator emerges as microtubule minus-end binding and stabilizing factor in mitosis. In *Nature communications* 6, p. 7889. DOI: 10.1038/ncomms8889.

Miller, T.; Krogan, N. J.; Dover, J.; Erdjument-Bromage, H.; Tempst, P.; Johnston, M. et al. (2001): COMPASS: a complex of proteins associated with a trithorax-related SET domain protein. In *Proceedings of the National Academy of Sciences of the United States of America* 98 (23), pp. 12902–12907. DOI: 10.1073/pnas.231473398.

Min, Sang-Hyun; Lau, Alan W.; Lee, Tae Ho; Inuzuka, Hiroyuki; Wei, Shuo; Huang, Pengyu et al. (2012): Negative regulation of the stability and tumor suppressor function of Fbw7 by the Pin1 prolyl isomerase. In *Molecular cell* 46 (6), pp. 771–783. DOI: 10.1016/j.molcel.2012.04.012.

Minella, Alex C.; Swanger, Jherek; Bryant, Eileen; Welcker, Markus; Hwang, Harry; Clurman, Bruce E. (2002): p53 and p21 Form an Inducible Barrier that Protects Cells against Cyclin E-cdk2 Deregulation. In *Current Biology* 12 (21), pp. 1817–1827. DOI: 10.1016/s0960-9822(02)01225-3.

Mo, Jung-Soon; Ann, Eun-Jung; Yoon, Ji-Hye; Jung, Jane; Choi, Yun-Hee; Kim, Hwa-Young et al. (2011): Serum- and glucocorticoid-inducible kinase 1 (SGK1) controls Notch1 signaling by downregulation of protein stability through Fbw7 ubiquitin ligase. In *Journal of cell science* 124 (Pt 1), pp. 100–112. DOI: 10.1242/jcs.073924.

Moberg, K. H.; Bell, D. W.; Wahrer, D. C.; Haber, D. A.; Hariharan, I. K. (2001): Archipelago regulates Cyclin E levels in Drosophila and is mutated in human cancer cell lines. In *Nature* 413 (6853), pp. 311–316. DOI: 10.1038/35095068.

Mosadeghi, Ruzbeh; Reichermeier, Kurt M.; Winkler, Martin; Schreiber, Anne; Reitsma, Justin M.; Zhang, Yaru et al. (2016): Structural and kinetic analysis of the COP9-Signalosome activation and the cullin-RING ubiquitin ligase deneddylation cycle. In *eLife* 5. DOI: 10.7554/eLife.12102.

Moscat, Jorge; Karin, Michael; Diaz-Meco, Maria T. (2016): p62 in Cancer: Signaling Adaptor Beyond Autophagy. In *Cell* 167 (3), pp. 606–609. DOI: 10.1016/j.cell.2016.09.030.

Mueller, Susanne; Wahlander, Asa; Selevsek, Nathalie; Otto, Claudia; Ngwa, Elsy Mankah; Poljak, Kristina et al. (2015): Protein degradation corrects for imbalanced subunit stoichiometry in OST complex assembly. In *Molecular biology of the cell* 26 (14), pp. 2596–2608. DOI: 10.1091/mbc.E15-03-0168.

Murray, A. W.; Solomon, M. J.; Kirschner, M. W. (1989): The role of cyclin synthesis and degradation in the control of maturation promoting factor activity. In *Nature* 339 (6222), pp. 280–286. DOI: 10.1038/339280a0.

Murray, Andrew W. (2004): Recycling the Cell Cycle. In *Cell* 116 (2), pp. 221–234. DOI: 10.1016/s0092-8674(03)01080-8.

Nakagawa, Tadashi; Xiong, Yue (2011a): Chromatin regulation by CRL4 E3 ubiquitin ligases: CUL4B targets WDR5 ubiquitylation in the nucleus. In *Cell cycle (Georgetown, Tex.)* 10 (24), pp. 4197–4198. DOI: 10.4161/cc.10.24.18407.

Nakagawa, Tadashi; Xiong, Yue (2011b): X-linked mental retardation gene CUL4B targets ubiquitylation of H3K4 methyltransferase component WDR5 and regulates neuronal gene expression. In *Molecular cell* 43 (3), pp. 381–391. DOI: 10.1016/j.molcel.2011.05.033.

Nakayama, Keiichi I.; Nakayama, Keiko (2006): Ubiquitin ligases: cell-cycle control and cancer. In *Nature reviews. Cancer* 6 (5), pp. 369–381. DOI: 10.1038/nrc1881.

Nalepa, Grzegorz; Rolfe, Mark; Harper, J. Wade (2006): Drug discovery in the ubiquitin-proteasome system. In *Nature reviews. Drug discovery* 5 (7), pp. 596–613. DOI: 10.1038/nrd2056.

Nash, P.; Tang, X.; Orlicky, S.; Chen, Q.; Gertler, F. B.; Mendenhall, M. D. et al. (2001): Multisite phosphorylation of a CDK inhibitor sets a threshold for the onset of DNA replication. In *Nature* 414 (6863), pp. 514–521. DOI: 10.1038/35107009.

Neefjes, Jacques; Jongsma, Marlieke L. M.; Paul, Petra; Bakke, Oddmund (2011): Towards a systems understanding of MHC class I and MHC class II antigen presentation. In *Nature reviews. Immunology* 11 (12), pp. 823–836. DOI: 10.1038/nri3084.

Neilsen, Beth K.; Chakraborty, Binita; McCall, Jamie L.; Frodyma, Danielle E.; Sleightholm, Richard L.; Fisher, Kurt W.; Lewis, Robert E. (2018): WDR5 supports colon cancer cells by promoting methylation of H3K4 and suppressing DNA damage. In *BMC cancer* 18 (1), p. 673. DOI: 10.1186/s12885-018-4580-6.

Nguyen, Henry C.; Wang, Wei; Xiong, Yong (2017): Cullin-RING E3 Ubiquitin Ligases: Bridges to Destruction. In *Sub-cellular biochemistry* 83, pp. 323–347. DOI: 10.1007/978-3-319-46503-6_12.

Nicola, A. V.; Chen, W.; Helenius, A. (1999): Co-translational folding of an alphavirus capsid protein in the cytosol of living cells. In *Nature cell biology* 1 (6), pp. 341–345. DOI: 10.1038/14032.

Noda, Nobuo N.; Inagaki, Fuyuhiko (2015): Mechanisms of Autophagy. In *Annual review of biophysics* 44, pp. 101–122. DOI: 10.1146/annurev-biophys-060414-034248.

O'Connor, Hazel F.; Huibregtse, Jon M. (2017): Enzyme-substrate relationships in the ubiquitin system: approaches for identifying substrates of ubiquitin ligases. In *Cellular and molecular life sciences : CMLS* 74 (18), pp. 3363–3375. DOI: 10.1007/s00018-017-2529-6.

Odho, Zain; Southall, Stacey M.; Wilson, Jon R. (2010): Characterization of a novel WDR5-binding site that recruits RbBP5 through a conserved motif to enhance methylation of histone H3 lysine 4 by mixed lineage leukemia protein-1. In *The Journal of biological chemistry* 285 (43), pp. 32967–32976. DOI: 10.1074/jbc.M110.159921.

Oh, Eugene; Akopian, David; Rape, Michael (2018): Principles of Ubiquitin-Dependent Signaling. In *Annual review of cell and developmental biology* 34, pp. 137–162. DOI: 10.1146/annurev-cellbio-100617-062802.

Oh, Eugene; Mark, Kevin G.; Mocciaro, Annamaria; Watson, Edmond R.; Prabu, J. Rajan; Cha, Denny D. et al. (2020): Gene expression and cell identity controlled by anaphase-promoting complex. In *Nature* 579 (7797), pp. 136–140. DOI: 10.1038/s41586-020-2034-1.

Ohtake, Fumiaki; Saeki, Yasushi; Sakamoto, Kensaku; Ohtake, Kazumasa; Nishikawa, Hiroyuki; Tsuchiya, Hikaru et al. (2015): Ubiquitin acetylation inhibits polyubiquitin chain elongation. In *EMBO reports* 16 (2), pp. 192–201. DOI: 10.15252/embr.201439152.

Orlicky, Stephen; Tang, Xiaojing; Neduva, Victor; Elowe, Nadine; Brown, Eric D.; Sicheri, Frank; Tyers, Mike (2010): An allosteric inhibitor of substrate recognition by the SCF(Cdc4) ubiquitin ligase. In *Nature biotechnology* 28 (7), pp. 733–737. DOI: 10.1038/nbt.1646.

Orlicky, Stephen; Tang, Xiaojing; Willems, Andrew; Tyers, Mike; Sicheri, Frank (2003): Structural Basis for Phosphodependent Substrate Selection and Orientation by the SCFCdc4 Ubiquitin Ligase. In *Cell* 112 (2), pp. 243–256. DOI: 10.1016/s0092-8674(03)00034-5.

Orpinell, Meritxell; Fournier, Marjorie; Riss, Anne; Nagy, Zita; Krebs, Arnaud R.; Frontini, Mattia; Tora, Làszlò (2010): The ATAC acetyl transferase complex controls mitotic progression by targeting non-histone substrates. In *The EMBO journal* 29 (14), pp. 2381–2394. DOI: 10.1038/emboj.2010.125.

Pankiv, Serhiy; Alemu, Endalkachew A.; Brech, Andreas; Bruun, Jack-Ansgar; Lamark, Trond; Overvatn, Aud et al. (2010): FYCO1 is a Rab7 effector that binds to LC3 and PI3P to mediate microtubule plus end-directed vesicle transport. In *The Journal of cell biology* 188 (2), pp. 253–269. DOI: 10.1083/jcb.200907015.

Patel, Anamika; Dharmarajan, Venkatasubramanian; Cosgrove, Michael S. (2008a): Structure of WDR5 bound to mixed lineage leukemia protein-1 peptide. In *The Journal of biological chemistry* 283 (47), pp. 32158–32161. DOI: 10.1074/jbc.C800164200.

Patel, Anamika; Vought, Valarie E.; Dharmarajan, Venkatasubramanian; Cosgrove, Michael S. (2008b): A conserved arginine-containing motif crucial for the assembly and enzymatic activity of the mixed lineage leukemia protein-1 core complex. In *The Journal of biological chemistry* 283 (47), pp. 32162–32175. DOI: 10.1074/jbc.M806317200.

Patton, E. E.; Willems, A. R.; Sa, D.; Kuras, L.; Thomas, D.; Craig, K. L.; Tyers, M. (1998): Cdc53 is a scaffold protein for multiple Cdc34/Skp1/F-box proteincomplexes that regulate cell division and methionine biosynthesis in yeast. In *Genes & development* 12 (5), pp. 692–705. DOI: 10.1101/gad.12.5.692.

Pauwels, Kris; van Molle, Inge; Tommassen, Jan; van Gelder, Patrick (2007): Chaperoning Anfinsen: the steric foldases. In *Molecular microbiology* 64 (4), pp. 917–922. DOI: 10.1111/j.1365-2958.2007.05718.x.

Peng, Junmin; Schwartz, Daniel; Elias, Joshua E.; Thoreen, Carson C.; Cheng, Dongmei; Marsischky, Gerald et al. (2003): A proteomics approach to understanding protein ubiquitination. In *Nature biotechnology* 21 (8), pp. 921–926. DOI: 10.1038/nbt849.

Peth, Andreas; Uchiki, Tomoaki; Goldberg, Alfred L. (2010): ATP-dependent steps in the binding of ubiquitin conjugates to the 26S proteasome that commit to degradation. In *Molecular cell* 40 (4), pp. 671–681. DOI: 10.1016/j.molcel.2010.11.002.

Petronczki, Mark; Lénárt, Péter; Peters, Jan-Michael (2008): Polo on the Rise-from Mitotic Entry to Cytokinesis with Plk1. In *Developmental cell* 14 (5), pp. 646–659. DOI: 10.1016/j.devcel.2008.04.014.

Petroski, Matthew D. (2010): Mechanism-based neddylation inhibitor. In *Chemistry & biology* 17 (1), pp. 6–8. DOI: 10.1016/j.chembiol.2010.01.002.

Petroski, Matthew D.; Deshaies, Raymond J. (2005): Function and regulation of cullin-RING ubiquitin ligases. In *Nature reviews. Molecular cell biology* 6 (1), pp. 9–20. DOI: 10.1038/nrm1547.

Pierce, Nathan W.; Lee, J. Eugene; Liu, Xing; Sweredoski, Michael J.; Graham, Robert L. J.; Larimore, Elizabeth A. et al. (2013): Cand1 promotes assembly of new SCF complexes through dynamic exchange of F box proteins. In *Cell* 153 (1), pp. 206–215. DOI: 10.1016/j.cell.2013.02.024.

Piunti, Andrea; Shilatifard, Ali (2016): Epigenetic balance of gene expression by Polycomb and COMPASS families. In *Science (New York, N.Y.)* 352 (6290), aad9780. DOI: 10.1126/science.aad9780.

Pohl, Christian (2008): Coordination of late stages of cytokinesis by the inhibitor of apoptosis protein BRUCE.

Pohl, Christian; Jentsch, Stefan (2008): Final stages of cytokinesis and midbody ring formation are controlled by BRUCE. In *Cell* 132 (5), pp. 832–845. DOI: 10.1016/j.cell.2008.01.012.

Prakash, Sumit; Inobe, Tomonao; Hatch, Ace Joseph; Matouschek, Andreas (2009): Substrate selection by the proteasome during degradation of protein complexes. In *Nature chemical biology* 5 (1), pp. 29–36. DOI: 10.1038/nchembio.130.

Puklowski, Anja; Homsi, Yahya; Keller, Debora; May, Martin; Chauhan, Sangeeta; Kossatz, Uta et al. (2011): The SCF-FBXW5 E3-ubiquitin ligase is regulated by PLK4 and targets HsSAS-6 to control centrosome duplication. In *Nature cell biology* 13 (8), pp. 1004–1009. DOI: 10.1038/ncb2282.

Qian, Yingjuan; Chen, Xinbin (2013): Senescence regulation by the p53 protein family. In *Methods in molecular biology (Clifton, N.J.)* 965, pp. 37–61. DOI: 10.1007/978-1-62703-239-1_3.

Qiu, Xiao-Bo; Markant, Shirley L.; Yuan, Junying; Goldberg, Alfred L. (2004): Nrdp1-mediated degradation of the gigantic IAP, BRUCE, is a novel pathway for triggering apoptosis. In *The EMBO journal* 23 (4), pp. 800–810. DOI: 10.1038/sj.emboj.7600075.

Rajagopalan, Harith; Jallepalli, Prasad V.; Rago, Carlo; Velculescu, Victor E.; Kinzler, Kenneth W.; Vogelstein, Bert; Lengauer, Christoph (2004): Inactivation of hCDC4 can cause chromosomal instability. In *Nature* 428 (6978), pp. 77–81. DOI: 10.1038/nature02313.

Ravid, Tommer; Hochstrasser, Mark (2008): Diversity of degradation signals in the ubiquitin-proteasome system. In *Nature reviews. Molecular cell biology* 9 (9), pp. 679–690. DOI: 10.1038/nrm2468.

Reiterer, Veronika; Figueras-Puig, Cristina; Le Guerroue, Francois; Confalonieri, Stefano; Vecchi, Manuela; Jalapothu, Dasaradha et al. (2017): The pseudophosphatase STYX targets the F-box of FBXW7 and inhibits SCFFBXW7 function. In *The EMBO journal* 36 (3), pp. 260–273. DOI: 10.15252/embj.201694795.

Reits, E. A.; Benham, A. M.; Plougastel, B.; Neefjes, J.; Trowsdale, J. (1997): Dynamics of proteasome distribution in living cells. In *The EMBO journal* 16 (20), pp. 6087–6094. DOI: 10.1093/emboj/16.20.6087.

Richter, Kai T. (2017): Identification and characterization of novel regulators of the tumor suppressor and ubiquitin ligase SCF-FBXW7.

Richter, Kai T.; Kschonsak, Yvonne T.; Vodicska, Barbara; Hoffmann, Ingrid (2020): FBXO45-MYCBP2 regulates mitotic cell fate by targeting FBXW7 for degradation. In *Cell death and differentiation* 27 (2), pp. 758–772. DOI: 10.1038/s41418-019-0385-7.

Rieder, Conly L.; Maiato, Helder (2004): Stuck in division or passing through: what happens when cells cannot satisfy the spindle assembly checkpoint. In *Developmental cell* 7 (5), pp. 637–651. DOI: 10.1016/j.devcel.2004.09.002.

Roberts, J. R.; Allison, D. C.; Donehower, R. C.; Rowinsky, E. K. (1990): Development of polyploidization in taxol-resistant human leukemia cells in vitro. In *Cancer research* 50 (3), pp. 710–716.

Rosenblatt, J.; Gu, Y.; Morgan, D. O. (1992): Human cyclin-dependent kinase 2 is activated during the S and G2 phases of the cell cycle and associates with cyclin A. In *Proceedings of the National Academy of Sciences of the United States of America* 89 (7), pp. 2824–2828. DOI: 10.1073/pnas.89.7.2824.

Rossi, Mario; Duan, Shanshan; Jeong, Yeon-Tae; Horn, Moritz; Saraf, Anita; Florens, Laurence et al. (2013): Regulation of the CRL4(Cdt2) ubiquitin ligase and cell-cycle exit by the SCF(Fbxo11) ubiquitin ligase. In *Molecular cell* 49 (6), pp. 1159–1166. DOI: 10.1016/j.molcel.2013.02.004.

Russell, S. J.; Steger, K. A.; Johnston, S. A. (1999): Subcellular localization, stoichiometry, and protein levels of 26 S proteasome subunits in yeast. In *The Journal of biological chemistry* 274 (31), pp. 21943–21952. DOI: 10.1074/jbc.274.31.21943.

Saffie, Rizwan; Zhou, Nan; Rolland, Delphine; Önder, Özlem; Basrur, Venkatesha; Campbell, Sydney et al. (2020): FBXW7 Triggers Degradation of KMT2D to Favor Growth of Diffuse Large B-cell Lymphoma Cells. In *Cancer research* 80 (12), pp. 2498–2511. DOI: 10.1158/0008-5472.CAN-19-2247.

Sahu, Indrajit; Glickman, Michael H. (2021): Structural Insights into Substrate Recognition and Processing by the 20S Proteasome. In *Biomolecules* 11 (2). DOI: 10.3390/biom11020148.

Sakamoto, K. M.; Kim, K. B.; Kumagai, A.; Mercurio, F.; Crews, C. M.; Deshaies, R. J. (2001): Protacs: chimeric molecules that target proteins to the Skp1-Cullin-F box complex for ubiquitination and

degradation. In *Proceedings of the National Academy of Sciences of the United States of America* 98 (15), pp. 8554–8559. DOI: 10.1073/pnas.141230798.

Schibler, Andria; Koutelou, Evangelia; Tomida, Junya; Wilson-Pham, Marenda; Wang, Li; Lu, Yue et al. (2016): Histone H3K4 methylation regulates deactivation of the spindle assembly checkpoint through direct binding of Mad2. In *Genes & development* 30 (10), pp. 1187–1197. DOI: 10.1101/gad.278887.116.

Schuetz, Anja; Allali-Hassani, Abdellah; Martín, Fernando; Loppnau, Peter; Vedadi, Masoud; Bochkarev, Alexey et al. (2006): Structural basis for molecular recognition and presentation of histone H3 by WDR5. In *The EMBO journal* 25 (18), pp. 4245–4252. DOI: 10.1038/sj.emboj.7601316.

Schülein, Christina; Eilers, Martin; Popov, Nikita (2011): PI3K-dependent phosphorylation of Fbw7 modulates substrate degradation and activity. In *FEBS letters* 585 (14), pp. 2151–2157. DOI: 10.1016/j.febslet.2011.05.036.

Schulze, Volker K.; Klar, Ulrich; Kosemund, Dirk; Wengner, Antje M.; Siemeister, Gerhard; Stöckigt, Detlef et al. (2020): Treating Cancer by Spindle Assembly Checkpoint Abrogation: Discovery of Two Clinical Candidates, BAY 1161909 and BAY 1217389, Targeting MPS1 Kinase. In *Journal of medicinal chemistry* 63 (15), pp. 8025–8042. DOI: 10.1021/acs.jmedchem.9b02035.

Schweichel, J. U.; Merker, H. J. (1973): The morphology of various types of cell death in prenatal tissues. In *Teratology* 7 (3), pp. 253–266. DOI: 10.1002/tera.1420070306.

Schweiggert, Jörg; Habeck, Gregor; Hess, Sandra; Mikus, Felix; Beloshistov, Roman; Meese, Klaus et al. (2021): SCFFbxw5 targets kinesin-13 proteins to facilitate ciliogenesis. In *The EMBO journal* 40 (18), e107735. DOI: 10.15252/embj.2021107735.

Schwob, E. (1994): The B-type cyclin kinase inhibitor p40SIC1 controls the G1 to S transition in S. cerevisiae. In *Cell* 79 (2), pp. 233–244. DOI: 10.1016/0092-8674(94)90193-7.

Scott, Daniel C.; Sviderskiy, Vladislav O.; Monda, Julie K.; Lydeard, John R.; Cho, Shein Ei; Harper, J. Wade; Schulman, Brenda A. (2014): Structure of a RING E3 trapped in action reveals ligation mechanism for the ubiquitin-like protein NEDD8. In *Cell* 157 (7), pp. 1671–1684. DOI: 10.1016/j.cell.2014.04.037.

Scully, Ralph; Panday, Arvind; Elango, Rajula; Willis, Nicholas A. (2019): DNA double-strand break repair-pathway choice in somatic mammalian cells. In *Nature reviews. Molecular cell biology* 20 (11), pp. 698–714. DOI: 10.1038/s41580-019-0152-0.

Settembre, Carmine; Fraldi, Alessandro; Medina, Diego L.; Ballabio, Andrea (2013): Signals from the lysosome: a control centre for cellular clearance and energy metabolism. In *Nature reviews. Molecular cell biology* 14 (5), pp. 283–296. DOI: 10.1038/nrm3565.

Sherr, C. J.; Roberts, J. M. (1999): CDK inhibitors: positive and negative regulators of G1-phase progression. In *Genes & development* 13 (12), pp. 1501–1512. DOI: 10.1101/gad.13.12.1501.

Simmons Kovacs, Laura A.; Orlando, David A.; Haase, Steven B. (2008): Transcription networks and cyclin/CDKs: the yin and yang of cell cycle oscillators. In *Cell cycle (Georgetown, Tex.)* 7 (17), pp. 2626–2629. DOI: 10.4161/cc.7.17.6515.

Simonetta, Kyle R.; Taygerly, Joshua; Boyle, Kathleen; Basham, Stephen E.; Padovani, Chris; Lou, Yan et al. (2019): Prospective discovery of small molecule enhancers of an E3 ligase-substrate interaction. In *Nature communications* 10 (1), p. 1402. DOI: 10.1038/s41467-019-09358-9.

Sims, Joshua J.; Cohen, Robert E. (2009): Linkage-specific avidity defines the lysine 63-linked polyubiquitin-binding preference of rap80. In *Molecular cell* 33 (6), pp. 775–783. DOI: 10.1016/j.molcel.2009.02.011.

Singh, Neha; Zeke, András; Reményi, Attila (2022): Systematic Discovery of FBXW7-Binding Phosphodegrons Highlights Mitogen-Activated Protein Kinases as Important Regulators of Intracellular Protein Levels. In *International journal of molecular sciences* 23 (6). DOI: 10.3390/ijms23063320.

Sinha, Debottam; Duijf, Pascal H. G.; Khanna, Kum Kum (2019): Mitotic slippage: an old tale with a new twist. In *Cell cycle (Georgetown, Tex.)* 18 (1), pp. 7–15. DOI: 10.1080/15384101.2018.1559557.

Skaar, Jeffrey R.; Pagan, Julia K.; Pagano, Michele (2013): Mechanisms and function of substrate recruitment by F-box proteins. In *Nature reviews. Molecular cell biology* 14 (6), pp. 369–381. DOI: 10.1038/nrm3582.

Skowyra, Dorota; Craig, Karen L.; Tyers, Mike; Elledge, Stephen J.; Harper, J.Wade (1997): F-Box Proteins Are Receptors that Recruit Phosphorylated Substrates to the SCF Ubiquitin-Ligase Complex. In *Cell* 91 (2), pp. 209–219. DOI: 10.1016/s0092-8674(00)80403-1.

Sloss, Olivia; Topham, Caroline; Diez, Maria; Taylor, Stephen (2016): Mcl-1 dynamics influence mitotic slippage and death in mitosis. In *Oncotarget* 7 (5), pp. 5176–5192. DOI: 10.18632/oncotarget.6894.

Snow, Anson; Zeidner, Joshua F. (2022): The development of pevonedistat in myelodysplastic syndrome (MDS) and acute myeloid leukemia (AML): hope or hype? In *Therapeutic advances in hematology* 13, 20406207221112899. DOI: 10.1177/20406207221112899.

Sobhian, Bijan; Shao, Genze; Lilli, Dana R.; Culhane, Aedín C.; Moreau, Lisa A.; Xia, Bing et al. (2007): RAP80 Targets BRCA1 to Specific Ubiquitin Structures at DNA Damage Sites. In *Science (New York, N.Y.)* 316 (5828), pp. 1198–1202. DOI: 10.1126/science.1139516.

Song, Lei; Luo, Zhao-Qing (2019): Post-translational regulation of ubiquitin signaling. In *The Journal of cell biology* 218 (6), pp. 1776–1786. DOI: 10.1083/jcb.201902074.

Song, Xiangping; Shen, Lin; Tong, Jingshan; Kuang, Chaoyuan; Zeng, Shan; Schoen, Robert E. et al. (2020): Mcl-1 inhibition overcomes intrinsic and acquired regorafenib resistance in colorectal cancer. In *Theranostics* 10 (18), pp. 8098–8110. DOI: 10.7150/thno.45363.

Soucy, Teresa A.; Smith, Peter G.; Milhollen, Michael A.; Berger, Allison J.; Gavin, James M.; Adhikari, Sharmila et al. (2009): An inhibitor of NEDD8-activating enzyme as a new approach to treat cancer. In *Nature* 458 (7239), pp. 732–736. DOI: 10.1038/nature07884.

Spruck, Charles H.; Strohmaier, Heimo; Sangfelt, Olle; Müller, Hannes M.; Hubalek, Michael; Müller-Holzner, Elisabeth et al. (2002): hCDC4 gene mutations in endometrial cancer. In *Cancer research* 62 (16), pp. 4535–4539.

Sriramachandran, Annie M.; Dohmen, R. Jürgen (2014): SUMO-targeted ubiquitin ligases. In *Biochimica et biophysica acta* 1843 (1), pp. 75–85. DOI: 10.1016/j.bbamcr.2013.08.022.

Stolz, Ailine; Vogel, Celia; Schneider, Verena; Ertych, Norman; Kienitz, Anne; Yu, Hongtao; Bastians, Holger (2009): Pharmacologic abrogation of the mitotic spindle checkpoint by an indolocarbazole discovered by cellular screening efficiently kills cancer cells. In *Cancer research* 69 (9), pp. 3874–3883. DOI: 10.1158/0008-5472.CAN-08-3597.

Strausfeld, U. P.; Howell, M.; Descombes, P.; Chevalier, S.; Rempel, R. E.; Adamczewski, J. et al. (1996): Both cyclin A and cyclin E have S-phase promoting (SPF) activity in Xenopus egg extracts. In *Journal of cell science* 109 (Pt 6), pp. 1555–1563. DOI: 10.1242/jcs.109.6.1555.

Strohmaier, H.; Spruck, C. H.; Kaiser, P.; Won, K. A.; Sangfelt, O.; Reed, S. I. (2001): Human F-box protein hCdc4 targets cyclin E for proteolysis and is mutated in a breast cancer cell line. In *Nature* 413 (6853), pp. 316–322. DOI: 10.1038/35095076.

Sudakin, V.; Chan, G. K.; Yen, T. J. (2001): Checkpoint inhibition of the APC/C in HeLa cells is mediated by a complex of BUBR1, BUB3, CDC20, and MAD2. In *The Journal of cell biology* 154 (5), pp. 925–936. DOI: 10.1083/jcb.200102093.

Sudo, Tamotsu; Nitta, Masayuki; Saya, Hideyuki; Ueno, Naoto T. (2004): Dependence of paclitaxel sensitivity on a functional spindle assembly checkpoint. In *Cancer research* 64 (7), pp. 2502–2508. DOI: 10.1158/0008-5472.can-03-2013.

Sun, Yuting; Bell, Jessica L.; Carter, Daniel; Gherardi, Samuele; Poulos, Rebecca C.; Milazzo, Giorgio et al. (2015): WDR5 Supports an N-Myc Transcriptional Complex That Drives a Protumorigenic Gene Expression Signature in Neuroblastoma. In *Cancer research* 75 (23), pp. 5143–5154. DOI: 10.1158/0008-5472.CAN-15-0423.

Taggart, James Christopher; Zauber, Henrik; Selbach, Matthias; Li, Gene-Wei; McShane, Erik (2020): Keeping the Proportions of Protein Complex Components in Check. In *Cell systems* 10 (2), pp. 125–132. DOI: 10.1016/j.cels.2020.01.004.

Takada, Mamoru; Zhang, Weiguo; Suzuki, Aussie; Kuroda, Taruho S.; Yu, Zhouliang; Inuzuka, Hiroyuki et al. (2017): FBW7 Loss Promotes Chromosomal Instability and Tumorigenesis via Cyclin E1/CDK2-Mediated Phosphorylation of CENP-A. In *Cancer research* 77 (18), pp. 4881–4893. DOI: 10.1158/0008-5472.CAN-17-1240.

Tang, Wenqing; Xue, Ruyi; Weng, Shuqiang; Wu, Jian; Fang, Ying; Wang, Yi et al. (2015): BIRC6 promotes hepatocellular carcinogenesis: interaction of BIRC6 with p53 facilitating p53 degradation. In *International journal of cancer* 136 (6), E475-87. DOI: 10.1002/ijc.29194.

Tang, Xiaojing; Orlicky, Stephen; Lin, Zhenyuan; Willems, Andrew; Neculai, Dante; Ceccarelli, Derek et al. (2007): Suprafacial orientation of the SCFCdc4 dimer accommodates multiple geometries for substrate ubiquitination. In *Cell* 129 (6), pp. 1165–1176. DOI: 10.1016/j.cell.2007.04.042.

Teixeira, Leonardo K.; Reed, Steven I. (2013): Ubiquitin ligases and cell cycle control. In *Annual review of biochemistry* 82, pp. 387–414. DOI: 10.1146/annurev-biochem-060410-105307.

Thomas, Lance R.; Wang, Qingguo; Grieb, Brian C.; Phan, Jason; Foshage, Audra M.; Sun, Qi et al. (2015): Interaction with WDR5 promotes target gene recognition and tumorigenesis by MYC. In *Molecular cell* 58 (3), pp. 440–452. DOI: 10.1016/j.molcel.2015.02.028.

Tian, Jianhua; Teuscher, Kevin B.; Aho, Erin R.; Alvarado, Joseph R.; Mills, Jonathan J.; Meyers, Kenneth M. et al. (2020): Discovery and Structure-Based Optimization of Potent and Selective WD Repeat Domain 5 (WDR5) Inhibitors Containing a Dihydroisoquinolinone Bicyclic Core. In *Journal of medicinal chemistry* 63 (2), pp. 656–675. DOI: 10.1021/acs.jmedchem.9b01608.

Toh, Tan Boon; Lim, Jhin Jieh; Chow, Edward Kai-Hua (2017): Epigenetics in cancer stem cells. In *Molecular cancer* 16 (1), p. 29. DOI: 10.1186/s12943-017-0596-9.

Tong, J.; Tan, S.; Zou, F.; Yu, J.; Zhang, L. (2017): FBW7 mutations mediate resistance of colorectal cancer to targeted therapies by blocking Mcl-1 degradation. In *Oncogene* 36 (6), pp. 787–796. DOI: 10.1038/onc.2016.247.

Topham, Caroline; Tighe, Anthony; Ly, Peter; Bennett, Ailsa; Sloss, Olivia; Nelson, Louisa et al. (2015): MYC Is a Major Determinant of Mitotic Cell Fate. In *Cancer cell* 28 (1), pp. 129–140. DOI: 10.1016/j.ccell.2015.06.001.

Tripathi, Vivek; Kaur, Ekjot; Kharat, Suhas Sampat; Hussain, Mansoor; Damodaran, Arun Prasath; Kulshrestha, Swati; Sengupta, Sagar (2019): Abrogation of FBW7α-dependent p53 degradation enhances p53's function as a tumor suppressor. In *The Journal of biological chemistry* 294 (36), pp. 13224–13232. DOI: 10.1074/jbc.AC119.008483.

Tyanova, Stefka; Temu, Tikira; Sinitcyn, Pavel; Carlson, Arthur; Hein, Marco Y.; Geiger, Tamar et al. (2016): The Perseus computational platform for comprehensive analysis of (prote)omics data. In *Nature methods* 13 (9), pp. 731–740. DOI: 10.1038/nmeth.3901.

van Nocker, S.; Sadis, S.; Rubin, D. M.; Glickman, M.; Fu, H.; Coux, O. et al. (1996): The multiubiquitin-chain-binding protein Mcb1 is a component of the 26S proteasome in Saccharomyces cerevisiae and plays a nonessential, substrate-specific role in protein turnover. In *Molecular and cellular biology* 16 (11), pp. 6020–6028. DOI: 10.1128/MCB.16.11.6020.

Varshavsky, Alexander (1991): Naming a targeting signal. In *Cell* 64 (1), pp. 13–15. DOI: 10.1016/0092-8674(91)90202-A.

Varshavsky, Alexander (2017): The Ubiquitin System, Autophagy, and Regulated Protein Degradation. In *Annual review of biochemistry* 86, pp. 123–128. DOI: 10.1146/annurev-biochem-061516-044859.

Varshavsky, Alexander (2019): N-degron and C-degron pathways of protein degradation. In *Proceedings of the National Academy of Sciences of the United States of America* 116 (2), pp. 358–366. DOI: 10.1073/pnas.1816596116.

Vaz, Sara; Ferreira, Fábio J.; Macedo, Joana C.; Leor, Gil; Ben-David, Uri; Bessa, José; Logarinho, Elsa (2021): FOXM1 repression increases mitotic death upon antimitotic chemotherapy through BMF upregulation. In *Cell death & disease* 12 (6). DOI: 10.1038/s41419-021-03822-5.

Vembar, Shruthi S.; Brodsky, Jeffrey L. (2008): One step at a time: endoplasmic reticulum-associated degradation. In *Nature reviews. Molecular cell biology* 9 (12), pp. 944–957. DOI: 10.1038/nrm2546.

Verhagen, A. M.; Coulson, E. J.; Vaux, D. L. (2001): Inhibitor of apoptosis proteins and their relatives: IAPs and other BIRPs. In *Genome biology* 2 (7), REVIEWS3009. DOI: 10.1186/gb-2001-2-7-reviews3009.

Verma, R.; Feldman, R. M.; Deshaies, R. J. (1997): SIC1 is ubiquitinated in vitro by a pathway that requires CDC4, CDC34, and cyclin/CDK activities. In *Molecular biology of the cell* 8 (8), pp. 1427–1437. DOI: 10.1091/mbc.8.8.1427.

Verma, Rati; Oania, Robert; Graumann, Johannes; Deshaies, Raymond J. (2004): Multiubiquitin chain receptors define a layer of substrate selectivity in the ubiquitin-proteasome system. In *Cell* 118 (1), pp. 99–110. DOI: 10.1016/j.cell.2004.06.014.

Vogel, Celia; Kienitz, Anne; Hofmann, Irmgard; Müller, Rolf; Bastians, Holger (2004): Crosstalk of the mitotic spindle assembly checkpoint with p53 to prevent polyploidy. In *Oncogene* 23 (41), pp. 6845–6853. DOI: 10.1038/sj.onc.1207860.

Vucic, Domagoj; Dixit, Vishva M.; Wertz, Ingrid E. (2011): Ubiquitylation in apoptosis: a post-translational modification at the edge of life and death. In *Nature reviews. Molecular cell biology* 12 (7), pp. 439–452. DOI: 10.1038/nrm3143.

Walden, Helen; Rittinger, Katrin (2018): RBR ligase-mediated ubiquitin transfer: a tale with many twists and turns. In *Nature structural & molecular biology* 25 (6), pp. 440–445. DOI: 10.1038/s41594-018-0063-3.

Walter, David; Hoffmann, Saskia; Komseli, Eirini-Stavroula; Rappsilber, Juri; Gorgoulis, Vassilis; Sørensen, Claus Storgaard (2016): SCF(Cyclin F)-dependent degradation of CDC6 suppresses DNA re-replication. In *Nature communications* 7, p. 10530. DOI: 10.1038/ncomms10530.

Wang, Dong; Pierce, Angela; Veo, Bethany; Fosmire, Susan; Danis, Etienne; Donson, Andrew et al. (2021a): A Regulatory Loop of FBXW7-MYC-PLK1 Controls Tumorigenesis of MYC-Driven Medulloblastoma. In *Cancers* 13 (3). DOI: 10.3390/cancers13030387.

Wang, Haolan; Guo, Ming; Wei, Hudie; Chen, Yongheng (2021b): Targeting MCL-1 in cancer: current status and perspectives. In *Journal of hematology & oncology* 14 (1), p. 67. DOI: 10.1186/s13045-021-01079-1.

Wang, Xinmiao; Li, Rui; Wu, Luping; Chen, Yang; Liu, Shaopeng; Zhao, Hui et al. (2022): Histone methyltransferase KMT2D cooperates with MEF2A to promote the stem-like properties of oral squamous cell carcinoma. In *Cell & bioscience* 12 (1), p. 49. DOI: 10.1186/s13578-022-00785-8.

Weikel, Karen A.; Cacicedo, José M.; Ruderman, Neil B.; Ido, Yasuo (2016): Knockdown of GSK3β increases basal autophagy and AMPK signalling in nutrient-laden human aortic endothelial cells. In *Bioscience reports* 36 (5). DOI: 10.1042/BSR20160174.

Welburn, Julie P. I.; Vleugel, Mathijs; Liu, Dan; Yates, John R.; Lampson, Michael A.; Fukagawa, Tatsuo; Cheeseman, Iain M. (2010): Aurora B phosphorylates spatially distinct targets to differentially regulate the kinetochore-microtubule interface. In *Molecular cell* 38 (3), pp. 383–392. DOI: 10.1016/j.molcel.2010.02.034.

Welcker, Markus; Clurman, Bruce E. (2008): FBW7 ubiquitin ligase: a tumour suppressor at the crossroads of cell division, growth and differentiation. In *Nature reviews. Cancer* 8 (2), pp. 83–93. DOI: 10.1038/nrc2290.

Welcker, Markus; Larimore, Elizabeth A.; Swanger, Jherek; Bengoechea-Alonso, Maria T.; Grim, Jonathan E.; Ericsson, Johan et al. (2013): Fbw7 dimerization determines the specificity and robustness of substrate degradation. In *Genes & development* 27 (23), pp. 2531–2536. DOI: 10.1101/gad.229195.113.

Welcker, Markus; Orian, Amir; Jin, Jianping; Grim, Jonathan E.; Grim, Jonathan A.; Harper, J. Wade et al. (2004): The Fbw7 tumor suppressor regulates glycogen synthase kinase 3 phosphorylation-dependent c-Myc protein degradation. In *Proceedings of the National Academy of Sciences of the United States of America* 101 (24), pp. 9085–9090. DOI: 10.1073/pnas.0402770101.

Welcker, Markus; Singer, Jeffrey; Loeb, Keith R.; Grim, Jonathan; Bloecher, Andrew; Gurien-West, Mark et al. (2003): Multisite Phosphorylation by Cdk2 and GSK3 Controls Cyclin E Degradation. In *Molecular cell* 12 (2), pp. 381–392. DOI: 10.1016/s1097-2765(03)00287-9.

Welcker, Markus; Wang, Baiyun; Rusnac, Domniţa-Valeria; Hussaini, Yasser; Swanger, Jherek; Zheng, Ning; Clurman, Bruce E. (2022): Two diphosphorylated degrons control c-Myc degradation by the Fbw7 tumor suppressor. In *Science advances* 8 (4), eabl7872. DOI: 10.1126/sciadv.abl7872.

Werner, Achim; Disanza, Andrea; Reifenberger, Nina; Habeck, Gregor; Becker, Janina; Calabrese, Matthew et al. (2013): SCFFbxw5 mediates transient degradation of actin remodeller Eps8 to allow proper mitotic progression. In *Nature cell biology* 15 (2), pp. 179–188. DOI: 10.1038/ncb2661.

Wertz, Ingrid E.; Kusam, Saritha; Lam, Cynthia; Okamoto, Toru; Sandoval, Wendy; Anderson, Daniel J. et al. (2011): Sensitivity to antitubulin chemotherapeutics is regulated by MCL1 and FBW7. In *Nature* 471 (7336), pp. 110–114. DOI: 10.1038/nature09779.

Willems, Andrew R.; Lanker, Stefan; Patton, E.Elizabeth; Craig, Karen L.; Nason, Timothy F.; Mathias, Neal et al. (1996): Cdc53 Targets Phosphorylated G1 Cyclins for Degradation by the Ubiquitin Proteolytic Pathway. In *Cell* 86 (3), pp. 453–463. DOI: 10.1016/s0092-8674(00)80118-x.

Willems, Andrew R.; Schwab, Michael; Tyers, Mike (2004): A hitchhiker's guide to the cullin ubiquitin ligases: SCF and its kin. In *Biochimica et biophysica acta* 1695 (1-3), pp. 133–170. DOI: 10.1016/j.bbamcr.2004.09.027.

Wilson, Marenda A.; Meaux, Stacie; van Hoof, Ambro (2007): A Genomic Screen in Yeast Reveals Novel Aspects of Nonstop mRNA Metabolism. In *Genetics* 177 (2), pp. 773–784. DOI: 10.1534/genetics.107.073205.

Won, K. A.; Reed, S. I. (1996): Activation of cyclin E/CDK2 is coupled to site-specific autophosphorylation and ubiquitin-dependent degradation of cyclin E. In *The EMBO journal* 15 (16), pp. 4182–4193.

Wysocka, Joanna; Swigut, Tomek; Milne, Thomas A.; Dou, Yali; Zhang, Xin; Burlingame, Alma L. et al. (2005): WDR5 associates with histone H3 methylated at K4 and is essential for H3 K4 methylation and vertebrate development. In *Cell* 121 (6), pp. 859–872. DOI: 10.1016/j.cell.2005.03.036.

Xiao, Wenchang; Yeerken, Danna; Li, Jia; Li, Zhangfu; Jiang, Lanfang; Li, Dan et al. (2021): Nlp promotes autophagy through facilitating the interaction of Rab7 and FYCO1. In *Sig Transduct Target Ther* 6 (1). DOI: 10.1038/s41392-021-00543-1.

Xiong, Wenjun; Deng, Zhenxuan; Tang, Yuxin; Deng, Zhenwei; Li, Mingsong (2018): Downregulation of KMT2D suppresses proliferation and induces apoptosis of gastric cancer. In *Biochemical and Biophysical Research Communications* 504 (1), pp. 129–136. DOI: 10.1016/j.bbrc.2018.08.143.

Xu, Ping; Duong, Duc M.; Seyfried, Nicholas T.; Cheng, Dongmei; Xie, Yang; Robert, Jessica et al. (2009): Quantitative proteomics reveals the function of unconventional ubiquitin chains in proteasomal degradation. In *Cell* 137 (1), pp. 133–145. DOI: 10.1016/j.cell.2009.01.041.

Yada, Masayoshi; Hatakeyama, Shigetsugu; Kamura, Takumi; Nishiyama, Masaaki; Tsunematsu, Ryosuke; Imaki, Hiroyuki et al. (2004): Phosphorylation-dependent degradation of c-Myc is mediated by the F-box protein Fbw7. In *The EMBO journal* 23 (10), pp. 2116–2125. DOI: 10.1038/sj.emboj.7600217.

Yang, Liu; Jin, Mingli; Jung, Nahyun; Jeong, Kwang Won (2020): MLL2 regulates glucocorticoid receptor-mediated transcription of ENACα in human retinal pigment epithelial cells. In *Biochemical and Biophysical Research Communications* 525 (3), pp. 675–680. DOI: 10.1016/j.bbrc.2020.02.046.

Yeh, Chien-Hung; Bellon, Marcia; Nicot, Christophe (2018): FBXW7: a critical tumor suppressor of human cancers. In *Molecular cancer* 17 (1), p. 115. DOI: 10.1186/s12943-018-0857-2.

Yeh, Chi-Wei; Huang, Wei-Chieh; Hsu, Pang-Hung; Yeh, Kun-Hai; Wang, Li-Chin; Hsu, Paul Wei-Che et al. (2021): The C-degron pathway eliminates mislocalized proteins and products of deubiquitinating enzymes. In *The EMBO journal* 40 (7), e105846. DOI: 10.15252/embj.2020105846.

Yu, Li; Chen, Yang; Tooze, Sharon A. (2018): Autophagy pathway: Cellular and molecular mechanisms. In *Autophagy* 14 (2), pp. 207–215. DOI: 10.1080/15548627.2017.1378838.

Yu, Xufen; Li, Dongxu; Kottur, Jithesh; Shen, Yudao; Kim, Huen Suk; Park, Kwang-Su et al. (2021): A selective WDR5 degrader inhibits acute myeloid leukemia in patient-derived mouse models. In *Science translational medicine* 13 (613), eabj1578. DOI: 10.1126/scitranslmed.abj1578.

Yumimoto, Kanae; Nakayama, Keiichi I. (2020): Recent insight into the role of FBXW7 as a tumor suppressor. In *Seminars in cancer biology* 67 (Pt 2), pp. 1–15. DOI: 10.1016/j.semcancer.2020.02.017.

Yumimoto, Kanae; Yamauchi, Yuhei; Nakayama, Keiichi I. (2020): F-Box Proteins and Cancer. In *Cancers* 12 (5). DOI: 10.3390/cancers12051249.

Zeng, Xiaofang; Xu, Wendy Kaichun; Lok, Tsun Ming; Ma, Hoi Tang; Poon, Randy Y. C. (2019): Imbalance of the spindle-assembly checkpoint promotes spindle poison-mediated cytotoxicity with distinct kinetics. In *Cell death & disease* 10 (4), p. 314. DOI: 10.1038/s41419-019-1539-8.

Zhang, Naixia; Wang, Qinghua; Ehlinger, Aaron; Randles, Leah; Lary, Jeffrey W.; Kang, Yang et al. (2009): Structure of the s5a:k48-linked diubiquitin complex and its interactions with rpn13. In *Molecular cell* 35 (3), pp. 280–290. DOI: 10.1016/j.molcel.2009.06.010.

Zhang, Qiang; Karnak, David; Tan, Mingjia; Lawrence, Theodore S.; Morgan, Meredith A.; Sun, Yi (2016a): FBXW7 Facilitates Nonhomologous End-Joining via K63-Linked Polyubiquitylation of XRCC4. In *Molecular cell* 61 (3), pp. 419–433. DOI: 10.1016/j.molcel.2015.12.010.

Zhang, Qiang; Mady, Ahmed S. A.; Ma, Yuanyuan; Ryan, Caila; Lawrence, Theodore S.; Nikolovska-Coleska, Zaneta et al. (2019): The WD40 domain of FBXW7 is a poly(ADP-ribose)-binding domain that mediates the early DNA damage response. In *Nucleic acids research* 47 (8), pp. 4039–4053. DOI: 10.1093/nar/gkz058.

Zhang, Suyang; Chang, Leifu; Alfieri, Claudio; Zhang, Ziguo; Yang, Jing; Maslen, Sarah et al. (2016b): Molecular mechanism of APC/C activation by mitotic phosphorylation. In *Nature* 533 (7602), pp. 260–264. DOI: 10.1038/nature17973.

Zhang, Wei; Koepp, Deanna M. (2006): Fbw7 isoform interaction contributes to cyclin E proteolysis. In *Molecular cancer research : MCR* 4 (12), pp. 935–943. DOI: 10.1158/1541-7786.MCR-06-0253.

Zhao, Shuai; Allis, C. David; Wang, Gang Greg (2021): The language of chromatin modification in human cancers. In *Nature reviews. Cancer* 21 (7), pp. 413–430. DOI: 10.1038/s41568-021-00357-x.

Zheng, Jianyu; Yang, Xiaoming; Harrell, Jennifer M.; Ryzhikov, Sophia; Shim, Eun-Hee; Lykke-Andersen, Karin et al. (2002a): CAND1 Binds to Unneddylated CUL1 and Regulates the Formation of SCF Ubiquitin E3 Ligase Complex. In *Molecular cell* 10 (6), pp. 1519–1526. DOI: 10.1016/s1097-2765(02)00784-0.

Zheng, Nana; Wang, Zhiwei; Wei, Wenyi (2016): Ubiquitination-mediated degradation of cell cycle-related proteins by F-box proteins. In *The international journal of biochemistry & cell biology* 73, pp. 99–110. DOI: 10.1016/j.biocel.2016.02.005.

Zheng, Ning; Schulman, Brenda A.; Song, Langzhou; Miller, Julie J.; Jeffrey, Philip D.; Wang, Ping et al. (2002b): Structure of the Cul1-Rbx1-Skp1-F boxSkp2 SCF ubiquitin ligase complex. In *Nature* 416 (6882), pp. 703–709. DOI: 10.1038/416703a.

Zhou, Qianghua; Chen, Xu; He, Haixia; Peng, Shengmeng; Zhang, Yangjie; Zhang, Jingtong et al. (2021): WD repeat domain 5 promotes chemoresistance and Programmed Death-Ligand 1 expression in prostate cancer. In *Theranostics* 11 (10), pp. 4809–4824. DOI: 10.7150/thno.55814.

Zhu, Yanting; Zhou, Yuan; Shi, Jue (2014): Post-slippage multinucleation renders cytotoxic variation in anti-mitotic drugs that target the microtubules or mitotic spindle. In *Cell cycle (Georgetown, Tex.)* 13 (11), pp. 1756–1764. DOI: 10.4161/cc.28672.

6. Appendix

6.1 Flag-immunoprecipitation/mass-spectrometry substrate screen

Appendix table 1: Significantly enriched proteins from non-synchronized lysates identified by Flag-immunoprecipitation and mass spectrometry.
Label-free quantification (LFQ) results from mass spectrometry were compared to assess enrichment between samples using MaxQuant Perseus. Unpaired, two-tailed student's t-test, n=4. $p < 0.05$ was considered significant. All proteins listed were significantly enriched between EV and WT, grey background marks proteins significantly enriched in WT samples compared to WD40 samples. EV – empty vector, WT – wild type FBXW7, WD40 – FBXW7 S462A, T463V, R465A

Gene names	-log p-value EV vs WT asynchronous	Difference (log_2) EV vs WT asynchronous	-log p-value WT vs WD40 asynchronous	Difference (log_2) WT vs WD40 asynchronous
TP53	3,391	-11,944	3,069	10,398
PRR36	3,760	-8,646	3,867	10,109
FBXW7	4,465	-8,517	2,838	5,678
MED12	3,554	-8,066	2,999	7,262
MED1	3,828	-7,913	3,970	7,532
MYC	3,422	-7,243	2,767	7,235
MED24	2,941	-7,051	3,612	6,277
RADIL	2,958	-7,005	2,915	6,782
MED14	3,798	-6,777	3,698	6,970
NFKB2	3,445	-6,769	2,756	6,384
MED17	3,477	-6,429	2,901	6,738
MED13	3,712	-6,326	2,716	7,678
KPNA3	3,836	-5,955	3,925	5,547
KPNA4	3,566	-5,834	3,803	5,371
MED13L	7,575	-5,753	3,834	5,894
EP400	2,786	-5,511	2,334	4,598
MED15	3,028	-5,059	2,938	5,545
BIRC6	3,375	-4,941	1,698	4,277
CREB3L2	2,425	-4,916	2,376	4,461
RB1	2,623	-4,807	1,895	4,373
MED4	2,370	-4,565	2,391	4,723
MED27	3,614	-4,398	2,503	4,951
MED23	2,783	-4,318	1,885	4,244
ANKRD40	2,932	-4,054	2,183	6,127
MAX	3,918	-4,031	3,767	4,507
MED16	2,104	-3,711	2,735	5,387
MED20	2,315	-3,242	3,084	4,198
MED6	3,087	-3,056	2,352	3,777
MYCBP2	2,700	-10,751	1,500	1,055
RAE1	3,294	-9,188	1,435	1,131
CS	3,520	-9,038	1,042	1,406
FBXO45	4,142	-8,876	1,154	1,024
SPRYD3	3,568	-8,620	1,491	1,592

FBXW7 mutant	3,254	-8,440	0,465	0,307
SKP1	3,437	-7,764	1,116	0,551
CUL1	3,939	-7,508	0,996	0,500
LGALS3BP	3,744	-7,281	1,621	1,370
RBX1	3,847	-7,260	1,066	0,864
MYCBP2	2,778	-6,807	0,563	0,931
NUDC	4,502	-6,482	1,689	-2,473
ARIH1	3,040	-6,293	0,413	0,316
FBXW2	1,752	-5,734	0,392	0,212
DIABLO	2,645	-5,447	1,908	1,247
XIAP	3,250	-5,289	0,775	0,752
PSME4	4,312	-5,194	1,881	-1,535
NEDD8;NEDD8-MDP1	3,221	-5,148	0,253	0,398
TRRAP	2,373	-5,083	1,559	3,758
PSMA2	2,591	-4,961	1,101	-1,656
PSME3	2,003	-4,941	2,072	-1,391
PSMD8	2,519	-4,820	1,067	-0,880
PSMA7	2,384	-4,662	1,694	-1,134
TUBGCP4	2,495	-4,650	0,265	0,595
PSMB4	2,489	-4,497	1,226	-1,504
BOD1L1	1,934	-4,442	1,333	2,813
PSMB2	2,509	-4,317	1,289	-1,376
PSMD12	2,694	-4,308	2,053	-1,221
PSMD7	2,426	-4,179	1,881	-1,416
PSMA3	2,071	-4,129	0,799	-1,199
PSMA1	2,516	-3,992	1,146	-1,216
PSMB6	1,958	-3,963	1,602	-1,068
PSMB5	2,271	-3,884	0,455	-0,926
PSMA6	3,010	-3,870	1,674	-1,321
USP11	2,695	-3,850	0,656	1,160
PSMA5	3,902	-3,790	1,911	-1,217
PSMD13	2,918	-3,780	1,662	-1,055
CHTF18	1,654	-3,706	2,410	2,529
PSMB3	1,869	-3,662	1,094	-1,339
MED8	2,302	-3,591	2,471	2,595
PSMD14	4,577	-3,567	1,641	-1,280
PSMB7	2,322	-3,506	1,665	-2,005
METTL15	2,273	-3,455	0,914	1,394
CAPN1	2,259	-3,434	0,727	0,678
PSMC3	5,107	-3,433	2,650	-1,342
BAG2	4,161	-3,253	2,477	-1,782
DNAJC16	2,558	-3,206	0,507	-0,590

PSMC1	4,793	-3,175	2,335	-1,230
CDK8	2,501	-3,175	1,116	2,899
PSMC6	3,219	-3,052	2,241	-1,283
PSMD1	3,176	-3,040	1,947	-1,144
PSMD6	2,836	-2,919	1,491	-1,009
HUWE1	2,512	-2,903	1,318	-0,864
PSMD11	2,588	-2,880	2,328	-1,121
PSMD2	3,647	-2,846	1,696	-1,041
RPL22	2,101	3,284	0,089	-0,276
FXR2	1,850	3,539	0,034	-0,097

Appendix table 2: Significantly enriched proteins from mitotic lysates identified by Flag-immunoprecipitation and mass spectrometry.
Label-free quantification (LFQ) results from mass spectrometry were compared to assess enrichment between samples using MaxQuant Perseus. Unpaired, two-tailed student's t-test, n=4. $p < 0.05$ was considered significant. All proteins listed were significantly enriched between EV and WT, grey background marks proteins significantly enriched in WT samples compared to WD40 samples. EV – empty vector, WT – wild type FBXW7, WD40 – FBXW7 S462A, T463V, R465A

Gene names	-log p-value EV vs WT mitotic	Difference (log_2) EV vs WT mitotic	-log p-value WT vs WD40 mitotic	Difference (log_2) WT vs WD40 mitotic
TP53	3,258	-11,535	3,354	12,158
BIRC6	4,821	-9,417	4,413	9,857
MED12	3,900	-9,379	3,277	9,192
FBXW7	3,728	-9,211	2,673	8,492
PRR36	3,780	-8,804	4,830	10,353
MED1	4,041	-8,318	3,511	7,691
MED14	3,975	-7,315	2,803	6,261
MED17	3,693	-7,094	4,204	6,573
MYC	4,079	-6,868	4,022	7,931
MED13L	8,373	-6,842	3,780	8,243
MED13	4,226	-6,803	3,390	7,620
NFKB2	2,979	-6,784	2,971	6,318
MED24	2,141	-6,482	2,140	5,550
CREB3L2	3,077	-6,449	3,221	6,933
EP400	2,750	-6,144	3,534	4,920
RADIL	2,851	-5,983	3,054	6,032
TRRAP	2,639	-5,910	2,429	4,732
MED15	3,540	-5,781	2,338	5,838
FYCO1	1,984	-5,695	3,200	6,346
KPNA4	2,461	-5,537	1,860	5,121
NOTCH1	2,286	-5,397	2,228	6,161
BOD1L1	2,369	-5,293	3,888	4,099
MED4	2,609	-5,009	3,515	5,781
KPNA3	1,911	-4,993	1,838	4,900

MED27	3,979	-4,938	2,790	5,599
MED23	2,808	-4,729	2,067	4,370
MED8	2,580	-4,331	2,371	4,022
MED16	2,448	-4,168	2,960	5,587
MED6	3,544	-3,948	3,170	4,133
CDK8	2,917	-3,849	4,462	4,530
MAX	2,103	-3,373	2,111	4,059
MYCBP2	2,671	-10,603	0,641	0,744
FBXO45	4,200	-9,173	0,699	0,885
CS	3,370	-9,067	0,421	0,803
RAE1	3,207	-8,894	0,354	0,517
FBXW7 mutant	3,297	-8,597	0,197	0,134
SPRYD3	3,458	-8,274	1,426	1,469
SKP1	3,532	-8,187	0,370	0,445
LGALS3BP	4,193	-7,951	1,441	1,282
CUL1	3,906	-7,785	0,343	0,372
RBX1	4,059	-7,692	1,609	0,743
NUDC	4,033	-7,289	1,315	-1,901
ARIH1	3,200	-6,642	0,477	0,126
MYCBP2	2,691	-6,458	0,508	1,165
NEDD8;NEDD8-MDP1	3,083	-5,463	0,153	0,213
FBXW2	1,530	-5,363	0,302	-0,704
DIABLO	2,402	-5,327	0,577	1,912
RB1	3,199	-5,236	2,763	3,120
TUBGCP4	2,562	-5,235	0,709	2,488
USP11	2,884	-4,922	0,281	0,557
PSME4	3,990	-4,737	1,966	-1,674
XIAP	3,383	-4,727	0,261	0,537
PSMB4	2,701	-4,637	0,560	-0,911
PSMA2	1,899	-4,614	0,370	-1,294
PSME3	1,712	-4,479	0,887	-1,743
PSMA7	2,182	-4,335	1,108	-1,244
PSMD8	2,089	-4,219	0,656	-1,110
CHTF18	1,892	-4,200	2,794	2,259
PSMB2	2,440	-4,171	0,975	-1,265
PSMD12	2,586	-4,105	1,129	-1,194
HPS6	3,405	-4,092	1,684	4,087
PSMD7	2,111	-4,027	0,553	-1,097
PSMA6	3,001	-3,992	1,011	-1,051
PSMA3	1,922	-3,981	0,752	-1,246
PSMA1	2,430	-3,965	0,618	-0,946
METTL15	2,353	-3,953	0,688	1,090

MED20	2,664	-3,931	2,544	2,968
PSMB6	1,802	-3,659	0,691	-1,147
FAHD2A;FAHD2B	2,160	-3,597	0,258	0,835
PSMD13	2,733	-3,579	1,186	-1,167
PSMD14	4,862	-3,564	0,888	-1,177
CAPN1	2,179	-3,511	0,330	0,431
MAP7D1	4,104	-3,505	2,601	2,807
PSMC3	4,030	-3,389	0,663	-1,003
PSMA5	3,054	-3,351	1,064	-1,437
BAG2	2,439	-3,168	1,451	-1,703
BRD8	2,415	-3,158	3,194	3,129
PSMC1	5,185	-3,154	1,471	-1,139
PSMC6	3,319	-3,104	0,785	-0,954
CAND1	3,578	-3,100	2,169	-0,570
UBR5	3,832	-2,906	2,428	0,601
PSMD6	2,810	-2,894	0,868	-0,996
PSMD1	3,025	-2,776	1,303	-1,211

Appendix table 3: Significantly enriched proteins between FBXW7 WT from non-synchronized and mitotic cells identified by Flag-immunoprecipitation and mass spectrometry.
Label-free quantification (LFQ) results from mass spectrometry were compared to assess enrichment between samples using MaxQuant Perseus. Unpaired, two-tailed student's t-test, n=4. $p < 0.05$ was considered significant. All proteins listed were four-fold enriched between the samples, grey background marks proteins significantly enriched in WT FBXW7 samples from non-synchronized cells compared to mitotic cells. WT – wild type FBXW7

Gene names	-log p-value WT asynchronous vs WTmitotic	Difference (log_2) WT asynchronous vs WT mitotic
BIRC6	3,550	-4,476
FYCO1	3,612	-4,401
NOTCH1	1,814	-3,829
SETD4	0,508	-3,527
SGK3	1,752	-2,854
LGALS7	0,563	-2,645
ACTBL2	1,014	-2,552
MAP7D1	2,351	-2,502
NYNRIN	0,455	-2,437
TSPYL1	0,509	-2,380
TUBA4A	1,372	-2,261
CCNC	1,273	-2,260
S100A8	0,622	-2,250
DDX46	1,260	-2,220
ATP6V1B2	1,263	-2,202
VDAC3	1,398	-2,189
NOL10	1,001	-2,187

ANXA1	1,005	-2,183
KIF23	0,564	-2,170
GSPT1	0,937	-2,151
IMPDH2	0,669	-2,108
HNRNPK	1,062	-2,102
NUMA1	0,641	-2,092
FAM184B	0,568	-2,064
MRPL3	2,381	-2,060
HNRNPC	2,031	-2,042
MAP1S	2,226	-2,003

6.2 FYCO1 is not upregulated by knockdown of FBXW7

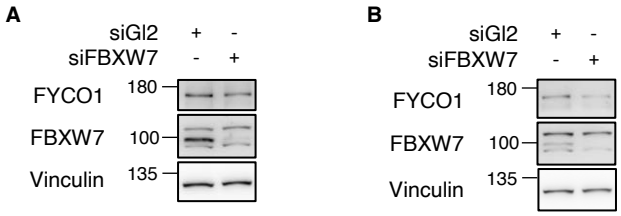

Appendix figure 1: FYCO1 protein levels are not stabilized after knockdown of FBXW7.
A U2OS cells or **B** HeLa cells were transfected with siRNA targeting FBXW7 or Gl2 for 72 h. Cell lysates were analyzed by Western blotting.

6.3 Abbreviations

APC/C	Anaphase-promoting complex/cyclosome
APS	Ammonium peroxodisulfate
ASH2L	ASH2-like protein
ATG	Autophagy-related proteins
ATM	Ataxia telangiectasia mutated
ATP	Adenosine triphosphate
BCL-2	B-cell lymphoma protein 2
BRB	Bric-a-brac/Tramtrack/Broad
BRUCE	BIR repeat-containing ubiquitin-conjugating enzyme
BSA	Bovine Serum Albumin
BUB1	Uninhibited by benzamidazole 1
C/EBPδ	CCAAT-enhancer-binding protein δ
CAND1	Cullin-associated and neddylation-dissociated protein 1
CDC4	Cell division protein 4
CDK	Cyclin-dependent kinase
CENPA	Centrosome-associated protein A
CIN	Chromosomal instability
CK2	Casein kinase 2
CP	Core protease

CP110	Centriolar coiled-coil protein of 110 kDa
CRBN	Cereblon
CRL	Cullin-RING E3 ubiquitin ligase
CUL	Cullin
DCAF	DDB1-CUL4-associated factor
DDB1	DNA damage-binding protein 1
DLBCL	Diffuse large B-cell lymphoma
DMEM	Dulbecco's Modified Eagle's Medium
DMSO	Dimethyl sulfoxide
DNA-PK	DNA-dependent protein kinase
Dox	Doxycycline
DTT	Dithiothreitol
DUB	Deubiquitylating enzyme
EDTA	Ethylenediaminetetraacetic acid
ELM	Eukaryotic Linear Motif resource
EMI1	early mitotic inhibitor 1
EPS8	Epidermal growth factor receptor kinase substrate 8
ERAD	Endoplasmatic reticulum-associated degradation
EV	Empty vector
F	Phenylalanine
FBS	Fetal bovine serum
FBXW7	F-box/WD40-repeat containing protein 7
Fig.	Figure
FOXM1	Forkhead box protein M1
GFP	Green fluorescent protein
GSK3β	Glycogen synthase kinase 3 beta
GST	Glutathione S-transferase
HECT	Homologous to the E6-associated protein carboxyl terminus
HRP	Horseradish peroxidase
hSAS6	Spindle assembly abnormal protein 6 homolog
HSP	Heat-shock protein
HtrA2	Serine protease high temperature requirement protein A2
IAP	Inhibitor of apoptosis
IP	Immunoprecipitation
IPTG	Isopropyl β- d-1-thiogalactopyranoside
K	Lysine
KANSL1	KAT8 regulatory NSL complex subunit 1
kDa	Kilodalton
KMT2D	SET-domain lysine methyltransferase 2D
KO	Knockout
l.e.	long exposure
LB	Lysogeny broth
LDS	Lithium dodecyl sulfate
LFQ	Label free quantification
LIR	LC3-interacting region
LSD1	Lysine-specific demethylase 1
LTN1	Listerin

MAD1	Mitotic arrest deficient
MCAK	Mitotic centromere-associated kinesin
MCC	Mitotic checkpoint complex
MCM	Minichromosome maintenance complex
MED13	Mediator of RNA polymerase II transcription
MPS1	Monopolar spindle 1
mRNA	messenger ribonucleic acid
MYCBP2	Myc-binding protein 2
NEHJ	Non-homologous end joining
NEM	N-ethylmaleimide
NOTCH1	Neurogenic locus notch homolog protein 1
P	Proline
PAGE	Polyacrylamide gel electrophoresis
PAR	polyADP-ribose
PCR	Polymerase chain reaction
PD	Pulldown
PEI	Polyethyleneimine
PI3K	phosphoinositide 3-kinase
PLK2	Polo-like kinase 2
PQC	Protein quality control system
PROTAC	Proteolysis-targeting chimera
PTM	Post-translational modification
qPCR	Quantitative real-time PCR
RBBP5	RB binding protein 5
RBR	RING-between-RING
RBX1	Ring-box protein 1
RING	Really Interesting New Gene
RP	Regulatory particle
RQC	Ribosome-associated protein quality control
RT	Room temperature
S	Serine
s.e.	short exposure
SAC	Spindle-assembly checkpoint
SCF	SKP1-CUL1-F-box protein complex
SDS	Sodium dodecyl sulfate
siRNA	Small interfering RNA
SKP1	S-phase kinase-associated protein 1
SOCS	Suppressor of cytokine signaling
SOX9	SRY-box transcription factor 9
SR	Substrate receptor
STYX	Serine/threonine/tyrosine-interacting protein
SUMO	small ubiquitin-like modifier
T	Threonine
T-ALL	T-cell acute lymphoblastic leukemia
T-LBL	T-cell lymphoblastic lymphoma
TMD	Transmembrane domain
TRIP13	Thyroid hormone receptor-interacting protein 13

UBC	Ubiquitin-conjugating domain
UBD	Ubiquitin-binding domain
UPS	Ubiquitin-proteasome system
USP9X	Probable ubiquitin carboxyl-terminal hydrolase FAF-X
VHL	Von Hippel-Lindau
WCE	Whole cell extract
WDR5	WD repeat-containing protein 5
WHB	Winged-helix B domain
WT	Wild-type
XRCC4	X-ray repair cross-complementing protein 4

6.4 List of figures

6.5 List of tables

7. Acknowledgements

I would like to express my gratitude to Prof. Dr. Ingrid Hoffmann for giving me the opportunity to join her lab and to work on this interesting research topic. I am grateful for the scientific discussions, the supporting environment, the encouragement and for the trust she showed me.

I would like to thank Prof. Dr. Frauke Melchior and Prof. Dr. Tobias Dick for being part of my thesis advisory committee and for their critical discussions and provided expertise. Additionally, I thank apl. Prof. Dr. Matthias Mayer for joining my thesis examination committee.

All of the current and past lab members of the Hoffmann lab helped me by providing a nice working atmosphere and giving advice and support: Kai Richter, Bettina Dörr, Yannik Dieter, Xu Holtkotte, Vesna Zivanovic, Kübra Gürkaslar, Bosco-Sungho Han, Josina Großmann and Alexandra Turi da Fonte Dias. I am very happy to have met all of you. In addition, I would like to thank Jörg Schweiggert for providing advice.

I would like to thank the DKFZ Light Microscope Facility, especially Manuela Brom, and the DKFZ MS-based Protein analysis Unit for their support and expertise.

Especially, I thank my whole family for their encouragement, support and understanding throughout the entire time. I would like to express my greatest gratitude towards my wife Rebecca for her patience, understanding and love. I could not have finished this journey without her support.